ISSN 1948-0210 (online)

World Journal of *Stem Cells*

World J Stem Cells 2019 February 26; 11(2): 55-146

Published by Baishideng Publishing Group Inc

WJSC

World Journal of Stem Cells

Contents

Monthly Volume 11 Number 2 February 26, 2019

Contents

World Journal of Stem Cells

Volume 11 Number 2 February 26, 2019

ABOUT COVER

Associate Editor of *World Journal of Stem Cells*, Dong-Wook Han, PhD, Professor, Department of Optics and Mechatronics Engineering, Pusan National University, Busan 46241, South Korea

AIMS AND SCOPE

World Journal of Stem Cells (*World J Stem Cells*, *WJSC*, online ISSN 1948-0210, DOI: 10.4252), is a peer-reviewed open access academic journal that aims to guide clinical practice and improve diagnostic and therapeutic skills of clinicians.

WJSC covers topics concerning all aspects of stem cells: embryonic, neural, hematopoietic, mesenchymal, tissue-specific, and cancer stem cells; the stem cell niche, stem cell genomics and proteomics, *etc*.

We encourage authors to submit their manuscripts to *WJSC*. We will give priority to manuscripts that are supported by major national and international foundations and those that are of great basic and clinical significance.

INDEXING/ABSTRACTING

The *WJSC* is now indexed in PubMed, PubMed Central, Science Citation Index Expanded (also known as SciSearch®), Journal Citation Reports/Science Edition, Biological Abstracts, and BIOSIS Previews. The 2018 Edition of Journal Citation Reports cites the 2017 impact factor for *WJSC* as 4.376 (5-year impact factor: N/A), ranking *WJSC* as 7 among 24 journals in Cell and Tissue Engineering (quartile in category Q2), and 65 among 190 journals in Cell Biology (quartile in category Q2).

RESPONSIBLE EDITORS FOR THIS ISSUE

Responsible Electronic Editor: *Ying-Na Bian* **Proofing Editorial Office Director:** *Jin-Lei Wang*

NAME OF JOURNAL
World Journal of Stem Cells

ISSN
ISSN 1948-0210 (online)

LAUNCH DATE
December 31, 2009

FREQUENCY
Monthly

EDITORS-IN-CHIEF
Tong Cao, Shengwen Calvin Li, Carlo Ventura

EDITORIAL BOARD MEMBERS
https://www.wjgnet.com/1948-0210/editorialboard.htm

EDITORIAL OFFICE
Jin-Lei Wang, Director

PUBLICATION DATE
February 26, 2019

INSTRUCTIONS TO AUTHORS
https://www.wjgnet.com/bpg/gerinfo/204

GUIDELINES FOR ETHICS DOCUMENTS
https://www.wjgnet.com/bpg/GerInfo/287

GUIDELINES FOR NON-NATIVE SPEAKERS OF ENGLISH
https://www.wjgnet.com/bpg/gerinfo/240

PUBLICATION MISCONDUCT
https://www.wjgnet.com/bpg/gerinfo/208

ARTICLE PROCESSING CHARGE
https://www.wjgnet.com/bpg/gerinfo/242

STEPS FOR SUBMITTING MANUSCRIPTS
https://www.wjgnet.com/bpg/GerInfo/239

ONLINE SUBMISSION
https://www.f6publishing.com

World Journal of Stem Cells

Submit a Manuscript: https://www.f6publishing.com

World J Stem Cells 2019 February 26; 11(2): 55-72

DOI: 10.4252/wjsc.v11.i2.55

ISSN 1948-0210 (online)

REVIEW

Rational use of mesenchymal stem cells in the treatment of autism spectrum disorders

Qiang Liu, Mo-Xian Chen, Lin Sun, Chloe U Wallis, Jian-Song Zhou, Li-Juan Ao, Qi Li, Pak C Sham

ORCID number: Qiang Liu (0000-0002-0167-2963); Mo-Xian Chen (0000-0001-6019-5776); Lin Sun (0000-0001-7496-7685); Chloe U Wallis (0000-0002-6770-8324); Jian-Song Zhou (0000-0002-4410-4202); Li-Juan Ao (0000-0002-5116-1993); Qi Li (0000-0002-3732-2578); Pak C Sham (0000-0002-2533-7270).

Author contributions: Liu Q and Chen MX contributed equally to this work; Liu Q, Chen MX, Li Q, Ao LJ, and Sham PC designed the research; Liu Q and Chen MX wrote the first draft of the article; Lin S, Zhou JS, and Wallis CU designed the tables and figures; Li Q and Wallis CU revised the draft; Ao LJ and Sham PC contributed to the funding support to this research.

Supported by National Nature Science Foundation of China, No. 81660381

Conflict-of-interest statement: All authors have no conflicts of interest to report.

Qiang Liu, Department of Surgery, The Chinese University of Hong Kong, Hong Kong, China

Mo-Xian Chen, Li-Juan Ao, School of Rehabilitation, Kunming Medical University, Kunming 650500, Yunnan Province, China

Lin Sun, Department of Psychology, Weifang Medical University, Weifang 261053, Shandong Province, China

Chloe U Wallis, Medical Sciences Division, University of Oxford, Oxford OX3 9DU, United Kingdom

Jian-Song Zhou, Mental Health Institute of the Second Xiangya Hospital, Central South University, Changsha 410011, Hunan Province, China

Qi Li, Pak C Sham, Department of Psychiatry, the University of Hong Kong, Hong Kong, China

Pak C Sham, State Key Laboratory of Brain and Cognitive Sciences, Center for Genomic Sciences, the University of Hong Kong, Hong Kong, China

Corresponding author: Qi Li, PhD, Postdoctoral Fellow, Department of Psychiatry, the University of Hong Kong, 21 Sasson Roads, Pokfulam, Hong Kong, China.
liqihku@gmail.com
Telephone: +852-39719588

Abstract

Autism and autism spectrum disorders (ASD) refer to a range of conditions characterized by impaired social and communication skills and repetitive behaviors caused by different combinations of genetic and environmental influences. Although the pathophysiology underlying ASD is still unclear, recent evidence suggests that immune dysregulation and neuroinflammation play a role in the etiology of ASD. In particular, there is direct evidence supporting a role for maternal immune activation during prenatal life in neurodevelopmental conditions. Currently, the available options of behavioral therapies and pharmacological and supportive nutritional treatments in ASD are only symptomatic. Given the disturbing rise in the incidence of ASD, and the fact that there is no effective pharmacological therapy for ASD, there is an urgent need for new therapeutic options. Mesenchymal stem cells (MSCs) possess immunomodulatory properties that make them relevant to several diseases associated with inflammation and tissue damage. The paracrine regenerative mechanisms of MSCs are also suggested to be therapeutically beneficial for ASD. Thus the underlying pathology in ASD, including immune system dysregulation and inflammation, represent potential targets for MSC therapy. This review will

Manuscript source: Unsolicited manuscript

Received: October 9, 2018
Peer-review started: October 10, 2018
First decision: November 27, 2018
Revised: December 30, 2018
Accepted: January 22, 2019
Article in press: January 23, 2019
Published online: February 26, 2019

focus on immune dysfunction in the pathogenesis of ASD and will further discuss the therapeutic potential for MSCs in mediating ASD-related immunological disorders.

Key words: Autism spectrum disorders; Mesenchymal stem cells; Major histocompatibility complex; Inflammation; Maternal immune activation; Cell therapy

Core tip: Autism spectrum disorder (ASD) is a complex, behaviorally defined disorder characterized by severe impairments in social communication and repetitive behavior. Because of an incomplete understanding of the pathology of ASD, available treatment options in ASD are only symptomatic. We discuss the role of immune dysfunction in the etiology of ASD and function of mesenchymal stem cells. We summarize the pre-clinical and clinical evidence for mesenchymal stem cell therapy in ASD and suggest that more basic experiments are needed to better understand the therapeutic mechanisms of mesenchymal stem cells in ASD.

Citation: Liu Q, Chen MX, Sun L, Wallis CU, Zhou JS, Ao LJ, Li Q, Sham PC. Rational use of mesenchymal stem cells in the treatment of autism spectrum disorders. *World J Stem Cells* 2019; 11(2): 55-72
URL: https://www.wjgnet.com/1948-0210/full/v11/i2/55.htm
DOI: https://dx.doi.org/10.4252/wjsc.v11.i2.55

INTRODUCTION

Autism spectrum disorder (ASD) is a complex, behaviorally defined disorder characterized by severe and pervasive impairments in social communication and repetitive behavior. According to the 5th edition of the diagnostic and statistical manual of mental disorders, ASD is diagnosed in individuals exhibiting three social communication and interaction deficits, at least two symptoms of restricted or repetitive behavior/interests/activities, and a variety of specific symptoms classified within each diagnostic category. ASD is one of the most common psychiatric disorders affecting 1 in 59 children aged 8 years based on the most recent estimates calculated by the United States Center of Disease Control[1]. There has recently been a steady and highly significant rise in the estimated prevalence of ASD, due both to a greater awareness of the disorder and broader diagnostic criteria[1,2]. ASD is a complex and heterogeneous psychiatric disorder, and early studies suggest a strong genetic component to autism. For example, identical twin studies estimate concordance for ASD to be between 70% and 90%[3-5]. However, growing evidence suggests that these previous studies may have overestimated the genetic component of autism because the heritability of autism and shared twin environment were similar[6]. Meanwhile, large numbers of ASD candidate genes have been uncovered by whole-genome linkage studies, gene association studies, copy number variation screening, and SNP analysis[7]. Many of the candidate genes, such as reelin (*RELN*)[8], SH3 and multiple ankyrin repeat domains 3 (*SHANK3*)[9], neuroligin 3 (*NLGN3*), *NLGN4X*[10], *MET*[11], gamma-aminobutyric acid type-A receptor beta3 subunit (*GABRB3*)[12], oxytocin receptor (*OXTR*)[13], serotonin transporter (*SLC6A4*)[14], and phosphatase and tensin homolog (*PTEN*)[15] have been demonstrated to be associated with ASD (Figure 1). Furthermore, single gene mutations cause several ASD-related syndromes, including Rett's syndrome (methyl CpG binding protein 2, *MECP2*)[16], Fragile X (fragile X mental retardation 1, *FMR1*)[17], and tuberous sclerosis (*TSC1* or *TSC2*)[18]. Proteins within the phosphoinositide-3-kinase pathway, including MET, PTEN, TSC1, and TSC2 have a major role in regulating interleukin (IL)-12 production and are involved in both innate and adaptive immunity[19]. Additionally, some of the ASD candidate genes, including the major histocompatibility complex class genes are traditionally thought to play a role exclusively in the immune system[20] (Figure 1). Even with the recent advances in identifying candidate genes involved in ASD, all identified genes account for < 20% of ASD cases[21]. Moreover, a number of these genetic risk factors are present in individuals without ASD suggesting additional risk factors are also necessary. For example, recent studies provided evidence for altered DNA

methylation in ASD[22,23]. Thus through epigenetic mechanisms, exposure to specific environmental factors may be responsible for triggering the development of ASD in some individuals (Figure 1). A variety of environmental risk factors have been identified to increase ASD risk including: maternal immune activation (MIA)[24-27]; prenatal or perinatal exposure to valproic acid (VPA)[28,29] and selective serotonin reuptake inhibitors (SSRI)[30-32]; early life exposure to stress[33,34]; advanced parental age, zinc deficiency, abnormal melatonin synthesis[35]; and environmental toxins[36] (Figure 1). MIA and maternal exposure to drugs such as SSRI and VPA are of particular interest given evidence from clinical and animal studies supporting the role for immune dysfunction and inflammation in the etiology of ASD.

The first part of this review discusses immune-related genetic and environmental risk factors for ASD, from both human and animal studies, and the role of immune activation in the etiology of ASD-related behavioral and neuropathological abnormalities. Understanding how immune abnormalities are involved in the etiology of ASD will provide a valuable starting point for further work towards potential stem cell therapies for ASD. There is great potential for the use of stem cells in the future of molecular and regenerative medicine. Amongst the various stem cell subtypes, mesenchymal stem cells (MSCs) are the most promising clinical candidate for the treatment of several diseases related with inflammation, tissue damage, and subsequent regeneration and repair[37]. Therefore, the second part of this review will focus on underlying treatment mechanism of MSCs in ASD.

EVIDENCE FOR IMMUNE ABNORMALITIES IN ASD

Immune-related genetic risk factors for ASD

Major histocompatibility complex molecules: Major histocompatibility complex (MHC) occurs on the short arm of chromosome 6 and is divided into three regions; MHC class I, II, and III (MHC-I, MHC-II, and MHC-III). The human leukocyte antigen refers to the MHC locus in humans, which contains a large number of genes involved in integrating the innate and adaptive immune system. MHC-I molecules are found on all nucleated cells, and present epitopes to T-cell receptor proteins on cytotoxic CD8+ T lymphocytes[38]. As a result of MHC-I presentation, cytotoxic CD8+ T lymphocytes become activated and play an important role in the clearance of bacterial and viral infections. While MHC-I molecules have long been known for their primary role in adaptive immunity, they also bind to inhibitory receptors on natural killer (NK) cells, which are part of the innate immune system[39,40]. Interestingly, some recent studies have demonstrated novel roles of MHC-I molecules in regulating synaptic function, plasticity of the cerebral cortex, and cortical glutamatergic connectivity[41-43]. Several lines of evidence have indicated that abnormalities in the balance between excitatory (glutamate-mediated) and inhibitory (gamma-Aminobutyric acid-mediated) neurotransmission may be a key pathological mechanism in autism[44-46]. MHC may also function in social communication and the formation of social memories[47,48]. Moreover, the class one allele of human leukocyte antigen-A2, an important MHC-I antigen presenting molecule, is linked to higher incidence of autism[49]. Thus, it is interesting to speculate that human leukocyte antigen polymorphisms might contribute to the abnormal social communication in ASD by altering excitatory/inhibitory balance in the brain.

Unlike MHC-I, MHC-II molecules are expressed exclusively by the antigen presenting cells, including B cells, dendritic cells, and macrophages, in response to inflammation signals[50]. In general, helper CD4+ T lymphocytes can recognize exogenous antigen presented on MHC-II through T cell receptors. Once activated, helper CD4+ T lymphocytes promote B cell differentiation and antibody production and secrete many cytokines and chemokines. MHC-II alleles are associated with autoimmune disease[51], and interestingly, many studies report that a family history of autoimmune disease is a significant risk factor for ASD[52]. Moreover, in the developing and adult brain, MHC-II molecules are expressed mainly on microglia, astrocytes, and perivascular monocytes[53-55]. *In vitro* experiments suggest that the expression of MHC-II differs in astrocytes and microglia. For example, glutamate, an excitatory neurotransmitter abundantly present in the central nervous system (CNS), inhibits expression of MHC-II induced by interferon-gamma (IFN-γ) on astrocytes, but not on microglia cells[54]. Hellendall and Ting[56] reported that cytokine (IFN-γ) induced expression of MHC-II on astrocytes is mediated through a cAMP and protein kinase C-dependent pathway. Whilst a mitogen-activated protein kinase (MAPK) signal pathway including extracellular signal-regulated kinases 1/2, c-Jun N-terminal kinase, and p38 MAPK and cyclic AMP responding element binding protein, may be involved in lipopolysaccharide (LPS)-activated microglia[57]. Altered microglial

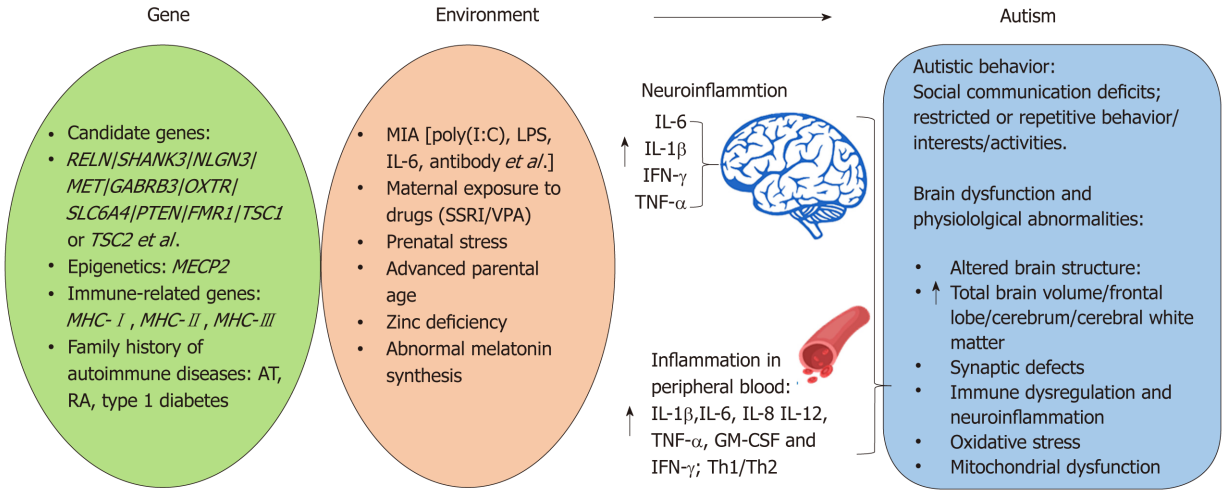

Figure 1 Genetic and environmental risk factors for autism spectrum disorders. Genetic risk factors for autism spectrum disorder (ASD) including: important candidate genes, immune-related genes (such as *MHC*), epigenetics, and family history of autoimmune disease. Prenatal infection, maternal exposure to drugs, prenatal stress, advanced parental age, zinc deficiency, and abnormal melatonin synthesis are important environmental risk factors for ASD. ASD children exhibit social communication deficits and repetitive behavior. Brain dysfunction and physiological abnormalities are observed in ASD patients and animal models. RELN: Reelin; GABRB3: Gamma-aminobutyric acid type-A receptor beta3 subunit; OXTR: Oxytocin receptor; SLC6A: PTEN: Phosphatase and tensin homolog; FMR1: Fragile X mental retardation 1; TSC1/2: Tuberous sclerosis 1/2; MECP2: Methyl CpG binding protein 2; MHC: Major histocompatibility complex; AT: Autoimmune thyroiditis; RA: Rheumatoid arthritis; MIA: Maternal immune activation; LPS: Lipopolysaccharide; SSRI: Selective serotonin reuptake inhibitors; VPA: Valproic acid.

activation in the brain is accompanied by the behavioral phenotype of autism (*e.g.*, anxiety, abnormal social interaction, and learning impairment) in MIA animal models[58,59]. Meanwhile, an increased average microglia somal volume in white matter and microglial density in grey matter has been reported in post-mortem studies of ASD[60,61]. Furthermore, several studies have reported that the *DRβ1*04* allele of the MHC-II region is associated with ASD[62-64].

The MHC-III region encodes a cluster of proteins with immune functions including complement proteins (C2 and C4), tumor necrosis factor (TNF)-α, and heat shock proteins. The CB4 null allele of MHC-III has been implicated in ASD[65]. In addition, strong evidence has demonstrated that MHC-III molecules play an important role in brain development and function. For example, TNF-α enhances dendrite growth and synaptic connectivity, balances neuronal excitation and inhibition, and alters synaptic plasticity[66-68].

Clearly, the MHC molecules play a vital role in the formation, refinement, maintenance, and plasticity of the brain. Thus, disruptions in the expression of MHC molecules in the developing brain induced by mutations and/or immune dysregulation might contribute to the altered brain function and endophenotypes of ASD.

Environmental risk factors in ASD

MIA and ASD: Epidemiological studies indicate that generalized activation of the maternal immune system caused by maternal infection during prenatal life is a strong risk factor for ASD[69-72]. Consistent with these reports, our research group and others have demonstrated non-specific induction of MIA using viral analogues such as the double stranded RNA poly(I:C), and this is sufficient to bring about neuropathologic, neuroimaging, and behavioral phenotypic changes in the offspring, which are analogous to those observed in human ASD[22,24-26,73,74]. In addition, MIA can be induced in both rodent and non-human primate models with influenza[75], IL-6[76], maternal anti-fetal brain antibody[77], and LPS[78]. Altogether, these large epidemiological findings and animal experiments point to a primary role for MIA in the etiology of ASD.

It is now well understood that shortly after maternal injection with poly(I:C), pro-inflammatory cytokines, including IL-1β, IL-6, and TNF-α are elevated in the maternal bloodstream, placenta, and fetal brain[59,79]. IL-6 in particular may be a crucial immunological mediator of the link between maternal immune activation and altered adult brain functions. This is because, unlike IL-1β and TNF-α, IL-6 may cross the placenta and enter the fetal brain after MIA[80,81]. Indeed, maternal IL-6 injection is sufficient to precipitate offspring prepulse inhibition and latent inhibition deficits usually consequent on poly(I:C) exposure[76]. Simultaneous injection of an anti-IL-6 antibody can prevent behavioral maldevelopment and gene expression changes

caused by MIA[76]. More convincingly, IL-6 knock-out mice are resistant to the effects of prenatal poly(I:C) exposure[76]. There is also evidence that maternal IL-6 dependent activation of the Janus kinase/signal transducer and activator of transcription 3 pathway in the placenta demonstrates a direct transfer of the MIA response from maternal to fetal cells[79]. Interestingly, pathways downstream of the Janus kinase/signal transducer and activator of transcription 3 signaling including the MAPK cascade that contains Ras/Raf, mitogen-activated protein kinase kinase 1, and phosphorylated extracellular signal-regulated kinases, have been demonstrated to contribute to the fetal brain dysfunction observed in the MIA mice model[82]. Moreover, several recent studies from our group and others report that MIA induces epigenetic alterations in the brain, suggesting that stable DNA methylation is a plausible mechanism underlying the disruption of gene transcription, brain development, and behavioral functions in response to immune challenge *in utero*[22,83-85].

Maternal exposure to SSRI and ASD: Depression during pregnancy is not uncommon; the prevalence is reported to be around 7%-12%[86,87]. SSRIs are the most frequently prescribed antidepressants during pregnancy because they are thought to be relatively safe for the fetus compared to other antidepressants. However, recent meta-analyses have suggested that SSRI exposure during pregnancy increases the risk for preterm birth and low birth weight[88], congenital malformation[89], and unfavorable effects on language or behavioral development in children[90]. SSRIs can cross the placenta and are able to reach the fetal brain, which might have long-term neurobehavioral and neurodevelopmental consequences in the offspring[91]. An imbalance of serotonin (5-HT) in prenatal life may be a risk factor for ASD. Experimental investigations have demonstrated that SSRIs have the potential to cause changes in brain circuitry and maladaptive behaviors, due to elevated levels of 5-HT[92]. *In utero*, exposure to an SSRI during a key developmental window lead to dysfunctional 5-HT signaling, loss of 5-HT terminals, and behavioral abnormalities in animals[92]. 5-HT levels are reported to be decreased in ASD patients[93]. Additionally, several clinical studies have reported that the use of SSRIs during pregnancy increases the risk of ASD in children[30,94-96]. Although several reviews and meta-analyses have recently been published addressing this issue, there are conflicting conclusions when controlling for maternal psychiatric disease and other confounding factors, such as genetic syndromes and congenital anomalies that are associated with ASD-like behavior[97-99]. To answer this question more accurately further investigation is warranted, in particular focusing on maternal psychiatric conditions and/or SSRI treated and untreated siblings.

Given that 5-HT plays a role as an immunomodulator, it is possible that prenatal SSRI exposure may contribute to the pathophysiology of ASD through interactions between an altered serotonergic system and the immune system. 5-HT modulates the function of a wide range of immune cells, including macrophages, NK cells, dendritic cells, T-cells, and B-cells through binding to 5-HT receptors during the immune response[100]. In addition, there is an association between serum 5-HT levels and the presence of certain MHC genes in ASD children[101]. It is possible that abnormal synaptic or extracellular levels of 5-HT may affect the immune system, triggering abnormalities as seen in ASD. However, a direct experimental investigation is needed to verify the 5-HT-mediated neuro-immune crosstalk in ASD.

Valproic acid and ASD: VPA has been used for the treatment of seizures and mood swings for more than 30 years. Several lines of clinical evidence have suggested that maternal exposure to VPA is associated with increased risk of ASD[102-104]. Our research group and others have shown that rodents exposed to VPA prenatally develop behavioral traits and neurochemical alterations that may be relevant to ASD[28,105]. Interestingly, prenatal exposure to VPA on gestation day 9 before neural tube closure disrupts the maturation of serotonergic neurons thereby interrupting early development of the serotonergic system[106]. In addition, prenatal exposure to VPA on gestation day 9 results in an elevated level of 5-HT in the hippocampus and hyperserotonemia in blood[107]. Furthermore, Dufour-Rainfray *et al*[108] reported that decreased 5-HT levels in the hippocampus of rats exposed to VPA at gestation day 9 may be associated with behavioral impairments. Therefore, these results suggest prenatal VPA exposure may play a role in the development of ASD through disruption of the normal development of the serotonin system. However, further research is required to elucidate the mechanisms by which this occurs. Clinical use of VPA is often associated with hepatotoxicity and the pathology of VPA-induced hepatotoxicity has been studied extensively. Oxidative stress and hepatic inflammation are apparent; elevated levels of nuclear NF-κB in the liver is accompanied by the induction of IL-1β, IL-6, and TNF-α, and these play important

roles in the pathology of VPA-induced hepatotoxicity[109]. Moreover, moderate or high doses of prenatal exposure to VPA can also induce toxicity and even death in the offspring in animals[28]. However, the underlying mechanism of VPA-induced toxicity in the CNS is not clear yet. We suspect that oxidative stress and/or neuroinflammation may also play an important role in the altered brain function observed in prenatal exposure to VPA. Further study is required to improve understanding of the mechanisms by which prenatal VPA exposure may induce ASD, through investigation of the serotoninergic system and immune responses in the fetal brain.

Inflammation in ASD

A consistent body of data has suggested that there is active inflammation in the CNS in ASD patients. Increased activation of astroglia and microglia has been found in the postmortem brain and cerebrospinal fluid samples in ASD patients[61]. In addition, elevated macrophage chemoattractant protein-1 and tumor growth factor-β1 derived from neuroglia are the most prominent cytokines in the brain samples of ASD patients; marked expression of a prominent inflammatory cytokine profile, macrophage chemoattractant protein-1, IL-6, IL-8, and IFN-γ is shown in the cerebrospinal fluid of ASD patients[61]. Another study further demonstrates that pro-inflammatory cytokines including TNF-α, IL-6, IL-8, granulocyte macrophage-colony stimulating factor, and IFN-γ (Th1 cytokines) are significantly increased in the brains of ASD patients[110]. However, there is no increase in IL-4 or IL-5 (Th2 cytokines), thus Th1/Th2 ratio is significantly raised in ASD patients, suggesting that the Th1 pathway is activated in ASD[110].

A number of studies have shown that IL-1β, IL-12, TNF-α, and IFN-γ are increased in the peripheral blood of autistic patients[111]. Two recent large case-control studies comparing ASD and typically developing children have further confirmed increased levels of plasma cytokines including the Th1-like IL-12p40 and pro-inflammatory cytokines IL-1β, IL-6, IL-8, and granulocyte macrophage-colony stimulating factor[112], and chemokines, including MCP-1, regulated on activation normal T cell expressed and secreted, and eotaxin[113]. These elevated levels of cytokines and chemokines are associated with behavioral and cognitive impairments[112,113].

POTENTIAL FOR MSCS IN THE TREATMENT OF ASD

MSCs

MSCs are a population of progenitor cells of mesodermal origin found principally in the bone marrow, which possess the capacity of self-renewal and also exhibit multilineage differentiation[114,115]. In addition to bone marrow, MSC populations can also be obtained readily from adipose tissue[116], placenta[117], skin[118], umbilical cord blood[119], umbilical cord perivascular cells[120], umbilical cord Wharton's jelly[121], amniotic fluid[122], synovial membrane[123], breast milk[124], alveolar epithelium[125], myocardium[126], menstrual blood[127], and endometrium[128] (Table 1). MSCs are relatively easy to isolate and expand in culture and capable of self-renewal and differentiation, making them a promising treatment option for a variety of clinical conditions. Although the multipotency of MSCs is demonstrated *in vitro*[129], this is still not definite *in vivo*. Until now, it is also still unclear whether MSCs isolated from different tissue sources have similar therapeutic potentials[130]. Furthermore, it is uncertain whether systematic delivery (*i.e.*, intravenous) of MSCs is sufficient to reach the brain as compared to direct implantation of MSCs[131,132]. Though intranasal application of cells provides an alternative, non-invasive method to deliver MSCs directly into the CNS[133]. At present, neither intravenous nor direct injection of MSCs have been able to yield consistent clinical results because infused cells exhibit limited survival and transient functionality in host tissues[134-136].

As well as the ability to self-renew and differentiate, MSCs can also secrete immunomodulatory, anti-apoptotic, anti-inflammatory, pro-angiogenic, pro-mitogenic, and antibacterial molecules that contribute to immunomodulatory and trophic effects[137]. Thus recent recognition of the immunomodulatory functions of MSCs may result in the exploration and development of new therapies for ASD.

Effects of MSCs on the nervous system in health and ASD

Although the mechanism of action of MSCs on the nervous system remains largely unknown, recent research suggests that neuroprotection, neurogenesis, and synaptogenesis may be involved[138]. Genetic findings linking ASD to synapse-associated genes, such as SH3 and multiple ankyrin repeat domains 3 (SHANK3) and mutations of other synaptic cell adhesion molecules, suggest that ASD may result, at

Table 1 Tissue sources of mesenchymal stem cells

Tissue sources	MSCs	Ref.
Bone marrow	BM-MSCs	[115]
Adipose	Ad-MSCs	[116]
Placenta	Pl-MSCs	[117]
Skin	S-MSCs	[118]
Umbilical cord blood	UCB-MSCs	[119]
Umbilical cord perivascular cells	UCPVC-MSCs	[120]
Umbilical cord Wharton's jelly	WJ-MSCs	[121]
Amniotic fluid	AF-MSCs	[122]
Synovial membrane	SM-MSCs	[123]
Breast milk	M-MSCs	[124]
Alveolar epithelium (lung)	AE-MSCs	[125]
Myocardium (heart)	Myo-MSCs	[126]
Menstrual blood	Men-MSCs	[127]
Endometrium	En-MSCs	[128]

MSCs: Mesenchymal stem cells; BM-MSCs: Bone marrow MSCs; Ad-MSCs: Adipose MSCs; UCB-MSCs: Umbilical cord blood MSCs.

least partially, from disruption of synapse function and plasticity[139]. MSCs act through several possible mechanisms to regulate synaptic function and plasticity, that is, secreting survival-promoting growth factors (*e.g.*, brain-derived neurotrophic factor; nerve growth factor), sustaining synaptic plasticity, restoring synaptic transmitter release by providing local re-innervations, integrating into existing synaptic networks, and re-establishing functional afferent and efferent connections[138,140,141].

Effects of MSCs on the immune system and autoimmune diseases in health and ASD

There is a considerable body of literature documenting the effects of MSCs on the immune system. MSCs act on both the adaptive and innate immune system by suppressing pro-inflammatory activities, inhibiting dendritic cell maturation, polarizing macrophages towards anti-inflammatory M2-like state, promoting the generation of regulatory T cells *via* IL-10, suppressing proliferation and cytotoxicity of NK cells, and reducing B cell activation and proliferation. These functions of MSCs on the immune system have been covered extensively in several reviews[142-146]. As discussed above in this review, ASD patients show an imbalance between Th1 and Th2, as well as NK cells, overproduction of pro-inflammation, and reduction of anti-inflammation. MSCs immunoregulatory effects have the potential to restore this immune imbalance, inhibit TNF-α, IL-1β and IFN-γ production, and increase IL-10 and IL-4 levels[147].

In addition, MSCs are capable of crossing the blood-brain-barrier and migrating to sites of tissue injury and inflammation[148,149]. MSCs act through Toll-like receptor (TLR) signaling to initiate the clearance of pathogens and promote the repair of injured tissue. These TLRs respond to so-called "danger signals" from microbial invasion, such as double-stranded RNA (dsRNA), LPS, and heat shock proteins, triggering intracellular signaling pathways. This results in the induction of inflammatory cytokines, type I IFNs, and upregulation of co-stimulatory molecules leading to the activation of the adaptive immune response[150]. As mentioned above, prenatal exposure to poly(I:C), a synthetic analog of dsRNA, elicits a plethora of intracellular signaling pathways through binding to TLR3 in a MIA model of ASD[151], whilst LPS elicits distinct molecular profiles through binding to TLR4[152]. In TLR3- and TLR4-mediated signaling pathways, toll–IL-1 receptor domain-containing adaptor inducing IFN-β (TRIF) leads to activation of the transcription factors interferon regulatory factor 3 (IRF3), which are responsible for induction of IFN-β[153] (Figure 2A). TRIF-dependent signaling pathway, both downstream of TLR-3 and TLR-4, also leads to activation of MAPKs and production of cytokines, such as IL-6 and TNF-α[153,154]. Interestingly, TLRs may polarize MSCs toward pro-inflammatory (MSC1) or anti-inflammatory (MSC2) phenotypes. For example, TLR4 (LPS) priming results in production of pro-inflammatory cytokines such as IL-6 or IL-8 (MSC1), while TLR3 (dsRNA, ployI:C) priming induces secretion of anti-inflammatory

molecules such as IL-10, IL-4, indoleamine 2,3-dioxygenase, or prostaglandin (MSC2)[155,156] (Figure 2B). These polarizing effects of TLR priming depend on the ligand concentration, timing, and kinetics of activation. This may also explain the contradictory results obtained so far regarding the effects of TLRs on immunomodulation by MSCs[155,156]. However, in contradiction to the reported LPS polarizing process (MSC1 phenotype) observed *in vitro*, several studies have reported beneficial effects of MSC treatment in animal models of LPS-induced tissue injury[157-159]. Therefore, the *in vivo* modulation of MSCs by TLR ligands deserves further investigation and clarification. In particular, the MIA model of prenatal exposure to poly(I:C) represents a good animal model in which to explore the underlying mechanism of MSC treatment in ASD.

Numerous autoimmune conditions have been associated with ASD, including autoimmune thyroiditis, rheumatoid arthritis, ulcerative colitis, celiac disease, and type 1 diabetes[160] (Table 2). The potential use of MSC therapy has been investigated in many of these conditions. Preclinical experiments and clinical trials have demonstrated the safety and efficacy of MSC therapy in rheumatoid arthritis animal models and patients[161]. In addition, MSC therapy has been reported to increase regulatory T cells, restore Th1/Th2 balance in blood and induce apoptosis of infiltrated leukocytes in pancreatic islet cells in mice with type 1 diabetes[162]. However, in order to translate this finding from bench to bedside, further in-depth mechanistic studies of the therapeutic effects of MSCs on type 1 diabetes are warranted. Recent pre-clinical research has shown the restorative effect of MSCs in mice with autoimmune thyroiditis through the MAPK signaling pathway[163]. Furthermore, graft-versus-host-disease and multiple sclerosis have been targeted for MSC treatment in both animal experiments and clinical trials[164-167] (Table 2). However, the use of MSCs in the treatment of graft-versus-host-disease has failed to give consistent results in animal experiments[167].

Pre-clinical and clinical evidence for MSC therapy in ASD

To date, only a few pre-clinical studies have demonstrated the therapeutic potential of MSC treatment in animal models of ASD. Ha *et al*[168] reported that adipose MSCs are transplanted intraventricularly into the brains of neonatal fetal pups at a very early stage. This early intervention reduces repetitive behavior and anxiety, and improves social deficits in mice prenatally exposed to VPA through the rescue of decreased IL-10 and vascular endothelial growth factor levels together with upregulation of reduced PTEN proteins in the brain. In addition, it has been demonstrated that by promoting the maturation of newly formed neurons in the granular cell layer of the dentate gyrus, MSC transplantation restores post-developmental hippocampal neurogenesis in VPA-exposed mice[169]. This is associated with improvements in cognitive and social behavior 2 wk after transplantation of the MSCs and thus may be related to the modulation of hippocampal neurogenesis[169].

A widely accepted mouse model of ASD is the BTBR T+, tf/J (Black and Tan Brachyury, BTBR) inbred mouse strain, which display autistic-like behavior and neuroanatomical abnormalities, including absence of corpus callosum and reduced hippocampal commissure, analogous to the core endophenotype of autism[170-172]. It has been shown that intracerebroventricular transplant of human MSCs into BTBR mice results in a reduction of stereotypical behaviors and cognitive rigidity and an improvement in social behavior[173]. Furthermore, elevated brain-derived neurotrophic factor levels and hippocampal neurogenesis were detected in the MSCs-transplanted BTBR mice[173]. This finding then promoted an investigation of the behavioral effects of transplanted MSCs, which were induced to secrete a higher amount of neurotrophic factors (NurOwn®) in BTBR mice[174]. This study demonstrated NurOwn®[175] are superior to MSCs without induced neurotrophic factors in several aspects. In particular, NurOwn® contains 2 and 5 fold levels of brain-derived neurotrophic factor and glial cell-derived neurotrophic factor, respectively, compared to MSCs from the same donor[176]. Moreover, NurOwn® transplantation increases male-female social interaction, decreases repetitive behavior (changes which can be sustained for 6 mo after treatment), and improves cognitive flexibility in BTBR mice[174]. Exosomes derived from MSCs serve as the main mediators of the therapeutic effect of MSC, with an involvement in repairing damaged tissues, suppressing inflammatory responses, and modulating the immune system[177,178]. Their potential as a surrogate of therapeutic MSCs has been widely explored. Recently, it has been shown that BTBR mice treated with exosomes derived from MSCs via intranasal administration present with significant behavioral improvements in social interaction and ultrasonic communication and reduced repetitive behavior. Interestingly, BTBR mothers that were treated with exosomes derived from MSCs showed improvements in maternal behaviors such as pup retrieval behavior[179].

Although there have been few pre-clinical studies of MSC therapy for ASD, several

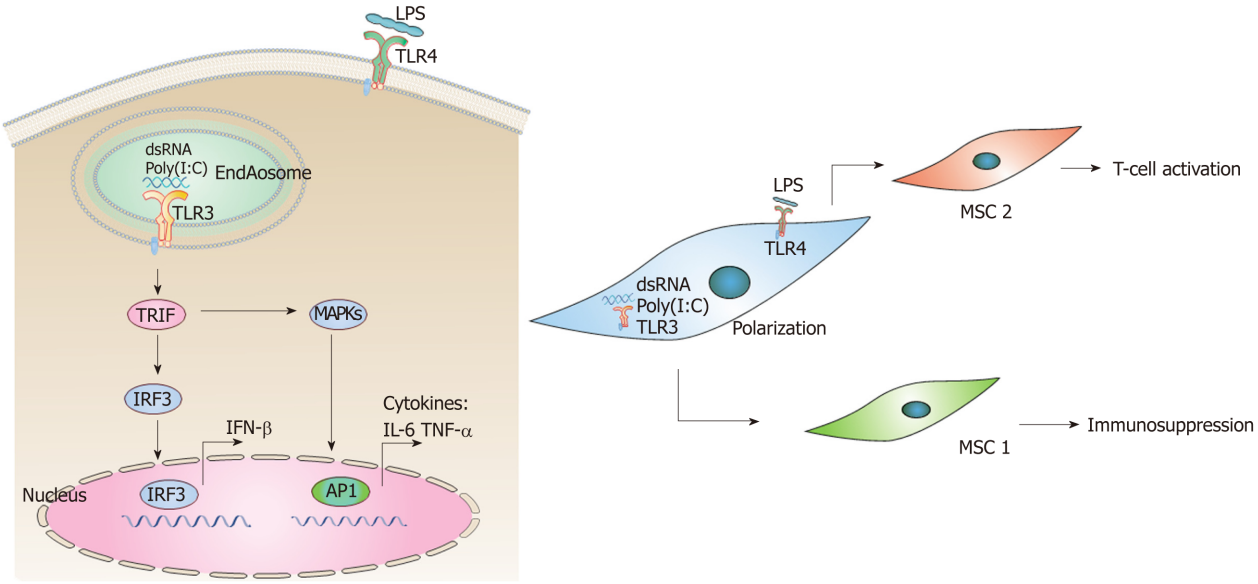

Figure 2 Poly(I:C)-toll-like receptor 3 signaling pathway and polarization of mesenchymal stem cells. A: Poly(I:C)-induced toll-like receptor 3(TLR3) signaling pathway. TLR3 recognizes dsRNA analog poly(I:C) in the endosomes and initiates signaling by TRIF, leading to activation of IRF3 and induction of IFN-β. TRIF-dependent signaling pathway also induces activation of MAPKs and AP-1, and culminates in the production of inflammatory cytokines, such as IL-6 and TNF-α; B: Polarization of MSCs into MSC1 (M1 type with a proinflammatory response) and MSC2 cells (M2 type with an anti-inflammatory response) as a result of activation of TLR3 and TLR4 respectively. Poly(I:C): polyinosinic–polycytidylic acid; dsRNA: Double-stranded RNA; TLR3: Toll-like receptor 3; TLR4: Toll-like receptor 4; TRIF: Toll–IL-1 receptor domain-containing adaptor inducing IFN-β; IRF3: Interferon regulatory factor 3; MAPKs: Mitogen-activated protein kinases; AP1: Activator protein 1; IFN-β: Interferon β; IL-6: Interleukin 6; TNF-α: Tumor necrosis factor α; LPS: Lipopolysaccharide.

clinical trials on human have been conducted. Lv *et al*[180] performed a non-randomized, open-label, controlled, proof-of-concept clinical trial to exam the treatment, safety and efficacy of umbilical cord blood MSCs and/or cord blood mononuclear cells in children with autism. At 24 wk post-treatment, significant reductions in symptom severity are observed with the greatest improvement in the combined group (umbilical cord blood-MSCs + cord blood mononuclear cells), suggesting a synergic effect of dual therapy[180]. There is no significant safety issue related to the treatment and no observed severe adverse effects.

Meanwhile, Sharma *et al*[181] conducted another open-label proof of concept study and reported on the use of intrathecal transplantation of autologous bone marrow mononuclear cells that contain MSCs in 32 patients with ASD. This study included children as well as adults with ASD (age 3-33). Most of the patients showed improved scores in various behavioral scales after a 26 mo follow up, including improvements in social relationships and reciprocity, emotional responsiveness, speech, language, communication, behavior patterns, sensory aspects, and cognition. Only a few adverse events (including seizures and hyperactivity) were observed, and these were controlled with medications[181]. It has been reported that cerebral hypoperfusion or insufficient blood flow in the brain occurs in many brain regions in ASD[182], and interestingly, their study suggested that the cell transplantation may have had a balancing effect on the brain metabolism[181]. Comparative Positron Emission Tomography-Computed Tomography scans before and 6 mo after cell transplantation showed increased ^{18}F-fluorodeoxyglucose uptake in the areas of frontal lobe, cerebellum, amygdala, hippocampus, parahippocampus, and mesial temporal lobe[181].

Another small pilot open label study recently investigated the clinical benefits of bone marrow aspirate concentrate stem cell with intrathecal transplantation in 10 ASD children (4-12 years of age)[183]. The maximal effect of cell therapy was observed within the first 12 mo following the treatment. Interestingly they also found that improvement decreased as the age of ASD child increased[183]. However, there was no control group and the number of subjects in this study was quite small. Dawson *et al*[184] conducted an open-label phase I clinical trial of a single intravenous infusion of autologous UCB (AUCB) on 25 ASD children aged between 2 and 5 years. They found that most of the significant improvements in behavior occurred during the first 6 mo and were sustained between 6 and 12 mo post-infusion. Thus whilst a single therapy did not improve all autistic symptoms, this work has demonstrated that it is safe and feasible to perform AUCB infusions for the effective treatment of ASD in young children[184]. Dawson's research team[185] performed a secondary follow up study and reported changes in electroencephalography spectral power by 12-mo post-treatment

Table 2 Autoimmune diseases, autism spectrum disorders, and mesenchymal stem cells

Autoimmune diseases	ASD	MSCs
Autoimmune thyroiditis	+	Pre-clinical experiment
Rheumatoid arthritis	+	Pre-clinical experiment; Clinical trials on-going
GVHD	-	Pre-clinical experiment; Clinical trials
MS	-	Pre-clinical experiment; Clinical trials on-going
Type 1 diabetes	+	Pre-clinical experiment; Clinical trials on-going

ASD: Autism spectrum disorders; MSCs: Mesenchymal stem cells; GVHD: graft-versus-host-disease; MS: Multiple sclerosis; +: An association between ASD and a family history of autoimmune diseases; -: No or lack of evidence of correlation between autoimmune diseases and ASD.

of AUCB on ASD children. Baseline posterior electroencephalography beta power was positively associated with an improvement in social communication symptoms in ASD children, suggesting the electroencephalography may be a useful biomarker to predict the outcome of clinical trials for ASD.

Recently, the first randomized, double-blinded, placebo-controlled clinical trial provided further evidence that AUCB was safe, but there was minimal clinical efficacy compared to the findings of the previous open-label trial[186]. Twenty-nine ASD children 2-6 years of age were infused with either AUCB or placebo, and evaluated at baseline, 12 wk, and 24 wk[186]. This study suggested that infusion of AUCB has no serious adverse events for the treatment of ASD and potentially had an impact on socialization for children with ASD.

While the clinical trials discussed above have generally reported a good safety profile for MSC transplantation in ASD children, the follow-up checks are currently only up to 12 mo after treatment. Thus caution should still prevail as no data of long-term effects such as 5 to 20 years posttreatment are currently available.

CONCLUSION

Despite the increasing incidence of ASD, autism currently remains untreatable. The available options of behavioral, pharmacological, and nutritional therapies are only supportive treatments[84,187,188]. The underlying pathology of ASD involves immune system dysregulation, autoimmunity, and inflammation[189], and these processes are targetable with MSC therapy. MSCs can be transplanted directly without genetic modification or pretreatment, differentiated according to the cues from the surrounding tissues, and do not cause uncontrollable growth or tumors[190]. Several proof-of-concept clinical studies mentioned above and meta-analyses have shown the safety and/or efficacy of MSCs treatment in autistic patients or other clinical conditions of immune dysregulation[180,181,184,190]. Although MSCs have the potential for clinical use in ASD, a number of methodological, technical, and safety challenges still need to be considered[191]. Additionally, their response to other pharmacological interventions, tissue distribution upon administration, and their long-term safety profile are key areas in need of further investigation. Currently, it is unclear how long a single dose of MSC can sustain anti-inflammatory effects or when would be the ideal age for intervention (the early the better?). Furthermore, the most recent randomized, double-blinded, placebo-controlled clinical trial, which had a much more rigorous design than other clinical trials mentioned in this review reported lack of efficacy of AUCB for the treatment of ASD. Given that the long-term safety and efficacy of MSC treatment cannot be fully ascertained, standardized trial design needs to be considered when designing future clinical trials.

More importantly, our understanding of basic MSC biology and underlying etiology of ASD is still limited. Further basic research into endogenous functions of MSC is warranted to elucidate the mechanism by which therapeutic MSCs for the treatment of ASD mediate their action. Animal models such as the MIA and BTBR mouse models may be vital for this as they allow the simultaneous measurement of peripheral and central immune function, quantitative neuronal modification, and behavioral changes in response to MSC treatment, thus enabling a better understanding of the therapeutic mechanisms of MSCs in ASD.

REFERENCES

1 **Baio J**, Wiggins L, Christensen DL, Maenner MJ, Daniels J, Warren Z, Kurzius-Spencer M, Zahorodny W, Robinson Rosenberg C, White T, Durkin MS, Imm P, Nikolaou L, Yeargin-Allsopp M, Lee LC, Harrington R, Lopez M, Fitzgerald RT, Hewitt A, Pettygrove S, Constantino JN, Vehorn A, Shenouda J, Hall-Lande J, Van Naarden Braun K, Dowling NF. Prevalence of Autism Spectrum Disorder Among Children Aged 8 Years - Autism and Developmental Disabilities Monitoring Network, 11 Sites, United States, 2014. *MMWR Surveill Summ* 2018; **67**: 1-23 [PMID: 29701730 DOI: 10.15585/mmwr.ss6706a1]

2 **Croen LA**, Grether JK, Hoogstrate J, Selvin S. The changing prevalence of autism in California. *J Autism Dev Disord* 2002; **32**: 207-215 [PMID: 12108622 DOI: 10.1023/A:1015453830880]

3 **Bailey A**, Le Couteur A, Gottesman I, Bolton P, Simonoff E, Yuzda E, Rutter M. Autism as a strongly genetic disorder: evidence from a British twin study. *Psychol Med* 1995; **25**: 63-77 [PMID: 7792363 DOI: 10.1017/S0033291700028099]

4 **Rosenberg RE**, Law JK, Yenokyan G, McGready J, Kaufmann WE, Law PA. Characteristics and concordance of autism spectrum disorders among 277 twin pairs. *Arch Pediatr Adolesc Med* 2009; **163**: 907-914 [PMID: 19805709 DOI: 10.1001/archpediatrics.2009.98]

5 **Steffenburg S**, Gillberg C, Hellgren L, Andersson L, Gillberg IC, Jakobsson G, Bohman M. A twin study of autism in Denmark, Finland, Iceland, Norway and Sweden. *J Child Psychol Psychiatry* 1989; **30**: 405-416 [PMID: 2745591 DOI: 10.1111/j.1469-7610.1989.tb00254.x]

6 **Hallmayer J**, Cleveland S, Torres A, Phillips J, Cohen B, Torigoe T, Miller J, Fedele A, Collins J, Smith K, Lotspeich L, Croen LA, Ozonoff S, Lajonchere C, Grether JK, Risch N. Genetic heritability and shared environmental factors among twin pairs with autism. *Arch Gen Psychiatry* 2011; **68**: 1095-1102 [PMID: 21727249 DOI: 10.1001/archgenpsychiatry.2011.76]

7 **Abrahams BS**, Geschwind DH. Advances in autism genetics: on the threshold of a new neurobiology. *Nat Rev Genet* 2008; **9**: 341-355 [PMID: 18414403 DOI: 10.1038/nrg2346]

8 **Skaar DA**, Shao Y, Haines JL, Stenger JE, Jaworski J, Martin ER, DeLong GR, Moore JH, McCauley JL, Sutcliffe JS, Ashley-Koch AE, Cuccaro ML, Folstein SE, Gilbert JR, Pericak-Vance MA. Analysis of the RELN gene as a genetic risk factor for autism. *Mol Psychiatry* 2005; **10**: 563-571 [PMID: 15558079 DOI: 10.1038/sj.mp.4001614]

9 **Moessner R**, Marshall CR, Sutcliffe JS, Skaug J, Pinto D, Vincent J, Zwaigenbaum L, Fernandez B, Roberts W, Szatmari P, Scherer SW. Contribution of SHANK3 mutations to autism spectrum disorder. *Am J Hum Genet* 2007; **81**: 1289-1297 [PMID: 17999366 DOI: 10.1086/522590]

10 **Jamain S**, Quach H, Betancur C, Råstam M, Colineaux C, Gillberg IC, Soderstrom H, Giros B, Leboyer M, Gillberg C, Bourgeron T; Paris Autism Research International Sibpair Study. Mutations of the X-linked genes encoding neuroligins NLGN3 and NLGN4 are associated with autism. *Nat Genet* 2003; **34**: 27-29 [PMID: 12669065 DOI: 10.1038/ng1136]

11 **Campbell DB**, Sutcliffe JS, Ebert PJ, Militerni R, Bravaccio C, Trillo S, Elia M, Schneider C, Melmed R, Sacco R, Persico AM, Levitt P. A genetic variant that disrupts MET transcription is associated with autism. *Proc Natl Acad Sci USA* 2006; **103**: 16834-16839 [PMID: 17053076 DOI: 10.1073/pnas.0605296103]

12 **Buxbaum JD**, Silverman JM, Smith CJ, Greenberg DA, Kilifarski M, Reichert J, Cook EH, Fang Y, Song CY, Vitale R. Association between a GABRB3 polymorphism and autism. *Mol Psychiatry* 2002; **7**: 311-316 [PMID: 11920158 DOI: 10.1038/sj.mp.4001011]

13 **Wu S**, Jia M, Ruan Y, Liu J, Guo Y, Shuang M, Gong X, Zhang Y, Yang X, Zhang D. Positive association of the oxytocin receptor gene (OXTR) with autism in the Chinese Han population. *Biol Psychiatry* 2005; **58**: 74-77 [PMID: 15992526 DOI: 10.1016/j.biopsych.2005.03.013]

14 **Brune CW**, Kim SJ, Salt J, Leventhal BL, Lord C, Cook EH. 5-HTTLPR Genotype-Specific Phenotype in Children and Adolescents With Autism. *Am J Psychiatry* 2006; **163**: 2148-2156 [PMID: 17151167 DOI: 10.1176/ajp.2006.163.12.2148]

15 **Frazier TW**, Embacher R, Tilot AK, Koenig K, Mester J, Eng C. Molecular and phenotypic abnormalities in individuals with germline heterozygous PTEN mutations and autism. *Mol Psychiatry* 2015; **20**: 1132-1138 [PMID: 25288137 DOI: 10.1038/mp.2014.125]

16 **Lam CW**, Yeung WL, Ko CH, Poon PM, Tong SF, Chan KY, Lo IF, Chan LY, Hui J, Wong V, Pang CP, Lo YM, Fok TF. Spectrum of mutations in the MECP2 gene in patients with infantile autism and Rett syndrome. *J Med Genet* 2000; **37**: E41 [PMID: 11106359 DOI: 10.1136/jmg.37.12.e41]

17 **Belmonte MK**, Bourgeron T. Fragile X syndrome and autism at the intersection of genetic and neural networks. *Nat Neurosci* 2006; **9**: 1221-1225 [PMID: 17001341 DOI: 10.1038/nn1765]

18 **Wiznitzer M**. Autism and tuberous sclerosis. *J Child Neurol* 2004; **19**: 675-679 [PMID: 15563013 DOI: 10.1177/08830738040190090701]

19 **Fukao T**, Tanabe M, Terauchi Y, Ota T, Matsuda S, Asano T, Kadowaki T, Takeuchi T, Koyasu S. PI3K-mediated negative feedback regulation of IL-12 production in DCs. *Nat Immunol* 2002; **3**: 875-881 [PMID: 12154357 DOI: 10.1038/ni825]

20 **Needleman LA**, McAllister AK. The major histocompatibility complex and autism spectrum disorder. *Dev Neurobiol* 2012; **72**: 1288-1301 [PMID: 22760919 DOI: 10.1002/dneu.22046]

21 **Abrahams BS**, Geschwind DH. Connecting genes to brain in the autism spectrum disorders. *Arch Neurol* 2010; **67**: 395-399 [PMID: 20385903 DOI: 10.1001/archneurol.2010.47]

22 **Basil P**, Li Q, Dempster EL, Mill J, Sham PC, Wong CC, McAlonan GM. Prenatal maternal immune activation causes epigenetic differences in adolescent mouse brain. *Transl Psychiatry* 2014; **4**: e434 [PMID: 25180573 DOI: 10.1038/tp.2014.80]

23 **Wong CC**, Meaburn EL, Ronald A, Price TS, Jeffries AR, Schalkwyk LC, Plomin R, Mill J. Methylomic analysis of monozygotic twins discordant for autism spectrum disorder and related behavioural traits. *Mol Psychiatry* 2014; **19**: 495-503 [PMID: 23608919 DOI: 10.1038/mp.2013.41]

24 **Li Q**, Cheung C, Wei R, Cheung V, Hui ES, You Y, Wong P, Chua SE, McAlonan GM, Wu EX. Voxel-based analysis of postnatal white matter microstructure in mice exposed to immune challenge in early or late pregnancy. *Neuroimage* 2010; **52**: 1-8 [PMID: 20399275 DOI: 10.1016/j.neuroimage.2010.04.015]

25 **Li Q**, Cheung C, Wei R, Hui ES, Feldon J, Meyer U, Chung S, Chua SE, Sham PC, Wu EX, McAlonan GM. Prenatal immune challenge is an environmental risk factor for brain and behavior change relevant to schizophrenia: evidence from MRI in a mouse model. *PLoS One* 2009; **4**: e6354 [PMID: 19629183 DOI: 10.1371/journal.pone.0006354]

26 **Meyer U**. Prenatal poly(i:C) exposure and other developmental immune activation models in rodent systems. *Biol Psychiatry* 2014; **75**: 307-315 [PMID: 23938317 DOI: 10.1016/j.biopsych.2013.07.011]

27 **Brown AS**. Epidemiologic studies of exposure to prenatal infection and risk of schizophrenia and autism. *Dev Neurobiol* 2012; **72**: 1272-1276 [PMID: 22488761 DOI: 10.1002/dneu.22024]

28 **Wei R**, Li Q, Lam S, Leung J, Cheung C, Zhang X, Sham PC, Chua SE, McAlonan GM. A single low dose of valproic acid in late prenatal life alters postnatal behavior and glutamic acid decarboxylase levels in the mouse. *Behav Brain Res* 2016; **314**: 190-198 [PMID: 27498245 DOI: 10.1016/j.bbr.2016.08.006]

29 **Christensen J**, Grønborg TK, Sørensen MJ, Schendel D, Parner ET, Pedersen LH, Vestergaard M. Prenatal valproate exposure and risk of autism spectrum disorders and childhood autism. *JAMA* 2013; **309**: 1696-1703 [PMID: 23613074 DOI: 10.1001/jama.2013.2270]

30 **Croen LA**, Grether JK, Yoshida CK, Odouli R, Hendrick V. Antidepressant use during pregnancy and childhood autism spectrum disorders. *Arch Gen Psychiatry* 2011; **68**: 1104-1112 [PMID: 21727247 DOI: 10.1001/archgenpsychiatry.2011.73]

31 **Olivier JD**, Vallès A, van Heesch F, Afrasiab-Middelman A, Roelofs JJ, Jonkers M, Peeters EJ, Korte-Bouws GA, Dederen JP, Kiliaan AJ, Martens GJ, Schubert D, Homberg JR. Fluoxetine administration to pregnant rats increases anxiety-related behavior in the offspring. *Psychopharmacology (Berl)* 2011; **217**: 419-432 [PMID: 21487650 DOI: 10.1007/s00213-011-2299-z]

32 **Simpson KL**, Weaver KJ, de Villers-Sidani E, Lu JY, Cai Z, Pang Y, Rodriguez-Porcel F, Paul IA, Merzenich M, Lin RC. Perinatal antidepressant exposure alters cortical network function in rodents. *Proc Natl Acad Sci USA* 2011; **108**: 18465-18470 [PMID: 22025710 DOI: 10.1073/pnas.1109353108]

33 **Ronald A**, Pennell CE, Whitehouse AJ. Prenatal Maternal Stress Associated with ADHD and Autistic Traits in early Childhood. *Front Psychol* 2011; **1**: 223 [PMID: 21833278 DOI: 10.3389/fpsyg.2010.00223]

34 **Fine R**, Zhang J, Stevens HE. Prenatal stress and inhibitory neuron systems: implications for neuropsychiatric disorders. *Mol Psychiatry* 2014; **19**: 641-651 [PMID: 24751963 DOI: 10.1038/mp.2014.35]

35 **Grabrucker AM**. Environmental factors in autism. *Front Psychiatry* 2013; **3**: 118 [PMID: 23346059 DOI: 10.3389/fpsyt.2012.00118]

36 **Landrigan PJ**. What causes autism? Exploring the environmental contribution. *Curr Opin Pediatr* 2010; **22**: 219-225 [PMID: 20087185 DOI: 10.1097/MOP.0b013e328336eb9a]

37 **Keating A**. Mesenchymal stromal cells: new directions. *Cell Stem Cell* 2012; **10**: 709-716 [PMID: 22704511 DOI: 10.1016/j.stem.2012.05.015]

38 **Machold RP**, Ploegh HL. Intermediates in the assembly and degradation of class I major histocompatibility complex (MHC) molecules probed with free heavy chain-specific monoclonal antibodies. *J Exp Med* 1996; **184**: 2251-2259 [PMID: 8976180 DOI: 10.1084/jem.184.6.2251]

39 **Krzewski K**, Strominger JL. The killer's kiss: the many functions of NK cell immunological synapses. *Curr Opin Cell Biol* 2008; **20**: 597-605 [PMID: 18639449 DOI: 10.1016/j.ceb.2008.05.006]

40 **Long EO**. Negative signaling by inhibitory receptors: the NK cell paradigm. *Immunol Rev* 2008; **224**: 70-84 [PMID: 18759921 DOI: 10.1111/j.1600-065X.2008.00660.x]

41 **Garay PA**, McAllister AK. Novel roles for immune molecules in neural development: implications for neurodevelopmental disorders. *Front Synaptic Neurosci* 2010; **2**: 136 [PMID: 21423522 DOI: 10.3389/fnsyn.2010.00136]

42 **Needleman LA**, Liu XB, El-Sabeawy F, Jones EG, McAllister AK. MHC class I molecules are present both pre- and postsynaptically in the visual cortex during postnatal development and in adulthood. *Proc Natl Acad Sci USA* 2010; **107**: 16999-17004 [PMID: 20837535 DOI: 10.1073/pnas.1006087107]

43 **Glynn MW**, Elmer BM, Garay PA, Liu XB, Needleman LA, El-Sabeawy F, McAllister AK. MHCI negatively regulates synapse density during the establishment of cortical connections. *Nat Neurosci* 2011; **14**: 442-451 [PMID: 21358642 DOI: 10.1038/nn.2764]

44 **Yizhar O**, Fenno LE, Prigge M, Schneider F, Davidson TJ, O'Shea DJ, Sohal VS, Goshen I, Finkelstein J, Paz JT, Stehfest K, Fudim R, Ramakrishnan C, Huguenard JR, Hegemann P, Deisseroth K. Neocortical excitation/inhibition balance in information processing and social dysfunction. *Nature* 2011; **477**: 171-178 [PMID: 21796121 DOI: 10.1038/nature10360]

45 **Rubenstein JL**, Merzenich MM. Model of autism: increased ratio of excitation/inhibition in key neural systems. *Genes Brain Behav* 2003; **2**: 255-267 [PMID: 14606691 DOI: 10.1034/j.1601-183X.2003.00037.x]

46 **Chao HT**, Chen H, Samaco RC, Xue M, Chahrour M, Yoo J, Neul JL, Gong S, Lu HC, Heintz N, Ekker M, Rubenstein JL, Noebels JL, Rosenmund C, Zoghbi HY. Dysfunction in GABA signalling mediates autism-like stereotypies and Rett syndrome phenotypes. *Nature* 2010; **468**: 263-269 [PMID: 21068835 DOI: 10.1038/nature09582]

47 **Ruff JS**, Nelson AC, Kubinak JL, Potts WK. MHC signaling during social communication. *Adv Exp Med Biol* 2012; **738**: 290-313 [PMID: 22399386 DOI: 10.1007/978-1-4614-1680-7_17]

48 **St Pourcain B**, Whitehouse AJ, Ang WQ, Warrington NM, Glessner JT, Wang K, Timpson NJ, Evans DM, Kemp JP, Ring SM, McArdle WL, Golding J, Hakonarson H, Pennell CE, Smith GD. Common variation contributes to the genetic architecture of social communication traits. *Mol Autism* 2013; **4**: 34 [PMID: 24047820 DOI: 10.1186/2040-2392-4-34]

49 **Torres AR**, Sweeten TL, Cutler A, Bedke BJ, Fillmore M, Stubbs EG, Odell D. The association and linkage of the HLA-A2 class I allele with autism. *Hum Immunol* 2006; **67**: 346-351 [PMID: 16720216 DOI: 10.1016/j.humimm.2006.01.001]

50 **Kambayashi T**, Laufer TM. Atypical MHC class II-expressing antigen-presenting cells: can anything replace a dendritic cell? *Nat Rev Immunol* 2014; **14**: 719-730 [PMID: 25324123 DOI: 10.1038/nri3754]

51 **Unanue ER**, Turk V, Neefjes J. Variations in MHC Class II Antigen Processing and Presentation in Health and Disease. *Annu Rev Immunol* 2016; **34**: 265-297 [PMID: 26907214 DOI: 10.1146/annurev-immunol-041015-055420]

52 **Wu S**, Ding Y, Wu F, Li R, Xie G, Hou J, Mao P. Family history of autoimmune diseases is associated with an increased risk of autism in children: A systematic review and meta-analysis. *Neurosci Biobehav Rev* 2015; **55**: 322-332 [PMID: 25981892 DOI: 10.1016/j.neubiorev.2015.05.004]

53 **Wierzba-Bobrowicz T**, Kosno-Kruszewska E, Lewandowska E, Lechowicz W, Schmidt-Sidor B. Major histocompatibility complex class II (MHC II) expression during development of human fetal brain and haemopoietic organs. *Adv Exp Med Biol* 2001; **495**: 93-101 [PMID: 11774614 DOI: 10.1007/978-1-4615-0685-0_13]

54 **Lee SC**, Collins M, Vanguri P, Shin ML. Glutamate differentially inhibits the expression of class II MHC antigens on astrocytes and microglia. *J Immunol* 1992; **148**: 3391-3397 [PMID: 1350289]

55 **Perlmutter LS**, Scott SA, Barrón E, Chui HC. MHC class II-positive microglia in human brain: association with Alzheimer lesions. *J Neurosci Res* 1992; **33**: 549-558 [PMID: 1484388 DOI: 10.1002/jnr.490330407]

56 **Hellendall RP**, Ting JP. Differential regulation of cytokine-induced major histocompatibility complex

class II expression and nitric oxide release in rat microglia and astrocytes by effectors of tyrosine kinase, protein kinase C, and cAMP. *J Neuroimmunol* 1997; **74**: 19-29 [PMID: 9119973 DOI: 10.1016/S0165-5728(96)00202-0]

57 **Ajmone-Cat MA**, De Simone R, Nicolini A, Minghetti L. Effects of phosphatidylserine on p38 mitogen activated protein kinase, cyclic AMP responding element binding protein and nuclear factor-kappaB activation in resting and activated microglial cells. *J Neurochem* 2003; **84**: 413-416 [PMID: 12559004 DOI: 10.1046/j.1471-4159.2003.01562.x]

58 **Singer HS**, Morris C, Gause C, Pollard M, Zimmerman AW, Pletnikov M. Prenatal exposure to antibodies from mothers of children with autism produces neurobehavioral alterations: A pregnant dam mouse model. *J Neuroimmunol* 2009; **211**: 39-48 [PMID: 19362378 DOI: 10.1016/j.jneuroim.2009.03.011]

59 **Meyer U**, Nyffeler M, Engler A, Urwyler A, Schedlowski M, Knuesel I, Yee BK, Feldon J. The time of prenatal immune challenge determines the specificity of inflammation-mediated brain and behavioral pathology. *J Neurosci* 2006; **26**: 4752-4762 [PMID: 16672647 DOI: 10.1523/JNEUROSCI.0099-06.2006]

60 **Morgan JT**, Chana G, Pardo CA, Achim C, Semendeferi K, Buckwalter J, Courchesne E, Everall IP. Microglial activation and increased microglial density observed in the dorsolateral prefrontal cortex in autism. *Biol Psychiatry* 2010; **68**: 368-376 [PMID: 20674603 DOI: 10.1016/j.biopsych.2010.05.024]

61 **Vargas DL**, Nascimbene C, Krishnan C, Zimmerman AW, Pardo CA. Neuroglial activation and neuroinflammation in the brain of patients with autism. *Ann Neurol* 2005; **57**: 67-81 [PMID: 15546155 DOI: 10.1002/ana.20315]

62 **Johnson WG**, Buyske S, Mars AE, Sreenath M, Stenroos ES, Williams TA, Stein R, Lambert GH. HLA-DR4 as a risk allele for autism acting in mothers of probands possibly during pregnancy. *Arch Pediatr Adolesc Med* 2009; **163**: 542-546 [PMID: 19487610 DOI: 10.1001/archpediatrics.2009.74]

63 **Lee LC**, Zachary AA, Leffell MS, Newschaffer CJ, Matteson KJ, Tyler JD, Zimmerman AW. HLA-DR4 in families with autism. *Pediatr Neurol* 2006; **35**: 303-307 [PMID: 17074598 DOI: 10.1016/j.pediatrneurol.2006.06.006]

64 **Torres AR**, Maciulis A, Stubbs EG, Cutler A, Odell D. The transmission disequilibrium test suggests that HLA-DR4 and DR13 are linked to autism spectrum disorder. *Hum Immunol* 2002; **63**: 311-316 [PMID: 12039413 DOI: 10.1016/S0198-8859(02)00374-9]

65 **Odell D**, Maciulis A, Cutler A, Warren L, McMahon WM, Coon H, Stubbs G, Henley K, Torres A. Confirmation of the association of the C4B null allelle in autism. *Hum Immunol* 2005; **66**: 140-145 [PMID: 15694999 DOI: 10.1016/j.humimm.2004.11.002]

66 **Beattie EC**, Stellwagen D, Morishita W, Bresnahan JC, Ha BK, Von Zastrow M, Beattie MS, Malenka RC. Control of synaptic strength by glial TNFalpha. *Science* 2002; **295**: 2282-2285 [PMID: 11910117 DOI: 10.1126/science.1067859]

67 **Stellwagen D**. The contribution of TNFα to synaptic plasticity and nervous system function. *Adv Exp Med Biol* 2011; **691**: 541-557 [PMID: 21153360 DOI: 10.1007/978-1-4419-6612-4_57]

68 **Albensi BC**, Mattson MP. Evidence for the involvement of TNF and NF-kappaB in hippocampal synaptic plasticity. *Synapse* 2000; **35**: 151-159 [PMID: 10611641 DOI: 10.1002/(SICI)1098-2396(200002)35:2<151::AID-SYN8>3.0.CO;2-P]

69 **Chess S**. Autism in children with congenital rubella. *J Autism Child Schizophr* 1971; **1**: 33-47 [PMID: 5172438 DOI: 10.1007/BF01537741]

70 **Atladóttir HÓ**, Henriksen TB, Schendel DE, Parner ET. Autism after infection, febrile episodes, and antibiotic use during pregnancy: an exploratory study. *Pediatrics* 2012; **130**: e1447-e1454 [PMID: 23147969 DOI: 10.1542/peds.2012-1107]

71 **Zerbo O**, Iosif AM, Walker C, Ozonoff S, Hansen RL, Hertz-Picciotto I. Is maternal influenza or fever during pregnancy associated with autism or developmental delays? Results from the CHARGE (CHildhood Autism Risks from Genetics and Environment) study. *J Autism Dev Disord* 2013; **43**: 25-33 [PMID: 22562209 DOI: 10.1007/s10803-012-1540-x]

72 **Lee BK**, Magnusson C, Gardner RM, Blomström Å, Newschaffer CJ, Burstyn I, Karlsson H, Dalman C. Maternal hospitalization with infection during pregnancy and risk of autism spectrum disorders. *Brain Behav Immun* 2015; **44**: 100-105 [PMID: 25218900 DOI: 10.1016/j.bbi.2014.09.001]

73 **Meyer U**, Feldon J, Schedlowski M, Yee BK. Immunological stress at the maternal-foetal interface: a link between neurodevelopment and adult psychopathology. *Brain Behav Immun* 2006; **20**: 378-388 [PMID: 16378711 DOI: 10.1016/j.bbi.2005.11.003]

74 **McAlonan GM**, Li Q, Cheung C. The timing and specificity of prenatal immune risk factors for autism modeled in the mouse and relevance to schizophrenia. *Neurosignals* 2010; **18**: 129-139 [PMID: 21042002 DOI: 10.1159/000321080]

75 **Fatemi SH**, Earle J, Kanodia R, Kist D, Emamian ES, Patterson PH, Shi L, Sidwell R. Prenatal viral infection leads to pyramidal cell atrophy and macrocephaly in adulthood: implications for genesis of autism and schizophrenia. *Cell Mol Neurobiol* 2002; **22**: 25-33 [PMID: 12064515 DOI: 10.1023/A:1015337611258]

76 **Smith SE**, Li J, Garbett K, Mirnics K, Patterson PH. Maternal immune activation alters fetal brain development through interleukin-6. *J Neurosci* 2007; **27**: 10695-10702 [PMID: 17913903 DOI: 10.1523/JNEUROSCI.2178-07.2007]

77 **Martin LA**, Ashwood P, Braunschweig D, Cabanlit M, Van de Water J, Amaral DG. Stereotypies and hyperactivity in rhesus monkeys exposed to IgG from mothers of children with autism. *Brain Behav Immun* 2008; **22**: 806-816 [PMID: 18262386 DOI: 10.1016/j.bbi.2007.12.007]

78 **Romero E**, Guaza C, Castellano B, Borrell J. Ontogeny of sensorimotor gating and immune impairment induced by prenatal immune challenge in rats: implications for the etiopathology of schizophrenia. *Mol Psychiatry* 2010; **15**: 372-383 [PMID: 18414405 DOI: 10.1038/mp.2008.44]

79 **Hsiao EY**, Patterson PH. Activation of the maternal immune system induces endocrine changes in the placenta via IL-6. *Brain Behav Immun* 2011; **25**: 604-615 [PMID: 21195166 DOI: 10.1016/j.bbi.2010.12.017]

80 **Xing Z**, Gauldie J, Cox G, Baumann H, Jordana M, Lei XF, Achong MK. IL-6 is an antiinflammatory cytokine required for controlling local or systemic acute inflammatory responses. *J Clin Invest* 1998; **101**: 311-320 [PMID: 9435302 DOI: 10.1172/JCI1368]

81 **Zaretsky MV**, Alexander JM, Byrd W, Bawdon RE. Transfer of inflammatory cytokines across the placenta. *Obstet Gynecol* 2004; **103**: 546-550 [PMID: 14990420 DOI: 10.1097/01.AOG.0000114980.40445.83]

82 **Deng MY**, Lam S, Meyer U, Feldon J, Li Q, Wei R, Luk L, Chua SE, Sham P, Wang Y, McAlonan GM. Frontal-subcortical protein expression following prenatal exposure to maternal inflammation. *PLoS One*

2011; **6**: e16638 [PMID: 21347362 DOI: 10.1371/journal.pone.0016638]
83 **Richetto J**, Massart R, Weber-Stadlbauer U, Szyf M, Riva MA, Meyer U. Genome-wide DNA Methylation Changes in a Mouse Model of Infection-Mediated Neurodevelopmental Disorders. *Biol Psychiatry* 2017; **81**: 265-276 [PMID: 27769567 DOI: 10.1016/j.biopsych.2016.08.010]
84 **Basil P**, Li Q, Gui H, Hui TCK, Ling VHM, Wong CCY, Mill J, McAlonan GM, Sham PC. Prenatal immune activation alters the adult neural epigenome but can be partly stabilised by a n-3 polyunsaturated fatty acid diet. *Transl Psychiatry* 2018; **8**: 125 [PMID: 29967385 DOI: 10.1038/s41398-018-0167-x]
85 **Labouesse MA**, Dong E, Grayson DR, Guidotti A, Meyer U. Maternal immune activation induces GAD1 and GAD2 promoter remodeling in the offspring prefrontal cortex. *Epigenetics* 2015; **10**: 1143-1155 [PMID: 26575259 DOI: 10.1080/15592294.2015.1114202]
86 **Le Strat Y**, Dubertret C, Le Foll B. Prevalence and correlates of major depressive episode in pregnant and postpartum women in the United States. *J Affect Disord* 2011; **135**: 128-138 [PMID: 21802737 DOI: 10.1016/j.jad.2011.07.004]
87 **Gavin NI**, Gaynes BN, Lohr KN, Meltzer-Brody S, Gartlehner G, Swinson T. Perinatal depression: a systematic review of prevalence and incidence. *Obstet Gynecol* 2005; **106**: 1071-1083 [PMID: 16260528 DOI: 10.1097/01.AOG.0000183597.31630.db]
88 **Huang H**, Coleman S, Bridge JA, Yonkers K, Katon W. A meta-analysis of the relationship between antidepressant use in pregnancy and the risk of preterm birth and low birth weight. *Gen Hosp Psychiatry* 2014; **36**: 13-18 [PMID: 24094568 DOI: 10.1016/j.genhosppsych.2013.08.002]
89 **Myles N**, Newall H, Ward H, Large M. Systematic meta-analysis of individual selective serotonin reuptake inhibitor medications and congenital malformations. *Aust N Z J Psychiatry* 2013; **47**: 1002-1012 [PMID: 23761574 DOI: 10.1177/0004867413492219]
90 **Malm H**. Prenatal exposure to selective serotonin reuptake inhibitors and infant outcome. *Ther Drug Monit* 2012; **34**: 607-614 [PMID: 23042258 DOI: 10.1097/FTD.0b013e31826d07ea]
91 **Lattimore KA**, Donn SM, Kaciroti N, Kemper AR, Neal CR, Vazquez DM. Selective serotonin reuptake inhibitor (SSRI) use during pregnancy and effects on the fetus and newborn: a meta-analysis. *J Perinatol* 2005; **25**: 595-604 [PMID: 16015372 DOI: 10.1038/sj.jp.7211352]
92 **Borue X**, Chen J, Condron BG. Developmental effects of SSRIs: lessons learned from animal studies. *Int J Dev Neurosci* 2007; **25**: 341-347 [PMID: 17706396 DOI: 10.1016/j.ijdevneu.2007.06.003]
93 **McDougle CJ**, Naylor ST, Cohen DJ, Aghajanian GK, Heninger GR, Price LH. Effects of tryptophan depletion in drug-free adults with autistic disorder. *Arch Gen Psychiatry* 1996; **53**: 993-1000 [PMID: 8911222 DOI: 10.1001/archpsyc.1996.01830110029004]
94 **Rai D**, Lee BK, Dalman C, Golding J, Lewis G, Magnusson C. Parental depression, maternal antidepressant use during pregnancy, and risk of autism spectrum disorders: population based case-control study. *BMJ* 2013; **346**: f2059 [PMID: 23604083 DOI: 10.1136/bmj.f2059]
95 **Gidaya NB**, Lee BK, Burstyn I, Yudell M, Mortensen EL, Newschaffer CJ. In utero exposure to selective serotonin reuptake inhibitors and risk for autism spectrum disorder. *J Autism Dev Disord* 2014; **44**: 2558-2567 [PMID: 24803368 DOI: 10.1007/s10803-014-2128-4]
96 **Man KK**, Tong HH, Wong LY, Chan EW, Simonoff E, Wong IC. Exposure to selective serotonin reuptake inhibitors during pregnancy and risk of autism spectrum disorder in children: a systematic review and meta-analysis of observational studies. *Neurosci Biobehav Rev* 2015; **49**: 82-89 [PMID: 25498856 DOI: 10.1016/j.neubiorev.2014.11.020]
97 **Gentile S**. Prenatal antidepressant exposure and the risk of autism spectrum disorders in children. Are we looking at the fall of Gods? *J Affect Disord* 2015; **182**: 132-137 [PMID: 25985383 DOI: 10.1016/j.jad.2015.04.048]
98 **Brown HK**, Hussain-Shamsy N, Lunsky Y, Dennis CE, Vigod SN. The Association Between Antenatal Exposure to Selective Serotonin Reuptake Inhibitors and Autism: A Systematic Review and Meta-Analysis. *J Clin Psychiatry* 2017; **78**: e48-e58 [PMID: 28129495 DOI: 10.4088/JCP.15r10194]
99 **Kaplan YC**, Keskin-Arslan E, Acar S, Sozmen K. Prenatal selective serotonin reuptake inhibitor use and the risk of autism spectrum disorder in children: A systematic review and meta-analysis. *Reprod Toxicol* 2016; **66**: 31-43 [PMID: 27667009 DOI: 10.1016/j.reprotox.2016.09.013]
100 **Jaiswal P**, Mohanakumar KP, Rajamma U. Serotonin mediated immunoregulation and neural functions: Complicity in the aetiology of autism spectrum disorders. *Neurosci Biobehav Rev* 2015; **55**: 413-431 [PMID: 26021727 DOI: 10.1016/j.neubiorev.2015.05.013]
101 **Warren RP**, Singh VK. Elevated serotonin levels in autism: association with the major histocompatibility complex. *Neuropsychobiology* 1996; **34**: 72-75 [PMID: 8904735 DOI: 10.1159/000119295]
102 **Williams G**, King J, Cunningham M, Stephan M, Kerr B, Hersh JH. Fetal valproate syndrome and autism: additional evidence of an association. *Dev Med Child Neurol* 2001; **43**: 202-206 [PMID: 11263692 DOI: 10.1111/j.1469-8749.2001.tb00188.x]
103 **Evatt ML**, DeLong MR, Grant WB, Cannell JJ, Tangpricha V. Autism spectrum disorders following in utero exposure to antiepileptic drugs. *Neurology* 2009; **73**: 997 [PMID: 19770480 DOI: 10.1212/WNL.0b013e3181af0b95]
104 **Dean JC**, Hailey H, Moore SJ, Lloyd DJ, Turnpenny PD, Little J. Long term health and neurodevelopment in children exposed to antiepileptic drugs before birth. *J Med Genet* 2002; **39**: 251-259 [PMID: 11950853 DOI: 10.1136/jmg.39.4.251]
105 **Wagner GC**, Reuhl KR, Cheh M, McRae P, Halladay AK. A new neurobehavioral model of autism in mice: pre- and postnatal exposure to sodium valproate. *J Autism Dev Disord* 2006; **36**: 779-793 [PMID: 16609825 DOI: 10.1007/s10803-006-0117-y]
106 **Miyazaki K**, Narita N, Narita M. Maternal administration of thalidomide or valproic acid causes abnormal serotonergic neurons in the offspring: implication for pathogenesis of autism. *Int J Dev Neurosci* 2005; **23**: 287-297 [PMID: 15749253 DOI: 10.1016/j.ijdevneu.2004.05.004]
107 **Narita N**, Kato M, Tazoe M, Miyazaki K, Narita M, Okado N. Increased monoamine concentration in the brain and blood of fetal thalidomide- and valproic acid-exposed rat: putative animal models for autism. *Pediatr Res* 2002; **52**: 576-579 [PMID: 12357053 DOI: 10.1203/00006450-200210000-00018]
108 **Dufour-Rainfray D**, Vourc'h P, Le Guisquet AM, Garreau L, Ternant D, Bodard S, Jaumain E, Gulhan Z, Belzung C, Andres CR, Chalon S, Guilloteau D. Behavior and serotonergic disorders in rats exposed prenatally to valproate: a model for autism. *Neurosci Lett* 2010; **470**: 55-59 [PMID: 20036713 DOI: 10.1016/j.neulet.2009.12.054]
109 **Jin J**, Xiong T, Hou X, Sun X, Liao J, Huang Z, Huang M, Zhao Z. Role of Nrf2 activation and NF-κB inhibition in valproic acid induced hepatotoxicity and in diammonium glycyrrhizinate induced protection in mice. *Food Chem Toxicol* 2014; **73**: 95-104 [PMID: 25152329 DOI: 10.1016/j.fct.2014.08.009]

110 **Li X**, Chauhan A, Sheikh AM, Patil S, Chauhan V, Li XM, Ji L, Brown T, Malik M. Elevated immune response in the brain of autistic patients. *J Neuroimmunol* 2009; **207**: 111-116 [PMID: 19157572 DOI: 10.1016/j.jneuroim.2008.12.002]

111 **Onore C**, Careaga M, Ashwood P. The role of immune dysfunction in the pathophysiology of autism. *Brain Behav Immun* 2012; **26**: 383-392 [PMID: 21906670 DOI: 10.1016/j.bbi.2011.08.007]

112 **Ashwood P**, Krakowiak P, Hertz-Picciotto I, Hansen R, Pessah I, Van de Water J. Elevated plasma cytokines in autism spectrum disorders provide evidence of immune dysfunction and are associated with impaired behavioral outcome. *Brain Behav Immun* 2011; **25**: 40-45 [PMID: 20705131 DOI: 10.1016/j.bbi.2010.08.003]

113 **Ashwood P**, Krakowiak P, Hertz-Picciotto I, Hansen R, Pessah IN, Van de Water J. Associations of impaired behaviors with elevated plasma chemokines in autism spectrum disorders. *J Neuroimmunol* 2011; **232**: 196-199 [PMID: 21095018 DOI: 10.1016/j.jneuroim.2010.10.025]

114 **Collins E**, Gu F, Qi M, Molano I, Ruiz P, Sun L, Gilkeson GS. Differential efficacy of human mesenchymal stem cells based on source of origin. *J Immunol* 2014; **193**: 4381-4390 [PMID: 25274529 DOI: 10.4049/jimmunol.1401636]

115 **Friedenstein AJ**, Gorskaja JF, Kulagina NN. Fibroblast precursors in normal and irradiated mouse hematopoietic organs. *Exp Hematol* 1976; **4**: 267-274 [PMID: 976387]

116 **Zuk PA**, Zhu M, Ashjian P, De Ugarte DA, Huang JI, Mizuno H, Alfonso ZC, Fraser JK, Benhaim P, Hedrick MH. Human adipose tissue is a source of multipotent stem cells. *Mol Biol Cell* 2002; **13**: 4279-4295 [PMID: 12475952 DOI: 10.1091/mbc.e02-02-0105]

117 **In't Anker PS**, Scherjon SA, Kleijburg-van der Keur C, de Groot-Swings GM, Claas FH, Fibbe WE, Kanhai HH. Isolation of mesenchymal stem cells of fetal or maternal origin from human placenta. *Stem Cells* 2004; **22**: 1338-1345 [PMID: 15579651 DOI: 10.1634/stemcells.2004-0058]

118 **Shih DT**, Lee DC, Chen SC, Tsai RY, Huang CT, Tsai CC, Shen EY, Chiu WT. Isolation and characterization of neurogenic mesenchymal stem cells in human scalp tissue. *Stem Cells* 2005; **23**: 1012-1020 [PMID: 15941858 DOI: 10.1634/stemcells.2004-0125]

119 **Erices A**, Conget P, Minguell JJ. Mesenchymal progenitor cells in human umbilical cord blood. *Br J Haematol* 2000; **109**: 235-242 [PMID: 10848804 DOI: 10.1046/j.1365-2141.2000.01986.x]

120 **Sarugaser R**, Lickorish D, Baksh D, Hosseini MM, Davies JE. Human umbilical cord perivascular (HUCPV) cells: a source of mesenchymal progenitors. *Stem Cells* 2005; **23**: 220-229 [PMID: 15671145 DOI: 10.1634/stemcells.2004-0166]

121 **Wang HS**, Hung SC, Peng ST, Huang CC, Wei HM, Guo YJ, Fu YS, Lai MC, Chen CC. Mesenchymal stem cells in the Wharton's jelly of the human umbilical cord. *Stem Cells* 2004; **22**: 1330-1337 [PMID: 15579650 DOI: 10.1634/stemcells.2004-0013]

122 **Nadri S**, Soleimani M. Comparative analysis of mesenchymal stromal cells from murine bone marrow and amniotic fluid. *Cytotherapy* 2007; **9**: 729-737 [PMID: 17917881 DOI: 10.1080/14653240701656061]

123 **De Bari C**, Dell'Accio F, Tylzanowski P, Luyten FP. Multipotent mesenchymal stem cells from adult human synovial membrane. *Arthritis Rheum* 2001; **44**: 1928-1942 [PMID: 11508446 DOI: 10.1002/1529-0131(200108)44:8<1928::AID-ART331>3.0.CO;2-P]

124 **Patki S**, Kadam S, Chandra V, Bhonde R. Human breast milk is a rich source of multipotent mesenchymal stem cells. *Hum Cell* 2010; **23**: 35-40 [PMID: 20712706 DOI: 10.1111/j.1749-0774.2010.00083.x]

125 **Griffiths MJ**, Bonnet D, Janes SM. Stem cells of the alveolar epithelium. *Lancet* 2005; **366**: 249-260 [PMID: 16023517 DOI: 10.1016/S0140-6736(05)66916-4]

126 **Beltrami AP**, Barlucchi L, Torella D, Baker M, Limana F, Chimenti S, Kasahara H, Rota M, Musso E, Urbanek K, Leri A, Kajstura J, Nadal-Ginard B, Anversa P. Adult cardiac stem cells are multipotent and support myocardial regeneration. *Cell* 2003; **114**: 763-776 [PMID: 14505575 DOI: 10.1016/S0092-8674(03)00687-1]

127 **Hida N**, Nishiyama N, Miyoshi S, Kira S, Segawa K, Uyama T, Mori T, Miyado K, Ikegami Y, Cui C, Kiyono T, Kyo S, Shimizu T, Okano T, Sakamoto M, Ogawa S, Umezawa A. Novel cardiac precursor-like cells from human menstrual blood-derived mesenchymal cells. *Stem Cells* 2008; **26**: 1695-1704 [PMID: 18420831 DOI: 10.1634/stemcells.2007-0826]

128 **Gargett CE**, Schwab KE, Zillwood RM, Nguyen HP, Wu D. Isolation and culture of epithelial progenitors and mesenchymal stem cells from human endometrium. *Biol Reprod* 2009; **80**: 1136-1145 [PMID: 19228591 DOI: 10.1095/biolreprod.108.075226]

129 **Pittenger MF**, Mackay AM, Beck SC, Jaiswal RK, Douglas R, Mosca JD, Moorman MA, Simonetti DW, Craig S, Marshak DR. Multilineage potential of adult human mesenchymal stem cells. *Science* 1999; **284**: 143-147 [PMID: 10102814 DOI: 10.1126/science.284.5411.143]

130 **Prasanna SJ**, Gopalakrishnan D, Shankar SR, Vasandan AB. Pro-inflammatory cytokines, IFNgamma and TNFalpha, influence immune properties of human bone marrow and Wharton jelly mesenchymal stem cells differentially. *PLoS One* 2010; **5**: e9016 [PMID: 20126406 DOI: 10.1371/journal.pone.0009016]

131 **Kim SM**, Jeong CH, Woo JS, Ryu CH, Lee JH, Jeun SS. In vivo near-infrared imaging for the tracking of systemically delivered mesenchymal stem cells: tropism for brain tumors and biodistribution. *Int J Nanomedicine* 2015; **11**: 13-23 [PMID: 26719691 DOI: 10.2147/IJN.S97073]

132 **Karp JM**, Leng Teo GS. Mesenchymal stem cell homing: the devil is in the details. *Cell Stem Cell* 2009; **4**: 206-216 [PMID: 19265660 DOI: 10.1016/j.stem.2009.02.001]

133 **Danielyan L**, Schäfer R, von Ameln-Mayerhofer A, Buadze M, Geisler J, Klopfer T, Burkhardt U, Proksch B, Verleysdonk S, Ayturan M, Buniatian GH, Gleiter CH, Frey WH 2nd. Intranasal delivery of cells to the brain. *Eur J Cell Biol* 2009; **88**: 315-324 [PMID: 19324456 DOI: 10.1016/j.ejcb.2009.02.001]

134 **Eggenhofer E**, Benseler V, Kroemer A, Popp FC, Geissler EK, Schlitt HJ, Baan CC, Dahlke MH, Hoogduijn MJ. Mesenchymal stem cells are short-lived and do not migrate beyond the lungs after intravenous infusion. *Front Immunol* 2012; **3**: 297 [PMID: 23056000 DOI: 10.3389/fimmu.2012.00297]

135 **Liu XB**, Chen H, Chen HQ, Zhu MF, Hu XY, Wang YP, Jiang Z, Xu YC, Xiang MX, Wang JA. Angiopoietin-1 preconditioning enhances survival and functional recovery of mesenchymal stem cell transplantation. *J Zhejiang Univ Sci B* 2012; **13**: 616-623 [PMID: 22843181 DOI: 10.1631/jzus.B1201004]

136 **Eggenhofer E**, Luk F, Dahlke MH, Hoogduijn MJ. The life and fate of mesenchymal stem cells. *Front Immunol* 2014; **5**: 148 [PMID: 24904568 DOI: 10.3389/fimmu.2014.00148]

137 **Caplan AI**, Correa D. The MSC: an injury drugstore. *Cell Stem Cell* 2011; **9**: 11-15 [PMID: 21726829 DOI: 10.1016/j.stem.2011.06.008]

138 **Gesundheit B**, Ashwood P, Keating A, Naor D, Melamed M, Rosenzweig JP. Therapeutic properties of mesenchymal stem cells for autism spectrum disorders. *Med Hypotheses* 2015; **84**: 169-177 [PMID: 25592283 DOI: 10.1016/j.mehy.2014.12.016]

139 **Ebert DH**, Greenberg ME. Activity-dependent neuronal signalling and autism spectrum disorder. *Nature* 2013; **493**: 327-337 [PMID: 23325215 DOI: 10.1038/nature11860]
140 **Chopp M**, Li Y. Treatment of neural injury with marrow stromal cells. *Lancet Neurol* 2002; **1**: 92-100 [PMID: 12849513 DOI: 10.1016/S1474-4422(02)00040-6]
141 **Spejo AB**, Carvalho JL, Goes AM, Oliveira AL. Neuroprotective effects of mesenchymal stem cells on spinal motoneurons following ventral root axotomy: synapse stability and axonal regeneration. *Neuroscience* 2013; **250**: 715-732 [PMID: 23896572 DOI: 10.1016/j.neuroscience.2013.07.043]
142 **Nauta AJ**, Fibbe WE. Immunomodulatory properties of mesenchymal stromal cells. *Blood* 2007; **110**: 3499-3506 [PMID: 17664353 DOI: 10.1182/blood-2007-02-069716]
143 **Chen PM**, Yen ML, Liu KJ, Sytwu HK, Yen BL. Immunomodulatory properties of human adult and fetal multipotent mesenchymal stem cells. *J Biomed Sci* 2011; **18**: 49 [PMID: 21762539 DOI: 10.1186/1423-0127-18-49]
144 **Uccelli A**, Moretta L, Pistoia V. Mesenchymal stem cells in health and disease. *Nat Rev Immunol* 2008; **8**: 726-736 [PMID: 19172693 DOI: 10.1038/nri2395]
145 **Li N**, Hua J. Interactions between mesenchymal stem cells and the immune system. *Cell Mol Life Sci* 2017; **74**: 2345-2360 [PMID: 28214990 DOI: 10.1007/s00018-017-2473-5]
146 **Gao F**, Chiu SM, Motan DA, Zhang Z, Chen L, Ji HL, Tse HF, Fu QL, Lian Q. Mesenchymal stem cells and immunomodulation: current status and future prospects. *Cell Death Dis* 2016; **7**: e2062 [PMID: 26794657 DOI: 10.1038/cddis.2015.327]
147 **Aggarwal S**, Pittenger MF. Human mesenchymal stem cells modulate allogeneic immune cell responses. *Blood* 2005; **105**: 1815-1822 [PMID: 15494428 DOI: 10.1182/blood-2004-04-1559]
148 **Girard SD**, Virard I, Lacassagne E, Paumier JM, Lahlou H, Jabes F, Molino Y, Stephan D, Baranger K, Belghazi M, Deveze A, Khrestchatisky M, Nivet E, Roman FS, Féron F. From Blood to Lesioned Brain: An In Vitro Study on Migration Mechanisms of Human Nasal Olfactory Stem Cells. *Stem Cells Int* 2017; **2017**: 1478606 [PMID: 28698717 DOI: 10.1155/2017/1478606]
149 **Rüster B**, Göttig S, Ludwig RJ, Bistrian R, Müller S, Seifried E, Gille J, Henschler R. Mesenchymal stem cells display coordinated rolling and adhesion behavior on endothelial cells. *Blood* 2006; **108**: 3938-3944 [PMID: 16896152 DOI: 10.1182/blood-2006-05-025098]
150 **Delarosa O**, Dalemans W, Lombardo E. Toll-like receptors as modulators of mesenchymal stem cells. *Front Immunol* 2012; **3**: 182 [PMID: 22783256 DOI: 10.3389/fimmu.2012.00182]
151 **Park C**, Lee S, Cho IH, Lee HK, Kim D, Choi SY, Oh SB, Park K, Kim JS, Lee SJ. TLR3-mediated signal induces proinflammatory cytokine and chemokine gene expression in astrocytes: differential signaling mechanisms of TLR3-induced IP-10 and IL-8 gene expression. *Glia* 2006; **53**: 248-256 [PMID: 16265667 DOI: 10.1002/glia.20278]
152 **Joh EH**, Gu W, Kim DH. Echinocystic acid ameliorates lung inflammation in mice and alveolar macrophages by inhibiting the binding of LPS to TLR4 in NF-κB and MAPK pathways. *Biochem Pharmacol* 2012; **84**: 331-340 [PMID: 22564908 DOI: 10.1016/j.bcp.2012.04.020]
153 **Meylan E**, Tschopp J, Karin M. Intracellular pattern recognition receptors in the host response. *Nature* 2006; **442**: 39-44 [PMID: 16823444 DOI: 10.1038/nature04946]
154 **Pisegna S**, Pirozzi G, Piccoli M, Frati L, Santoni A, Palmieri G. p38 MAPK activation controls the TLR3-mediated up-regulation of cytotoxicity and cytokine production in human NK cells. *Blood* 2004; **104**: 4157-4164 [PMID: 15315972 DOI: 10.1182/blood-2004-05-1860]
155 **Waterman RS**, Tomchuck SL, Henkle SL, Betancourt AM. A new mesenchymal stem cell (MSC) paradigm: polarization into a pro-inflammatory MSC1 or an Immunosuppressive MSC2 phenotype. *PLoS One* 2010; **5**: e10088 [PMID: 20436665 DOI: 10.1371/journal.pone.0010088]
156 **Shirjang S**, Mansoori B, Solali S, Hagh MF, Shamsasenjan K. Toll-like receptors as a key regulator of mesenchymal stem cell function: An up-to-date review. *Cell Immunol* 2017; **315**: 1-10 [PMID: 28284487 DOI: 10.1016/j.cellimm.2016.12.005]
157 **Mei SH**, McCarter SD, Deng Y, Parker CH, Liles WC, Stewart DJ. Prevention of LPS-induced acute lung injury in mice by mesenchymal stem cells overexpressing angiopoietin 1. *PLoS Med* 2007; **4**: e269 [PMID: 17803352 DOI: 10.1371/journal.pmed.0040269]
158 **Xu J**, Woods CR, Mora AL, Joodi R, Brigham KL, Iyer S, Rojas M. Prevention of endotoxin-induced systemic response by bone marrow-derived mesenchymal stem cells in mice. *Am J Physiol Lung Cell Mol Physiol* 2007; **293**: L131-L141 [PMID: 17416739 DOI: 10.1152/ajplung.00431.2006]
159 **Nemeth K**, Mayer B, Mezey E. Modulation of bone marrow stromal cell functions in infectious diseases by toll-like receptor ligands. *J Mol Med (Berl)* 2010; **88**: 5-10 [PMID: 19756450 DOI: 10.1007/s00109-009-0523-7]
160 **Gesundheit B**, Rosenzweig JP, Naor D, Lerer B, Zachor DA, Procházka V, Melamed M, Kristt DA, Steinberg A, Shulman C, Hwang P, Koren G, Walfisch A, Passweg JR, Snowden JA, Tamouza R, Leboyer M, Farge-Bancel D, Ashwood P. Immunological and autoimmune considerations of Autism Spectrum Disorders. *J Autoimmun* 2013; **44**: 1-7 [PMID: 23867105 DOI: 10.1016/j.jaut.2013.05.005]
161 **Pistoia V**, Raffaghello L. Mesenchymal stromal cells and autoimmunity. *Int Immunol* 2017; **29**: 49-58 [PMID: 28338763 DOI: 10.1093/intimm/dxx008]
162 **Zhao Y**, Lin B, Darflinger R, Zhang Y, Holterman MJ, Skidgel RA. Human cord blood stem cell-modulated regulatory T lymphocytes reverse the autoimmune-caused type 1 diabetes in nonobese diabetic (NOD) mice. *PLoS One* 2009; **4**: e4226 [PMID: 19156219 DOI: 10.1371/journal.pone.0004226]
163 **Ma S**, Chen X, Wang L, Wei Y, Ni Y, Chu Y, Liu Y, Zhu H, Zheng R, Zhang Y. Repairing effects of ICAM-1-expressing mesenchymal stem cells in mice with autoimmune thyroiditis. *Exp Ther Med* 2017; **13**: 1295-1302 [PMID: 28413469 DOI: 10.3892/etm.2017.4131]
164 **Uccelli A**, Laroni A, Freedman MS. Mesenchymal stem cells for the treatment of multiple sclerosis and other neurological diseases. *Lancet Neurol* 2011; **10**: 649-656 [PMID: 21683930 DOI: 10.1016/S1474-4422(11)70121-1]
165 **Le Blanc K**, Frassoni F, Ball L, Locatelli F, Roelofs H, Lewis I, Lanino E, Sundberg B, Bernardo ME, Remberger M, Dini G, Egeler RM, Bacigalupo A, Fibbe W, Ringdén O; Developmental Committee of the European Group for Blood and Marrow Transplantation. Mesenchymal stem cells for treatment of steroid-resistant, severe, acute graft-versus-host disease: a phase II study. *Lancet* 2008; **371**: 1579-1586 [PMID: 18468541 DOI: 10.1016/S0140-6736(08)60690-X]
166 **El-Akabawy G**, Rashed LA. Beneficial effects of bone marrow-derived mesenchymal stem cell transplantation in a non-immune model of demyelination. *Ann Anat* 2015; **198**: 11-20 [PMID: 25660362 DOI: 10.1016/j.aanat.2014.12.002]
167 **Boieri M**, Shah P, Dressel R, Inngjerdingen M. The Role of Animal Models in the Study of Hematopoietic

Stem Cell Transplantation and GvHD: A Historical Overview. *Front Immunol* 2016; **7**: 333 [PMID: 27625651 DOI: 10.3389/fimmu.2016.00333]
168 **Ha S**, Park H, Mahmood U, Ra JC, Suh YH, Chang KA. Human adipose-derived stem cells ameliorate repetitive behavior, social deficit and anxiety in a VPA-induced autism mouse model. *Behav Brain Res* 2017; **317**: 479-484 [PMID: 27717813 DOI: 10.1016/j.bbr.2016.10.004]
169 **Gobshtis N**, Tfilin M, Wolfson M, Fraifeld VE, Turgeman G. Transplantation of mesenchymal stem cells reverses behavioural deficits and impaired neurogenesis caused by prenatal exposure to valproic acid. *Oncotarget* 2017; **8**: 17443-17452 [PMID: 28407680 DOI: 10.18632/oncotarget.15245]
170 **Ellegood J**, Crawley JN. Behavioral and Neuroanatomical Phenotypes in Mouse Models of Autism. *Neurotherapeutics* 2015; **12**: 521-533 [PMID: 26036957 DOI: 10.1007/s13311-015-0360-z]
171 **Wahlsten D**, Metten P, Crabbe JC. Survey of 21 inbred mouse strains in two laboratories reveals that BTBR T/+ tf/tf has severely reduced hippocampal commissure and absent corpus callosum. *Brain Res* 2003; **971**: 47-54 [PMID: 12691836 DOI: 10.1016/S0006-8993(03)02354-0]
172 **Faraji J**, Karimi M, Lawrence C, Mohajerani MH, Metz GAS. Non-diagnostic symptoms in a mouse model of autism in relation to neuroanatomy: the BTBR strain reinvestigated. *Transl Psychiatry* 2018; **8**: 234 [PMID: 30367028 DOI: 10.1038/s41398-018-0280-x]
173 **Segal-Gavish H**, Karvat G, Barak N, Barzilay R, Ganz J, Edry L, Aharony I, Offen D, Kimchi T. Mesenchymal Stem Cell Transplantation Promotes Neurogenesis and Ameliorates Autism Related Behaviors in BTBR Mice. *Autism Res* 2016; **9**: 17-32 [PMID: 26257137 DOI: 10.1002/aur.1530]
174 **Perets N**, Segal-Gavish H, Gothelf Y, Barzilay R, Barhum Y, Abramov N, Hertz S, Morozov D, London M, Offen D. Long term beneficial effect of neurotrophic factors-secreting mesenchymal stem cells transplantation in the BTBR mouse model of autism. *Behav Brain Res* 2017; **331**: 254-260 [PMID: 28392323 DOI: 10.1016/j.bbr.2017.03.047]
175 **Bahat-Stroomza M**, Barhum Y, Levy YS, Karpov O, Bulvik S, Melamed E, Offen D. Induction of adult human bone marrow mesenchymal stromal cells into functional astrocyte-like cells: potential for restorative treatment in Parkinson's disease. *J Mol Neurosci* 2009; **39**: 199-210 [PMID: 19127447 DOI: 10.1007/s12031-008-9166-3]
176 **Gothelf Y**, Abramov N, Harel A, Offen D. Safety of repeated transplantations of neurotrophic factors-secreting human mesenchymal stromal stem cells. *Clin Transl Med* 2014; **3**: 21 [PMID: 25097724 DOI: 10.1186/2001-1326-3-21]
177 **Yu B**, Zhang X, Li X. Exosomes derived from mesenchymal stem cells. *Int J Mol Sci* 2014; **15**: 4142-4157 [PMID: 24608926 DOI: 10.3390/ijms15034142]
178 **Xin H**, Li Y, Buller B, Katakowski M, Zhang Y, Wang X, Shang X, Zhang ZG, Chopp M. Exosome-mediated transfer of miR-133b from multipotent mesenchymal stromal cells to neural cells contributes to neurite outgrowth. *Stem Cells* 2012; **30**: 1556-1564 [PMID: 22605481 DOI: 10.1002/stem.1129]
179 **Perets N**, Hertz S, London M, Offen D. Intranasal administration of exosomes derived from mesenchymal stem cells ameliorates autistic-like behaviors of BTBR mice. *Mol Autism* 2018; **9**: 57 [PMID: 30479733 DOI: 10.1186/s13229-018-0240-6]
180 **Lv YT**, Zhang Y, Liu M, Qiuwaxi JN, Ashwood P, Cho SC, Huan Y, Ge RC, Chen XW, Wang ZJ, Kim BJ, Hu X. Transplantation of human cord blood mononuclear cells and umbilical cord-derived mesenchymal stem cells in autism. *J Transl Med* 2013; **11**: 196 [PMID: 23978163 DOI: 10.1186/1479-5876-11-196]
181 **Sharma A**, Gokulchandran N, Sane H, Nagrajan A, Paranjape A, Kulkarni P, Shetty A, Mishra P, Kali M, Biju H, Badhe P. Autologous bone marrow mononuclear cell therapy for autism: an open label proof of concept study. *Stem Cells Int* 2013; **2013**: 623875 [PMID: 24062774 DOI: 10.1155/2013/623875]
182 **Bjørklund G**, Kern JK, Urbina MA, Saad K, El-Houfey AA, Geier DA, Chirumbolo S, Geier MR, Mehta JA, Aaseth J. Cerebral hypoperfusion in autism spectrum disorder. *Acta Neurobiol Exp (Wars)* 2018; **78**: 21-29 [PMID: 29694338 DOI: 10.21307/ane-2018-005]
183 **Bansal H**, Verma P, Agrawal A, Leon J, Sundell IB, Koka PS. A Short Study Report on Bone Marrow Aspirate Concentrate Cell Therapy in Ten South Asian Indian Patients with Autism. *J Stem Cells* 2016; **11**: 25-36 [PMID: 28296862]
184 **Dawson G**, Sun JM, Davlantis KS, Murias M, Franz L, Troy J, Simmons R, Sabatos-DeVito M, Durham R, Kurtzberg J. Autologous Cord Blood Infusions Are Safe and Feasible in Young Children with Autism Spectrum Disorder: Results of a Single-Center Phase I Open-Label Trial. *Stem Cells Transl Med* 2017; **6**: 1332-1339 [PMID: 28378499 DOI: 10.1002/sctm.16-0474]
185 **Murias M**, Major S, Compton S, Buttinger J, Sun JM, Kurtzberg J, Dawson G. Electrophysiological Biomarkers Predict Clinical Improvement in an Open-Label Trial Assessing Efficacy of Autologous Umbilical Cord Blood for Treatment of Autism. *Stem Cells Transl Med* 2018; **7**: 783-791 [PMID: 30070044 DOI: 10.1002/sctm.18-0090]
186 **Chez M**, Lepage C, Parise C, Dang-Chu A, Hankins A, Carroll M. Safety and Observations from a Placebo-Controlled, Crossover Study to Assess Use of Autologous Umbilical Cord Blood Stem Cells to Improve Symptoms in Children with Autism. *Stem Cells Transl Med* 2018; **7**: 333-341 [PMID: 29405603 DOI: 10.1002/sctm.17-0042]
187 **Li Q**, Leung YO, Zhou I, Ho LC, Kong W, Basil P, Wei R, Lam S, Zhang X, Law AC, Chua SE, Sham PC, Wu EX, McAlonan GM. Dietary supplementation with n-3 fatty acids from weaning limits brain biochemistry and behavioural changes elicited by prenatal exposure to maternal inflammation in the mouse model. *Transl Psychiatry* 2015; **5**: e641 [PMID: 26393487 DOI: 10.1038/tp.2015.126]
188 **Sharma SR**, Gonda X, Tarazi FI. Autism Spectrum Disorder: Classification, diagnosis and therapy. *Pharmacol Ther* 2018; **190**: 91-104 [PMID: 29763648 DOI: 10.1016/j.pharmthera.2018.05.007]
189 **Estes ML**, McAllister AK. Immune mediators in the brain and peripheral tissues in autism spectrum disorder. *Nat Rev Neurosci* 2015; **16**: 469-486 [PMID: 26189694 DOI: 10.1038/nrn3978]
190 **Lalu MM**, McIntyre L, Pugliese C, Fergusson D, Winston BW, Marshall JC, Granton J, Stewart DJ; Canadian Critical Care Trials Group. Safety of cell therapy with mesenchymal stromal cells (SafeCell): a systematic review and meta-analysis of clinical trials. *PLoS One* 2012; **7**: e47559 [PMID: 23133515 DOI: 10.1371/journal.pone.0047559]
191 **Simberlund J**, Ferretti CJ, Hollander E. Mesenchymal stem cells in autism spectrum and neurodevelopmental disorders: pitfalls and potential promises. *World J Biol Psychiatry* 2015; **16**: 368-375 [PMID: 26230216 DOI: 10.3109/15622975.2015.1067372]

P- Reviewer: Fatkhudinov T, Miloso M, Oltra E
S- Editor: Ma YJ **L- Editor:** Filipodia **E- Editor:** Bian YN

World Journal of Stem Cells

Submit a Manuscript: https://www.f6publishing.com

World J Stem Cells 2019 February 26; 11(2): 73-83

DOI: 10.4252/wjsc.v11.i2.73

ISSN 1948-0210 (online)

MINIREVIEWS

Human cord blood-derived viral pathogens as the potential threats to the hematopoietic stem cell transplantation safety: A mini review

Ali Noroozi-aghideh, Maryam Kheirandish

ORCID number: Ali Noroozi-aghideh (0000-0002-2811-2659); Maryam Kheirandish (0000-0002-9856-0844).

Author contributions: The author contributed equally to this work.

Conflict-of-interest statement: Authors of this manuscript have no conflicts of interest to disclose.

Manuscript source: Invited manuscript

Received: December 12, 2018
Peer-review started: December 12, 2018
First decision: December 24, 2018
Revised: January 14, 2019
Accepted: January 26, 2019
Article in press: January 26, 2019
Published online: February 26, 2019

Ali Noroozi-aghideh, Department of Hematology, Faculty of Paramedicine, Aja University of Medical Sciences, Tehran 14665-1157, Iran

Maryam Kheirandish, Immunology Department, Blood Transfusion Research Center, High Institute for Research and Education in Transfusion Medicine (IBTO), Tehran 14665-1157, Iran

Corresponding author: Maryam Kheirandish, PhD, Associate Professor, Immunology Department, Blood Transfusion Research Center, High Institute for Research and Education in Transfusion Medicine (IBTO), Hemmat high way next to Milad tower, Tehran 14665-1157, Iran. m.kheirandish@ibto.ir
Telephone: +98-21-88629538
Fax: +98-21-88601577

Abstract

Umbilical cord blood (UCB) is a valuable source of hematopoietic stem cells (HSCs) and potential alternative for bone marrow transplantation for patients who lack human leukocyte antigen (HLA)-matched donors. The main practical advantages of UCB over other HSC sources are the immediate availability, lower incidence of graft-versus-host disease, minimal risk to the donor, and lower requirement for HLA compatibility. However, the use of UCB is limited by delayed engraftment and poor immune reconstitution, leading to a high rate of infection-related mortality. Therefore, severe infectious complications, especially due to viral pathogens remain the leading cause of morbidity and mortality during the post-UCB transplantation (UCBT) period. In this context, careful screening and excluding the viral-contaminated UCB units might be an effective policy to reduce the rate of UCBT-related infection and mortality. Taken together, complete prevention of the transmission of donor-derived viral pathogens in stem cell transplantation is not possible. However, having the knowledge of the transmission route and prevalence of viruses will improve the safety of transplantation. To the best of our knowledge, there are few studies that focused on the risk of virus transmission through the UCB transplant compared to other HSC sources. This review summarizes the general aspects concerning the prevalence, characteristics, and risk factors of viral infections with a focus on the impact of viral pathogens on cord blood transplantation safety.

Key words: Cord blood; Transplantation safety; Viral pathogens

Core tip: Severe infectious complications, especially due to viral pathogens remain the leading cause of the post-transplantation morbidity and mortality. In this context, excluding the viral-contaminated umbilical cord blood (UCB) units might be an effective policy to reduce the infection rate after UCB transplantation (UCBT). Complete prevention of the transmission of donor-derived viral pathogens via UCB is not possible. However, having the knowledge of the transmission route and the prevalence of viruses will improve the transplantation safety by controlled patient management. This minireview summarizes the general aspects concerning the prevalence, characteristics and risk factors of viral infections with a focus on the impact on UCBT safety.

Citation: Noroozi-aghideh A, Kheirandish M. Human cord blood-derived viral pathogens as the potential threats to the hematopoietic stem cell transplantation safety: A mini review. *World J Stem Cells* 2019; 11(2): 73-83
URL: https://www.wjgnet.com/1948-0210/full/v11/i2/73.htm
DOI: https://dx.doi.org/10.4252/wjsc.v11.i2.73

INTRODUCTION

In past years, allogeneic hematopoietic stem cell transplantation (allo-HSCT) has made considerable progress in the treatment of a large variety of malignant and nonmalignant disorders. Human leukocyte antigen (HLA)-identical sibling and HLA-matched unrelated donors are typically the first choices, although it can be achieved for only about 30% of patients. So, umbilical cord blood transplantation (UCBT) is an alternative option for patients with no HLA-matched bone marrow donors[1,2].

Benefits of using cord blood cells include immediate availability of banked UCB units, lower incidence of graft-versus-host disease (GVHD), minimal risk to the donor, and a lower requirement for HLA compatibility between the donor and the recipient[3].

Despite these advantages, UCBT is associated with delayed engraftment and poor immune reconstitution, leading to a high rate of infection-related mortality, up to about 50% in several historical series. Viral infections are important causes of morbidity and mortality in patients undergoing allo-HSCT. Therefore, careful screening and testing of UCB units seems be critical to exclude the potential UCB units with viral contaminations and to reduce the risk of UCB-related virus transmission[4,5].

Fortunately, improvements in molecular diagnostic methods, such as Multiplex polymerase chain reaction (PCR) and Real-time quantitative PCR (RQ-PCR) have facilitated the early diagnosis of viral infections and selection of "virus-safe" UCB units[6-8] (Table 1).

There have been significant strides in using UCB stem cells in cellular therapy, particularly those for neurologic[9-11] or hematopoietic[12-14] cell differentiation, because of their excellent therapeutic efficacy in bone marrow recovery and regenerative medicine. However, the necessity of increase of transplantation safety is recommended. To the best of our knowledge, there are few studies that focused on the risk of virus transmission through the UCB transplant compared to other HSC sources.

Here, we reviewed the prevalence, characteristics, and risk factors of viral infections in UCB transplantation settings.

COMMON VIRAL INFECTIONS IN HSCT RECIPIENTS

Cytomegalovirus (CMV)

Human CMV, also known as human herpesvirus-5 (HHV-5), is a ubiquitous beta-herpesvirus that infects 60%-95% of healthy adults worldwide[15]. This virus is the most common cause of congenital infection worldwide, impacting about one million newborns annually[16].

CMV infection is a leading opportunistic infectious agent in allogeneic HSCT. It has been noted that 30% and 5% of the recipients of allogeneic and autologous HSCT develop CMV disease, respectively. Moreover, the risk of CMV transmission from a seropositive donor to a seronegative recipient is about 30%[17,18].

Table 1 Umbilical cord blood transplantation-related viral infection

Virus type	UCBT-related primary viral infection	UCBT-related virus reactivation	Ref.
CMV	Albano *et al*		[4]
	Abedi *et al*		[6]
	Shin *et al*		[80]
	Al-Awadhi *et al*		[81]
		Tong *et al*	[20]
		Beck *et al*	[21]
		O'Connor *et al*	[22]
		Sinclair *et al*	[23]
	Weinberg *et al*		[26]
HCV	Benova *et al*		[41]
VZV	Tomonari *et al*		[44]
	Patrick *et al*		[45]
	Vandenbosch *et al*		[47]
HHV-6	D'Agaro *et al*		[53]
		Scheurer *et al*	[48]
		Yamane *et al*	[49]
		Hill *et al*	[50]
		Tomonari *et al*	[51]
		Sashihara *et al*	[52]
HHV-7	Abedi *et al*		[8]
HHV-8	Golchin *et al*		[7]
EBV	Hassan *et al*		[62]
	Haut *et al*		[63]
	Ohga *et al*		[64]
	Reddiconto *et al*		[65]
		Auger *et al*	[61]
		Barker *et al*	[67]
		Blaes *et al*	[69]
		Brunstein *et al*	[70]
		Dumas *et al*	[71]
		Kalra *et al*	[72]
AVs		Robin *et al*	[79]

UCBT: Umbilical cord blood transplantation; CMV: Cytomegalovirus; HCV: Hepatitis C virus; VZV: Varicella-zoster virus; HHV-6: Human herpesvirus-6; HHV-7: Human herpesvirus-7; HHV-8: Human herpesvirus-8; EBV: Epstein-Barr virus; AVs: Adenoviruses.

The initial infection is generally asymptomatic or associated with mild flu-like symptoms. In rare cases, it may cause a serious end-organ disease or systemic syndrome, either early or late period after transplantation with a poor prognosis. In some cases of congenital infections, CMV causes severe and permanent consequences such as sensorineural hearing loss, growth retardation, intellectual disability, and even death nevertheless, there are no effective interventions to interrupt the intrauterine transmission[16,19].

CMV infection can indirectly increase the risk of transplant-related mortality (TRM) by mediating the immunosuppressive effects. In this context, CMV has been related to the development of GVHD and bacterial or fungal superinfection, particularly in CMV-seronegative patients who received seropositive allografts[19,20].

Despite the advances in current preventive antiviral strategies and sensitive diagnostic techniques such as PCR-based assays, CMV remains the important cause of serious viral infections in the recipients of UCBT, as well as in allogeneic marrow or peripheral blood SCT. In this way, CMV reactivation rate following UCBT is noted to be 21%-100% and is similar when compared to peripheral blood or bone marrow SCT[21].

It has been reported that up to 30%-40% of seronegative pregnant women who infected by CMV transmit the virus to their fetus, suggesting a high incidence of cord blood contamination by CMV[16]. It has been shown that CMV can establish a lifelong

latency in hematopoietic progenitors and monocytes. Therefore, the virus might be transmitted by these infected cells to the immunocompromised recipient and then become reactivated[22,23] (Table 1). Pergam *et al*[24] indicated that high allograft white blood cell count is an important risk factor associated with CMV transmission due to the role of myeloid cells as a reservoir of latent CMV. In this context, Abedi *et al*[6] analyzed 825 UCB-derived buffy coat samples and reported that 17 samples have been positive for CMV latent infection.

The serostatus of the donor and recipient is the most important risk factor for CMV disease in allo-HSCT recipients. In this regard, CMV-seropositive recipients have been identified to be highly susceptible to developing CMV infection and CMV complications are primarily associated with viral reactivation. Seronegative patients who receive seropositive allografts are also susceptible to CMV transmission. As mentioned above, the risk for transmission of latent CMV from a CMV-seropositive donor to a CMV-seronegative patient is relatively low, but it increases TRM, mainly due to an increased risk for severe bacterial or fungal superinfection[24,25]. Therefore, for a CMV-seronegative recipient, it is preferable to select a CMV-seronegative donor to reduce the possibility of CMV transmission through allograft. On the contrary, using a seropositive donor for a seropositive recipient will probably result in a better outcome. This fact may be related to the transfer of primed CMV-specific T cells present in the allograft to the recipient[24].

Since the pediatric recipients of UCB transplant are primarily CMV-seronegative, CMV transmission by allograft is often of more importance than reactivation of the latent virus in the recipient[24,26]. Therefore, excluding the UCB donations from CMV seropositive mothers might be effective to prevent UCB-related CMV transmission.

Hepatitis B virus

Hepatitis B virus (HBV) is a double-stranded DNA virus, classified in the Hepadnaviridae family. Chronic HBV infection is a serious problem of public health affecting over 240 million people worldwide[27].

In the immunocompetent host, HBV infection is responsible for acute hepatitis, which may progress to chronic infection and lead to cirrhosis or hepatocellular carcinoma. Most HBV carriers, however, may never experience severe liver complications during their lifetime. While the risk of acquiring HBV infection *via* blood transfusion is nowadays extremely low, allogeneic HSCT patients still represent a high-risk group, being susceptible to be infected due to the lack of efficient immunity given both the disease and receiving the conditioning regimen before the transplantation. The prevalence of HBV infection in these patients ranges from 1% to 28%, according to geographic areas. The results of a multicenter study showed that the risk of HBV reactivation, two years after HSCT was 81% for allogeneic and 66% for autologous cases. Patients undergoing HSCT can also develop a de novo HBV infection following the transplantation. The risk of HBV transmission to uninfected recipients of bone marrow transplantation (BMT) is not 100% and the exact risk remains unclear[28,29].

Huang *et al*[30] exposed UCB-derived HSCs to HBV and demonstrated that HBV not only can infect these cells but also can replicate in them, and then suggested the possible role of HSCs as extrahepatic HBV reservoir. On the other hand, other studies have shown the risk of intrauterine transmission of HBV *via* peripheral blood mononuclear cells in addition to transplacental leakage and placental infection. These findings suggest the possibility of HBV transmission by UCB mononuclear cells to the recipient and highlight the importance of routine screening of UCB units[31,32]. To the best of our knowledge, very little published data are available about the prevalence and risk factors for HBV transmission by HSC transplant from UCB source.

Hepatitis C virus

Hepatitis C virus (HCV) is a double-stranded RNA virus of the Flaviviridae family. Global incidence of chronic HCV infection is about 170 million people and approximately 3-4 million more are infected each year[29,33]. As for HBV, patients infected with HCV show a mild to moderate liver disease on long-term monitoring depending on age at infection and host immune response[34].

HCV infection in HSCT recipients might be because of both virus reactivation and de novo infection. HCV reactivation after immunosuppressive therapy has led to fulminant hepatic failure in some cases. Accordingly, in a multicenter study by Locasciulli *et al*[35] the risk of HCV reactivation at 24 mo after HSCT has been 100% and 16% for allogeneic and autologous cases, respectively.

On the other hand, the rate of de novo HCV infection in HSCT recipients of donor-cell origin is controversial. In this context, 50% of the patients receiving an infected marrow became viraemic in a study by Locasciulli *et al*[36], while Shuhart *et al*[37] observed a 100% rate of virus transmission in such cases. Moreover, it has been

reported that HCV can infect HSCs and therefore, virus transmission from HCV-RNA positive donor to an uninfected recipient is possible[38].

HSCT has not a contraindication in HCV infected recipients without any evidence of liver damage. However, HCV-infected HSCT recipients are more prone to develop GVHD and fatal liver failure in comparison with non-infected recipients. Furthermore, outcomes in long-term survivors are significant, and they should be monitored carefully by regular examinations[39,40].

Anti-HCV positive but HCV-RNA negative donors are improbable to infect the recipients and may be selected for transplant donation for the patients without an alternative donor. Accordingly, all anti-HCV-positive donors should be tested for HCV-RNA. However, high-risk anti-HCV negative donors should also be tested for HCV-RNA[33,40].

The risk of vertical HCV transmission is lower than in HBV including 1.7% and 4.3% in children born to women positive for hepatitis C antibody or HCV-RNA, respectively. Despite the possibility of vertical HCV transmission from mother to fetus and possible contamination of UCB units, there is a paucity of published data that have focused on the possibility and outcomes of HCV transmission by UCBT. Future studies using molecular diagnostic methods and clinical monitoring will clarify the prevalence and importance of UCB-related HCV transmission[32,41].

Varicella-zoster virus

Varicella-zoster virus (VZV) or HHV-3 is an exclusively human alphaherpesvirus. The primary infection occurs typically as childhood chickenpox (varicella). As a common feature to all members of the Herpesviridae family, VZV is capable to establish latent infection in its host. It remains in a latent form for decades in cranial nerve ganglia and dorsal root ganglia, and then might become reactivated under the certain conditions. Reactivation of the virus, either spontaneously or following the post-transplant immunosuppression, may cause a painful and debilitating disease known as herpes zoster (shingles)[42,43].

The estimated prevalence of post-SCT VZV infection either primary infection or reactivation in children is as high as 22% to 32% after allogeneic and 9% to 46% after autologous transplantation. Based on previous studies, Older age, pre-transplant irradiation, HLA-mismatched transplantation, chronic GVHD, and recipient pre-transplant VZV seropositivity have been described as predisposing risk factors for VZV disease[44,45]. Accordingly, Umezawa *et al*.[46] retrospectively analyzed the clinical symptoms of VZV disease and risk factors for disease progression in allogeneic HSCT patients. They suggested that gender and total body irradiation did not affect the development of VZV dissemination, and concluded that delayed antiviral therapy is a serious risk factor for VZV dissemination following the allogeneic HSCT.

It has also been shown that VZV disease is more frequent and more severe after UCBT than other types of HSCT. In this regard, Tomonari[44] showed 80% cumulative incidence of VZV reactivation in adult patients who had undergone UCBT from unrelated donors. In another study, Vandenbosch and colleagues[47] compared the VZV reactivation rate in the total of 114 VZV seropositive children who had received UCBT or T-replete BMT and reported an incidence of 46% of VZV disease at 3 years after UCBT. This higher frequency in UCBT recipients may be related to delayed immune reconstitution after UCBT and therefore, necessitates the preemptive therapy or prophylaxis in these patients.

On the other hand, Patrick *et al*.[45] conducted a retrospective study to assess the efficacy of routine screening for identification of HSV or VZV viremia following HSCT. They aimed to discuss whether this screening identifies any patients with viremia who had not been identified via clinical manifestations. Finally, they concluded in agreement with the recommendation of the European Conference on Infections in Leukemia that routine screening for VZV is not obligatory in the pediatric HSCT recipients but regular clinical assessment should be performed.

HHV-6

HHV-6 belongs to the beta herpesviridae subfamily and exists as two closely related variants (A and B). Pathogenicity of HHV-6A is uncertain, whereas HHV-6B is the most frequent causative agent of HHV-6-related human diseases[48].

This virus is an opportunistic ubiquitous agent that infects most children in the early years of life. Primary infection is mainly associated with exanthema subitum (also called roseola infantum) and related febrile rash illnesses. Like the other herpesviruses, HHV-6 has the ability to persist in various cells of the host, especially in monocyte/macrophages and then become reactivated from latency during immunodeficiency, especially in HSCT recipients[26].

Several retrospective studies have shown the higher incidence of HHV-6 reactivation in the recipients of UCB than in patients receiving other stem cell sources,

and suggested to be related with high mortality rate and fatal complications including acute GVHD, bone marrow suppression, and CNS disease, especially the syndrome of post-transplantation acute limbic encephalitis called HHV-6-PALE[48,49]. Scheurer *et al*[48] conducted a systematic literature review and meta-analysis to investigate the prevalence and clinical significance of HHV-6 reactivation in UCBT recipients. They showed that prevalence of HHV-6 reactivation and related- encephalitis were significantly higher in UCB than non-UCB recipients, and emphasized the monitoring of UCB recipients for HHV-6 reactivation.

However, literature focusing on HHV-6 primary infection after UCBT and especially, HHV-6 transmission by UCB is scarce. Based on available data, HHV-6 DNA is detectable in plasma samples from 40% to 50% of HSC transplant recipients from adult donors and up to 80% of unrelated UCB recipients within 6 wk after transplantation[50]. Accordingly, Tomonari *et al*[51] have also shown the higher HHV-6 viral load using quantitative PCR in adult patients who underwent UCBT compared with unrelated BMT.

These reports in addition to the possibility of intrauterine transmission of HHV-6 and contamination of UCB cells suggest the possibility of HHV-6 transmission by UCB allograft and subsequent primary infection. This phenomenon might be associated with less efficient immunity against HHV6 in cord blood[52,53]. While more studies are needed to confirm and define the importance of UCBT in HHV-6 transmission, routine screening for HHV-6 and exclusion of PCR-positive UCB units seems to be efficient to prevent UCB-mediated virus transmission and related serious outcomes.

HHV-7

HHV-7 is a member of the beta herpesviridae family. Like HHV-6, it causes primary infection most commonly in infancy and childhood and is able to cause roseola. However, symptomatic HHV-7 infection is less common and occurs at a later age than with HHV-6. This virus remains latent in the human host and can become reactivated after transplantation. Right now, no clinical symptoms or significant laboratory abnormalities were found to be related to HHV-7 reactivation[54].

Owing to its selective tropism for CD4+ T lymphocytes and possibility of worsening the immunodeficiency state, the HHV-7 infection might be a serious threat in transplant recipients and impair the transplant engraftment. Mirandola *et al*[55] incubated cord blood CD34+ cells with HHV-7 and showed that HHV-7 affects the differentiation and survival of CD34+ hematopoietic progenitors. Consistently, Gonelli *et al*[56] showed that HHV-7 induces apoptosis of cord blood CD61+ megakaryocytic cells in vitro and may impair the development of megakaryocytic cells. Accordingly, Chan *et al*[57] noted the association of HHV-7 reactivation with delayed neutrophil engraftment following BMT. These findings are real causes for concern in patients with high risk of HHV-7 infection, such as HSCT patients.

Abedi *et al*[8] assayed a large number of UCB samples by quantitative real-time PCR and reported that 3.2% and 0.48% were positive for HHV-7 DNA in buffy coat and plasma as latent and active infections, respectively. In contrast, none of the samples were positive for HHV-7 DNA in the study by Weinberg[26].

Based on the high seroprevalence of HHV-7 in the general population and the role of this virus in myelopoiesis impairment, it seems that detection of HHV-7 in UCB donors could be a useful tool for prevention of UCB- associated HHV-7 transmission[55].

HHV-8

HHV-8, also called Kaposi sarcoma (KS)-associated herpesvirus, is a gamma-herpesvirus. Apart from KS, HHV-8 is the causative agent of lymphoproliferative disorders such as primary effusion lymphoma and multicentric Castleman's disease in immunosuppressed adults. HHV-8 has also been related to fatal hematopoiesis impairment in an autologous stem cell recipient[58,59].

The certain ways of HHV-8 transmission are unclear. Previous studies have suggested the sexual mode of virus transmission in homosexual men and horizontal transmission *via* saliva in endemic areas. Notably, HHV-8 from seropositive donor cell origin may be transmitted to the recipient[7,58].

Previous studies have indicated the minimum risk for vertical transmission of HHV-8 from mother to child during pregnancy, and therefore, the low seroprevalence of HHV-8 infection in UCB samples[7,26]. Accordingly, Golchin *et al*[7] surveyed a large number of UCB samples by real-time PCR and reported an only 1.38% HHV-8 prevalence in UCB mononuclear cells. However, HHV-8 has the ability to infect cord blood mononuclear cells and cause post-UCBT infection, and therefore it deserves the attention in UCBT settings[26].

Accordingly, defining the HHV-8 serostatus and avoiding matches between HHV-

8-positive donors and HHV-8-negative recipients appear to be effective to prevent virus transmission by UCBT in areas of high endemicity.

Epstein-Barr virus

Epstein-Barr virus (EBV) is a widespread gammaherpesvirus that infects over 90% of humans. In healthy individuals, EBV infection is tightly controlled by the immune system. After primary infection, EBV establishes a lifelong asymptomatic latent infection in B-cells of immunocompetent hosts. Later, immunosuppressive therapy given at HSCT may lead to EBV reactivation and subsequent EBV diseases, particularly life-threatening post-transplant lymphoproliferative disease (PTLD)[60,61]. Some studies have also reported the cases of UCB-transplanted patients who developed the EBV-related PTLD from graft-cell origin and proved the transmission of EBV infection by donor cells[62-65] (Table 1). EBV reactivation frequently occurs in patients having allogeneic HSCT and several risk factors for the development of EBV disease after HSCT have been reported, such as T-cell depletion, donor stem cell source, HLA mismatch, severe acute GVHD, EBV serostatus, the presence of CMV disease and possibly younger age[60,61].

Blood EBV DNA level has proven to be a predictive biomarker in allogeneic HSCT patients. In a clinical follow-up project, Li *et al*[61] evaluated the impact of EBV load on the survival of patients who had received transplant form different sources of stem cells, and found that patients with very low or high EBV-DNA load early after transplantation had a poor prognosis, compared to patients with intermediate levels.

Sundin and others have demonstrated that PTLD mostly originates from donor-derived cells, and risk for PTLD increases in positive donor/negative recipient (D+/R−) pairs. Therefore, selection of EBV-seronegative donors could reduce the risk of PTLD development[66-68]. There are also reports concerning the higher incidence of PTLD in patients who underwent UCBT compared with other HSC sources, especially when anti-thymocyte globulin is added to conditioning regimen[69,70]. Contrary to these findings, in a retrospective multicenter study, Dumas *et al*[71] studied 175 UCBT recipients for whom EBV RQ-PCR monitoring was performed, and concluded conversely that UCBT recipients are not more susceptible to EBV events if EBV load is regularly monitored and preemptive treatment performed.

Despite the low incidence of congenital EBV infection, the occurrence of EBV-associated PTLD is possible at least in unrelated UCBT setting and adds one additional fatal complication following UCBT. Therefore, EBV screening by sensitive and reliable tests may play an important role in the future evaluation of UCB units to use in transplantation[71,72].

Human adenoviruses

Human adenoviruses (AVs) are non-enveloped double-stranded DNA viruses that belong to the Adenoviridae family. AVs are divided into six subgroups (A through G) based on common biologic, immunologic, morphologic and genetic features[73].

In immunocompetent individuals, AV primary infection is mostly subclinical and self-limiting, although some severe courses have been described[74]. However, AV infection is more clinically important in patients with impaired immunity, particularly in HSCT patients and causes fatal complications. It is also more common to children than adults following the HSCT. In this regard, two studies compared the rates of AV isolation in children and adults after BMT and found 21% and 23% of children to be positive compared with 9% in adults, respectively[75,76].

In the allogeneic HSCT setting, AV infection can arise from *de novo* infection or reactivation of the latent endogenous virus. *De novo* infection can occur by transmission of the exogenous virus in D+/R− pairs. In this context, previous studies have demonstrated the 4-fold higher risk of primary AV infections in patients that received HSC graft from seropositive donors compared to seronegative ones. However, reactivation of endogenous latent AV seems to be the main cause of AV-associated fatal complication in immunocompromised patients[74,77,78].

Main risk factors predisposing an invasive AV infection include childhood, donor AV serostatus, severe GVHD, HLA-mismatched transplantation, CMV viremia, and T-cell depletion. Furthermore, UCBT is suggested to be an independent risk factor for AV infection probably due to the lack of mature lymphocytes in CB, as cellular components of antiviral defense[79].

Runde *et al*[77] studied the prevalence and risk factors of AV infection in allo-HSCT recipients and showed that AV antibody status of the donor had a strong impact on the development of AV infection in the recipients. Their finding supports indirectly the hypothesis that AV infection following HSCT is not always the result of virus reactivation, and the virus might be transmitted by infected cells from AV seropositive donors to the recipients. This hypothesis is proved if the same AV is detected by molecular analyses in donors and corresponding recipients.

To the best of our knowledge, there are few studies that have focused on the risk of AV transmission by UCB transplant compared to other HSC sources. However, the presence of AV DNA positive cells besides naivety of T cells serves UCB as a putative source of AV infection in the immunocompromised recipients.

CONCLUSION

The amount of threat for transmission of infections carried with allogeneic transplantation, notably of viruses, is largely unknown and difficult to assess. The approach to virological screening of UCB stem cell donors varies with national and regional regulations. Over recent years, UCBT has become a valuable alternative for patients who lack a suitably matched bone marrow donor. However, UCBT is associated with several limitations, in particular, the low number of mature lymphocytes and poor immune reconstitution. Given these limitations, virus transmission *via* UCB may cause serious infectious complication in the immunocompromised recipients, and therefore, excluding the viral-contaminated UCB units might be an effective policy to reduce the rate of UCBT-related infection and mortality. Taken together, complete prevention of the transmission of donor-derived viral pathogens in SCT is not possible. However, having the knowledge of the transmission route and the prevalence of viruses will improve the safety of transplantation.

REFERENCES

1 **Ballen KK**, Koreth J, Chen YB, Dey BR, Spitzer TR. Selection of optimal alternative graft source: mismatched unrelated donor, umbilical cord blood, or haploidentical transplant. *Blood* 2012; **119**: 1972-1980 [PMID: 22210876 DOI: 10.1182/blood-2011-11-354563]

2 **Ballen KK**, Gluckman E, Broxmeyer HE. Umbilical cord blood transplantation: the first 25 years and beyond. *Blood* 2013; **122**: 491-498 [PMID: 23673863 DOI: 10.1182/blood-2013-02-453175]

3 **Montoro J**, Piñana JL, Moscardó F, Sanz J. Infectious Complications after Umbilical Cord-Blood Transplantation from Unrelated Donors. *Mediterr J Hematol Infect Dis* 2016; **8**: e2016051 [PMID: 27872731 DOI: 10.4084/MJHID.2016.051]

4 **Albano MS**, Ciubotariu R, Dobrila L, Tarnawski M, DeLeon M, Watanabe C, Krishnan S, Scaradavou A, Rubinstein P. Cytomegalovirus viral load in cord blood and impact of congenital infection on markers of hematopoietic progenitor cell potency. *Transfusion* 2017; **57**: 2768-2774 [PMID: 28758211 DOI: 10.1111/trf.14257]

5 **Meissner-Roloff M**, Gaggia L, Vermeulen M, Mazanderani AFH, du Plessis NM, Steel HC, Pepper MS. Strategies for screening cord blood for a public cord blood bank in high HIV prevalence regions. *Glob Health Epidemiol Genom* 2018; **3**: e9 [PMID: 30263133 DOI: 10.1017/gheg.2018.6]

6 **Abedi E**, Kheirandish M, Sharifi Z, Samiee S, Kokhaei P, Pourpak Z, Ashraf MJ. Quantification of Active and Latent Form of Human Cytomegalovirus Infection in Umbilical Cord Blood Donors by Real-Time PCR. *Int J Organ Transplant Med* 2017; **8**: 140-145 [PMID: 28924462]

7 **Golchin N**, Kheirandish M, Sharifi Z, Samiee S, Kokhaei P, Pourpak Z. Quantification of viral genome in cord blood donors by real time PCR to investigate human herpesvirus type 8 active infection. *Transfus Apher Sci* 2015; **53**: 378-380 [PMID: 26283174 DOI: 10.1016/j.transci.2015.08.001]

8 **Abedi E**, Kheirandish M, Sharifi Z, Samiee S, Kokhaei P, Pourpak Z, Ashraf MJ. Quantitative polymerase chain reaction for detection of human herpesvirus-7 infection in umbilical cord blood donors. *Transpl Infect Dis* 2015; **17**: 21-24 [PMID: 25440722 DOI: 10.1111/tid.12319]

9 **Rafieemehr H**, Kheyrandish M, Soleimani M. Neuroprotective Effects of Transplanted Mesenchymal Stromal Cells-derived Human Umbilical Cord Blood Neural Progenitor Cells in EAE. *Iran J Allergy Asthma Immunol* 2015; **14**: 596-604 [PMID: 26725557]

10 **Kheirandish M**, Gavgani SP, Samiee S. The effect of hypoxia preconditioning on the neural and stemness genes expression profiling in human umbilical cord blood mesenchymal stem cells. *Transfus Apher Sci* 2017; **56**: 392-399 [PMID: 28428031 DOI: 10.1016/j.transci.2017.03.015]

11 **Rafieemehr H**, Kheirandish M, Soleimani M. Improving the neuronal differentiation efficiency of umbilical cord blood-derived mesenchymal stem cells cultivated under appropriate conditions. *Iran J Basic Med Sci* 2015; **18**: 1100-1106 [PMID: 26949497]

12 **Aghideh AN**, Kheirandish M, Abolghasemi H, Gharehbaghian A. Platelet growth factors suppress ex vivo expansion and enhance differentiation of umbilical cord blood CD133+ stem cells to megakaryocyte progenitor cells. *Growth Factors* 2010; **28**: 409-416 [PMID: 20854188 DOI: 10.3109/08977194.2010.504722]

13 **Dezaki ZA**, Kheirandish M. Hypoxia Preconditioning Promotes Survival And Clonogenic Capacity of Human Umbilical Cord Blood Mesenchymal Stem Cells. *IJBC* 2018; **10**: 43-49

14 **Rafieemehr H**, Kheirandish M, Soleimani M. A New Two Step Induction Protocol for Neural Differentiation of Human Umbilical Cord Blood- Derived Mesenchymal Stem Cells. *IJBC* 2015; **7**: 111-116

15 **Wu SJ**, Villarreal DO, Shedlock DJ, Weiner DB. Synthetic DNA approach to cytomegalovirus vaccine/immune therapy. *Adv Exp Med Biol* 2015; **848**: 131-148 [PMID: 25757619 DOI: 10.1007/978-1-4939-2432-5_7]

16 **Itell HL**, Nelson CS, Martinez DR, Permar SR. Maternal immune correlates of protection against placental transmission of cytomegalovirus. *Placenta* 2017; **60** Suppl 1: S73-S79 [PMID: 28456432 DOI: 10.1016/j.placenta.2017.04.011]

17 **Ljungman P**, Hakki M, Boeckh M. Cytomegalovirus in hematopoietic stem cell transplant recipients.

Hematol Oncol Clin North Am 2011; **25**: 151-169 [PMID: 21236396 DOI: 10.1016/j.hoc.2010.11.011]
18 **Azevedo LS**, Pierrotti LC, Abdala E, Costa SF, Strabelli TM, Campos SV, Ramos JF, Latif AZ, Litvinov N, Maluf NZ, Caiaffa Filho HH, Pannuti CS, Lopes MH, Santos VA, Linardi Cda C, Yasuda MA, Marques HH. Cytomegalovirus infection in transplant recipients. *Clinics (Sao Paulo)* 2015; **70**: 515-523 [PMID: 26222822 DOI: 10.6061/clinics/2015(07)09]
19 **Solano C**, Navarro D. Clinical virology of cytomegalovirus infection following hematopoietic transplantation. *Future Virol* 2010; **5**: 111-124 [DOI: 10.2217/fvl.09.64]
20 **Tong J**, Sun Z, Liu H, Geng L, Zheng C, Tang B, Song K, Yao W, Liu X. Risk factors of CMV infection in patients after umbilical cord blood transplantation: a multicenter study in China. *Chin J Cancer Res* 2013; **25**: 695-703 [PMID: 24385697 DOI: 10.3978/j.issn.1000-9604.2013.11.08]
21 **Beck JC**, Wagner JE, DeFor TE, Brunstein CG, Schleiss MR, Young JA, Weisdorf DH, Cooley S, Miller JS, Verneris MR. Impact of cytomegalovirus (CMV) reactivation after umbilical cord blood transplantation. *Biol Blood Marrow Transplant* 2010; **16**: 215-222 [PMID: 19786112 DOI: 10.1016/j.bbmt.2009.09.019]
22 **O'Connor CM**, Murphy EA. A myeloid progenitor cell line capable of supporting human cytomegalovirus latency and reactivation, resulting in infectious progeny. *J Virol* 2012; **86**: 9854-9865 [PMID: 22761372 DOI: 10.1128/JVI.01278-12]
23 **Sinclair J**. Human cytomegalovirus: Latency and reactivation in the myeloid lineage. *J Clin Virol* 2008; **41**: 180-185 [PMID: 18164651 DOI: 10.1016/j.jcv.2007.11.014]
24 **Pergam SA**, Xie H, Sandhu R, Pollack M, Smith J, Stevens-Ayers T, Ilieva V, Kimball LE, Huang ML, Hayes TS, Corey L, Boeckh MJ. Efficiency and risk factors for CMV transmission in seronegative hematopoietic stem cell recipients. *Biol Blood Marrow Transplant* 2012; **18**: 1391-1400 [PMID: 22387334 DOI: 10.1016/j.bbmt.2012.02.008]
25 **Ciáurriz M**, Zabalza A, Beloki L, Mansilla C, Pérez-Valderrama E, Lachén M, Bandrés E, Olavarría E, Ramírez N. The immune response to cytomegalovirus in allogeneic hematopoietic stem cell transplant recipients. *Cell Mol Life Sci* 2015; **72**: 4049-4062 [PMID: 26174234 DOI: 10.1007/s00018-015-1986-z]
26 **Weinberg A**, Enomoto L, Li S, Shen D, Coll J, Shpall EJ. Risk of transmission of herpesviruses through cord blood transplantation. *Biol Blood Marrow Transplant* 2005; **11**: 35-38 [PMID: 15625542 DOI: 10.1016/j.bbmt.2004.09.005]
27 **Caligiuri P**, Cerruti R, Icardi G, Bruzzone B. Overview of hepatitis B virus mutations and their implications in the management of infection. *World J Gastroenterol* 2016; **22**: 145-154 [PMID: 26755866 DOI: 10.3748/wjg.v22.i1.145]
28 **Chakrabarti S**, Mukherjee S. Prevention and treatment of hepatitis virus infections in hematopoietic stem cell transplant recipients. *Mediterr J Hematol Infect Dis* 2009; **1**: e2009017 [PMID: 21415956 DOI: 10.4084/MJHID.2009.017]
29 **Locasciulli A**, Montante B, Morelli E, Gulino V, Proia A, Pinazzi MB. Hepatitis B and C in hematopoietic stem cell transplant. *Mediterr J Hematol Infect Dis* 2009; **1**: e2009016 [PMID: 21415955 DOI: 10.4084/MJHID.2009.016]
30 **Huang Y**, Yan Q, Fan R, Song S, Ren H, Li Y, Lan Y. Hepatitis B Virus Replication in CD34+ Hematopoietic Stem Cells From Umbilical Cord Blood. *Med Sci Monit* 2016; **22**: 1673-1681 [PMID: 27188537 DOI: 10.12659/MSM.898680]
31 **Borgia G**, Maraolo AE, Gentile I. Hepatitis B mother-to-child transmission and infants immunization: we have not come to the end of the story yet. *Infect Dis (Lond)* 2017; **49**: 584-587 [PMID: 28316268 DOI: 10.1080/23744235.2017.1303746]
32 **Mavilia MG**, Wu GY. Mechanisms and Prevention of Vertical Transmission in Chronic Viral Hepatitis. *J Clin Transl Hepatol* 2017; **5**: 119-129 [PMID: 28660149 DOI: 10.14218/JCTH.2016.00067]
33 **Shi Y**, Lan Y, Cao F, Teng Y, Li L, Wang F, Li J, Zhou J, Li Y. Infected hematopoietic stem cells and with integrated HBV DNA generate defective T cells in chronic HBV infection patients. *J Viral Hepat* 2014; **21**: e39-e47 [PMID: 24620791 DOI: 10.1111/jvh.12236]
34 **Manns MP**, Buti M, Gane E, Pawlotsky JM, Razavi H, Terrault N, Younossi Z. Hepatitis C virus infection. *Nat Rev Dis Primers* 2017; **3**: 17006 [PMID: 28252637 DOI: 10.1038/nrdp.2017.6]
35 **Locasciulli A**, Bruno B, Alessandrino EP, Meloni G, Arcese W, Bandini G, Cassibba V, Rotoli B, Morra E, Majolino I, Alberti A, Bacigalupo A; Italian Cooperative Group for Blood and Marrow Transplantation. Hepatitis reactivation and liver failure in haemopoietic stem cell transplants for hepatitis B virus (HBV)/hepatitis C virus (HCV) positive recipients: a retrospective study by the Italian group for blood and marrow transplantation. *Bone Marrow Transplant* 2003; **31**: 295-300 [PMID: 12621466 DOI: 10.1038/sj.bmt.1703826]
36 **Locasciulli A**, Testa M, Valsecchi MG, Bacigalupo A, Solinas S, Tomas JF, Ljungman P, Alberti A. The role of hepatitis C and B virus infections as risk factors for severe liver complications following allogeneic BMT: a prospective study by the Infectious Disease Working Party of the European Blood and Marrow Transplantation Group. *Transplantation* 1999; **68**: 1486-1491 [PMID: 10589944]
37 **Shuhart MC**, Myerson D, Childs BH, Fingeroth JD, Perry JJ, Snyder DS, Spurgeon CL, Bevan CA, McDonald GB. Marrow transplantation from hepatitis C virus seropositive donors: transmission rate and clinical course. *Blood* 1994; **84**: 3229-3235 [PMID: 7949194]
38 **Pascutti MF**, Erkelens MN, Nolte MA. Impact of Viral Infections on Hematopoiesis: From Beneficial to Detrimental Effects on Bone Marrow Output. *Front Immunol* 2016; **7**: 364 [PMID: 27695457 DOI: 10.3389/fimmu.2016.00364]
39 **Socié G**, de Latour RP, McDonald GB. Hepatitis C virus and allogeneic stem cell transplantation still matters! *Haematologica* 2009; **94**: 170-172 [PMID: 19181791 DOI: 10.3324/haematol.2008.002048]
40 **Thomas P**, Santiago T, Dallas MH. Treatment of hepatitis C in a pediatric patient using simeprevir and sofosbuvir immediately after an umbilical cord blood transplantation. *Bone Marrow Transplant* 2016; **51**: 735-737 [PMID: 26752145 DOI: 10.1038/bmt.2015.309]
41 **Benova L**, Mohamoud YA, Calvert C, Abu-Raddad LJ. Vertical transmission of hepatitis C virus: systematic review and meta-analysis. *Clin Infect Dis* 2014; **59**: 765-773 [PMID: 24928290 DOI: 10.1093/cid/ciu447]
42 **Kennedy PG**, Rovnak J, Badani H, Cohrs RJ. A comparison of herpes simplex virus type 1 and varicella-zoster virus latency and reactivation. *J Gen Virol* 2015; **96**: 1581-1602 [PMID: 25794504 DOI: 10.1099/vir.0.000128]
43 **Mueller N**, Gilden D, Cohrs R, Mahalingam R, Nagel M. Varicella zoster virus infection: clinical features, molecular pathogenesis of disease, and latency. *Neurol Clin* 2008; **26**: 675-697 [DOI: 10.1016/j.ncl.2008.03.011]

44 **Tomonari A**, Iseki T, Takahashi S, Ooi J, Takasugi K, Shimohakamada Y, Ohno N, Nagamura F, Uchimaru K, Tani K, Tojo A, Asano S. Varicella-zoster virus infection in adult patients after unrelated cord blood transplantation: a single institute experience in Japan. *Br J Haematol* 2003; **122**: 802-805 [PMID: 12930392 DOI: 10.1046/j.1365-2141.2003.04496.x]

45 **Patrick K**, Ali M, Richardson SE, Gassas A, Egeler M, Krueger J, Lowry J, Allen U, Schechter T. The yield of monitoring for HSV and VZV viremia in pediatric hematopoietic stem cell transplant patients. *Pediatr Transplant* 2015; **19**: 640-644 [PMID: 26148054 DOI: 10.1111/petr.12551]

46 **Umezawa Y**, Kakihana K, Oshikawa G, Kobayashi T, Doki N, Sakamaki H, Ohashi K. Clinical features and risk factors for developing varicella zoster virus dissemination following hematopoietic stem cell transplantation. *Transpl Infect Dis* 2014; **16**: 195-202 [PMID: 24438510 DOI: 10.1111/tid.12181]

47 **Vandenbosch K**, Ovetchkine P, Champagne MA, Haddad E, Alexandrov L, Duval M. Varicella-zoster virus disease is more frequent after cord blood than after bone marrow transplantation. *Biol Blood Marrow Tr* 2008; **14**: 867-871 [DOI: 10.1016/j.bbmt.2008.05.006]

48 **Scheurer ME**, Pritchett JC, Amirian ES, Zemke NR, Lusso P, Ljungman P. HHV-6 encephalitis in umbilical cord blood transplantation: a systematic review and meta-analysis. *Bone Marrow Transplant* 2013; **48**: 574-580 [PMID: 23000642 DOI: 10.1038/bmt.2012.180]

49 **Yamane A**, Mori T, Suzuki S, Mihara A, Yamazaki R, Aisa Y, Nakazato T, Shimizu T, Ikeda Y, Okamoto S. Risk factors for developing human herpesvirus 6 (HHV-6) reactivation after allogeneic hematopoietic stem cell transplantation and its association with central nervous system disorders. *Biol Blood Marrow Transplant* 2007; **13**: 100-106 [PMID: 17222758 DOI: 10.1016/j.bbmt.2006.09.003]

50 **Hill JA**, Koo S, Guzman Suarez BB, Ho VT, Cutler C, Koreth J, Armand P, Alyea EP, Baden LR, Antin JH, Soiffer RJ, Marty FM. Cord-blood hematopoietic stem cell transplant confers an increased risk for human herpesvirus-6-associated acute limbic encephalitis: a cohort analysis. *Biol Blood Marrow Transplant* 2012; **18**: 1638-1648 [PMID: 22564265 DOI: 10.1016/j.bbmt.2012.04.016]

51 **Tomonari A**, Takahashi S, Ooi J, Iseki T, Takasugi K, Uchiyama M, Konuma T, Futami M, Ohno N, Uchimaru K, Tojo A, Asano S. Human herpesvirus 6 variant B infection in adult patients after unrelated cord blood transplantation. *Int J Hematol* 2005; **81**: 352-355 [PMID: 15914369 DOI: 10.1532/IJH97.04183]

52 **Sashihara J**, Tanaka-Taya K, Tanaka S, Amo K, Miyagawa H, Hosoi G, Taniguchi T, Fukui T, Kasuga N, Aono T, Sako M, Hara J, Yamanishi K, Okada S. High incidence of human herpesvirus 6 infection with a high viral load in cord blood stem cell transplant recipients. *Blood* 2002; **100**: 2005-2011 [PMID: 12200359]

53 **D'Agaro P**, Burgnich P, Comar M, Dal Molin G, Bernardon M, Busetti M, Alberico S, Poli A, Campello C; SIGO Italian Group. HHV-6 is frequently detected in dried cord blood spots from babies born to HIV-positive mothers. *Curr HIV Res* 2008; **6**: 441-446 [PMID: 18855654 DOI: 10.2174/157016208785861122]

54 **Grinde B**. Herpesviruses: latency and reactivation - viral strategies and host response. *J Oral Microbiol* 2013; **5** [PMID: 24167660 DOI: 10.3402/jom.v5i0.22766]

55 **Mirandola P**, Secchiero P, Pierpaoli S, Visani G, Zamai L, Vitale M, Capitani S, Zauli G. Infection of CD34(+) hematopoietic progenitor cells by human herpesvirus 7 (HHV-7). *Blood* 2000; **96**: 126-131 [PMID: 10891440]

56 **Gonelli A**, Mirandola P, Grill V, Secchiero P, Zauli G. Human herpesvirus 7 infection impairs the survival/differentiation of megakaryocytic cells. *Haematologica* 2002; **87**: 1223-1225 [PMID: 12414354]

57 **Chan PK**, Peiris JS, Yuen KY, Liang RH, Lau YL, Chen FE, Lo SK, Cheung CY, Chan TK, Ng MH. Human herpesvirus-6 and human herpesvirus-7 infections in bone marrow transplant recipients. *J Med Virol* 1997; **53**: 295-305 [PMID: 9365899]

58 **Heyrman B**, De Becker A, Schots R. A case report of immunosuppression-related Kaposi's sarcoma after autologous stem cell transplantation. *BMC Res Notes* 2016; **9**: 188 [PMID: 27012530 DOI: 10.1186/s13104-016-1991-9]

59 **Cuzzola M**, Irrera G, Iacopino O, Cuzzocrea A, Messina G, Console G, Iacopino G, Morabito F. Bone marrow failure associated with herpesvirus 8 infection in a patient undergoing autologous peripheral blood stem cell transplantation. *Clin Infect Dis* 2003; **37**: e102-106 [DOI: 10.1086/377268]

60 **Li Q**, Rane L, Poiret T, Zou J, Magalhaes I, Ahmed R, Du Z, Vudattu N, Meng Q, Gustafsson-Jernberg Å, Winiarski J, Ringdén O, Maeurer M, Remberger M, Ernberg I. Both high and low levels of cellular Epstein-Barr virus DNA in blood identify failure after hematologic stem cell transplantation in conjunction with acute GVHD and type of conditioning. *Oncotarget* 2016; **7**: 30230-30240 [PMID: 27102298 DOI: 10.18632/oncotarget.8803]

61 **Auger S**, Orsini M, Céballos P, Fegueux N, Kanouni T, Caumes B, Klein B, Villalba M, Rossi JF. Controlled Epstein-Barr virus reactivation after allogeneic transplantation is associated with improved survival. *Eur J Haematol* 2014; **92**: 421-428 [PMID: 24400833 DOI: 10.1111/ejh.12260]

62 **Hassan R**, Stefanoff CG, Maradei S, Fernandes GA, Barros MH, Carestiato FN, Romano SO, Bouzas LF, Zalcberg IR. EBV-associated post transplant lymphoproliferative disorder of the 'loser' graft cell origin following double unrelated umbilical cord blood transplantation. *Bone Marrow Transplant* 2009; **44**: 193-195 [PMID: 19204712 DOI: 10.1038/bmt.2008.445]

63 **Haut PR**, Kovarik P, Shaw PH, Walterhouse D, Jenson HB, Kletzel M. Detection of EBV DNA in the cord blood donor for a patient developing Epstein-Barr virus-associated lymphoproliferative disorder following mismatched unrelated umbilical cord blood transplantation. *Bone Marrow Transplant* 2001; **27**: 761-765 [PMID: 11360119 DOI: 10.1038/sj.bmt.1702770]

64 **Ohga S**, Kanaya Y, Maki H, Takada H, Ohshima K, Kanda M, Nomura A, Suminoe A, Matsuzaki A, Hara T. Epstein-Barr virus-associated lymphoproliferative disease after a cord blood transplant for Diamond-Blackfan anemia. *Bone Marrow Transplant* 2000; **25**: 209-212 [PMID: 10673683 DOI: 10.1038/sj.bmt.1702138]

65 **Reddiconto G**, Chiusolo P, Fiorini A, Farina G, Laurenti L, Martini M, Marchetti S, Fadda G, Leone G, Sica S. Assessment of cellular origin and EBV status in a PTLD after double cord blood transplantation. *Leukemia* 2007; **21**: 2552-2554 [PMID: 17597809 DOI: 10.1038/sj.leu.2404818]

66 **Sundin M**, Le Blanc K, Ringdén O, Barkholt L, Omazic B, Lergin C, Levitsky V, Remberger M. The role of HLA mismatch, splenectomy and recipient Epstein-Barr virus seronegativity as risk factors in post-transplant lymphoproliferative disorder following allogeneic hematopoietic stem cell transplantation. *Haematologica* 2006; **91**: 1059-1067 [PMID: 16885046]

67 **Barker JN**, Doubrovina E, Sauter C, Jaroscak JJ, Perales MA, Doubrovin M, Prockop SE, Koehne G, O'Reilly RJ. Successful treatment of EBV-associated posttransplantation lymphoma after cord blood transplantation using third-party EBV-specific cytotoxic T lymphocytes. *Blood* 2010; **116**: 5045-5049

[PMID: 20826724 DOI: 10.1182/blood-2010-04-281873]
68 **Heslop HE**, Savoldo B, Rooney CM. Cellular therapy of Epstein-Barr-virus-associated post-transplant lymphoproliferative disease. *Best Pract Res Clin Haematol* 2004; **17**: 401-413 [PMID: 15498712 DOI: 10.1016/j.beha.2004.05.007]
69 **Blaes AH**, Cao Q, Wagner JE, Young JA, Weisdorf DJ, Brunstein CG. Monitoring and preemptive rituximab therapy for Epstein-Barr virus reactivation after antithymocyte globulin containing nonmyeloablative conditioning for umbilical cord blood transplantation. *Biol Blood Marrow Transplant* 2010; **16**: 287-291 [PMID: 19835968 DOI: 10.1016/j.bbmt.2009.10.008]
70 **Brunstein CG**, Weisdorf DJ, DeFor T, Barker JN, Tolar J, van Burik JA, Wagner JE. Marked increased risk of Epstein-Barr virus-related complications with the addition of antithymocyte globulin to a nonmyeloablative conditioning prior to unrelated umbilical cord blood transplantation. *Blood* 2006; **108**: 2874-2880 [PMID: 16804113 DOI: 10.1182/blood-2006-03-011791]
71 **Dumas PY**, Ruggeri A, Robin M, Crotta A, Abraham J, Forcade E, Bay JO, Michallet M, Bertrand Y, Socié G, Ionescu I, Gluckman E, Milpied N, Rocha V. Incidence and risk factors of EBV reactivation after unrelated cord blood transplantation: a Eurocord and Société Française de Greffe de Moelle-Therapie Cellulaire collaborative study. *Bone Marrow Transplant* 2013; **48**: 253-256 [PMID: 22773124 DOI: 10.1038/bmt.2012.117]
72 **Kalra A**, Roessner C, Jupp J, Williamson T, Tellier R, Chaudhry A, Khan F, Taparia M, Jimenez-Zepeda VH, Stewart DA, Daly A, Storek J. Epstein-barr virus DNAemia monitoring for the management of post-transplant lymphoproliferative disorder. *Cytotherapy* 2018; **20**: 706-714 [PMID: 29580864 DOI: 10.1016/j.jcyt.2018.02.367]
73 **Russell WC**. Adenoviruses: update on structure and function. *J Gen Virol* 2009; **90**: 1-20 [PMID: 19088268 DOI: 10.1099/vir.0.003087-0]
74 **Lion T**. Adenovirus infections in immunocompetent and immunocompromised patients. *Clin Microbiol Rev* 2014; **27**: 441-462 [PMID: 24982316 DOI: 10.1128/CMR.00116-13]
75 **Baldwin A**, Kingman H, Darville M, Foot AB, Grier D, Cornish JM, Goulden N, Oakhill A, Pamphilon DH, Steward CG, Marks DI. Outcome and clinical course of 100 patients with adenovirus infection following bone marrow transplantation. *Bone Marrow Transplant* 2000; **26**: 1333-1338 [PMID: 11223974 DOI: 10.1038/sj.bmt.1702716]
76 **Howard DS**, Phillips II GL, Reece DE, Munn RK, Henslee-Downey J, Pittard M, Barker M, Pomeroy C. Adenovirus infections in hematopoietic stem cell transplant recipients. *Clin Infect Dis* 1999; **29**: 1494-1501 [PMID: 10585802 DOI: 10.1086/313514]
77 **Runde V**, Ross S, Trenschel R, Lagemann E, Basu O, Renzing-Köhler K, Schaefer UW, Roggendorf M, Holler E. Adenoviral infection after allogeneic stem cell transplantation (SCT): report on 130 patients from a single SCT unit involved in a prospective multi center surveillance study. *Bone Marrow Transplant* 2001; **28**: 51-57 [PMID: 11498744 DOI: 10.1038/sj.bmt.1703083]
78 **Walls T**, Shankar AG, Shingadia D. Adenovirus: an increasingly important pathogen in paediatric bone marrow transplant patients. *Lancet Infect Dis* 2003; **3**: 79-86 [PMID: 12560192 DOI: 10.1016/S1473-3099(03)00515-2]
79 **Robin M**, Marque-Juillet S, Scieux C, Peffault de Latour R, Ferry C, Rocha V, Molina JM, Bergeron A, Devergie A, Gluckman E, Ribaud P, Socié G. Disseminated adenovirus infections after allogeneic hematopoietic stem cell transplantation: incidence, risk factors and outcome. *Haematologica* 2007; **92**: 1254-1257 [PMID: 17666361 DOI: 10.3324/haematol.11279]
80 **Shin S**, Roh EY, Oh S, Song EY, Kim EC, Yoon JH. Excluding Anti-cytomegalovirus Immunoglobulin M-Positive Cord Blood Units Has a Minimal Impact on the Korean Public Cord Blood Bank Inventory. *Cell Transplant* 2017; **26**: 63-70 [PMID: 27524276 DOI: 10.3727/096368916X692825]
81 **Al-Awadhi R**, Al-Harmi J, Alfadhli S. Prevalence of cytomegalovirus DNA in cord blood and voided urine obtained from pregnant women at the end of pregnancy. *Med Princ Pract* 2013; **22**: 194-199 [PMID: 23075743 DOI: 10.1159/000343167]

P- Reviewer: Labusca L, Jun YM
S- Editor: Dou Y **L- Editor:** A **E- Editor:** Bian YN

World Journal of Stem Cells

Submit a Manuscript: https://www.f6publishing.com

World J Stem Cells 2019 February 26; 11(2): 84-99

DOI: 10.4252/wjsc.v11.i2.84

ISSN 1948-0210 (online)

ORIGINAL ARTICLE

Basic Study

Anti-inflammatory potential of human corneal stroma-derived stem cells determined by a novel *in vitro* corneal epithelial injury model

Mariana Lizeth Orozco Morales, Nagi M Marsit, Owen D McIntosh, Andrew Hopkinson, Laura E Sidney

ORCID number: Mariana Lizeth Orozco Morales (0000-0002-8287-753X); Nagi M Marsit (0000-0003-2952-7896); Owen D McIntosh (0000-0001-5184-6055); Andrew Hopkinson (0000-0002-8801-7485); Laura E Sidney (0000-0003-1466-7597).

Author contributions: Orozco Morales ML performed the majority of the data acquisition and analysis; Marsit NM processed all amniotic membrane used and helped with acquisition of data; McIntosh OD contributed to conception of the study and acquisition of data; Hopkinson A contributed to conception of the study; Sidney LE contributed to conception of the study, design of experiments, data acquisition, data analysis, and interpretation of data; all authors contributed to drafting the article, making revisions, and had final approval of the manuscript.

Institutional review board statement: Human corneoscleral rims and human AM were used with approval by the Nottingham Research Ethics Committee (Ethics approval numbers: 07/H0403/140 and OY110101, respectively).

Informed consent statement: All corneal tissue was supplied anonymously through Manchester Eye Bank, and all informed consent forms are held at this institution. For amniotic membrane, all donors provided written informed consent prior to tissue collection. During research studies all tissue was anonymised to the researchers.

Conflict-of-interest statement:

Mariana Lizeth Orozco Morales, Nagi M Marsit, Owen D McIntosh, Andrew Hopkinson, Laura E Sidney, Academic Ophthalmology, Division of Clinical Neuroscience, University of Nottingham, Nottingham, NG7 2UH, United Kingdom

Corresponding author: Laura E Sidney, MSc, PhD, Senior Research Fellow, Academic Ophthalmology, Division of Clinical Neuroscience, University of Nottingham, Queen's Medical Centre Campus, Nottingham NG7 2UH, United Kingdom.
laura.sidney@nottingham.ac.uk
Telephone: +44-115-8230459

Abstract

BACKGROUND

An *in vitro* injury model mimicking a corneal surface injury was optimised using human corneal epithelial cells (hCEC).

AIM

To investigate whether corneal-stroma derived stem cells (CSSC) seeded on an amniotic membrane (AM) construct manifests an anti-inflammatory, healing response.

METHODS

Treatment of hCEC with ethanol and pro-inflammatory cytokines were compared in terms of viability loss, cytotoxicity, and pro-inflammatory cytokine release, in order to generate the *in vitro* injury. This resulted in an optimal injury of 20% (v/v) ethanol for 30 s with 1 ng/mL interleukin-1 (IL-1) beta. Co-culture experiments were performed with CSSC alone and with CSSC-AM constructs. The effect of injury and co-culture on viability, cytotoxicity, IL-6 and IL-8 production, and *IL1B*, *TNF*, *IL6*, and *CXCL8* mRNA expression were assessed.

RESULTS

Co-culture with CSSC inhibited loss of hCEC viability caused by injury. Enzyme linked immunosorbent assay and polymerase chain reaction showed a significant reduction in the production of IL-6 and IL-8 pro-inflammatory cytokines, and reduction in pro-inflammatory cytokine mRNA expression during co-culture with CSSC alone and with the AM construct. These results confirmed the therapeutic potential of the CSSC and the possible use of AM as a cell carrier for application to the ocular surface.

CONCLUSION

CSSC were shown to have a potentially therapeutic anti-inflammatory effect

There are no potential conflicts of interest relevant to this study reported by the authors.

Manuscript source: Invited manuscript

Received: July 24, 2018
Peer-review started: July 24, 2018
First decision: October 5, 2018
Revised: November 1, 2018
Accepted: January 1, 2019
Article in press: January 1, 2019
Published online: February 26, 2019

when treating injured hCEC, demonstrating an important role in corneal regeneration and wound healing, leading to an improved knowledge of their potential use for research and therapeutic purposes.

Key words: Cornea; Corneal injuries; Injury model; Corneal epithelium; Corneal stroma-derived stem cells; Amnion; Anti-inflammatory; Cell therapy

Core tip: We designed a novel *in vitro* inflammation model of the human corneal surface using human corneal epithelial cells treated with 20% (v/v) ethanol, followed by stimulation with 1 ng/mL interleukin-1β. We then used this model to demonstrate the anti-inflammatory and regenerative healing properties of human cornea stroma-derived stem cells seeded on an amniotic membrane substrate in a co-culture model. This study is the first step in building a topical regenerative therapy for the treatment of inflammatory disorders of the front of the eye.

Citation: Orozco Morales ML, Marsit NM, McIntosh OD, Hopkinson A, Sidney LE. Anti-inflammatory potential of human corneal stroma-derived stem cells determined by a novel *in vitro* corneal epithelial injury model. *World J Stem Cells* 2019; 11(2): 84-99
URL: https://www.wjgnet.com/1948-0210/full/v11/i2/84.htm
DOI: https://dx.doi.org/10.4252/wjsc.v11.i2.84

INTRODUCTION

The cornea is the transparent window of the eye. It functions to provide two thirds of the eye's refractive power, as well as being the major barrier to the inner content of the eye. At present, when the cornea is damaged or diseased, transplantation of a donor cornea, known as keratoplasty, is the most effective technique to restore vision[1]. However, worldwide 8-10 million individuals have no access to a corneal transplant. Furthermore, patients may suffer from rejection of allogeneic corneal tissue or have to wait for long periods before finding a viable donor graft. For these reasons, corneal research has turned to the use of stem cell-based regenerative therapies for corneal tissue regeneration[2].

Since their discovery, mesenchymal stromal cells (MSCs) have been recognised by different characteristics: differentiation capacity into the adipogenic, chondrogenic, and osteogenic lineages; possible isolation from several tissues; and regeneration of myocardial tissues, tendon, and bone, amongst others in animal models[3]. The interest in MSCs has been enhanced for therapeutic applications due to their non-immunogenic potential[4]. MSCs can be obtained from autologous tissue and expanded in culture, producing anti-inflammatory factors which participate in normal wound repair[5]. Several studies have shown that MSCs have the ability to migrate to sites of tissue injury and stop an on going immune response by inhibiting T-cell proliferation[6]. Additionally, MSCs secrete growth factors and cytokines with autocrine and paracrine activities such as fibrosis inhibition and apoptosis, mitosis stimulation, suppression of the local immune system, angiogenesis enhancement, and stem cell differentiation. These effects can be either direct, causing intracellular signalling, or indirect (referred to as trophic effects), causing other cells to secrete functionally active factors which facilitate tissue regeneration[7].

In 2008, Polisetty *et al*[8] demonstrated the presence of MSCs in the human corneal limbus, which were shown to be similar to bone marrow-MSCs, indicating that these cells are unique in the adult stem cell niche. In 2012, Branch *et al*[9] characterised and analysed the peripheral and limbal corneal stromal cells, later referred to as corneal-stroma derived stem cells (CSSC), against the criteria of the International Society of Cellular Therapy for identification of MSCs. Finding evidence of plastic adhesion, trilineage potential differentiation, correct profile, and expression of the cell-surface markers, revealing that ≥ 95% of the cells expressed CD105, CD90, and CD73, but were negative for CD11b, CD19, CD34, and HLA-DR (≤ 2%). Further characterisation of these cells was performed to demonstrate their MSC-like phenotype in different media and the ability to differentiate back to a keratocyte-like state[10-12].

Recent *in vitro* studies have shown that CSSC contribute to corneal tissue

homeostasis, presenting an immunomodulatory response, a non-immunogenic profile, and a regenerative role[13-15]. From this, we can infer that these cells have potential to control the microenvironment during local inflammation, and are candidates for allogeneic cell-based therapies. There have been several studies investigating the use of MSCs from other tissue (bone marrow or adipose tissue) in treating corneal disease to differing success[16-19]. The use of MSCs from tissues other than the cornea has shown limitations for corneal disease models. In 2015, Fuentes-Julián *et al*[20] aimed to prevent transplant rejection with an adipose-derived MSC treatment while increasing the length of graft survival in a rabbit corneal inflammation model. However, the treatment had the opposite effect and increased the inflammation. Additionally, it is well known that even if MSCs share biological functions and molecular expression profiles across different tissues, they retain a differentiation preference due to their tissue origins[21]. Thus, corneal-derived MSCs, such as CSSCs, may be considered a more appropriate cell source for corneal regeneration.

The amniotic membrane (AM) is the inner most membrane encapsulating the foetus in the amniotic cavity, and consists of a simple epithelium, avascular stroma, and basement membrane[22]. The first therapeutic application of AM was reported in 1913 as a surgical procedure for skin[23]. In the 1940s, AM was first used in the ophthalmology field as a patch to cover defects in the conjunctival epithelium[24]. Subsequently, several studies have demonstrated that AM maintains an anti-scarring and anti-inflammatory action during pregnancy[25], providing evidence of these properties for ocular disorders[26,27]. Alongside its therapeutic properties, AM has been widely used as a cell carrier for different conditions such as chemical burns, ocular cicatricial pemphigoid, severe pterygium, and Stevens-Johnson syndrome[28,29], providing an effective cell-delivery method and a more effective therapeutic effect[30].

In this study, the optimization of an *in vitro* injury model based on 20% (v/v) ethanol (EtOH) and pro-inflammatory cytokine stimulation has been performed using an immortalised human corneal epithelial cell (hCEC) line with the aim of assessing the therapeutic potential of both the CSSC and the AM in a co-culture system by performing the following analyses: cell viability, cytotoxicity, interleukin (IL)-6, IL-8 production, and quantitative reverse transcription polymerase chain reaction (RT-qPCR) for the genes *IL1B*, *TNF*, *IL6*, and *CXCL8*.

MATERIALS AND METHODS

Human tissue

Human corneoscleral rims and human AM were used with approval by the Nottingham Research Ethics Committee (07/H0403/140 and OY110101, respectively) and in accordance with the tenets of the Declaration of Helsinki. Informed consent was obtained from the donors and/or their relatives.

Culture of immortalised human corneal epithelial cells

SV40-immortalised human corneal epithelial cells (hCEC)[31] were cultured in supplemented basal epithelial cell medium EpiLife® (Gibco, ThermoFisher, United Kingdom) containing 5 mL human keratinocyte growth supplement (Gibco, ThermoFisher) and 1% (v/v) antibiotic-antimycotic (AbAm, Sigma-Aldrich, United Kingdom). Cells were incubated at 37 °C, 5% CO_2 (standard conditions), and the medium changed every 2-3 d. hCEC were passaged at approximately 80% confluency using TrypLE Express dissociation reagent (ThermoFisher). hCEC were used between passages 24-31 and seeded at 5×10^4 cell/cm^2 density.

Isolation and culture of CSSC

CSSC were isolated as previously described[11]. Briefly, corneoscleral rims were washed with PBS containing 1% (v/v) AbAm. Residual sclera was removed with a scalpel and the rim was cut in small pieces, placed into 1 mg/mL collagenase type IA (Sigma-Aldrich) solution in basal medium 199 (M199) with 1% (v/v) AbAm, before incubation at 37 °C under slow agitation for 7 h. Digests were filtered through a 40 μm cell-strainer to remove debris and the cells seeded in appropriate culture medium. Culture medium either consisted of M199 (Sigma-Aldrich) supplemented with 20% (v/v) foetal bovine serum (Sigma-Aldrich), 1% (v/v) L-Glutamine (Sigma-Aldrich), and 1% (v/v) AbAm or stem cell medium (SCM) consisting of Dulbecco's modified Eagle's medium: nutrient mixture F-12 (Gibco, ThermoFisher) supplemented with 20% (v/v) knockout serum replacement (Gibco, ThermoFisher), 1% (v/v) MEM non-essential amino acids (Gibco, ThermoFisher), 4 ng/mL basic-fibroblast growth factor (Gibco), 5 ng/mL human leukaemia inhibitory factor (Cell Signalling Technologies,

United Kingdom), and 1% (v/v) AbAm. Finally, the cell suspension was transferred to a 0.1% (v/v) bovine gelatine (Sigma-Aldrich) coated T25 cm^2 flask and incubated at standard conditions. Medium was changed every 3-4 d. CSSC passaging was performed using TrypLE Express dissociation reagent and cells were used experimentally between passages 4-6 and seeded at 2×10^4 cell/cm^2 density, unless otherwise stated.

Experimental culture medium

To assess optimal growth conditions for co-culture of hCEC with CSSC, four media were tested: M199, SCM, EpiLife supplemented as previously mentioned, and keratinocyte-serum free medium (K-SFM, Gibco, ThermoFisher) supplemented with keratinocyte supplement (bovine pituitary extract, epidermal growth factor) and 1% (v/v) AbAm.

Cell viability and proliferation assay

PrestoBlue Cell Viability Reagent (Invitrogen, ThermoFisher) was used to assess cell viability and proliferation. At each time point, culture medium was removed from the cells and a 10% (v/v) PrestoBlue solution in Hank's balanced salt solution was added to each well before incubation for 30 min at 37 °C. Aliquots of 100 μL from each well were transferred to a black 96-well plate and fluorescence readings were taken at 560 nm excitation/590 nm emission with a CLARIOstar microplate reader (BMG LabTech, Buckinghamshire, United Kingdom). Results were corrected for background fluorescence from blank readings.

Injury model optimisation

The effect of combinations of the following conditions were assessed on the hCEC: treatment with 20% (v/v) absolute ethanol (EtOH) in PBS for 30 seconds; application of 1 ng/mL human IL-1β (R and D Systems, United Kingdom) in the media and/or application of 10 ng/mL human tumour necrosis factor (TNF)-α (R and D Systems, United Kingdom). The effect of culturing with IL-1β and TNF-α was assessed on the CSSC. The final injury model used in further co-culture studies consisted of treatment of the hCEC with 20% EtOH for 30 s followed by incubation with 1 ng/mL IL-1β. CSSC were not treated with EtOH during any experiments.

Cytotoxicity

The Pierce lactate dehydrogenase (LDH) Cytotoxicity Assay Kit (ThermoScientific, United Kingdom) was used to quantify cytotoxicity caused by the injury model by measuring LDH release into the culture medium. The assay was performed according to the manufacturer's protocol. Briefly, 50 μL of cell supernatant and 50 μL of reaction mixture were transferred into a 96-well plate, and incubated at room temperature for 30 min. The optical absorbance was read on the plate reader at 490 nm with background correction at 690 nm. Data was converted to a percentage using a maximum LDH release control reading to create a percentage cytotoxicity and corrected for cell viability.

Cytokine production

Human IL-6 and CXCL8/IL-8 DuoSet enzyme linked immunosorbent assay (R and D Systems, Abingdon, United Kingdom) were used in combination with the appropriate DuoSet Ancillary Reagent Kit (R and D Systems), according to manufacturer's instructions, to detect cytokine protein levels in a sample. Briefly, the supernatant samples were diluted 1:20. Optical density at 450 nm with background correction at 540 nm was determined immediately after the addition of the stop solution. Cytokine concentration was determined using 4-parameter fit standard. Data was corrected for the number of cells using viability data.

LIVE/DEAD™ viability assay

The LIVE/DEAD viability kit for mammalian cells (Invitrogen, ThermoFisher) was used to simultaneously stain live (green) and dead (red) cells after injury was performed. hCEC were seeded in 8-well Permanox Lab-Tek chamber slides (ThermoFisher Scientific). Cell monolayers were incubated with a solution containing 2 μmol/L calcein AM and 4 μmol/L ethidium homodimer-1 in PBS for 30 min. After incubation, the staining solution was discarded, chambers removed, and slides mounted under coverslips in fluorescent mounting media (Dako, United Kingdom). Imaging was performed using an upright fluorescence microscope (BX51, Olympus, Southend-on-Sea, United Kingdom) with images captured with a black and white camera (XM-10, Olympus) and Cell^F software (Olympus).

Collection of conditioned medium

Conditioned medium was collected from CSSC at P4 cultured in SCM and SCM supplemented with 1 ng/mL IL-1β. CSSC were seeded at 10000 cells/cm^2 in T75 cm^2 flasks. Conditioned medium was produced by adding 12 mL appropriate media and culturing for 72 h, before collection and filtering through a 0.22 μm filter.

Co-culture

hCEC were seeded in 12-well plates at a density of 5 × 10^4 cell/cm^2 and CSSC were seeded separately at 2 × 10^4 cell/cm^2 into 12 mm transwells with 0.4 μm polyester membrane insert (Corning). On the day of the injury model, hCEC were treated with 20% (v/v) EtOH for 30 s, prior to the CSSC-seeded transwells being added to the co-culture. SCM containing 1 ng/mL IL-1β was then added to cover both cell types. Controls for co-culture experiments included no injury, hCEC only, and CSSC only to correct for background production.

RT-qPCR

RT-qPCR was performed as previously described[10]. Briefly, RNA was extracted from cells using an RNeasy mini kit (Qiagen, Manchester, United Kingdom) according to manufacturer's instructions and quantified using an LVis-plate in a CLARIOstar plate reader. RNA transcription to single-stranded cDNA synthesis was performed with 1 μg of the total RNA using the SuperScript III First Strand Synthesis Kit (Invitrogen, ThermoFisher) using random hexamers. For PCR, 1 μL cDNA was used with inventoried TaqMan assays (Applied Biosystems, ThermoFisher) to detect *GAPDH* (Hs99999905_m1), *IL1B* (Hs01555410_m1), *TNF* (Hs00174128_m1), *IL6* (Hs00985639_m1), and *CXCL8* (Hs00174103_m1). Gene amplification was performed on an Mx3005P multi-colour 96-well PCR-system (Stratagene, Agilent Technologies). Results were analysed with the RT-qPCR Miner algorithm[32]. All readings were normalised using the endogenous reference gene *GAPDH*.

CSSC-AM construct preparation

Preparation of the dried, vacuum-packed AM was performed as previously described[33]. Briefly, AM was separated from chorion and triple washed in sodium chloride, before the spongy layer was removed. After incubation in 100 mmol/L raffinose pentahydrate (Acros Organics, United Kingdom) in PBS for 2 h, the AM was dried with main drying at a shelf temperature of 15 °C, vacuum 1.03 mbar for 30 min, followed by a final drying phase, shelf temperature 15 °C, vacuum pressure 0.001 mbar for 15 min in a cooled freeze dryer (Alpha 1-4 LSC, Advanced Freeze Dryer, Christ Osterode, Germany).

To culture CSSC on AM, a novel method designed in our laboratory was employed (Figure 1). Single use 30 mm diameter Millicell tissue culture inserts (Millipore, United Kingdom) were used without filtration membranes. A sterilisable polytetrafluoroethylene O-ring was placed in the centre of a 5 cm diameter rehydrated AM, epithelial side up. The AM was then trimmed to create a 1 cm frill around the inside of the O-ring, which was subsequently firmly wrapped over the O-ring edges creating a taut wrinkle free-surface. Forceps were used to position the O-ring-AM construct into the Millicell insert and the O-ring-AM construct was then gently pushed by the edges to the bottom. The AM-insert was placed in a 6-well tissue culture plate and the AM soaked in culture medium overnight. CSSC were seeded on the AM construct 7 d before inducing the injury model. On a separate 6-well plate, hCEC were seeded at 5 × 10^4 cell/cm^2 density 72 h before injury. On the injury day, the hCEC were treated with 20% (v/v) EtOH for 30 s, the CSSC-AM constructs were moved into the wells for co-culture studies and SCM containing 1 ng/mL IL-1β added. Controls for CSSC-AM co-culture experiments included no-injury, hCEC only, CSSC only, and AM only.

Statistical analysis

Statistical significances were calculated using GraphPad Prism v.7.00.

RESULTS

M199 and SCM support both hCEC and CSSC viability and proliferation

To determine an optimal medium for co-culturing hCEC and CSSC, both cell types were cultured in EpiLife, K-SFM, M199, and SCM with viability assays performed at 24 h and 144 h (Figure 2). hCEC showed significant proliferation in EpiLife, SCM, and M199 (Figure 2A). Contrary to expectations, hCEC in K-SFM did not proliferate. CSSC only demonstrated significant proliferation in SCM, but did not lose viability in M199. Culture in EpiLife and K-SFM significantly reduced CSSC viability (Figure 2B). As M199 and SCM supported both cell types, both media were selected for further

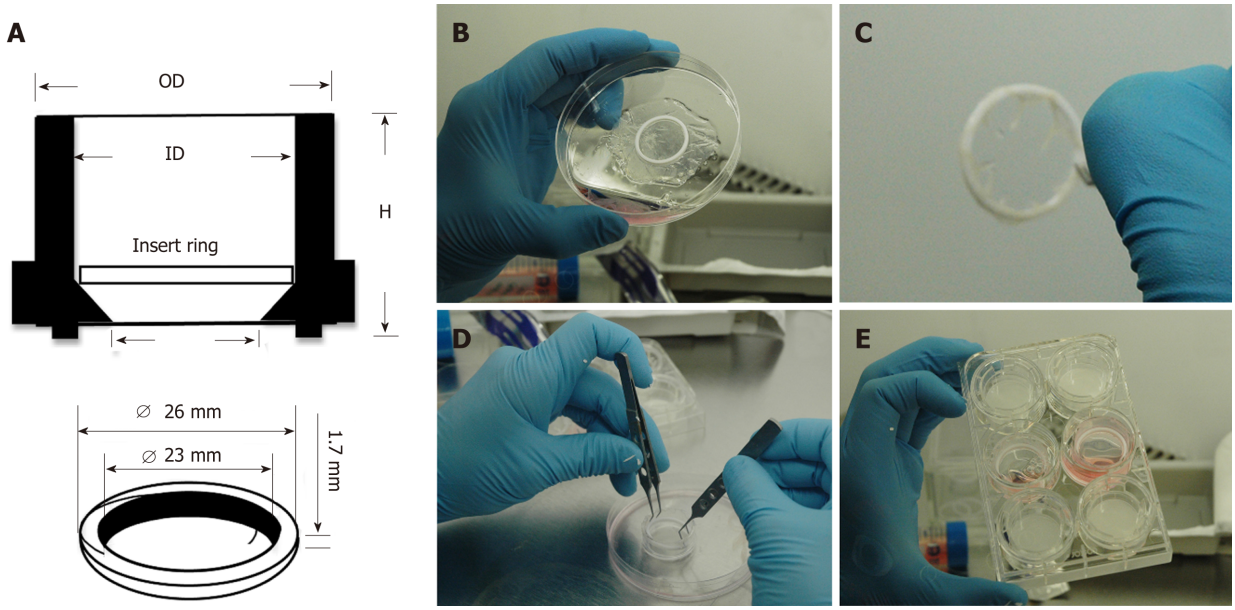

Figure 1 Culture system enabling seeding of corneal-stroma derived stem cells on amniotic membrane. A: Schematic showing dimensions and arrangement of polytetrafluoroethylene (PTFE) O-ring inside 30 mm tissue culture insert; B: The PTFE ring is placed on the epithelial side of hydrated amniotic membrane (AM); C: The AM is firmly wrapped over the O-ring edges leaving a taut membrane surface for cell seeding; D: The O-ring containing the AM is placed within the tissue culture insert; E: The tissue culture insert is placed within a 6-well plate and culture medium applied.

experiments.

An injury model of 20% (v/v) EtOH and 1 ng/mL IL-1β creates a balance between cell viability reduction and pro-inflammatory cytokine production

Different combinations of EtOH injury with and without inflammatory stimulus were tested on hCEC cultured in SCM and M199 to determine an optimised injury model (Figure 3). Viability assays were performed 72 h after injury with/without IL-1β and/or TNF-α supplementing the culture medium for the entire time (Figure 3A and 3B). For cells cultured in M199, all injury treatments caused significant reductions in cell viability, with EtOH with IL-1β and TNF-α treatment causing the largest reduction (Figure 3A). For cells cultured in SCM, there was no significant drop in viability when cells were treated with only IL-1β; the remaining treatments all caused over 50% reduction in viability (Figure 3B) with EtOH with IL-1β and TNF-α treatment causing the largest reduction.

Cytotoxicity caused by the injury was measured by levels of the LDH enzyme within the supernatant 72 h after injury began (Figure 3C and 3D). In both M199 and SCM, only treatment with EtOH with IL-1β, or EtOH with IL-1β and TNF-α caused significant levels of cytotoxicity compared with the no injury controls. Levels of inflammation within the injury models were assessed by measuring IL-6 and IL-8 concentration within the hCEC supernatant 72 h after initial injury (Figure 3E, 3F, 3G, and 3H). Significant concentrations of IL-6 were found with treatment of EtOH with IL-1β, or EtOH with IL-1β and TNF-α in both M199 (Figure 3E) and SCM (Figure 3F). IL-8 production was only significant in M199 when treated with EtOH with IL-1β and TNF-α (Figure 3G), but in SCM was significant when treated with EtOH with IL-1β, or EtOH with IL-1β and TNF-α (Figure 3H). Representative LIVE/DEAD staining images of hCEC cultured in SCM 72 h after initial injury can be seen in Figure 3I. When EtOH treatment was not used, 1 ng/mL IL-1β treatment showed an almost comparable cell confluence to the control. All other treatments evidenced a decrease in cell number, with EtOH with IL-1β and TNF-α being the most toxic.

These results taken as a whole suggest that combining EtOH treatment with both IL-1β and TNF-α generates high, but unnecessary, inflammatory and toxic damage to the cells, leaving few cells alive for further analysis. The most balanced treatment was 20% (v/v) EtOH with 1 ng/mL IL-1β, which led to significant production of pro-inflammatory cytokines, significant cytotoxicity, and a significant but not excessive reduction in viability. Thus, this injury model was chosen for further experiments. It was also decided to continue co-culture experiments in SCM only.

CSSC viability remains stable after treatment with IL-1β but production of IL-6 and IL-8 is increased

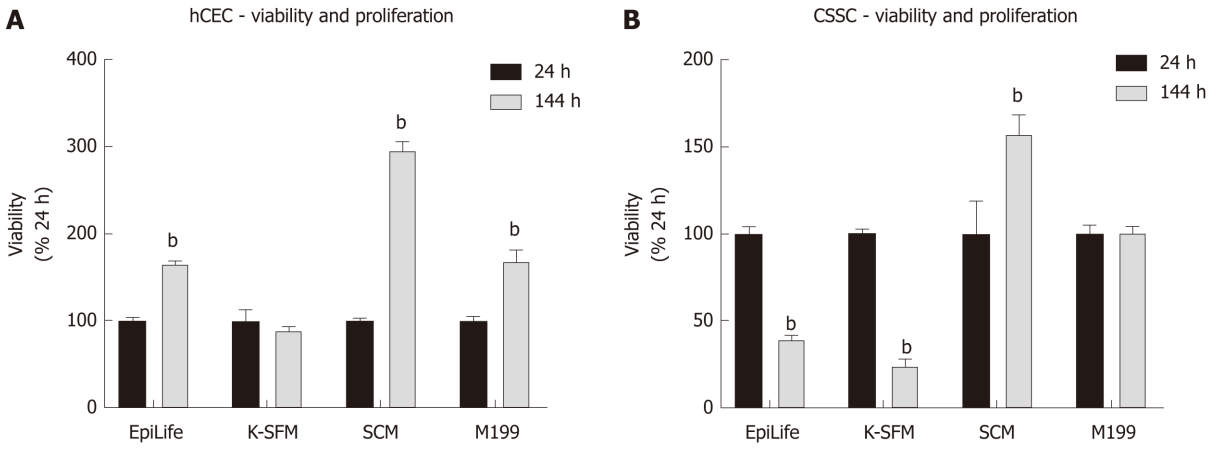

Figure 2 Effect of culture medium on human corneal epithelial cells and corneal-stroma derived stem cells viability and proliferation. A, B: Human corneal epithelial cells (A) and corneal-stroma derived stem cells (B) were seeded in EpiLife, keratinocyte-serum free medium, stem cell medium, and M199. Presto Blue viability assay was performed at 24 h and 144 h. Each time point is represented relative to the viability in that media type at 24 h. Data shown as mean ± SEM of six replicates (n = 6) each with 3 samples. Statistical significance compared to 24 h, analysed by two-way ANOVA, represented by $^{b}P \leq 0.0001$. CSSC: Corneal-stroma derived stem cells; hCEC: Human corneal epithelial cells; K-SFM: Keratinocyte-serum free medium; SCM: Stem cell medium.

CSSC cultured in both M199 and SCM were stimulated with IL-1β and TNF-α and assessed with identical assays to those described above, in preparation for co-culture with hCEC (Figure 4). Viability assays were performed at 72 h of cytokine stimulation (Figure 4A and 4B). A significant reduction in viability compared to non-injured controls was seen when IL-1β and TNF-α together were present in the medium. LDH concentration in the media, indicating cytotoxicity, was assessed after 72 h stimulation (Figure 4C and 4D). Significant cytotoxicity was only seen in M199 when treated with both IL-1β and TNF-α. Assessment of IL-6 (Figure 4E and 4F) and IL-8 (Figure 4G and 4H) production showed significant production of IL-6 in both media due to IL-1β treatment alone and with TNF-α. IL-8 was produced in significant levels in SCM due to IL-1β treatment alone and with TNF-α but only in M199 when both cytokines were present. Overall production of IL-6 and IL-8 by CSSC was far lower than that of hCEC.

CSSC conditioned medium does not inhibit hCEC viability loss but shows some inhibition of LDH, IL-6, and IL-8 production after injury.

CSSC were used to obtain conditioned SCM medium in order to determine if secreted factors alone were adequate for producing an anti-inflammatory response. hCEC were injured with EtOH for 30 s. Subsequently, SCM control, CSSC-conditioned medium, or CSSC-conditioned medium pre-treated with IL-1β were applied along with the extra IL-1β inflammatory stimulus for 72 h before analysis (Figure 5). No inhibition in the reduction of viability due to the injury was seen in any group, although there was significant reduction in viability of non-injured hCEC due to the presence of conditioned medium (Figure 5A). There was significant reduction in the levels of cytotoxicity caused by the injury with treatment with both types of conditioned medium, however there was still significant levels of cytotoxicity compared to non-injured controls (Figure 5B). There was significant reduction in the production of IL-6 by injured hCEC when treated with CSSC-conditioned medium with and without IL-1β pre-treatment; however, levels were still significantly higher than non-injured controls (Figure 5C). IL-8 production by hCEC in response to injury was not significant compared to the non-injured control when treated with CSSC-conditioned medium. However, when treated with the conditioned medium from the CSSC that had IL-1β pre-treatment, there was a significant increase in the levels of IL-8, potentially due to the high levels of IL-1β (Figure 5D).

Co-culture of CSSC with injured hCEC improves hCEC viability and reduces post-injury inflammation

hCEC were treated with the standard injury of EtOH for 30 s followed by IL-1β stimulation. During the IL-1β treatment, co-cultures of CSSC were added and analysis of viability, cytotoxicity, cytokine production, and gene expression were performed after 72 h (Figure 6). There was a significant reduction in viability of the injured hCEC compared to non-injured cells, as previously shown. However, the addition of the CSSC in co-culture to the injured hCEC showed a significant inhibition of this viability decrease, with a significantly higher viability shown in the co-culture injured

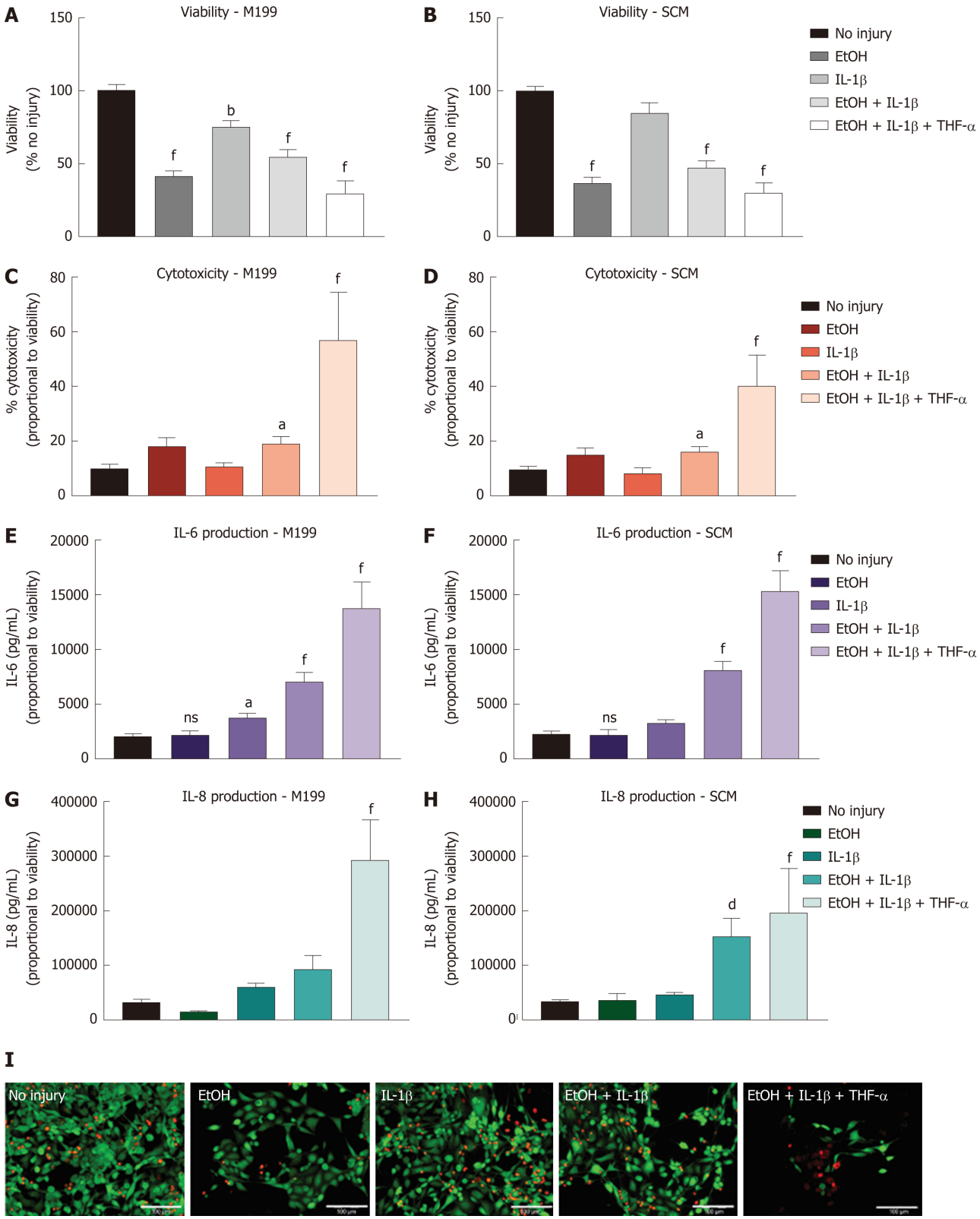

Figure 3 Injury model optimisation for human corneal epithelial cells. Injury model optimisation was performed with human corneal epithelial cells (hCEC) cultured in both M199 (A, C, E, G) and stem cell medium (B, D, F, H). Injuries consisted of the following treatments: 20% (v/v) ethanol (EtOH); 1 ng/mL interleukin (IL)-1β in the medium; 20% (v/v) EtOH with 1 ng/mL IL-1β in the medium; and 20% (v/v) EtOH with 1 ng/mL IL-1β and 10 ng/mL TNF-α in the medium. A, B: PrestoBlue viability assay performed 72 h after the different treatments. Data represented relative to reading for no injury control; C, D: LDH assay performed on supernatant 72 h after injury. Data displayed as percentage cytotoxicity and relative to cell viability; E, F: Concentration of IL-6 in the supernatant 72 h after injury. Data displayed relative to cell viability; G, H: Concentration of IL-8 in the supernatant 72 h after injury. Data displayed relative to cell viability. Data for all graphs shown as mean ± SEM of five independent experiments, with three to six replicates each. Statistical significance compared to no injury controls analysed by one-way ANOVA represented by $^{a}P \leq 0.05$, $^{b}P \leq 0.01$, $^{d}P \leq 0.001$, $^{f}P \leq 0.0001$; I: LIVE/DEAD staining performed on hCEC cultured in stem cell medium for hCEC untreated control (A), 20% (v/v) EtOH (B), 1 ng/mL IL-1β (C), EtOH + 1 ng/mL IL-1β (D), EtOH + 10 ng/mL IL-1β (E), and EtOH+ 1 ng/mL IL-1β + 10 ng/mL TNF-α (F). Live staining (green) is shown with FITC, and dead staining (red) is shown with TRITC. Scale bar = 100 μm. hCEC: Human corneal epithelial cells; IL: Interleukin; SCM: Stem cell medium; TNF: Tumour necrosis factor.

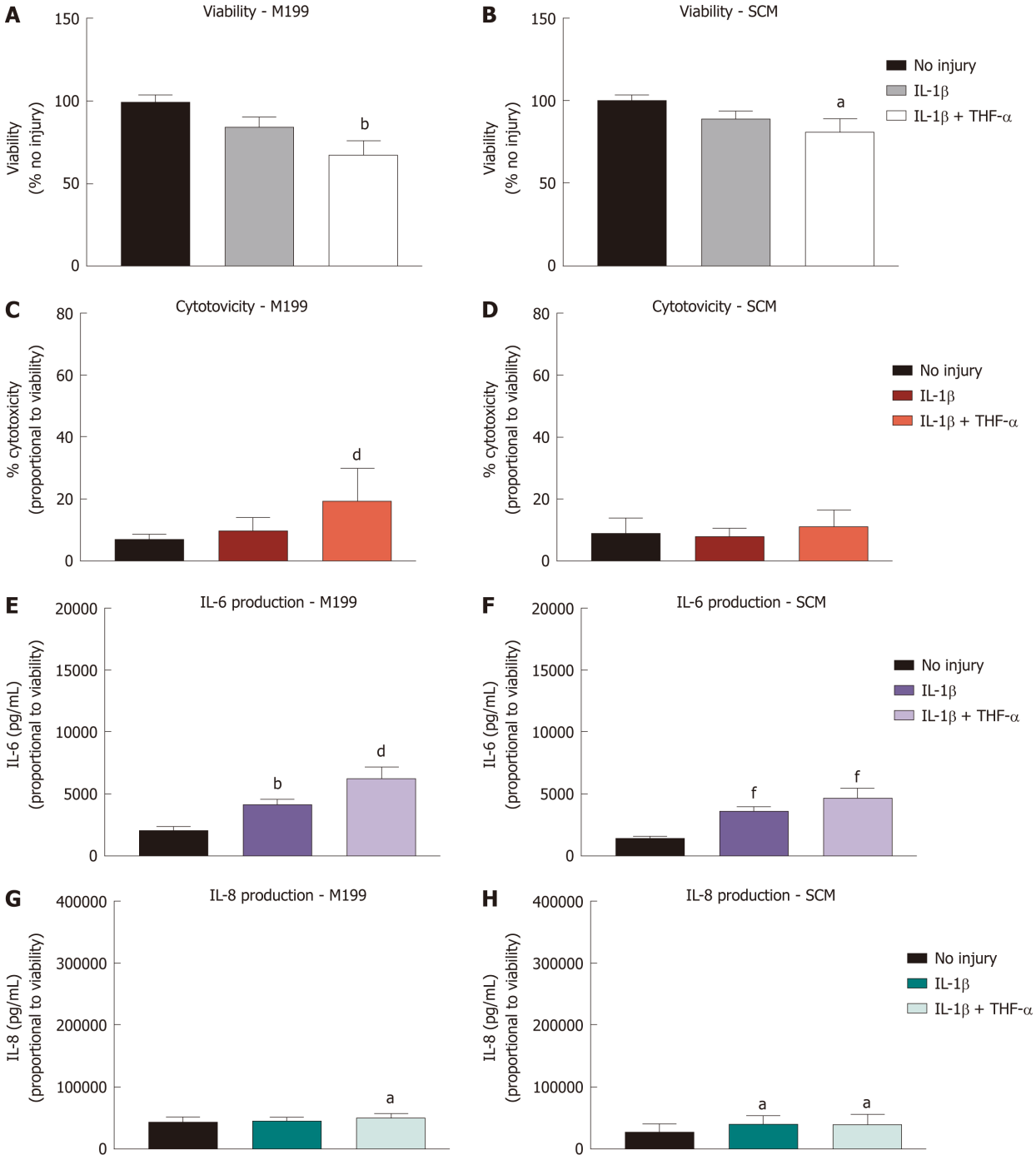

Figure 4 Effect of treatment with pro-inflammatory cytokines on corneal-stroma derived stem cells. Treatment of corneal-stroma derived stem cells cultured in stem cell medium or M199 with 1 ng/mL IL-1β with/without 10 ng/mL tumour necrosis factor-α was performed for 72 h. A: PrestoBlue viability assay after 72 h stimulation. Data represented relative to reading for no injury control; B: Lactate dehydrogenase cytotoxicity assay performed on cell supernatants after 72 h treatment. Data displayed as percentage cytotoxicity and relative to cell viability; C: Concentration of IL-6 in the supernatant 72 h after injury. Data displayed relative to cell viability; D: Concentration of IL-8 in the supernatant 72 h after injury. Data displayed relative to cell viability. Data for all graphs shown as mean ± SEM of five independent experiments with three to six replicates each. Statistical significance compared to no injury controls analysed by one-way ANOVA represented by $^{a}P \leq 0.05$, $^{b}P \leq 0.01$, $^{d}P \leq 0.001$, $^{f}P \leq 0.0001$. IL: Interleukin; TNF: Tumour necrosis factor; SCM: Stem cell medium.

group than in non-co-culture (Figure 6A). Levels of cytotoxicity were significantly reduced in the co-culture systems when compared to hCEC only, with no significant difference shown between no injury and injury (Figure 6B). Both IL-6 (Figure 6C) and IL-8 (Figure 6D) production was significantly reduced when in co-culture compared to the hCEC only injured group. Gene expression of *IL1B* (Figure 6E), *IL6* (Figure 6G) and *CXCL8* (IL-8, Figure 6H) by injured hCEC was also significantly reduced by co-culture with CSSC. *TNF* expression was not significantly reduced (Figure 6F).

Co-culture of injured hCEC with the CSSC-AM construct improves hCEC viability

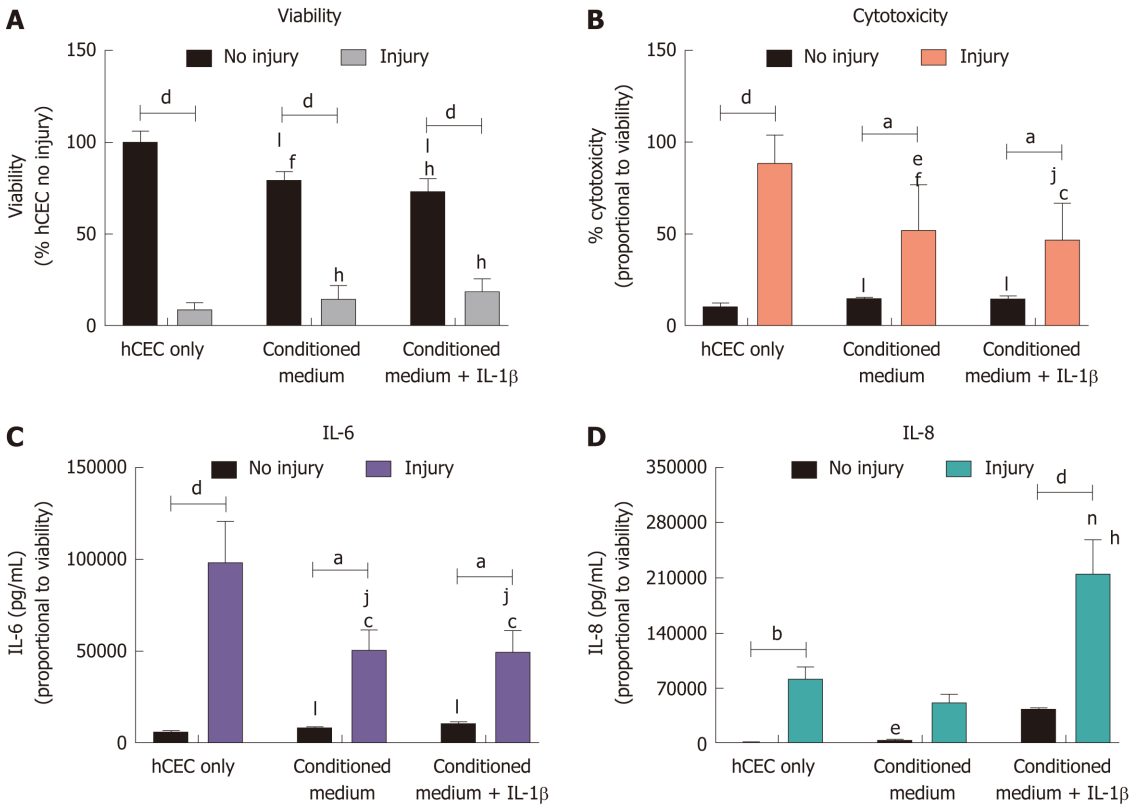

Figure 5 Effect of corneal-stroma derived stem cells-conditioned medium on human corneal epithelial cells treated with the injury model. Human corneal epithelial cells (hCEC) were treated with an injury model consisting of 30 s ethanol treatment followed by stimulation with 1 ng/mL IL-1β for 72 h. Medium conditioned by corneal-stroma derived stem cells with and without pre-treatment with IL-1β was applied to the hCEC after ethanol treatment during stimulation with IL-1β. A: PrestoBlue viability assay after 72 h. Data represented relative to reading for hCEC no injury control; B: Lactate dehydrogenase cytotoxicity assay performed on cell supernatants after 72 h treatment. Data displayed as percentage cytotoxicity and relative to cell viability; C: Concentration of IL-6 in the supernatant 72 h after injury. Data displayed relative to cell viability; D: Concentration of IL-8 in the supernatant 72 h after injury. Data displayed relative to cell viability. Data shown as mean ± SEM of three independent experiments with four to six replicates each. Statistical significance analysed by two-way ANOVA. Significance compared to non-injured, same treatment represented by $^{a}P \leq 0.05$, $^{b}P \leq 0.01$, $^{d}P \leq 0.0001$. Significance compared to hCEC, no injury represented by $^{c}P \leq 0.05$, $^{f}P \leq 0.01$, $^{h}P \leq 0.0001$. Significance compared to hCEC, injury represented by $^{e}P \leq 0.05$, $^{i}P \leq 0.01$, $^{n}P \leq 0.001$, $^{l}P \leq 0.0001$. hCEC: Human corneal epithelial cells; IL: Interleukin.

while reducing pro-inflammatory cytokines and pro-inflammatory cytokine mRNA expression after injury

hCEC were treated with the standard injury of EtOH followed by IL-1β stimulation in the culture medium. During the IL-1β stimulation, constructs of AM only and CSSC-AM were added in co-culture. After 72 h, analysis of viability, cytotoxicity, cytokine production, and mRNA expression of the hCEC were performed (Figure 7). As seen previously, there was a loss in hCEC viability when the injury was performed without co-culture. This loss in viability was not inhibited by the presence of AM alone, but significant inhibition of viability loss was demonstrated when injured hCEC were co-cultured with the CSSC-AM construct (Figure 7A). Increased cytotoxicity was seen when hCEC were injured without co-culture; this was not inhibited by the AM construct, but was significantly inhibited by co-culture with the CSSC-AM construct (Figure 7B). IL-6 and IL-8 release into the media due to injury was significantly inhibited during co-culture with the CSSC-AM construct (Figure 7C and 7D). IL-8 production was also significantly inhibited by the presence of AM only. Unlike, the previous co-culture experiment, expression of *IL1B* was not significantly reduced by either co-culture during injury (Figure 7E). Expression of *TNF* was also unaffected by co-culture (Figure 7F). Expression of *IL6* (Figure 7G) and *CXCL8* (IL-8, Figure 7H) mRNA were significantly reduced when injured hCEC were co-cultured with CSSC-AM. This reduction did not occur with AM only.

DISCUSSION

In the last few decades, MSCs have been widely studied for viable medical applications due to their therapeutic properties[34,35]. Moreover, CSSC have a huge potential in the ophthalmology field as these stem cells may play an important role in

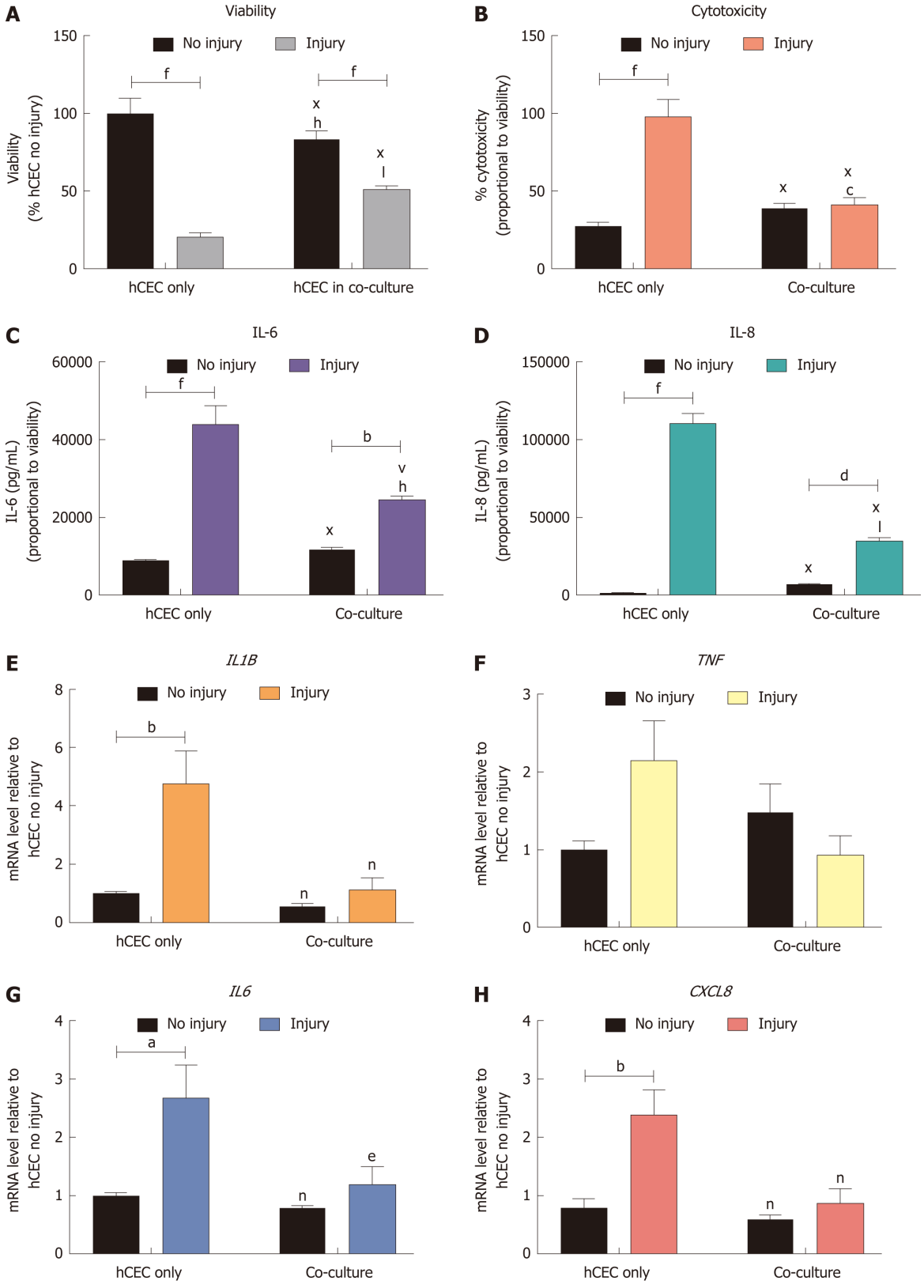

Figure 6 Effect of co-culture with corneal-stroma derived stem cells on human corneal epithelial cells response after injury. Human corneal epithelial cells (hCEC) were treated with an injury model consisting of 30 s ethanol treatment followed by stimulation with 1 ng/mL IL-1β for 72 h. During IL-1β stimulation corneal-stroma derived stem cells (CSSC) were co-cultured with CSSC in a transwell system. A: PrestoBlue viability assay after 72 h. Data represented relative to reading for hCEC only, no injury control; B: Lactate dehydrogenase cytotoxicity assay performed on cell supernatants after 72 h treatment. Data displayed as percentage cytotoxicity and relative to cell viability; C: Concentration of IL-6 in the supernatant 72 h after injury. Data displayed relative to cell viability; D: Concentration of IL-8 in the supernatant 72 h after injury. Data displayed relative to cell viability; E-H: RT-qPCR performed to show mRNA expression of *IL1B* (E), *TNF* (F), *IL6* (G), and *CXCL8* (H). Expression of each target gene normalised to *GAPDH* and represented relative to hCEC only, no injury. Data for all graphs shown as mean ± SEM of three independent experiments with five replicates each. Statistical significance analysed by two-way ANOVA. Significance compared to non-injured, same group, represented by $^{a}P \leq 0.05$, $^{b}P \leq 0.01$, $^{d}P \leq 0.001$, $^{f}P \leq 0.0001$. Significance compared to hCEC only, no injury represented by $^{c}P \leq 0.05$, $^{h}P \leq 0.01$, $^{i}P \leq 0.001$, $^{l}P \leq 0.0001$. Significance compared to hCEC, injury represented by $^{e}P \leq 0.05$, $^{n}P \leq 0.01$, $^{v}P \leq 0.001$, $^{x}P \leq 0.0001$. CSSC: Corneal-stroma derived stem cells; hCEC:

Human corneal epithelial cells; IL: Interleukin.

corneal regeneration and wound healing[36]. Some of their important functions are the transdifferentiation capacity from the mesenchymal to the epithelial phenotype[15,37] and the generation of progenitors with MSC potential[38].

Although CSSC provide positive results as therapy for sight-threatening corneal diseases[14], an optimal cell-delivery format is essential for a cell-based therapy to succeed. The choice of the delivery method depends on both the tissue and the disease to be treated, looking for a high cell retention and integration capacity for the cells to repopulate, release healing factors, or help the surrounding tissues and cells to recover their normal functions[39]. For corneal disease, AM shows high promise as a biocompatible scaffold, demonstrating properties which enhance the delivery of a cell-based therapy to the eye's surface through a topical application[26,30].

Herein, a comparison between four injury models was undertaken on hCEC to generate an *in vitro* model to mimic a keratitis condition in the cornea with the aim of demonstrating the therapeutic potential of CSSC. The second stage was to build a construct of CSSC on AM to investigate if the CSSC maintained their anti-inflammatory properties when using the membrane as a carrier and to discern if the AM added extra anti-inflammatory value.

Several factors had to be considered to develop a functional inflammatory model. Firstly, the comparison between K-SFM, EpiLife, SCM, and M199 took place in order to provide an optimal growth environment for both hCEC and CSSC when co-cultured. EpiLife is serum-free and commercially available for human epidermal keratinocytes, and it has been previously used and approved for hCEC culture[40]. K-SFM is another serum-free medium for epithelial cells, supplemented with epidermal growth factor and basic-fibroblast growth factor, which has been shown to be efficient for keratocyte[41] and hCEC[42] maintenance and proliferation. M199 was the only serum-containing medium tested in this study and it has previously demonstrated to maintain an MSC-like cell-surface marker profile when culturing CSSC[9,12]. Finally, SCM is mostly related with induced pluripotent stem cells and human embryonic stem cells. It contains basic-fibroblast growth factor, human leukaemia inhibitory factor, and knockout serum replacement and has been associated with the maintenance of pluripotency markers in CSSC cultures[10]. In this investigation, SCM and M199 maintained the proliferation and viability for both hCEC and CSSC, confirming previous studies performed on CSSC by our research group. However, as the ultimate outcome for this research is to translate the investigation into a cell-therapy based on maintenance and viability of the CSSC to heal the cornea and recover vision, an FBS-containing medium is not appropriate due to its variability in composition from batch-to-batch and its animal origin[43]. Moreover, despite the fact that M199 accomplished the minimal criteria for maintaining an MSC phenotype it does not share the advantages of SCM for the promotion of SC/progenitor markers while maintaining a MSC phenotype. Therefore, SCM is the best prospect for therapeutic applications[10].

Four models were initially tested against the hCEC to generate an injury. The 1 ng/mL IL-1β only treatment was not potent enough to significantly reduce the cell proliferation and it did not develop effective levels of inflammation. This response is supported by studies showing that IL-1β promotes differentiation of progenitor cells as well as maturation and survival of differentiated cells[44,45]. Treatment of 20% (v/v) EtOH only significantly reduced the cell viability/proliferation and caused an initial injury as supported by previous studies[46]. However, it did not activate the cells to generate inflammation through production of pro-inflammatory cytokines. In contrast, the IL-1β and TNF-α treatments both generated an inflammatory response. Combining both cytokines was too aggressive, allowing only a few cells to recover for further analysis. On the other hand, the 20% (v/v) EtOH with 1 ng/mL IL-1β treatment provided a balance between injury and inflammatory response, proving to be the optimal injury model to mimic an *in vitro* keratitis model. This outcome is consistent with the reviewed literature, as the inflammatory properties of IL-1β and TNF-α had only been tested individually[47,48]. However, to the best of the author's knowledge this was the first time that these combinations were used for the generation of an *in vitro* injury model.

CSSC-conditioned medium was used on the hCEC injury model to assess potential anti-inflammatory action. The conditioned medium showed no significant effect improving hCEC viability, but did demonstrate some positive effects by reducing cytotoxicity and IL-6/IL-8 production, demonstrating that CSSC secrete factors into the media that have a positive anti-inflammatory effect.

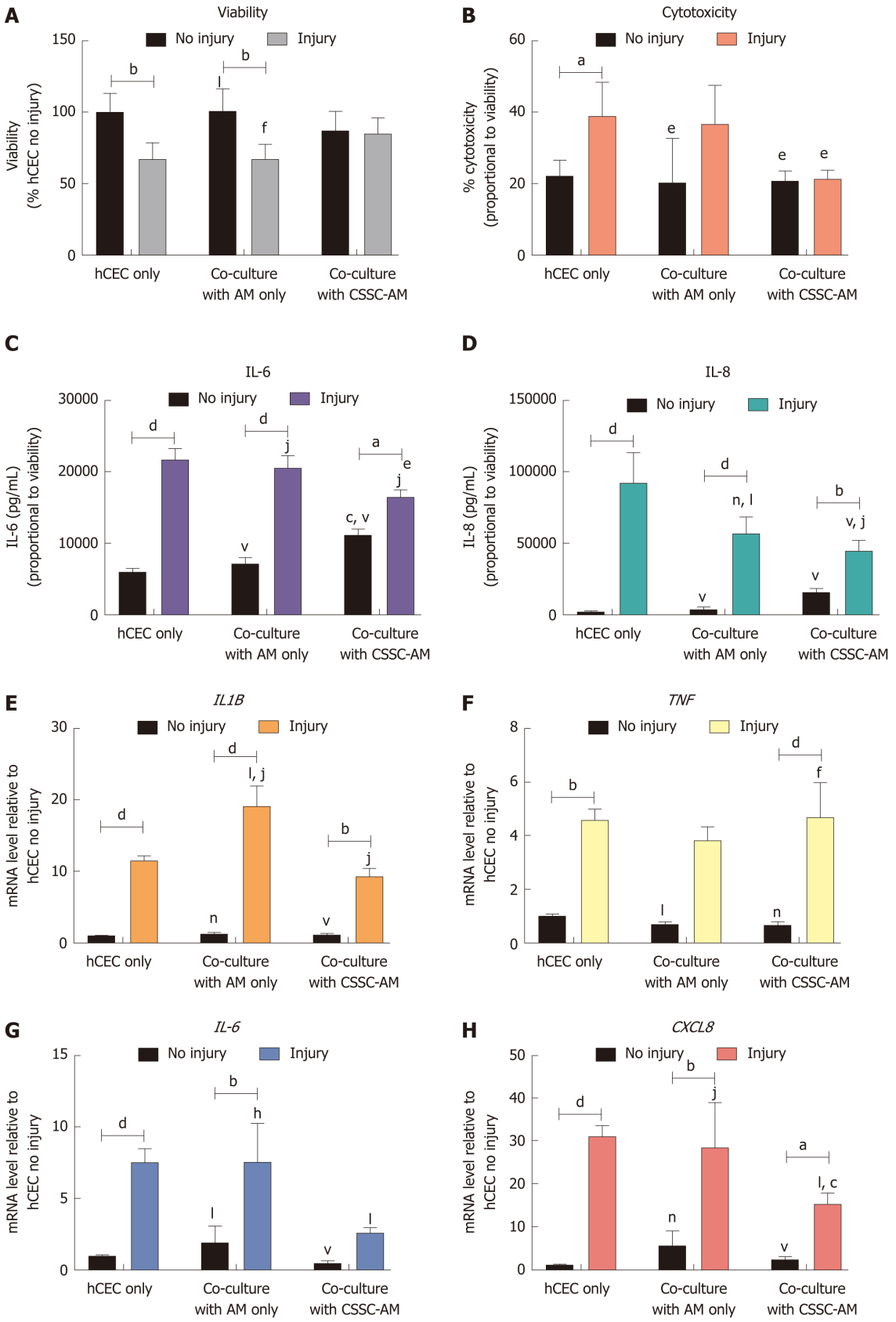

Figure 7 Effect of co-culture with corneal-stroma derived stem cells-amniotic membrane constructs on human corneal epithelial cells response after injury. Human corneal epithelial cells (hCEC) were treated with an injury model consisting of 30 s ethanol treatment followed by stimulation with 1 ng/mL IL-1β for 72 h. During IL-1β stimulation hCEC were co-cultured with either amniotic membrane (AM) only or a corneal-stroma derived stem cells-AM construct. A: PrestoBlue viability assay after 72 h. Data represented relative to reading for hCEC only, no injury control; B: Lactate dehydrogenase cytotoxicity assay performed on cell supernatants after 72 h treatment. Data displayed as percentage cytotoxicity and relative to cell viability; C: Concentration of IL-6 in the supernatant 72 h after injury. Data displayed relative to cell viability; D: Concentration of IL-8 in the supernatant 72 h after injury. Data displayed relative to cell viability; E-H: RT-qPCR performed to show mRNA expression of *IL1B* (E), *TNF* (F), *IL6* (G), and *CXCL8* (H). Expression of each target gene normalised to *GAPDH* and represented relative to hCEC only, no injury. Data for all graphs shown as mean ± SEM of three independent experiments with five replicates each. Statistical significance analysed by two-way ANOVA.

Significance compared to non-injured, same group, represented by $^{a}P \leq 0.05$, $^{b}P \leq 0.01$, $^{d}P \leq 0.0001$. Significance compared to hCEC only, no injury represented by $^{c}P \leq 0.05$, $^{f}P \leq 0.01$, $^{h}P \leq 0.001$, $^{i}P \leq 0.0001$. Significance compared to hCEC, injury represented by $^{e}P \leq 0.05$, $^{l}P \leq 0.01$, $^{n}P \leq 0.001$, $^{v}P \leq 0.0001$. AM: Amniotic membrane; CSSC: Corneal-stroma derived stem cells; hCEC: Human corneal epithelial cells; IL: Interleukin.

Both the CSSC alone and the CSSC-AM constructs inhibited the hCEC viability loss seen when the injury was performed. Furthermore, both systems showed beneficial anti-inflammatory effects as production of pro-inflammatory cytokines, pro-inflammatory mRNA expression, and cytotoxicity levels were significantly reduced. The beneficial therapeutic effect of the CSSC was further evidenced by the fact that the AM construct without CSSC had few inhibitory effects on the injury. Investigations for similar constructs have been performed before with positive results; Li *et al*[49] developed a construct where corneal stroma and limbal epithelium with SCs promoted cell proliferation. Additionally, a model using real architecture for 3D-tissue tissue equivalents as a substrate for co-culturing limbal epithelial cells and CSSC showed a positive impact on the expansion of the epithelial cells while maintaining the MSC-markers CD73 and CD90, confirming the CSSC phenotype[50]. Contrary to our findings, previous work on burned rat corneas showed that MSCs increased *IL6* expression but still reduced corneal inflammation[51].

In conclusion, an *in vitro* injury model was developed using hCEC culture, allowing the initial testing into the anti-inflammatory potential of CSSC. However, it is well known that *in vitro* observations are not always able to reflect an *in vivo* phenomenon; it would therefore be necessary to validate these findings in preclinical animal models in order to validate efficacy to proceed to clinical trials. Nevertheless, this investigation demonstrated that CSSC have an important role in corneal regeneration and wound healing and is a stepping stone towards further preclinical investigation.

ARTICLE HIGHLIGHTS

Research background

The cornea provides two thirds of the eye's refractive power as well as being the major barrier to the inner content of the eye. At present, the most effective treatment of a diseased or damaged cornea is transplantation of a donor cornea (keratoplasty). However, this is not feasible for 8-10 million individuals. Corneal research has turned to the use of stem cell-based regenerative therapies for corneal tissue regeneration. Recent *in vitro* studies have shown that mesenchymal stem cell-like cells from the corneal stroma (corneal-derived stromal stem cells, CSSC) contribute to corneal tissue homeostasis, presenting an immunomodulatory response, a non-immunogenic profile, and a regenerative role. Thus, CSSC may be considered an appropriate cell source for the treatment of inflammatory disorders of the cornea.

Research motivation

To investigate whether CSSC seeded on an amniotic membrane (AM) substrate have the ability to modulate an inflamed environment, and therefore whether they were suitable candidates for developing a cell therapy for the front of the eye.

Research objectives

The first objective was to optimise an *in vitro* injury model mimicking a corneal surface using human corneal epithelial cells (hCEC) stimulated with various injurious agents. Once optimised the second objective was to investigate whether CSSC conditioned media and then CSSC in co-culture could modulate the injury environment. The final objective was to seed CSSC on AM and investigate whether the CSSC-AM construct provided an anti-inflammatory, healing response to the injury.

Research methods

Treatment of hCEC with ethanol and pro-inflammatory cytokines were compared in terms of viability loss, cytotoxicity, and pro-inflammatory cytokine release in order to generate the novel *in vitro* injury. Co-culture experiments were performed with CSSC alone and with CSSC-AM constructs. The effect of injury and co-culture on viability, cytotoxicity, interleukin (IL)-6 and IL-8 production, and *IL1B*, *TNF*, *IL6*, and *CXCL8* mRNA expression were assessed.

Research results

An optimal injury of 20% (v/v) ethanol for 30 s with 1 ng/mL IL-1 beta was developed. Co-culture of the injury model with CSSC inhibited loss of hCEC viability caused by injury. Enzyme linked immunosorbent assay and PCR showed a significant reduction in the production of IL-6 and IL-8 pro-inflammatory cytokines and reduction in pro-inflammatory cytokine mRNA expression during co-culture with CSSC alone and with the AM construct.

Research conclusions

The novel findings of this study confirm the therapeutic potential of the CSSC and the possible

use of AM as a cell carrier for application to the ocular surface.

Research perspectives

The novel injury model developed in this study can be adapted for studying the therapeutic effects of many different agents. The findings of this study may lead to the development of practise changing cell therapies for treatment of inflammatory disorders of the cornea in clinic.

REFERENCES

1 **Thompson RW**, Price MO, Bowers PJ, Price FW. Long-term graft survival after penetrating keratoplasty. *Ophthalmology* 2003; **110**: 1396-1402 [PMID: 12867398 DOI: 10.1016/S0161-6420(03)00463-9]

2 **Du Y**, Funderburgh ML, Mann MM, SundarRaj N, Funderburgh JL. Multipotent stem cells in human corneal stroma. *Stem Cells* 2005; **23**: 1266-1275 [PMID: 16051989 DOI: 10.1634/stemcells.2004-0256]

3 **Aggarwal S**, Pittenger MF. Human mesenchymal stem cells modulate allogeneic immune cell responses. *Blood* 2005; **105**: 1815-1822 [PMID: 15494428 DOI: 10.1182/blood-2004-04-1559]

4 **Rohaina CM**, Then KY, Ng AM, Wan Abdul Halim WH, Zahidin AZ, Saim A, Idrus RB. Reconstruction of limbal stem cell deficient corneal surface with induced human bone marrow mesenchymal stem cells on amniotic membrane. *Transl Res* 2014; **163**: 200-210 [PMID: 24286920 DOI: 10.1016/j.trsl.2013.11.004]

5 **Prockop DJ**, Oh JY. Mesenchymal stem/stromal cells (MSCs): role as guardians of inflammation. *Mol Ther* 2012; **20**: 14-20 [PMID: 22008910 DOI: 10.1038/mt.2011.211]

6 **Tse WT**, Pendleton JD, Beyer WM, Egalka MC, Guinan EC. Suppression of allogeneic T-cell proliferation by human marrow stromal cells: implications in transplantation. *Transplantation* 2003; **75**: 389-397 [PMID: 12589164 DOI: 10.1097/01.tp.0000045055.63901.a9]

7 **Caplan AI**, Dennis JE. Mesenchymal stem cells as trophic mediators. *J Cell Biochem* 2006; **98**: 1076-1084 [PMID: 16619257 DOI: 10.1002/jcb.20886]

8 **Polisetty N**, Fatima A, Madhira SL, Sangwan VS, Vemuganti GK. Mesenchymal cells from limbal stroma of human eye. *Mol Vis* 2008; **14**: 431-442 [PMID: 18334960]

9 **Branch MJ**, Hashmani K, Dhillon P, Jones DR, Dua HS, Hopkinson A. Mesenchymal stem cells in the human corneal limbal stroma. *Invest Ophthalmol Vis Sci* 2012; **53**: 5109-5116 [PMID: 22736610 DOI: 10.1167/iovs.11-8673]

10 **Sidney LE**, Branch MJ, Dua HS, Hopkinson A. Effect of culture medium on propagation and phenotype of corneal stroma-derived stem cells. *Cytotherapy* 2015; **17**: 1706-1722 [PMID: 26454751 DOI: 10.1016/j.jcyt.2015.08.003]

11 **Sidney LE**, McIntosh OD, Hopkinson A. Phenotypic Change and Induction of Cytokeratin Expression During In Vitro Culture of Corneal Stromal Cells. *Invest Ophthalmol Vis Sci* 2015; **56**: 7225-7235 [PMID: 26544791 DOI: 10.1167/iovs.15-17810]

12 **Sidney LE**, Hopkinson A. Corneal keratocyte transition to mesenchymal stem cell phenotype and reversal using serum-free medium supplemented with fibroblast growth factor-2, transforming growth factor-β3 and retinoic acid. *J Tissue Eng Regen Med* 2018; **12**: e203-e215 [PMID: 27685949 DOI: 10.1002/term.2316]

13 **Bray LJ**, Heazlewood CF, Munster DJ, Hutmacher DW, Atkinson K, Harkin DG. Immunosuppressive properties of mesenchymal stromal cell cultures derived from the limbus of human and rabbit corneas. *Cytotherapy* 2014; **16**: 64-73 [PMID: 24094499 DOI: 10.1016/j.jcyt.2013.07.006]

14 **Veréb Z**, Póliska S, Albert R, Olstad OK, Boratkó A, Csortos C, Moe MC, Facskó A, Petrovski G. Role of Human Corneal Stroma-Derived Mesenchymal-Like Stem Cells in Corneal Immunity and Wound Healing. *Sci Rep* 2016; **6**: 26227 [PMID: 27195722 DOI: 10.1038/srep26227]

15 **Hashmani K**, Branch MJ, Sidney LE, Dhillon PS, Verma M, McIntosh OD, Hopkinson A, Dua HS. Characterization of corneal stromal stem cells with the potential for epithelial transdifferentiation. *Stem Cell Res Ther* 2013; **4**: 75 [PMID: 23800436 DOI: 10.1186/scrt226]

16 **Jia Z**, Li F, Zeng X, Lv Y, Zhao S. The effects of local administration of mesenchymal stem cells on rat corneal allograft rejection. *BMC Ophthalmol* 2018; **18**: 139 [PMID: 29884142 DOI: 10.1186/s12886-018-0802-6]

17 **Song HB**, Park SY, Ko JH, Park JW, Yoon CH, Kim DH, Kim JH, Kim MK, Lee RH, Prockop DJ, Oh JY. Mesenchymal Stromal Cells Inhibit Inflammatory Lymphangiogenesis in the Cornea by Suppressing Macrophage in a TSG-6-Dependent Manner. *Mol Ther* 2018; **26**: 162-172 [PMID: 29301108 DOI: 10.1016/j.ymthe.2017.09.026]

18 **Mittal SK**, Omoto M, Amouzegar A, Sahu A, Rezazadeh A, Katikireddy KR, Shah DI, Sahu SK, Chauhan SK. Restoration of Corneal Transparency by Mesenchymal Stem Cells. *Stem Cell Reports* 2016; **7**: 583-590 [PMID: 27693426 DOI: 10.1016/j.stemcr.2016.09.001]

19 **Luo X**, Li J, Yin L, Pan J, Zhang Y, Jiang Z. Role of microRNA 146a on the healing of cornea alkali burn treated with mesenchymal stem cells. *Mol Med Rep* 2018; **18**: 3203-3210 [PMID: 30066863 DOI: 10.3892/mmr.2018.9328]

20 **Fuentes-Julián S**, Arnalich-Montiel F, Jaumandreu L, Leal M, Casado A, García-Tuñon I, Hernández-Jiménez E, López-Collazo E, De Miguel MP. Adipose-derived mesenchymal stem cell administration does not improve corneal graft survival outcome. *PLoS One* 2015; **10**: e0117945 [PMID: 25730319 DOI: 10.1371/journal.pone.0117945]

21 **Hong HS**, Kim YH, Son Y. Perspectives on mesenchymal stem cells: tissue repair, immune modulation, and tumor homing. *Arch Pharm Res* 2012; **35**: 201-211 [PMID: 22370775 DOI: 10.1007/s12272-012-0201-0]

22 **Tseng SC**, He H, Zhang S, Chen SY. Niche Regulation of Limbal Epithelial Stem Cells: Relationship between Inflammation and Regeneration. *Ocul Surf* 2016; **14**: 100-112 [PMID: 26769483 DOI: 10.1016/j.jtos.2015.12.002]

23 **Stern M**. The grafting of preserved amniotic membrane to burned and ulcerated surfaces, substituting skin grafts: A preliminary report. *JAMA* 1913; **60**: 973-974 [DOI: 10.1001/jama.1913.04340130021008]

24 **SORSBY A**, SYMONS HM. Amniotic membrane grafts in caustic burns of the eye (burns of the second degree). *Br J Ophthalmol* 1946; **30**: 337-345 [PMID: 20985210 DOI: 10.1136/bjo.30.6.337]

25 **Hao Y**, Ma DH, Hwang DG, Kim WS, Zhang F. Identification of antiangiogenic and antiinflammatory proteins in human amniotic membrane. *Cornea* 2000; **19**: 348-352 [PMID: 10832697 DOI:

10.1097/00003226-200005000-00018]
26 **Shimmura S**, Shimazaki J, Ohashi Y, Tsubota K. Antiinflammatory effects of amniotic membrane transplantation in ocular surface disorders. *Cornea* 2001; **20**: 408-413 [PMID: 11333331 DOI: 10.1097/00003226-200105000-00015]
27 **Bauer D**, Wasmuth S, Hennig M, Baehler H, Steuhl KP, Heiligenhaus A. Amniotic membrane transplantation induces apoptosis in T lymphocytes in murine corneas with experimental herpetic stromal keratitis. *Invest Ophthalmol Vis Sci* 2009; **50**: 3188-3198 [PMID: 19255156 DOI: 10.1167/iovs.08-3041]
28 **Lee SH**, Tseng SC. Amniotic membrane transplantation for persistent epithelial defects with ulceration. *Am J Ophthalmol* 1997; **123**: 303-312 [PMID: 9063239 DOI: 10.1016/S0002-9394(14)70125-4]
29 **Shimazaki J**, Yang HY, Tsubota K. Amniotic membrane transplantation for ocular surface reconstruction in patients with chemical and thermal burns. *Ophthalmology* 1997; **104**: 2068-2076 [PMID: 9400767 DOI: 10.1016/S0161-6420(97)30057-8]
30 **Koizumi N**, Inatomi T, Quantock AJ, Fullwood NJ, Dota A, Kinoshita S. Amniotic membrane as a substrate for cultivating limbal corneal epithelial cells for autologous transplantation in rabbits. *Cornea* 2000; **19**: 65-71 [PMID: 10632011 DOI: 10.1097/00003226-200001000-00013]
31 **Araki-Sasaki K**, Ohashi Y, Sasabe T, Hayashi K, Watanabe H, Tano Y, Handa H. An SV40-immortalized human corneal epithelial cell line and its characterization. *Invest Ophthalmol Vis Sci* 1995; **36**: 614-621 [PMID: 7534282]
32 **Zhao S**, Fernald RD. Comprehensive algorithm for quantitative real-time polymerase chain reaction. *J Comput Biol* 2005; **12**: 1047-1064 [PMID: 16241897 DOI: 10.1089/cmb.2005.12.1047]
33 **Allen CL**, Clare G, Stewart EA, Branch MJ, McIntosh OD, Dadhwal M, Dua HS, Hopkinson A. Augmented dried versus cryopreserved amniotic membrane as an ocular surface dressing. *PLoS One* 2013; **8**: e78441 [PMID: 24205233 DOI: 10.1371/journal.pone.0078441]
34 **da Silva Meirelles L**, Chagastelles PC, Nardi NB. Mesenchymal stem cells reside in virtually all post-natal organs and tissues. *J Cell Sci* 2006; **119**: 2204-2213 [PMID: 16684817 DOI: 10.1242/jcs.02932]
35 **Chamberlain G**, Fox J, Ashton B, Middleton J. Concise review: mesenchymal stem cells: their phenotype, differentiation capacity, immunological features, and potential for homing. *Stem Cells* 2007; **25**: 2739-2749 [PMID: 17656645 DOI: 10.1634/stemcells.2007-0197]
36 **Ye J**, Yao K, Kim JC. Mesenchymal stem cell transplantation in a rabbit corneal alkali burn model: engraftment and involvement in wound healing. *Eye (Lond)* 2006; **20**: 482-490 [PMID: 15895027 DOI: 10.1038/sj.eye.6701913]
37 **Perrella G**, Scott CA, Spelat R, Brusini P, D'Aurizio F, De Pol I, Dua HS. Cultured hyman keratocytes from the limbus and cornea both express epithelial cytokeratin 3: Possible mesenchymal-epithelial transition. *Int J Ophthalmic Pathol* 2012; **1**: 1-7 [DOI: 10.4172/2324-8599.1000101]
38 **Li GG**, Zhu YT, Xie HT, Chen SY, Tseng SC. Mesenchymal stem cells derived from human limbal niche cells. *Invest Ophthalmol Vis Sci* 2012; **53**: 5686-5697 [PMID: 22836771 DOI: 10.1167/iovs.12-10300]
39 **Kelm JM**, Fussenegger M. Scaffold-free cell delivery for use in regenerative medicine. *Adv Drug Deliv Rev* 2010; **62**: 753-764 [PMID: 20153387 DOI: 10.1016/j.addr.2010.02.003]
40 **Lekhanont K**, Choubtum L, Chuck RS, Sa-ngiampornpanit T, Chuckpaiwong V, Vongthongsri A. A serum- and feeder-free technique of culturing human corneal epithelial stem cells on amniotic membrane. *Mol Vis* 2009; **15**: 1294-1302 [PMID: 19578552]
41 **Kawakita T**, Espana EM, He H, Smiddy R, Parel JM, Liu CY, Tseng SC. Preservation and expansion of the primate keratocyte phenotype by downregulating TGF-beta signaling in a low-calcium, serum-free medium. *Invest Ophthalmol Vis Sci* 2006; **47**: 1918-1927 [PMID: 16638999 DOI: 10.1167/iovs.05-1040]
42 **Postnikoff CK**, Pintwala R, Williams S, Wright AM, Hileeto D, Gorbet MB. Development of a curved, stratified, in vitro model to assess ocular biocompatibility. *PLoS One* 2014; **9**: e96448 [PMID: 24837074 DOI: 10.1371/journal.pone.0096448]
43 **Wappler J**, Rath B, Läufer T, Heidenreich A, Montzka K. Eliminating the need of serum testing using low serum culture conditions for human bone marrow-derived mesenchymal stromal cell expansion. *Biomed Eng Online* 2013; **12**: 15 [PMID: 23425366 DOI: 10.1186/1475-925X-12-15]
44 **Mills KH**, Dunne A. Immune modulation: IL-1, master mediator or initiator of inflammation. *Nat Med* 2009; **15**: 1363-1364 [PMID: 19966773 DOI: 10.1038/nm1209-1363]
45 **Vela JM**, Molina-Holgado E, Arévalo-Martín A, Almazán G, Guaza C. Interleukin-1 regulates proliferation and differentiation of oligodendrocyte progenitor cells. *Mol Cell Neurosci* 2002; **20**: 489-502 [PMID: 12139924 DOI: 10.1006/mcne.2002.1127]
46 **Oh JY**, Yu JM, Ko JH. Analysis of ethanol effects on corneal epithelium. *Invest Ophthalmol Vis Sci* 2013; **54**: 3852-3856 [PMID: 23674759 DOI: 10.1167/iovs.13-11717]
47 **Mohan RR**, Mohan RR, Kim WJ, Wilson SE. Modulation of TNF-alpha-induced apoptosis in corneal fibroblasts by transcription factor NF-kappaB. *Invest Ophthalmol Vis Sci* 2000; **41**: 1327-1336 [PMID: 10798647]
48 **Kimura K**, Teranishi S, Nishida T. Interleukin-1beta-induced disruption of barrier function in cultured human corneal epithelial cells. *Invest Ophthalmol Vis Sci* 2009; **50**: 597-603 [PMID: 19171646 DOI: 10.1167/iovs.08-2606]
49 **Li DQ**, Wang Z, Yoon KC, Bian F. Characterization, isolation, expansion and clinical therapy of human corneal epithelial stem/progenitor cells. *J Stem Cells* 2014; **9**: 79-91 [PMID: 25158157]
50 **Kureshi AK**, Dziasko M, Funderburgh JL, Daniels JT. Human corneal stromal stem cells support limbal epithelial cells cultured on RAFT tissue equivalents. *Sci Rep* 2015; **5**: 16186 [PMID: 26531048 DOI: 10.1038/srep16186]
51 **Oh JY**, Kim MK, Shin MS, Lee HJ, Ko JH, Wee WR, Lee JH. The anti-inflammatory and anti-angiogenic role of mesenchymal stem cells in corneal wound healing following chemical injury. *Stem Cells* 2008; **26**: 1047-1055 [PMID: 18192235 DOI: 10.1634/stemcells.2007-0737]

P- Reviewer: Liu L, Micheu MM, Vladimir H
S- Editor: Ji FF **L- Editor:** Filipodia **E- Editor:** Bian YN

World Journal of Stem Cells

Submit a Manuscript: https://www.f6publishing.com

World J Stem Cells 2019 February 26; 11(2): 100-123

DOI: 10.4252/wjsc.v11.i2.100

ISSN 1948-0210 (online)

ORIGINAL ARTICLE

Basic Study

Triple-modal imaging of stem-cells labeled with multimodal nanoparticles, applied in a stroke model

Helio Rodrigues da Silva, Javier Bustamante Mamani, Mariana Penteado Nucci, Leopoldo Penteado Nucci, Andrea Tiemi Kondo, Daianne Maciely Carvalho Fantacini, Lucas Eduardo Botelho de Souza, Virginia Picanço-Castro, Dimas Tadeu Covas, José Mauro Kutner, Fernando Anselmo de Oliveira, Nelson Hamerschlak, Lionel Fernel Gamarra

ORCID number: Helio Rodrigues da Silva (0000-0002-1173-745X); Javier Bustamante Mamani (0000-0001-5038-0070); Mariana Penteado Nucci (0000-0002-1502-9215); Leopoldo Penteado Nucci (0000-0002-1234-5845); Andrea Tiemi Kondo (0000-0002-4228-8503); Daianne Maciely Carvalho Fantacini (0000-0003-2694-0132); Lucas Eduardo Botelho de Souza (0000-0003-4254-7509); Virginia Picanço-Castro (0000-0002-3914-0938); Dimas Tadeu Maciely Covas (0000-0002-7364-2595); José Mauro Kutner (0000-0003-3784-6731); Fernando Anselmo de Oliveira (0000-0002-7226-1694); Nelson Hamerschlak (0000-0002-5140-5310); Lionel Fernel Gamarra (0000-0002-3910-0047).

Author contributions: da Silva HR and Gamarra LF conceptualized the original idea; da Silva HR, Mamani JB, Nucci MP and Gamarra LF designed and performed the experiments and analyzed the data; Nucci LP and de Oliveira FA performed analysis of the data and animal management; Fantacini DMC, de Souza LEB, Picanço-Castro V and Covas DT performed the cellular culture for transduction of luciferase and the writing of the original draft; Kondo AT, Kutner JM, Nucci LP and Hamerschlak N performed the stem cell isolation and immunophenotype characterization; Mamani JB, Nucci

Helio Rodrigues da Silva, Javier Bustamante Mamani, Andrea Tiemi Kondo, José Mauro Kutner, Fernando Anselmo de Oliveira, Nelson Hamerschlak, Lionel Fernel Gamarra, Hospital Israelita Albert Einstein, São Paulo 05651-900, Brazil

Mariana Penteado Nucci, LIM44, Hospital das Clinicas HCFMUSP, Faculdade de Medicina, Universidade de São Paulo, São Paulo 05403-010, Brazil

Leopoldo Penteado Nucci, Centro Universitário do Planalto Central, Brasilia 72445-020, Brazil

Daianne Maciely Carvalho Fantacini, Lucas Eduardo Botelho de Souza, Virginia Picanço-Castro, Dimas Tadeu Covas, Faculdade de Medicina de Ribeirão Preto, Universidade de São Paulo, São Paulo 05403-010, Brazil

Corresponding author: Lionel Fernel Gamarra, PhD, Senior Scientist, Group of nanobiotechnology of The Albert Einstein Hospital, Hospital Israelita Albert Einstein, Avenida Albert Einstein, 627/701 - Morumbi, São Paulo 05651-900, Brazil. lgamarra@einstein.br
Telephone: +55-11-21510243

Abstract

BACKGROUND

Mesenchymal stem cells (MSCs) have been widely tested for their therapeutic efficacy in the ischemic brain and have been shown to provide several benefits. A major obstacle to the clinical translation of these therapies has been the inability to noninvasively monitor the best route, cell doses, and collateral effects while ensuring the survival and effective biological functioning of the transplanted stem cells. Technological advances in multimodal imaging have allowed *in vivo* monitoring of the biodistribution and viability of transplanted stem cells due to a combination of imaging technologies associated with multimodal nanoparticles (MNPs) using new labels and covers to achieve low toxicity and longtime residence in cells.

AIM

To evaluate the sensitivity of triple-modal imaging of stem cells labeled with MNPs and applied in a stroke model.

METHODS

After the isolation and immunophenotypic characterization of human bone

MP, Nucci LP and Gamarra LF did the writing - original draft and writing - review and editing; Gamarra LF performed funding acquisition, investigation, project administration, resources and supervision.

Supported by Conselho Nacional de Desenvolvimento Científico e Tecnológico, No. CNPq-465259/2014-6, and No. CNPq-400856/2016-6; São Paulo State Research Support Foundation, No. 2014/50983-3, and No. 2016/21470-3.

Institutional review board statement: The study was approved by the Ethics Committee for Research at the Instituto Israelita de Ensino e Pesquisa Albert Eisntein, Brazil (CAAE - 27665714.4.0000.0071) for the use of human mesenchymal stem cells after the donors informed consent.

Institutional animal care and use committee statement: The study was approved by the Ethics in Animal Research Committee of the Hospital Israelita Albert Einstein (HIAE) with approval number 1906-13. The vivarium of the Experimental Surgical Training Center (Centro de Experimentação e Treinamento em Cirurgia - CETEC) was accredited by the Association for the Assessment and Accreditation of Laboratory Animal Care International (AAALAC International).

Conflict-of-interest statement: The authors have declared that no competing interests exist.

Data sharing statement: The datasets supporting the conclusions of this article are included within in the article.

ARRIVE guidelines statement: The authors have read the ARRIVE guidelines - Animal Research: Reporting *In vivo* Experiments, and the manuscript was prepared and revised according to the ARRIVE guidelines.

marrow MSCs (hBM-MSCs), our team carried out lentiviral transduction of these cells for the evaluation of bioluminescent images (BLIs) *in vitro* and *in vivo*. In addition, MNPs that were previously characterized (regarding hydrodynamic size, zeta potential, and optical properties), and were used to label these cells, analyze cell viability *via* the 3-[4,5-dimethylthiazol-2-yl]-2,5 diphenyl tetrazolium bromide assay and BLI analysis, and quantify the internalization process and iron load in different concentrations of MNPs *via* magnetic resonance imaging (MRI), near-infrared fluorescence (NIRF), and inductively coupled plasma-mass spectrometry (ICP-MS). In *in vivo* analyses, the same labeled cells were implanted in a sham group and a stroke group at different times and under different MNP concentrations (after 4 h or 6 d of cell implantation) to evaluate the sensitivity of triple-modal images.

RESULTS

hBM-MSC collection and isolation after immunophenotypic characterization were demonstrated to be adequate in hBM samples. After transduction of these cells with luciferase (hBM-MSC$_{Luc}$), we detected a maximum BLI intensity of 2.0 x 10^8 photons/s in samples of 10^6 hBM-MSCs. Analysis of the physicochemical characteristics of the MNPs showed an average hydrodynamic diameter of 38.2 ± 0.5 nm, zeta potential of 29.2 ± 1.9 mV and adequate colloidal stability without agglomeration over 18 h. The signal of iron load internalization in hBM-MSC$_{Luc}$ showed a close relationship with the corresponding MNP-labeling concentrations based on MRI, ICP-MS and NIRF. Under the highest MNP concentration, cellular viability showed a reduction of less than 10% compared to the control. Correlation analysis of the MNP load internalized into hBM-MSC$_{Luc}$ determined *via* the MRI, ICP-MS and NIRF techniques showed the same correlation coefficient of 0.99. Evaluation of the BLI, NIRF, and MRI signals *in vivo* and *ex vivo* after labeled hBM-MSC$_{Luc}$ were implanted into animals showed differences between different MNP concentrations and signals associated with different techniques (MRI and NIRF; 5 and 20 μg Fe/mL; $P < 0.05$) in the sham groups at 4 h as well as a time effect (4 h and 6 d; $P < 0.001$) and differences between the sham and stroke groups in all images signals ($P < 0.001$).

CONCLUSION

This study highlighted the importance of quantifying MNPs internalized into cells and the efficacy of signal detection under the triple-image modality in a stroke model.

Key words: Multimodal nanoparticles; Human bone marrow mesenchymal stem cells; Near-infrared fluorescence image; Magnetic resonance image; Bioluminescence; Stroke

Core tip: Multimodal imaging techniques provide morpho-functional information for studying pathological events following ischemia associated with new tracers. Molecular imaging innovations will contribute to the further understanding of stem cell transplantation, allowing an assessment of their therapeutic effects at the molecular scale. In this study, we evaluate the sensitivity of triple-modal imaging of human bone marrow mesenchymal stem cells labeled with multimodal nanoparticles (MNPs) to quantify the internalized iron load and cellular viability as well as the correlation of quantification results between the techniques. We demonstrate the importance of quantifying the MNP load internalized into cells *via* triple-image evaluation and the efficacy of signal detection in a stroke model.

Citation: da Silva HR, Mamani JB, Nucci MP, Nucci LP, Kondo AT, Fantacini DMC, de Souza LEB, Picanço-Castro V, Covas DT, Kutner JM, de Oliveira FA, Hamerschlak N, Gamarra LF. Triple-modal imaging of stem-cells labeled with multimodal nanoparticles, applied in a stroke model. *World J Stem Cells* 2019; 11(2): 100-123
URL: https://www.wjgnet.com/1948-0210/full/v11/i2/100.htm
DOI: https://dx.doi.org/10.4252/wjsc.v11.i2.100

Manuscript source: Unsolicited manuscript

Received: October 22, 2018
Peer-review started: October 23, 2018
First decision: November 14, 2018
Revised: December 5, 2018
Accepted: December 17, 2018
Article in press: December 17, 2018
Published online: February 26, 2019

INTRODUCTION

Mesenchymal stem cells (MSCs) have been widely tested for therapeutic efficacy in the ischemic brain. The important roles of paracrine and immune modulatory mechanisms in the beneficial effects exerted by MSCs have been recognized in many studies[1]. Due to the relative ease of isolation, low immunogenicity, and good proliferation, differentiation, and paracrine potential of MSCs, these stem cells have become the main source for tissue engineering of bone, cartilage, muscle, marrow stroma, fat, and other connective tissues[2]. Moreover, we and others have shown that cellular therapy using MSC transplantation has the potential to improve the symptoms of various aging diseases, such as Parkinson's disease, stroke, amyotrophic lateral sclerosis, and multiple sclerosis[1,2].

Several preclinical investigations have indicated that the MSCs are unable to replace dead neurons following ischemic events; nevertheless, they provide various other types of benefits *via* parallel processes, including growth factor upregulation at the injured site, decreasing apoptosis, reducing glial scar formation, promoting axonal outgrowth, synaptic remodeling, neurogenesis, angiogenesis, and astrocyte and oligodendrocyte growth factors[1]. Intravenous injection is an often-used route for the delivery of MSCs in pre-clinical and clinical trials[3]. It was recently discovered that a large proportion of MSCs injected intravenously are trapped in the pulmonary vasculature, leading to a low delivery efficiency to target organs[4]. Nevertheless, it remains difficult to non-invasively monitor the delivery and biodistribution of administered cells in target organs in a quantitative way over a long period, without relying on behavioral endpoints or tissue histology[5].

Therefore, a major obstacle to the clinical translation of these therapies has been the inability to noninvasively monitor the best route, cell doses, and collateral or epigenomic effects, while ensuring survival and the effective biological functioning of the transplanted stem cells[6].

Consequently, there is a need for technological advances in the development of non-invasive imaging techniques with a high spatial and temporal resolution that allow *in vivo* monitoring of the biodistribution and viability of transplanted stem cells[7]. These requirements can be met through a combination of imaging technologies, also known as multimodal imaging[8]. In parallel with this increase in technological image-based verification, multimodal nanoparticles (MNPs) have been developed to show lower toxicity and an increased residence time in cells with the use of new labels and covers[9].

Currently, multimodal imaging techniques provide morpho-functional information at different times, which improves the field of diagnostic imaging, in addition to generating detailed information on diseases from multiple images and allowing simultaneous diagnosis and therapy[10]. Technological innovations and the development of new tracers and smart probes have further promoted these multimodal imaging techniques, providing safe improvement of contrast and multidimensional functional, structural and morphological information[9].

Superparamagnetic iron oxide nanoparticles (SPIONs), which are known for their magnetic properties (superparamagnetic), biocompatibility, biodegradability, surface-to-volume ratio, and greater surface area (sizes as small as 100 nm), exhibit diverse potential applications, such as drug delivery for magnetic resonance imaging (MRI), diagnostics, specific cell labeling and tracking of cell separation and bio-catalysis. Surface modification with polymeric stabilizers and inorganic molecules (*e.g.*, silica, gold, gadolinium, fluorescent dyes) increases sensibility and specificity in certain medical diagnoses, thus making this approach ideal for increasing accuracy in many biomedical applications[11].

SPION labeling with near-infrared (NIR) dye, which further improves probe capabilities, reveals deeper tissue penetration due to minimal absorbency of the surface tissue in the spectral region[12]. *In vivo* fluorescence imaging has undergone remarkable growth with the use of the novel NIR fluorescence (NIRF) probes and optical instruments that allow evaluation of the dynamic migration and distribution of transplanted MSCs as well as the stem cell-based regeneration of tissue[13].

The bioluminescent imaging (BLI) technique is complementary to NIRF imaging, enhancing the monitoring of ischemic and inflammation processes and viable cells after engraftment reduction. The BLI method requires genetic modification of cells to express the luciferase enzyme signal. Despite the low spatial resolution, the resulting images exhibit a good temporal resolution, and cell morphology is not altered[14].

Promising studies have focused on engineering MSCs for targeted delivery in specific targets. Additional efforts would benefit from imaging technologies for quantitatively monitoring *in vivo* cell localization and in real time[15]. One previous study by our group examining *in vivo* dual-modal imaging techniques (MRI combined with NIRF) and cytology demonstrated that the infused labeled cells could be

efficiently tracked in a Parkinson`s disease model. However, cellular viability could not be assessed due to the lack of another imaging modality[16]. Therefore, the present study aimed to evaluate two procedures: (1) we evaluate the sensitivity of triple-modal imaging (NIRF, MRI and BLI) of stem cells labeled with multimodal nanoparticles for quantification of the iron load internalized and cellular viability *in vitro* as well as the correlation of quantification results between the techniques of inductively coupled plasma-mass spectrometry (ICP-MS), MRI and NIRF; (2) we verify whether the images of stem cells labeled with multimodal nanoparticles maintain the same properties after application in a stroke model.

MATERIALS AND METHODS

In vitro study

Isolation and culture of human bone marrow MSCs: hMSCs were isolated from the bone marrow of normal donors who had provided informed consent for the research project (CAAE - 27665714.4.0000.0071), which was approved by the ethics committee for research at the Instituto Israelita de Ensino e Pesquisa Albert Eisntein (São Paulo, Brazil).

The aspirated bone marrow was diluted with phosphate-buffered saline (PBS) (Gibco®, Carlsbad, CA, United States) (1:3) then centrifuged with 20 mL of Ficoll/Hypaque (GE Healthcare) for 30 min at 500 *x*g and 22 °C. Following centrifugation, the cells were removed from the plasma/Ficoll-Hypaque interface, washed 3 times with PBS, and resuspended in Dulbecco's modified Eagle's medium - high glucose (DMEM-HG) (Gibco®, Carlsbad, CA, United States) supplemented with 15% fetal bovine serum (FBS) (Gibco®, Carlsbad, CA, United States).

The hBM-MSCs were cultivated in 75 cm^2 flasks with DMEM - low glucose (DMEM-LG) (GIBCO - Invitrogen Technologies, New York, USA), supplemented with 10% FBS, 1% de L-glutamine, 100 U/mL streptomycin and 100 U/mL penicillin (GIBCO - Invitrogen Technologies, New York, United States) and were maintained in humidified incubators with 5% CO_2 at 37 ºC, to favor the attachment of cells to the flask bottom.

Immunophenotypic characterization of hBM-MSCs: Cell-surface expression was analyzed with a predefined set of protein markers. In brief, cells at the third passage with 70% confluency were stained with the selected monoclonal antibodies and incubated in the dark for 30 min at 4 ºC. The cells were then washed and fixed with 1% paraformaldehyde. The following positive human marker antibodies were used: CD29-PE (clone: MAR4; BD Pharmingen), CD44-PE (clone: 515; BD Pharmingen), CD73-PE (clone: AD2; BD Pharmingen), CD90-APC (clone: 5E10; BD Pharmingen), and CD105-PE (clone: 8E11; Chemicon, Temecula, CA, United States). The negative markers were as follows: CD14-FITC (clone: M5E2; BD Pharmingen, San Diego, CA, United States), CD19-APC (clone: SJ25C1; Biosciences), CD31-PE (clone: WM59; BD Pharmingen), CD34-PE (clone: 581; BD Pharmingen), CD45-PerCP-Cy5 (clone: 2D1; Biosciences, San Jose, CA, United States), CD106-FITC (clone: 51-10C9; BD Pharmingen), and human leukocyte antigen HLA-DR-PerCPCy5 (clone: L243; Biosciences). The cells were analyzed using FACSARia flow cytometry equipment (Becton Dickinson, San Jose, CA, United States), and the acquired data were analyzed using FLOWJO (Tree Star, Ashland, OR) software.

The hBM-MSCs were also subjected to differentiation induction to evaluate the multipotentiality characteristics and differentiation capacity of the cells into two cellular types: adipocytes and osteoblasts.

Lentiviral transduction of hBM-MSCs for BLI analysis: Cells were genetically engineered to generate luciferase-expressing hBM-MSCs (hBM-MSC_{Luc}). Briefly, hBM-MSCs were transduced with the glycoprotein of the vesicular stomatitis virus (VSV-G) from pseudotyped viruses carrying the lentiviral vector (pMSCV_Luc2_T2A_Puro). The vector encodes the bioluminescent reporter luciferase-2 and the puromycin resistance gene puromycin N-acetyl-transferase under the control of a murine stem cell virus (MSCV) promoter.

For virion production, human embryonic kidney 293FT cells grown at 80% confluence in 150 mm Petri dishes (about 20 million cells/dish) were simultaneously transfected with 30 μg/dish of the vector pMSCV-Luc2-T2A-Puro along with two other helper vectors: 20 μg/dish of pCMV-dr8.91 and 10 μg/dish of pMD2.G. Transfection was conducted with 25-kDa linear polyethylenimine (PEI, Alfa Ansar) as previously reported[17]. Two days after transfection, the viral supernatant was collected and filtered through 0.45 μm polyvinylidene fluoride (PVDF) filters and concentrated by ultracentrifugation. As described in previous reports, the copy

number of integrated lentiviral vector sequences was determined *via* quantitative real-time polymerase chain reaction (PCR).

For lentiviral transduction, virions were added to cultures of 1 × 10^6 hBM-MSCs at a multiplicity of infection of 3 (MOI = 3) in the presence of 8 μg/mL polybrene (Sigma-Aldrich). The medium was replaced after 18 h, and the cells were cultured for an additional 48 h. After this period, the cells were selected for incubation with 1 μg/mL puromycin every other day for 8 d.

Bioluminescence signal expression in hBM-MSC$_{Luc}$: The expression of the bioluminescence (BLI) signal in hBM-MSC$_{Luc}$ was analyzed in the following cell concentrations/well: 1 × 10^4, 1 × 10^5 and 1 × 10^6, in triplicate samples in a 24-well plate, using IVIS® Lumina LT Series III equipment (Xenogen Corp. CA, EUA). Images were captured before and after the addition of 100 μL of D-luciferin (50 mg/mL) (XenoLight, PerkinElmer), and the intensity of the BLI signal was detected under the following parameters: Exposure time of 2 ms with a 5 min interval between each image acquisition, over a total of 490 min. The kinetics of BLI expression were registered and analyzed with Living Image Software version 4.3.1 (IVIS Imaging System) in radiation absolute units (photons/s).

MNP with magnetic and fluorescent properties: We used multimodal nanoparticles (MNP-IR750; Molday ION™750 - BioPal) with an 8 nm iron oxide (Fe_3O_4) nucleus, a hydrodynamic size of 35 nm (coated with dextran), and a zeta potential of approximately +31 mV, which were conjugated with fluorophores that emitted fluorescence with of NIR absorption/emission wavelengths of 755/777 nm. The MNP-IR750 has magnetic and fluorescent properties detectable in MRI and NIR images.

MNP-IR750 characterization: Hydrodynamic size, zeta potential and optical properties: The hydrodynamic size and zeta potential of MNP-IR750 were measured using the dynamic light scattering (DLS) technique with the Zetasizer Nano S system (Malvern, United Kingdom). The hydrodynamic size distribution was obtained at an angle of 173°, with the number of averages set at 20 and a time of 5 s per mean. Measurements were performed in a fixed position at 25 °C with a 60 s equilibrium period. In addition, to obtain information about possible agglomeration of nanoparticles, we performed an analysis of the stability of MNP-IR750 using DMEM-LG supplemented with 10% FBS over 18 h. The hydrodynamic size and zeta potential (surface charge) measurements were performed at a concentration of 50 μg Fe/mL and a pH of 7.4.

To verify the optical properties of MNP-IR750 excitation/emission, the corresponding spectrum was acquired using a Shimadzu RF-6000 fluorometer at a concentration of 100 μg Fe/mL, maintaining the temperature at 37 °C.

hBM-MSC$_{Luc}$ labeled with MNP-IR750: For hBM-MSC$_{Luc}$ labeling with MNP-IR750, triplicate samples of 1 × 10^4 cells were placed in a 24-well plate in DMEM-LG, supplemented with 15% FBS, penicillin (100 U/mL), streptomycin (100 μg/mL) and 1% L-glutamine. After 24 h of hBM-MSC$_{Luc}$ adhesion, the cells were washed twice with 300 μL of PBS and incubated for 18 h (at 37 °C and 5% CO_2), with MNP-IR750 added at the following concentrations: 5, 10, 20, 30, 40 and 50 μg Fe/mL, in DMEM-LG supplemented with 15% FBS. After incubation, the culture medium was removed, and the cells were washed three times with PBS.

Following the labeling of hBM-MSC$_{Luc}$ with MNP-IR750, the evaluation of MNP-IR750 internalized was performed *via* MRI, NIRF and BLI, and the viability of the labeled cells was assessed *via* the 3-[4,5-dimethylthiazol-2-yl]-2,5 diphenyl tetrazolium bromide (MTT) assay and the BLI technique.

Internalization of MNP-IR750 into hBM-MSC$_{Luc}$: Confirmation of the labeling of hBM-MSC$_{Luc}$ with MPN-IR750 was performed at the following concentrations: 5, 10, 20, 30, 40 and 50 μg/mL of MNP-IR750 in culture plates, *via* Prussian Blue staining[16,18]. Cells that were previously labeled and fixed in plates were washed twice with PBS and incubated with a staining solution composed of 0.25 mg of potassium ferrocyanide [K4Fe(CN)$_6$] (SIGMA, United States) and 5% hydrochloric acid (HCl) in a proportion of 1:1, in a volume of 1000 μL per well over 5 min at room temperature, protected from light. After this period, the Prussian Blue solution was removed, and the wells containing hBM-MSC$_{Luc}$ were washed twice with 500 μL of PBS. Thereafter, 500 μl of Nuclear Fast Red staining solution (SIGMA, United States) was added to the wells, followed by incubation for 10 min. After staining, the cells were washed again with PBS (2x), and light-field images were obtained under a Nikon TI® inverted microscope.

MRI, NIRF and BLI signals after internalization of MNP-IR750 by hBM-MSC$_{Luc}$: MRI, NIRF and BLI signals were evaluated in hBM-MSC$_{Luc}$ after labeling with MNP-IR750 at the following concentrations: 5, 10, 20, 30, 40 and 50 μg/mL.

For MRI signal evaluation, the labeled hBM-MSC$_{Luc}$ were mixed with 1% agarose (Sigma-Aldrich Chemie GmbH, Germany) and plated in culture wells. Images were acquired on a 3T RM scanner with a head coil of 32 channels (Magnetom Vision, Siemens, Germany) using the T2-weighted imaging sequence, following the protocol described in a previous study[19].

NIRF and BLI images were acquired after the plating of labeled hBM-MSC$_{Luc}$. The BLI signal was acquired after the addition of 100 μL of luciferin (1 mmol/L in PBS), the maximum time of intensity of the BLI signal determined *via* kinetic BLI analysis (section 2.4), using an exposure time of 2 ms, binning of 2 and f/stop of 4. The NIRF signal was acquired in the same samples used for BLI, applying an excitation of 745 nm, registered in a range of emission of 810-875 nm. Both imaging analyses were performed with IVIS® Lumina LT Series III equipment, and the signals were analyzed in radiation absolute units (photons/s). The experiments were performed with hBM-MSC$_{Luc}$ between the fifth and seventh passages.

Viability of hBM-MSC$_{Luc}$ labeled with MNP-IR750 - MTT and BLI: Evaluation of the viability of hBM-MSC$_{Luc}$ labeled with MNP-IR750 was performed using the MTT and BLI assays.

In the MTT assay, hBM-MSC$_{Luc}$ were grown in 96-well plates until they were subconfluent. MPN-IR750 were then added to the cells at defined concentrations of 5, 10, 20, 30, 40 and 50 μg Fe/mL, followed by incubation overnight. After incubation, the culture medium was discarded, and 100 μL of fresh medium per well was added to the cells, after thorough washing with PBS. Then, 100 μL of the MTT reagent (1 mg/mL - final concentration) was added per well, and the plate was incubated for four h in an incubator, at 37 °C in 5% CO_2. Actinomycin D (Sigma-Aldrich) was used as positive control for cell death in this assay. The "cell death dose" concentration identified in this assay was 0.25 μg/mL. After incubation, the medium was discarded from the wells, and 100 μL of dimethyl sulphoxide (DMSO Hybri-Max - Sigma-Aldrich) was added to solubilize the formazan crystals that had formed. Readings were then taken in a DTX 880 Multimode Detector reader (Beckman Coulter) at 490 nm, with subtraction for plate absorbance at 650 nm. The viability percentage of the cells was calculated as the ratio of the mean absorbance of triplicate readings with respect to the mean absorbance of control wells, as cell viability = (sample/control) × 100.

The viability assays were verified using the BLI technique. Similar samples to those used in the MTT assays were used for the BLI assay, adding 100 mL of luciferin in each well, and acquiring the BLI images using IVIS® Lumina LT Series III equipment. For BLI intensity analysis (photons/s), a region of interest (ROI) of 2.5 cm^2 was selected. The viability percentage was calculated with the formula (sample/control) × 100.

Quantification of MNP-IR750 internalized into hBM-MSC$_{Luc}$: Quantification of MNP-IR750 after hBM-MSC$_{Luc}$ labeling was performed *via* MRI, ICP-MS and NIR imaging. The samples used for quantification were prepared with 1 × 10^6 hBM-MSC$_{Luc}$ that either were not labeled (control) or were labeled with MNP-IR750 at the following concentrations: 5, 10, 20, 30, 40 and 50 μg Fe/mL.

Quantification of MNP-IR750 internalized into hBM-MSC$_{Luc}$*via* MRI. For quantification of the internalization process by MRI, the following equation was used:

(1) $1/(T_2^{\text{hBM-MSC}_{Luc}+\text{MNP\_IR750}}) = 1/(T_2^{\text{hBM-MSC}_{Luc}}) + [Fe] \times r_2$

where [Fe] is the concentration of intracellular iron internalized into hBM-MSC$_{Luc}$; r_2 is the relaxivity of the MNP-IR750; and T_2 is the transverse relaxation time for samples containing hBM-MSC$_{Luc}$ labeled with MNP-IR750 and control samples (hBM-MSC$_{Luc}$).

For the calculation of r_2, a phantom with 24 wells (culture plate) containing MNP-IR750 suspended in the following concentrations was used: 0, 2, 4, 6, 10, 15 and 20 μg Fe/mL, dispersed in 1% agarose. The phantom was subjected to MRI examination and the T_2 values of samples were determined from the relaxivity curves. The r_2 values were obtained *via* linear adjustment of the inverse of the transverse relaxation *vs* the concentration of MNP-IR750 used for cellular labeling.

For the calculation of $T_2^{\text{hBM-MSC}_{Luc}+\text{MNP\_IR750}}$, samples labeled with different concentrations of nanoparticles, as described above, were used; for the determination of $T_2^{\text{hBM-MSC}_{Luc}}$, only 1 × 10^6 hBM-MSC$_{Luc}$ from the samples were used. In both analyses, the samples were suspended in a 1% agarose solution and plated in a 24-well culture plate, then subjected to MRI examination.

T_2-weighted MRI images were acquired in a whole-body 3T scanner (Magneton Vision®, Siemens, Erlangen, Germany) with a 32-channel head coil using the following

parameters: Multicontrast turbo-spin echo sequence, repetition time (TR) of 1500 ms, echo time (TE) of 8-256 ms, field of view of 300 mm, 256 × 256 matrix, slice thickness of 3.0 mm and flip angle of 180°. The intensity curves of the MRI signals of the samples as a function of TE were analyzed using a selection of regions of interest with a fixed size. The T_2 of each sample was determined by adjusting the decay curve with a monoexponential linear algorithm: Intensity (TE) = C × $e^{(-TE/T2)}$.

From the MNP-IR750 load obtained from equation 1, the number of MNP-IR750 internalized into hBM-MSC_{Luc} was calculated with the following equation:

(2) Number of MNP_IR750 = $[6 \times load_{MNP\_IR750} \times (at\_m)]/[\pi \times \rho_{MNP\_IR750} \times M_{Fe} \times \varphi^3_{MNP\_IR750}]$

Where $load_{MNP\_IR750}$ is the internalization MNP-IR750 loaded into hBM-MSC_{Luc}; at_m is the atomic mass; ρ_{MNP_IR750} is the iron oxide density (Fe_3O_4); M_{Fe} is the molecular weight of iron; and φ_{MNP_IR750} is the diameter of MNP-IR750.

Quantification of MNP-IR750 internalized into hBM-MSC_{Luc}*via* ICP-MS. The samples were diluted in 1 mL of Milli-Q® water (EMD Millipore Corporation, Bedford MA, USA) and subjected to the digestion of organic components with 5 mL of nitric acid (37%) using a Titan Microwave sample preparation system (Perkin Elmer, USA). After digestion, the samples were analyzed with ICP-MS equipment (Perkin Elmer Nexion 350x, PerkinElmer Corporation, USA) to determine the iron content of each sample. Measurements of samples were performed in triplicate, and quantification was based on a calibration curve using certified standard iron (NexION # N8145054) at the following concentrations: 0, 10, 20, 30, 40 and 50 ng Fe/mL (ppb). Samples of 1 × 10^6 hBM-MSC_{Luc} without labeling were used as a control.

Quantification of MNP-IR750 internalized into hBM-MSC_{Luc}*via* NIRF imaging. NIRF images were acquired after trypsinization of the samples and washing with PBS. The NIRF signal was detected after excitation at 745 nm and was registered in the emission range of 810-875 nm using IVIS® Lumina LT Series III equipment. The absolute quantification was determined after establishing the calibration curve using known concentrations of 1, 2, 3, 4, 5 and 6 μg Fe/mL.

In vivo study

Animals and experimental design: We used 2-month-old male Wistar rats weighing 250-300 g. The animals were maintained at the vivarium of the Experimental Surgical Training Center (Centro de Experimentação e Treinamento em Cirurgia - CETEC) at 21 ± 2°C and 60% ± 5% relative humidity with full ventilation under a 12 h light/dark cycle (7 a.m. - 7 p.m.), and they had access to food and water *ad libitum*. This vivarium is accredited by the Association for the Assessment and Accreditation of Laboratory Animal Care International (AAALAC International), and the general conditions were monitored daily. The study was approved by the Ethics in Animal Research Committee of the Hospital Israelita Albert Einstein (HIAE) with approval number 1906-13

The experimental design of the *in vivo* study involved in two experiments:

Experiment 1 was conducted to analyze the sensitivity of the NIRF, BLI and MRI signals of the labeled hBM-MSC_{Luc} implanted at different concentrations in the animals in the sham group, after being subjected to a craniectomy procedure. These animals were divided into 4 groups (n = 7 rats/group): Group Sham_control (S_control) - implantation of 1 × 10^6 de hBM-MSC_{Luc}; Group Sham_5 - implantation of 1 × 10^6 de hBM-MSC_{Luc} labeled with 5 μg Fe/mL of MPN-IR750; Group Sham_20 implantation of 1 × 10^6 de hBM-MSC_{Luc} labeled with 20 μg Fe/mL of MPN-IR750; and Group Sham_50 implantation of 1 × 10^6 de hBM-MSC_{Luc} labeled with 50 μg Fe/mL of MPN-IR750.

Experiment 2 analyzed the NIRF, BLI and MRI signals of the labeled hBM-MSC_{Luc} implanted in the animals after being subjected to stroke induction. These animals were divided into 2 groups (n = 7 rats/group): Group Sham_50: implantation of 1 × 10^6 de hBM-MSC_{Luc} labeled with 50 μg Fe/mL of MPN-IR750; and Group Stroke_50: implantation of 1 × 10^6 de hBM-MSC_{Luc} labeled with MPN-IR750. The concentration of nanoparticles that was used was determined from the best conditions verified in experiment 1.

In both experiments, the animals were randomly allocated, coded and housed in individual cages.

Evaluation of NIRF, BLI and MRI signals after the implantation of hBM-MSC_{Luc} labeled with MNP-IR750 in animals (Experiment 1): A total of 28 Wistar rats were used to evaluate the behavior of the signals of the labeled and unlabeled hBM-MSC_{Luc} in the animals' brains. The animals were anesthetized with ketamine hydrochloride (100 mg/kg) and xylazine hydrochloride (20 mg/kg) i.p. and subjected to a craniectomy procedure to implant the cells at the following coordinates: 2.0 mm antero-posterior, 2.0 mm lateral to the midline and 2.5 mm deep, according to the

atlas of Paxinos and Watson (1986)[20]. The cells were infused at a rate of 10 μL/min using a 10 μL Hamilton syringe.

After 4 h of cell implantation, the animals were subjected to evaluation of BLI expression and NIRF detection *in vivo* using IVIS® Lumina LT Series III equipment. The NIRF signal measurements were obtained with an excitation wavelength of 745 nm and an emission wavelength of 810-875 nm. Soon thereafter, the animals received 150 mg/kg of luciferin i.p., and the BLI images were acquired with 10 min of latency. Both images were analyzed in radiation absolute units (photons/s).

The animals were euthanized after *in vivo* NIRF and BLI evaluation. Their brains were extracted to record NIRF emissions using the same parameters employed for *in vivo* image acquisition. Following *ex vivo* NIRF analysis, the brains were fixed with 4% paraformaldehyde, and brain phantoms were prepared with 1% agarose for MRI signal evaluation. The phantoms with brain tissue were analyzed by using a 3T scanner (Siemens), to track the hBM-MSC$_{Luc}$ labeled with MNP-IR750. The MRI images were obtained with a 3D Fast Low Angle Shot (FLASH) sequence, a matrix of 256x160x128, TR = 200 ms, TE = 20 ms, and a range of excitation angle of 20-25º.

Induction of a focal ischemic lesion *via* thermocoagulation (stroke): A focal brain ischemic lesion was induced *via* thermocoagulation in the pial blood vessels of the motor and somatosensory cortex as previously described[21]. Briefly, animals were anesthetized with ketamine hydrochloride (100 mg/kg, i.p.) and xylazine hydrochloride (20 mg/kg, i.p.) and placed in a stereotaxic apparatus (Harvard Apparatus, Holliston, United States). A craniectomy procedure was performed to expose the left somatosensory cortex (+ 2 to -6 mm in the anterior-posterior direction and +2 mm on the medial-lateral axis from the Bregma, according to the atlas of Paxinos and Watson)[20]. Superficial blood vessels were transdurally thermocoagulated by approximation of a hot probe to the dura matter (about 2 mm), maintaining a constant temperature of 400ºC for 30 min. The procedure was concluded with incision tissue suturing and the administration of a tramadol analgesic (5 mg/kg) (i.p.). Throughout anesthesia, the rats were placed on a heating pad to maintain the rectal temperature at 37.0 ± 0.5 ºC (PhysioSuite, kent Scientific Corporation, Torrington, CT, United States).

The ischemic lesion was confirmed through local blood perfusion analysis using a PeriCam Perfusion Speckle Imager (PSI) system (Perimed, Stockholm, Sweden) and TTC staining after 2 h of lesion induction, as described in a previous study[21]. The color changes of the targeted region, from light red to dark red, were also noted[22].

Implantation of hBM-MSC$_{Luc}$ labeled with MNP-IR750 and evaluation of the signal in the brains of animals after focal ischemic lesion induction (Experiment 2): In experiment 2, after 24 hs of focal brain ischemic induction, the animals were subjected to cell implantation in the same manner described above in section 2.13. Then, 6 d after stroke induction, we analyzed the signal behavior of the hBM-MSC$_{Luc}$ labeled with MNP-IR750 *via* BLI and NIRF imaging *in vivo* and MRI *ex vivo*, following the same procedures described in section 2.13. The concentration of MNP-IR750 implanted in the stroke group was determined from the best result for the signal detected in the presence of the different concentrations tested in experiment 1.

Statistical analysis

Data were presented as the mean and standard deviation in each analysis. For the *in vivo* study, the quantification of the effect of the MNP-IR750 concentration in the sham group was compared *via* the ANOVA test, following Bonferroni-corrected post hoc tests for each image technique (experiment 1). For temporal analysis in the sham groups (4 h *vs* 6 d, experiments 1 and 2, respectively) and group analysis for experiment 2 (sham *vs* stroke at 6 d), Student's *t*-test was applied, with previous verification of a normal distribution and homoscedasticity in the two groups. Finally, we compared the differences between NIRF and MRI *via* an independent samples *t*-test.

RESULTS

Characterization of hBM-MSCs

After the isolation and culture of hBM-MSCs, immunophenotypic characterization was performed using flow cytometry, which showed that showed positive surface markers for CD29 (93.7%), CD44 (94.9%), CD 73 (95.0%), CD90 (94.7%) and CD105 (93.2%) as depicted in Figure 1A-E, negative surface markers for CD14 (0.17%), CD19(0.87%), CD31(1.35%), CD34(1.47%), CD45 (0.83%) and CD106 (0.96%), as depicted in Figure 1F-K, with low levels of HLA-DR (2.82%, Figure 1L). These results

confirmed the immunophenotypic profile of the hBM-MSCs and demonstrated that the collection and isolation of these cells from human bone marrow samples were adequate.

hBM-MSC$_{Luc}$ bioluminescence signal

The hBM-MSC$_{Luc}$ bioluminescence signal was analyzed as a function of the number of cells over 490 min showing the intensity of the signal curves (Figure 2), in which we observed a peak of intensity at 10 min, followed by a decrease in the BLI signal intensity over time. These patterns were observed for all concentrations of cells tested, and the highest cell concentrations corresponded to the highest amplitude curves.

Images of circular ROIs represented the BLI intensity over time for each concentration of cells. The color variations of the ROIs were determined from the intensity of the BLI signal for each part of the curve, as represented by a color scale of intensity (Figure 2, blue to red scale). The BLI intensity of 10^6 hBM-MSC$_{Luc}$ samples revealed a maximum of 2.0×10^8 photons/s (Figure 2, peak of the blue curve) after luciferin addition, but the BLI intensity was almost null under the same concentration (10^6 hBM-MSC$_{Luc}$) without luciferin addition (inset in Figure 2, black curve). The peaks of BLI intensity for 10^4 hBM-MSC$_{Luc}$ and 10^5 hBM-MSC$_{Luc}$ were 0.3×10^7 and 0.25×10^8 photons/s, respectively (Figure 2, pink and red curves).

MNP-IR750 characterization

Figure 3 shows the curves of the hydrodynamic size distribution of MPN-IR750 acquired over 18 h. The curves for a polydispersed log-normal size distribution showed an average hydrodynamic diameter of 38.2 ± 0.5 nm. The curves obtained temporally showed a constant distribution of the hydrodynamic diameter in DMEM-LG culture supplemented with 10% PBS. MNP-IR750 did not agglomerate in the period of time analyzed, showing adequate stability during the analysis.

The MNP-IR750 surface charge determined from the zeta potential at pH 7.4 was $\xi = +29.2 \pm 1.9$ mV, as shown in Figure 3B, indicating a positive potential of MNP-IR750 that favors the electrostatic process with hBM-MSC$_{Luc}$.

The fluorescence optical properties of MNP-IR750 revealed peaks of intensity in the excitation/emission spectrum at 757.9 nm (excitation) and 779.4 nm (emission), as shown in Figure 3C. These values correspond to the infrared spectrum, which indicates high applicability in *in vivo* studies, due to low absorption of biologic molecules in this region of the spectrum.

Evaluation of the internalization of MNP-IR750 by hBM-MSC$_{Luc}$

After labeling hBM-MSC$_{Luc}$ with MNP-IR750 at concentrations of 5, 10, 20, 30, 40 and 50 μg Fe/mL, Prussian blue staining was performed. The optical microscopy images showed that the presence of MNP-IR750 was highlighted, due to the blue staining of iron oxide nuclei in the hBM-MSCLuc cytoplasm (Figure 4 A-N), demonstrating the efficacy of cellular labeling at all MNP-IR750 concentrations.

In addition to the adequate labeling intensity, the cellular morphology was preserved under all labeling conditions. However, the intensity of labeling was dependent on the MNP-IR750 concentration used. The cells labeled with 5 μg/mL of MNP-IR750 exhibited lower labeling in comparison to the other concentrations tested. The difference was discrete between 10 and 20 μg/mL of MNP-IR750 (Figure 4E-H) and between 30, 40 and 50 μg/mL of MNP-IR750 (Figure 4I-N). The contrast between the 5 and 10 μg/mL concentrations of MNP-IR750 (Figure 4C, D and 4E, F, respectively) and between 20 and 30 μg/mL of MNP-IR750 (Figure 4G, H and 4I, J, respectively) was more evident than those between the other concentrations.

Evaluation of hBM-MSC$_{Luc}$ labeled with MNP-IR750 based on fluorescent properties was not possible *via* the fluorescence microscopy technique, as the emission/absorption spectrum is within the NIR range.

Evaluation of the viability of hBM-MSC$_{Luc}$ labeled with MNP-IR750: MTT and BLI assays

The cellular viability analysis of hBM-MSC$_{Luc}$ labeled with different concentrations of MNP-IR750 indicated a discrete increase in toxicity due to increasing concentrations of MNP-IR750 compared to the control sample (hBM-MSC$_{Luc}$ unlabeled) (Figure 4O).

Under standard culture conditions, unlabeled hBM-MSC$_{Luc}$ (control) showed 100% relative cellular viability in both assays (Figure 4O). Cellular viability determined *via* the MTT assay decreased as the MNP-IR750 concentration rose, where the lowest MNP-IR750 concentration (5 μg Fe/mL) resulted in a viability of 98.9%, and while a viability of 90.5% was observed for the highest concentration of MNP-IR750 (50 μg Fe/mL). The difference between the highest concentration of MNP-IR750 (50 μg Fe/mL) and the control was 9.5%, with remarkable differences being found between 5 and 10 μg Fe/mL of MNP-IR750 (2.2%), 20 and 30 μg Fe/mL of MNP-IR750 (1.6%)

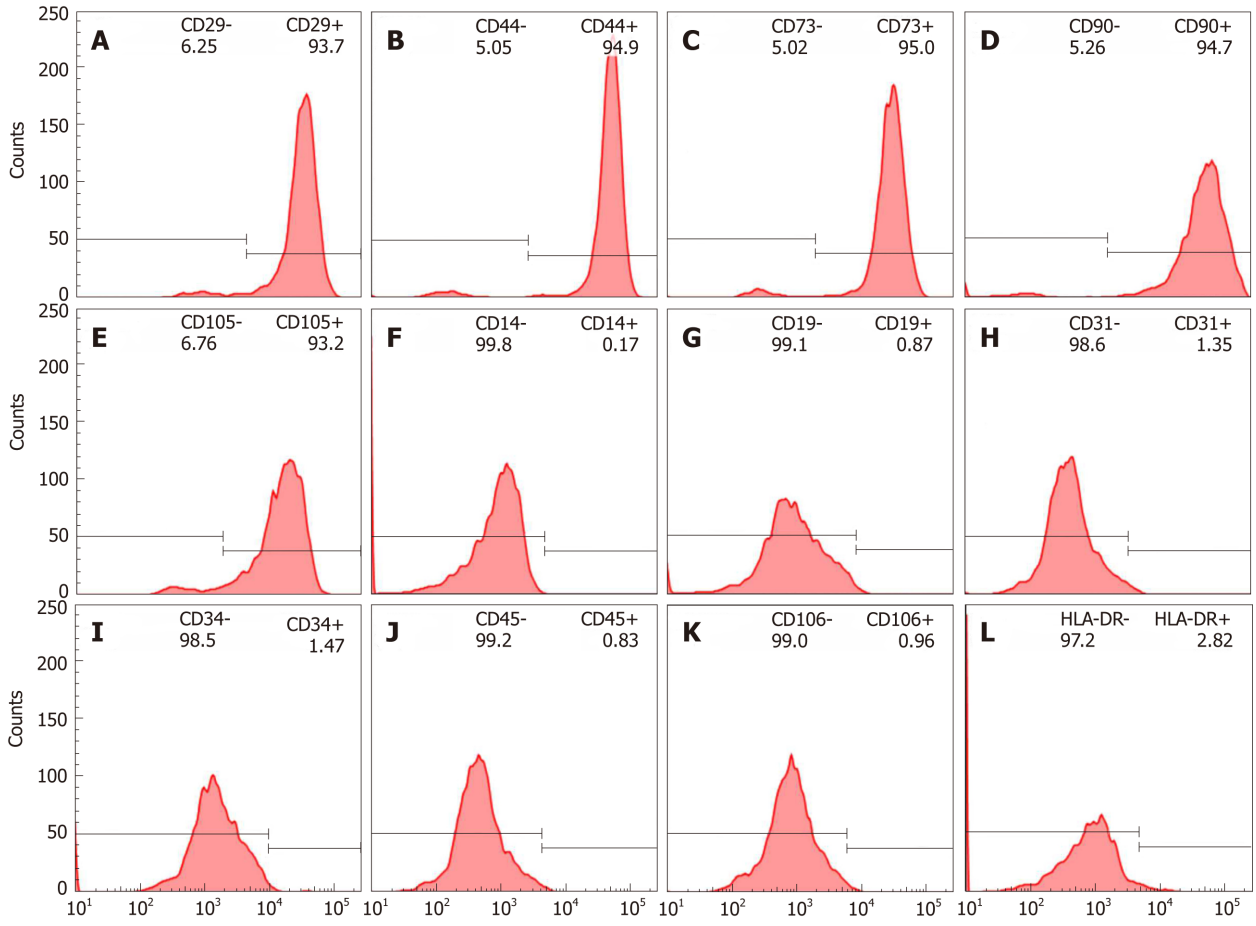

Figure 1 Immunophenotypic characterization of human bone marrow mesenchymal stem cells. A-D: Positive surface markers CD29, CD44, CD 73, CD90 and CD105; E-K: Negative surface markers CD14, CD19, CD31, CD34, CD45 and CD106; L: Low levels of HLA-DR.

and 30 and 40 μg Fe/mL of MNP-IR750 (3.0%). The lowest difference between the concentrations was found between 40 and 50 μg Fe/mL of MNP-IR750 (0.5%) (Figure 4O - red bars).

In the BLI assay, cellular viability decreased by 7.7% from the control to the highest concentration of MNP-IR750 (92.3% for 50 μg Fe/mL of MNP-IR750) (Figure 4O - blue bars). The viability observed under lower MNP-IR750 concentrations showed greater relevance (97.6% for 5 μg Fe/mL, 95.5% for 10 μg Fe/mL and 94.7% for 20 μg Fe/mL), while for the highest concentrations, viability was more constant (93.8% for 30 μg Fe/mL, 93.2% for 40 μg Fe/mL and 92.3% for 50 μg Fe/mL) (Figure 4O - blue bars).

The cellular viability showed dependence upon the dose applied but remained over 90% in both assays. Considering the small deviation observed for each MNP-IR750 concentrations, the viability values found in the MTT and BLI assays were highly similar.

Evaluation of MRI, NIRF and BLI signals after internalization of MNP-IR750 by hBM-MSC$_{Luc}$

After labeling hBM-MSC$_{Luc}$ with MNP-IR750 at concentrations of 5, 10, 20, 30, 40 and 50 μg Fe/mL, MRI images were acquired as a function of TE (Figure 5A, first and second phantom images). These images showed differences related to the different cellular concentrations and between short and long TEs (93.6 and 249.6 ms), mainly for the highest concentrations. From the MRI, it was possible to determine the T2 values presented in the gray columns of the graphic (Figure 5B), demonstrating that the signal decayed with the increase in the MPN-IR750 concentration for both TEs analyzed; a high signal intensity was also present when a short TE was used.

BLI and NIRF images were acquired with the same phantom used in MRI, but comparing the intensity signal before and after luciferin addition (Figure 5A, fourth and last phantom images). The NIRF images showed a discrete influence of the presence of luciferin during signal analysis (Figure 5C). However, considering the small discrepancy between the intensity values, the difference was actually practically null. The BLI intensity signal after luciferin addition showed a reduction with the

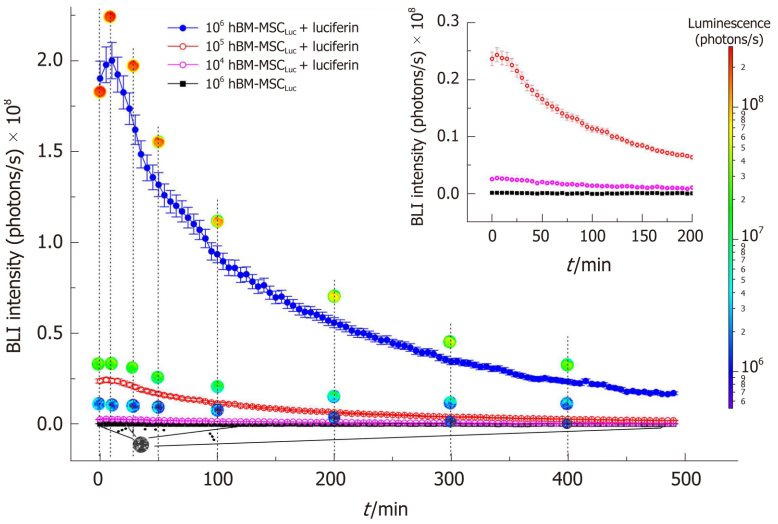

Figure 2 Expression of the bioluminescence signal as a function of number of human bone marrow mesenchymal stem cells$_{Luc}$ over 490 min. The 10^4, 10^5, and 10^6 hBM-MSC$_{Luc}$ groups with luciferin addition and the 10^6 hBM-MSC$_{Luc}$ group without luciferin addition are represented by curves in pink, red, blue and black, respectively. The inset shows the amplified signals of 10^4 and 10^5 hBM-MSC$_{Luc}$ with luciferin addition and 10^6 hBM-MSC$_{Luc}$ without luciferin addition. hBM-MSC: Human bone marrow mesenchymal stem cells.

increase in the MNP-IR750 concentration, due to the viability effect described above (Figure 5D).

Quantification of MNP-IR750 internalized by hBM-MSC$_{Luc}$ via MRI, ICP-MS and NIRF

Figure 6 shows the quantification of the iron load determined by using the MRI, ICP-MS and NIRF techniques. The process of quantification of the iron content internalized by hBM-MSC$_{Luc}$*via* MRI starts with relaxometry characterization, to determine the r^2 relaxivity of MNP-IR750 obtained upon T2-weighted image analysis (Figure 6A). The decay curves of the phantom signal related to the different concentrations of MNP-IR750 were obtained from of the ROI images shown in Figure 6A-I under the different TEs tested. The image obtained under the highest concentration of MNP-IR750 that is shown (Figure 6A-II) exhibited greater hypointensity in comparison with the control image; the gray image variations were proportional to the iron concentrations in the ROI, due to magnetic perturbation produced by the superparamagnetic properties of MNP-IR750.

The data adjustment of the relaxation rate as a function of the iron concentration (Figure 6A) followed a directly proportional straight line, which resulted in the r^2 angular coefficient value of (20.6 ± 1.4) × 10^{-4} μg Fe^{-1} ms^{-1} mL when adjusted by the method of least squares. The obtained r^2 value was characteristic of MRI contrast studies based on T2-weighted images using a 3T scanner.

Figure 6B shows the T2-weighted MRI signal intensity curves as a function of TE samples containing hBM-MSC$_{Luc}$ labeled in different concentrations of MNP-IR750. The curve decay was proportional to the iron load internalized by hBM-MSC$_{Luc}$. The T2 values of each sample were obtained from the adjustment of the MRI signal exponential decay curves, as shown in Figure 6B-IV. These values matched the MRI image of the ROI (Figure 6B-III) and were inversely proportional to the MNP-IR750 concentrations used for cellular labeling.

The MNP-IR750 load internalized by hBM-MSC$_{Luc}$ was determined from the obtained T2 values (Figure 6B, C) and r^2 values (Figure 6A) with equation 1. The number of MNP-IR750 per cell was calculated from the MNP-IR750 load using equation 2; these values were determined *via* the quantification of each labeling concentration, as shown in Table 1. The observed internalized MNP-IR750 loads $m_{cell}([Fe])$ as a function of the labeling concentration ([Fe]) were plotted and adjusted in an exponential curve, as shown in Figure 6C, following equation 3:

(3) $m_{cell}([Fe]) = m_{cell}^{max} \times (1\text{-}e^{-[Fe]/\varphi})$

where m_{cell}^{max} is the maximum number of MNP-IR750 that could be internalized by hBM-MSC$_{Luc}$ during the labeling process, and φ is a constant equivalent to the adequate MNP-IR750 concentration for achieving 63% of m_{cell}^{max} after cellular internalization. The obtained values of m_{cell}^{max} and φ are shown in Table 1, (m_{cell}^{max} = 7.91 ± 0.22 pg Fe/mL and φ = 14.46 ± 1.69 μg Fe/mL).

To verify the MRI quantification results, standard ICP-MS quantification was performed, as shown in Figure 6D. The MNP-IR750 load internalized by hBM-MSC$_{Luc}$

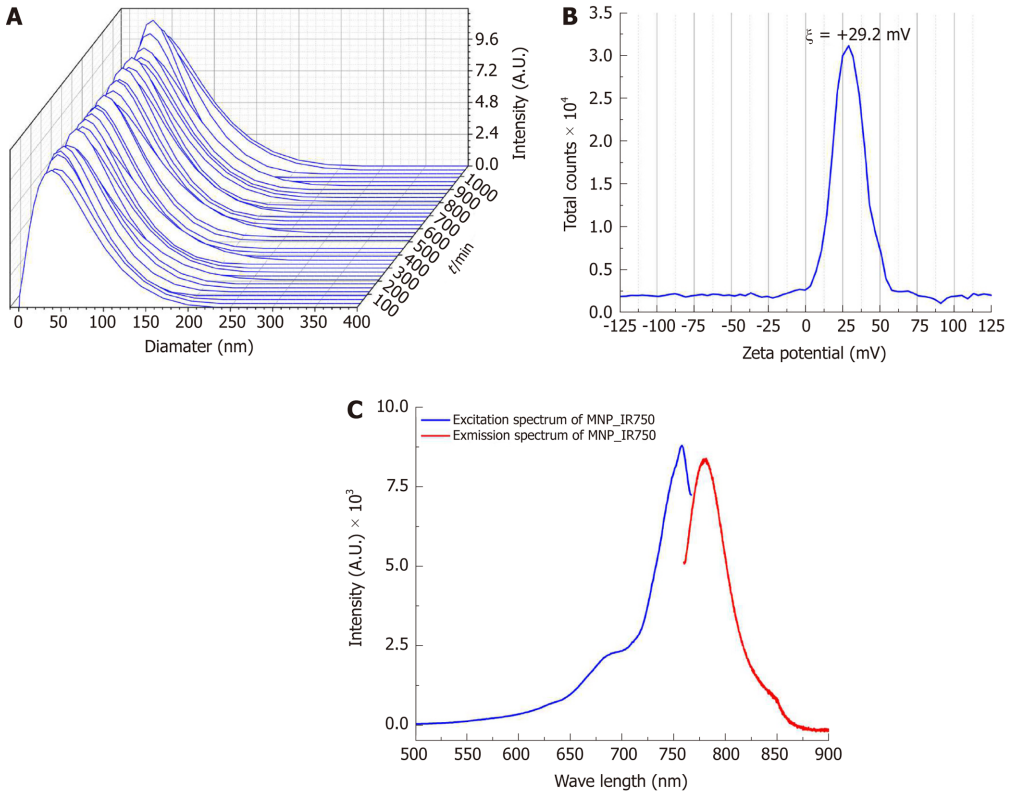

Figure 3 Characterization of the hydrodynamic diameter, zeta potential and optical properties of multimodal nanoparticles-IR750. A: Curves of the hydrodynamic size distribution of MNP-IR750 over 18 h; B: Spectrum of the surface charge of MNP-IR750 with a zeta potential at pH 7.4 of ξ = +29.2±1.9 mV; C: MNP-IR750 excitation/emission spectrum (blue and red curves, respectively), showing fluorescence intensity peaks of 757.9 and 779.4 nm, respectively. MNP: Multimodal nanoparticles.

was determined from the calibration curve generated using known MNP-IR750 concentrations, as depicted in Figure 6D,E, in which the adjustment curve presented correlation coefficient of R = 0.99. The number of MNP-IR750 internalized by hBM-MSC$_{Luc}$ at each labeling concentration was determined from the MNP-IR750 load internalized by hBM-MSC$_{Luc,}$ as shown in Table 1. m_{cell}^{max} = 7.91 ± 0.22 pg Fe/mL and φ = 14.46 ± 1.69 µg Fe/mL were determined from equation 3, as shown in Table 1.

The determination of the load and number of MNP-IR750 internalized by hBM-MSC$_{Luc}$*via* NIRF (Figure 6E) followed the same procedure used for ICP-MS after the calibration curve was generated (Figure 6E, F, R = 0.97). The values obtained for each MNP-IR750 concentration are shown in Table 1, along with the values adjusted based on an exponential curve with equation 3 (m_{cell}^{max} = 7.93 ± 0.40 pg Fe/mL and φ = 18.90 ± 2.14 µg Fe/mL).

The analysis of the correlation of the results regarding the MNP-IR750 load internalized by hBM-MSC$_{Luc}$ between the MRI, ICP-MS and NIRF techniques showed the same correlation coefficient of 0.99 (Figure 6F, blue dots for the correlation of ICP-MS - NIRF; green dots for the correlation of ICP-MS - MRI; and pink dots for the correlation of NIRF - MRI). The adjustment of the three correlation analyses is shown in Figure 6F (red dots).

Evaluation of the sensitivity of BLI, NIRF, and MRI signals of labeled hBM-MSC$_{Luc}$ implanted in animals

The evaluation of BLI, NIRF, and MRI signals *in vivo* and *ex vivo* after labeled hBM-MSC$_{Luc}$ were implanted in the animals in experiment 1 showed sensitivity in the detection of MNP-IR750 at concentrations of 5, 20 and 50 µg Fe/mL (Figure 7), after 4 h of cell implantation.

A BLI signal acquired after the implantation of the hBM-MSCLuc was present in all groups (S_control, S5, S20, and S50), even in the control group (1.31 ± 0.11; 10^7 photons/s), in which the implanted cells were not labeled with MNP-IR750 (Figure 7A-D and Figure 8J). The intensity of the BLI signal showed low variability in the S5 (1.36 ± 0.12) 10^7, S20 (1.23 ± 0.11) 10^7, and S50 (1.21 ± 0.10) 10^7 groups in relation to the increase in the MNP-IR750 concentrations (Figure 7 B-D), without any significant difference between all sham groups analyzed at each MNP-IR750 concentration (Figure 8J, *P* = 0.392).

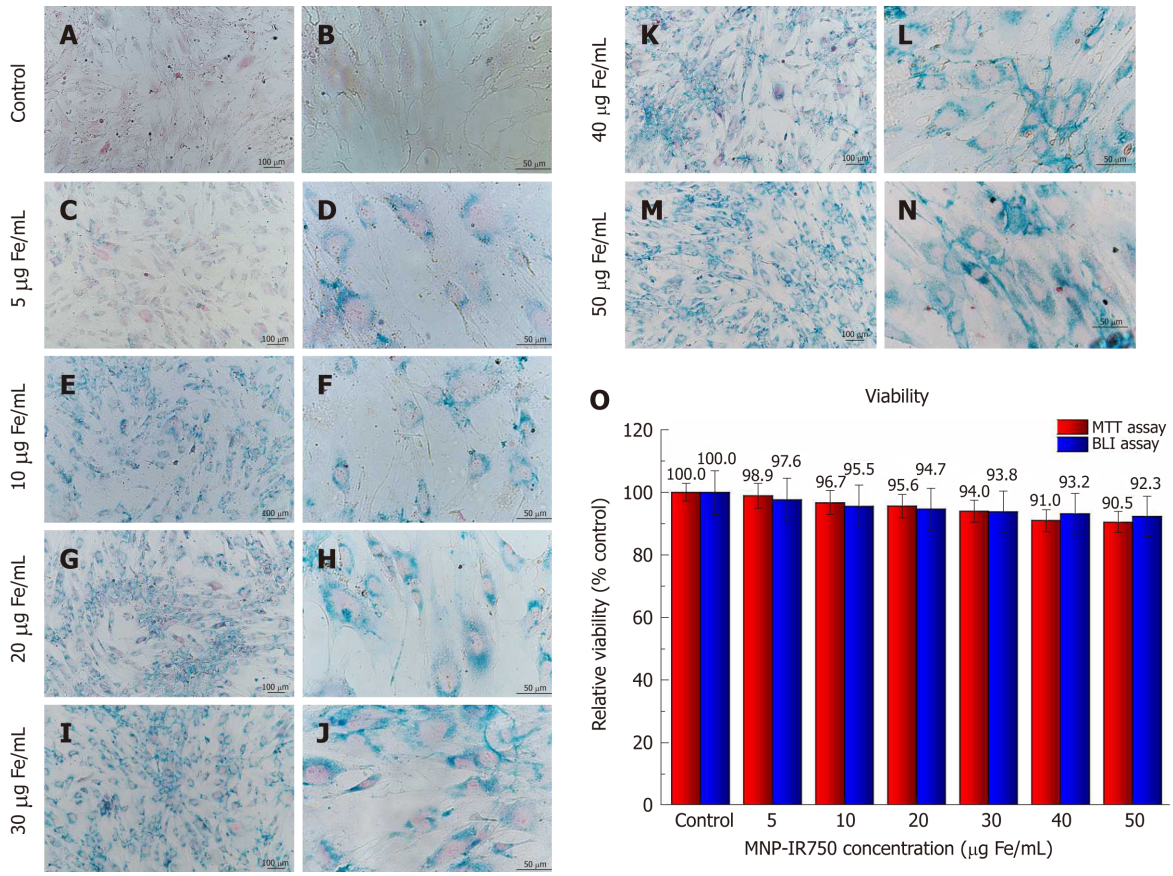

Figure 4 Internalization and viability analysis of human bone marrow mesenchymal stem cells$_{Luc}$ labeled with multimodal nanoparticles-IR750. A-N: Optical microscopy images of hBM-MSC$_{Luc}$ labeled with MNP-IR750, shown at 10 × (left column images) and 40 × (right column images); O: Cellular viability of hBM-MSC$_{Luc}$ after labeling in MTT (red bars) and BLI (blue bars) assays. Internalization of MPN-IR750 was performed at the following concentrations: 5, 10, 20, 30, 40 and 50 µg Fe/mL. hBM-MSC: Human bone marrow mesenchymal stem cells; MNP: Multimodal nanoparticles; MTT: The 3-[4,5-dimethylthiazol-2-yl]-2,5 diphenyl tetrazolium bromide; BLI: Bioluminescent images.

The NIRF signal was detected in the S5 (1.09 ± 0.19) µg Fe, S20 (3.10 ± 0.50) µg Fe and S50 (5.80 ± 0.73) µg Fe groups. A significant difference between MNP-IR750 concentrations was found *via* the ANOVA test, with a P value < 0.001(Figure 8H), where the increase in the NIRF intensity signal was proportional to the increase in the nanoparticle concentration (Figure 7 F-H). In the *ex vivo* evaluation, the NIRF signal was also detected and remained in the same brain region indicated in the *in vivo* NIRF examination (Figure 7 I-L). This evaluation also showed the same behavior with regard to intensity, but with high evidence of contrast (Figure 7 J-L), due to the decreased attenuation caused by the presence of tissue in *in vivo* images. The NIRF signal was not detected in the S_control group when evaluated *in vivo* (Figure 7E) or *ex vivo* (Figure 7I)

The *ex vivo* MRI intensity signal showed sensitivity in the detection of MNP-IR750 at different concentrations (Figure 7 M-T and Figure 8H), due to the magnetic properties of these nanoparticles. The values for each group were as follows: S5 (0.30 ± 0.15) µg Fe, S25 (1.10 ± 0.32) µg Fe and S50 (5.20 ± 0.78) µg Fe, and a significant difference was found in the comparison between them (P < 0.001). The post hoc test showed no difference between the S5 and S20 groups (P = 0.254), as shown in sagittal (Figure 7P) and coronal slices (Figure 7T). However, a more remarkable difference was revealed when comparing S50 with S5 or S20, and this difference remained significant after the post hoc test (P < 0.001), as shown in graphic representation of Figure 8H.

When the intensity quantification results were compared between techniques, a significant difference was detected between the NIRF and MRI results in the S5 and S25 groups (P = 0.005 and P = 0.004, respectively), as shown in Figure 8H.

Evaluation of the sensitivity of NIRF, BLI and MRI signals of labeled hBM-MSC$_{Luc}$ implanted in animals subjected to stroke induction

Before cellular implantation, a focal ischemic lesion induced by thermocoagulation (stroke induction) was confirmed from local blood perfusion images, which showed a

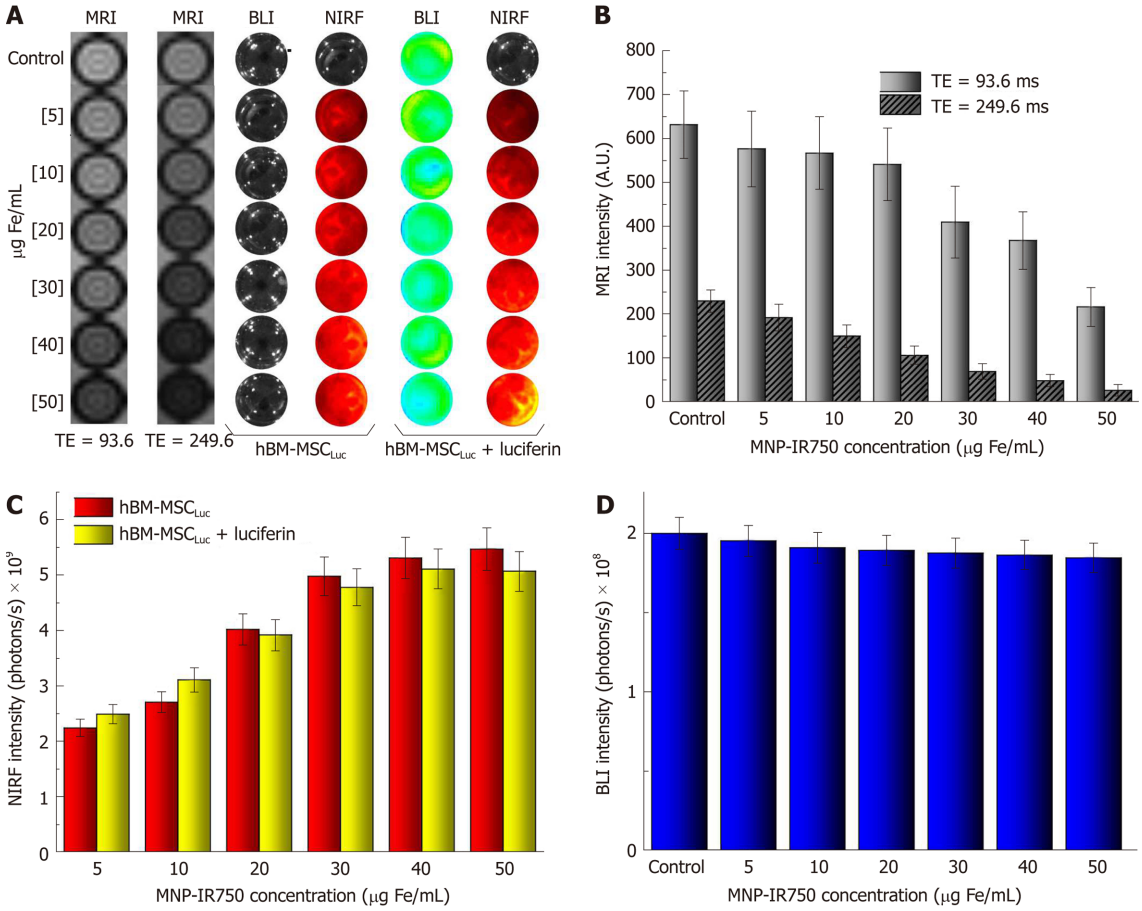

Figure 5 Evaluation of magnetic resonance imaging, near-infrared fluorescence and bioluminescent images intensity signals *in vitro*. A: Images of hBM-MSC$_{Luc}$ phantoms, labeled with different concentrations of MNP-IR750, comparing short *vs* long TEs *via* MRI and before *vs* after the addition of luciferin *via* NIRF and BLI; B: Graphic representation of the MRI signal intensity of all samples acquired with a TE of 93.6 ms (light gray bars) and a TE of 249.6 ms (dark gray bars); C: Graphic representation of the NIRF signal intensity of all samples acquiring before luciferin addition (red bars) and after luciferin addition (yellow bars); D: Graphic representation of BLI signal intensity after luciferin addition in all samples with different concentrations of MNP-IR750. hBM-MSC: Human bone marrow mesenchymal stem cells; MNP: Multimodal nanoparticles; MRI: Magnetic resonance imaging; NIRF: Near-infrared fluorescence; BLI: Bioluminescent images.

decrease in the local blood flow intensity between the basal image and the image acquired after 30 min of induction (Figure 8-I). This blood perfusion decrease represented graphically revealed a reduction of 75% ± 5% between the basal measurement and that performed after 30 min of induction (Figure 8 II). TTC staining performed 120 min after ischemic lesion induction complemented the blood perfusion analysis and showed an ischemic lesion in the pale area (non-TTC-stained) of the left sensorimotor cortex, extending to the corpus callosum and the subcortical brain region in the stroke group compared to the sham group, where the latter was only subjected to the craniectomy procedure (Figure 8 III).

The BLI intensity was found to decrease significantly in the sham_50 group (P < 0.001; Figure 8J) when the intensity of the image acquired at 4 h (1.21 ± 0.10) 10^7 (Figure 7D, J) was compared to that at 6 d after cell implantation (0.12 ± 0.07; 10^7 photons/s) (Figure 8AJ), with the same nanoparticle concentration in both groups. However, after 6 d of cell implantation, the stroke_50 group showed a significantly high signal intensity (3.02 ± 0.12; 10^7 photons/s) (Figure 8D, J) in relation to the sham_50 group (0.12 ± 0.07; 10^7 photons/s) in experiment 2 (P < 0.001; Figure 8A, J).

The NIRF and MRI images also showed a significant intensity reduction in the sham_50 group (P < 0.001; Figure 7H, L, P, T and 8B, C, E-H) when the two acquisition times were compared (4 h and 6 d) under the same nanoparticle concentration. Additionally, significant intensity increase was observed after 6 d of cell implantation under both techniques when the sham_50 group was compared to the stroke_50 group (P = 0.004 and P < 0.001, respectively; Figure 8H). The NIRF image intensity between times of acquisition was reduced from 5.80 ± 0.73 μg Fe in the S50 group (Figure 7H and Figure 8H) to 1.30 ± 0.21 μg Fe in the sham_50 group (Figure 8B, H), and the MRI intensity decreased from 5.20 ± 0.78 μg Fe in the S50 group (Figure 7P, T and Figure 8H) to 0.01 ± 0.01 μg Fe in the sham_50 group (Figure 8C, H). Regarding the difference between the sham and stroke groups at the same

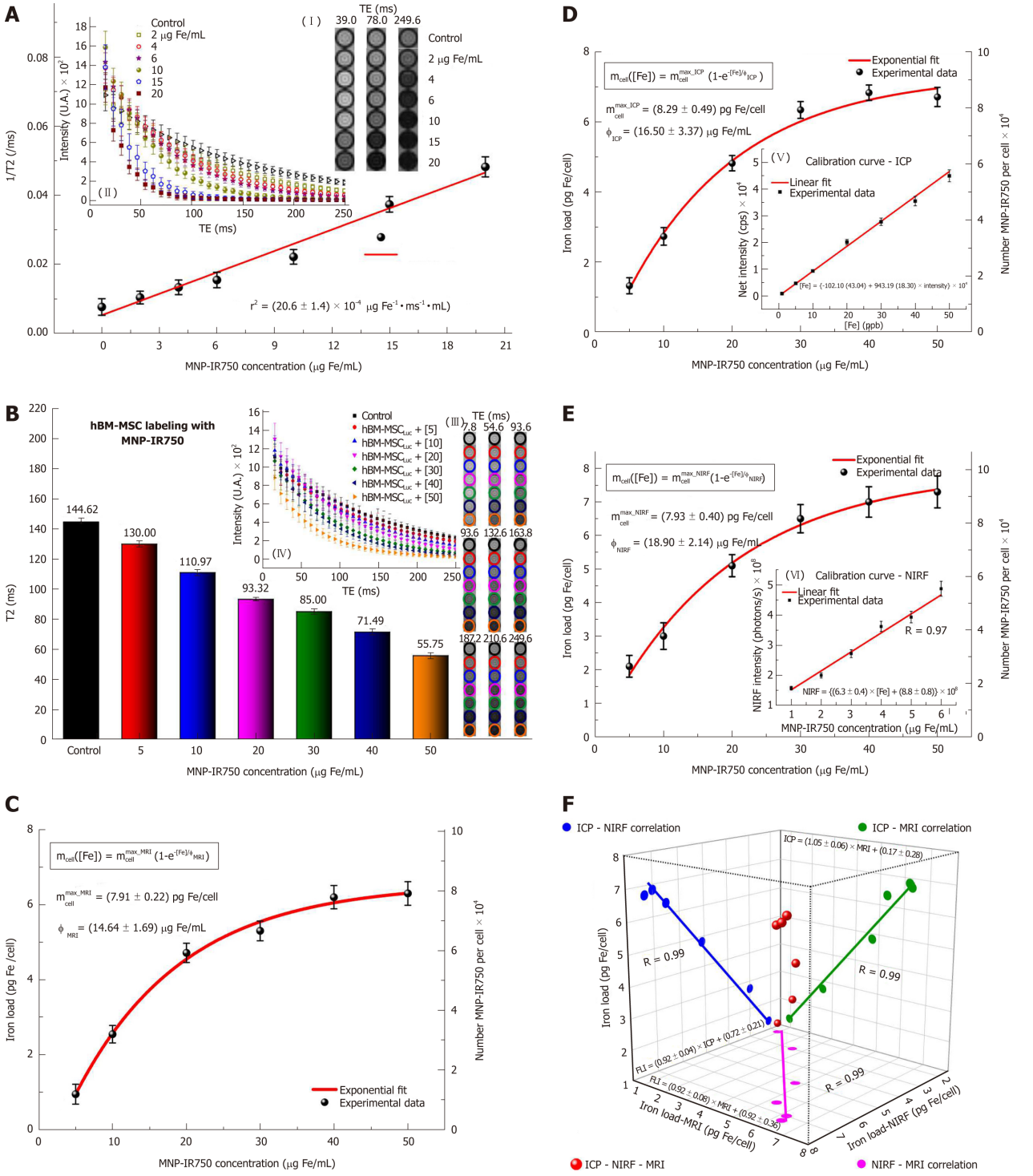

Figure 6 Quantification of multimodal nanoparticles-IR750 internalized by human bone marrow mesenchymal stem cells$_{Luc}$ using magnetic resonance imaging, inductively coupled plasma-mass spectrometry and near-infrared fluorescence images *in vitro*. For quantification *via* MRI, (A) the r_2 values were determined from the intensity signal of MNP-IR750 at different concentrations as a function of TEs (I-II); B: the T2 values of hBM-MSC$_{Luc}$ labeled with MNP-IR750 at different concentrations were determined based on the adjustment of the MRI signal exponential decay curves obtained for the MRI images of ROIs (III-IV); C: the MNP-IR750 load and number internalized per cell as a function of different labeling concentrations were determined *via* MRI, and these values were adjusted based on an exponential curve, following equation 3 and the parameters determined for this equation; D: the MNP-IR750 load and number internalized per cell as a function of different labeling concentrations were determined *via* ICP-MS (V) from the calibration curve generated using known MNP-IR750 concentrations, and the values determined *via* ICP-MS quantification were adjusted based on an exponential curve, following equation 3 and the parameters determined for this equation; E: the MNP-IR750 load and number internalized per cell as a function of different labeling concentrations were determined *via* NIRF imaging (VI) from the calibration curve generated using known MNP-IR750 concentrations, and the values determined *via* NIRF quantification were adjusted with an exponential curve, following equation 3 and the parameters determined for this equation; and F: the correlation of the MNP-IR750 load internalized by hBM-MSC$_{Luc}$ was compared between ICP-MS and NIRF (blue dots), ICP-MS and MRI (green dots), NIRF and MRI (pink dots). hBM-MSC: Human bone marrow mesenchymal stem cells; MNP: Multimodal nanoparticles; ICP-MS: Inductively coupled plasma-mass spectrometry; MRI: Magnetic resonance imaging; NIRF: Near-infrared fluorescence; BLI: Bioluminescent images.

Table 1 Quantification of the multimodal nanoparticles-IR750 load and number internalized by human bone marrow mesenchymal stem cells$_{Luc}$ *via* magnetic resonance imaging, inductively coupled plasma-mass spectrometry magnetic resonance imaging and near-infrared fluorescence

[Fe] in cell labeling (μg Fe/mL)	&Iron load /cell (pg Fe/mL)		
	¥[Number MNP-IR750 per cell × 10^4]		
	MRI	**ICP-MS**	**NIRF**
[5]	&0.94 ± 0.26	&1.32 ± 0.23	&2.12 ± 0.32
	¥1.19 ± 0.34	¥1.66 ± 0.28	¥2.64 ± 0.41
[10]	&2.54 ± 0.23	&2.73 ± 0.25	&3.02 ± 0.39
	¥3.20 ± 0.29	¥3.43 ± 0.31	¥3.77 ± 0.49
[20]	&4.71 ± 0.25	&4.82 ± 0.21	&5.14 ± 0.33
	¥5.92 ± 0.32	¥6.06 ± 0.26	¥6.41 ± 0.41
[30]	&5.31 ± 0.26	&6.34 ± 0.24	&6.52 ± 0.42
	¥6.66 ± 0.33	¥7.97 ± 0.30	¥8.17 ± 0.53
[40]	&6.20 ± 0.31	&6.83 ± 0.22	&7.12 ± 0.46
	¥7.79 ± 0.38	¥8.58 ± 0.27	¥8.79 ± 0.57
[50]	&6.30 ± 0.32	&6.71 ± 0.28	&7.3 ± 0.47
	¥7.92 ± 0.39	¥8.43 ± 0.35	¥9.17 ± 0.59
	Parameter fit curve		
	$m_{cell}([Fe]) = m_{cell}^{max} \times (1\text{-}e^{-[Fe]/\varphi})$		
Parameter	**MRI**	**ICP-MS**	**NIRF**
m_{cell}^{max} (pg Fe/mL)	7.91 ± 0.22	8.29 ± 0.49	7.93 ± 0.40
φ (μg Fe/mL)	14.64 ± 1.69	16.50 ± 3.37	18.90 ± 2.14

MRI: Magnetic resonance image; ICP-MS: Inductively coupled plasma - mass spectrometry; NIRF: Near-infrared fluorescence; $m_{cell}([Fe])$: MNP-IR750 load values internalized as a function of the labeling concentration; m_{cell}^{max}: maximum number of MNP-IR750 that could be internalized by hBM-MSC$_{Luc}$; φ: Constant equivalent of the adequate MNP-IR750 concentration for achieving 63% of m_{cell}^{max} after the cellular internalization process.

time point (6 d after cell implantation), the NIRF intensity increased from 1.30 ± 0.21 μg Fe in the sham_50 group (Figure 8B, H) to 2.80 ± 0.45 μg Fe in the stroke_50 group (Figure 8E,H), and the *ex vivo* MRI results increased from 0.01 ± 0.01 μg Fe in the sham_50 group (Figure 8C, H) to 3.20 ± 0.48 μg Fe in the stroke_50 group (Figure 8F-H). Figure 8F (yellow arrow) shows only an image of the stroke lesion, and the MRI hypointense image is indicated with red arrows in Figures 7N-P and 8F, G.

When the intensity quantification results were compared between techniques in experiment 2, a significant difference was detected between the NIRF and MRI results in the sham_50 group ($P < 0.001$), as shown in Figure 8H.

DISCUSSION

Although meta-analyses have examined the benefits of cell transplantation in experimental stroke[23], the low viable cell retention after transplantation in ischemic brain areas still represents the major obstacle to the successful clinical translation of cell-based stroke repair approaches. The present study showed high hBM-MSC viability upon transfection with luciferase and labeling with multimodal nanoparticles. These specific nanoparticles exhibit biocompatibility, magnetic and NIRF properties and a high positive zeta potential, which favors viability. The results further showed sensitivity in triple-image evaluations (MRI, BLI and NIRF), highlighting the importance of quantification of the MNP-IR750 load internalized by cells when different concentrations are used in *in vitro* analyses for application to *in vivo* analysis. These findings demonstrated effectiveness of signal detection under the triple-image modality with the highest concentration tested, as an approach for cellular therapy in a stroke lesion model.

Stem cells exhibit remarkable applicability in cellular therapy for drug discovery and regenerative medicine. Moreover, this type of therapy has increased the effectiveness of this approach when associated with noninvasive image modalities,

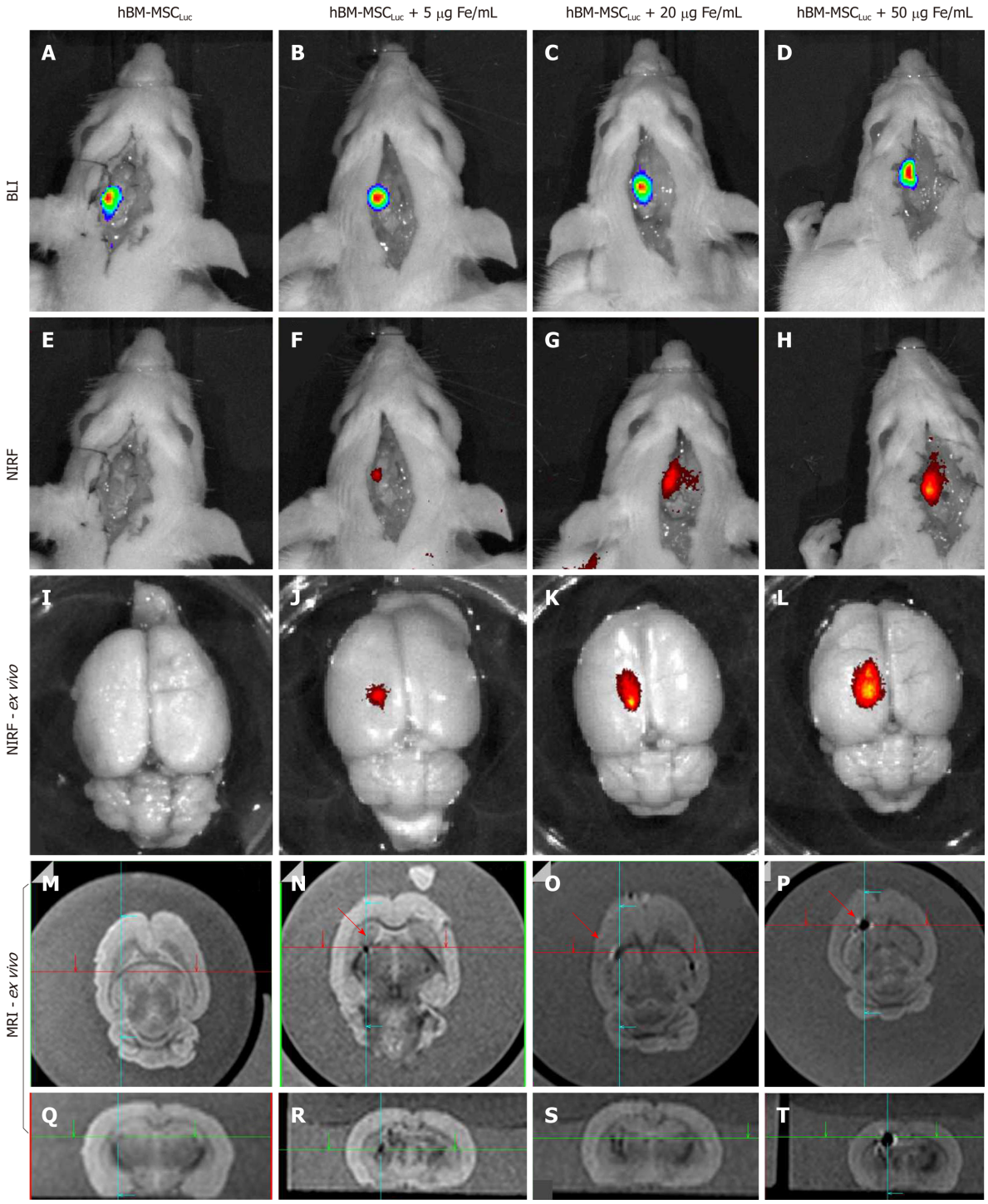

Figure 7 Evaluation of bioluminescent images, near-infrared fluorescence, and magnetic resonance imaging signals of labeled human bone marrow mesenchymal stem cells$_{Luc}$ implanted in animals (sham groups). A: BLI image of the sham_control group after luciferin addition; B-D: BLI images after luciferin addition in the sham_S5, sham_S20 and sham_S50 groups; E: NIRF image of the sham_control group; F-H: NIRF images of the sham_S5, sham_S20 and sham_S50 groups; I, L: *ex vivo* NIRF images of all groups; M-Q: Sagittal and coronal MRI of the sham_control group; N-P: Sagittal MRI of the sham_s5, sham_s20 and sham_S50 groups, showing the position of iron signal detection with red arrows; R-T: Coronal MRI of the sham_s5, sham_s20 and sham_S50 groups, showing the position of iron signal detection with crossing green lines. (n = 7 rats/group). BLI: Bioluminescent images; hBM-MSC: Human bone marrow mesenchymal stem cells; NIRF: Near-infrared fluorescence; MRI: Magnetic resonance imaging.

providing complementary information through the evaluation of cellular viability, the state of differentiation, cell numbers, cell tracking and cell fate. This approach also provides information about the behavior and function of stem cell protein expression levels and interactions between the cells and adjacent tissue[24].

It is important to select an appropriate imaging approach, taking into account factors such as the application, the experimental subject under study, and the goal of the experiment. The combined image modalities have improved the accuracy of

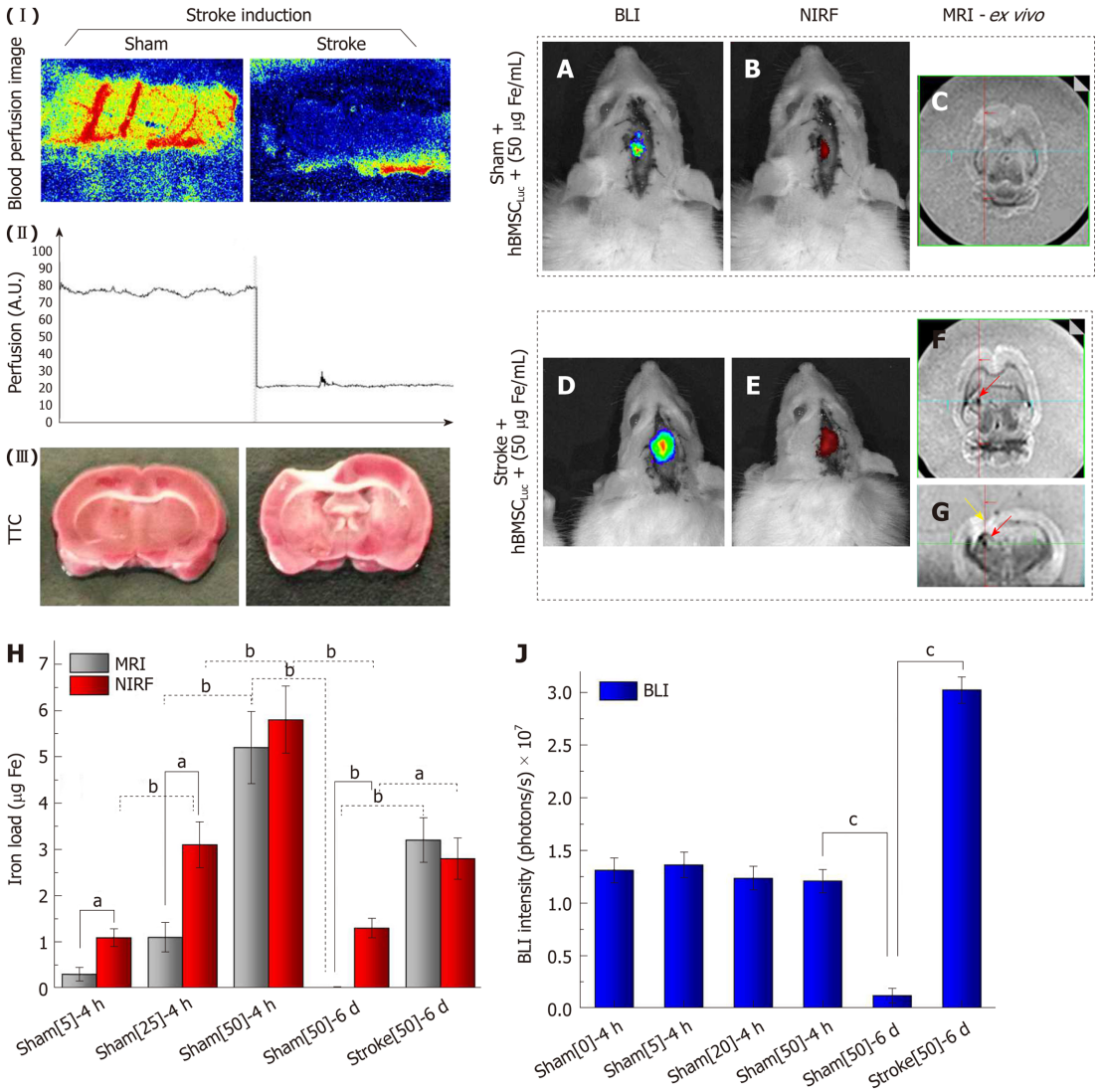

Figure 8 Evaluation of near-infrared fluorescence, bioluminescent images (*in vivo*) and magnetic resonance imaging signals (*ex vivo*) after 6 d of stroke induction. (I) Local blood perfusion images of the basal condition and 30 min after stroke induction by thermocoagulation; (II) graphic representation of local blood perfusion showing the decrease in perfusion from 80 to 20 au, comparing the basal condition to 30 min after stroke induction; (III) TTC staining of the sham and stroke groups performed 120 min after ischemic lesion induction; A, B: *In vivo* BLI and NIRF images of the sham_50 group; C: *Ex vivo* MRI results of the sham_50 group; D, E: *In vivo* BLI and NIRF images of the stroke_50 group; F, G: *Ex vivo* MRI results of the stroke_50 group (red arrows show the presence of nanoparticles, and a yellow arrow shows the stroke lesion); H: Graphic representation of quantification of the iron load *via* NIRF (red bars) and MRI (gray bars) in different groups in experiments 1 and 2, $^aP < 0.05$, $^bP < 0.001$, MRI *vs* NIRF; J: Graphic representation of BLI intensity (blue bars) in different groups in experiments 1 and 2, $^cP < 0.05$, *vs* sham[50]-6 d ($n = 7$ rats/group). BLI: Bioluminescent images; NIRF: Near-infrared fluorescence;

cellular therapy by using advanced technology to develop new hybrid tracers (multicomponent nanoparticles) containing two or more imaging contrast agents that permit several imaging techniques to be used in a hybrid manner, which is also known as multimodal imaging[25].

Dual-image modalities are often used in *in vivo* studies for homing and tracking evaluations under different approaches[10,26,27]. However, triple-image modality analyses, such as the analysis performed in this study, are currently scarce in the literature, and such analyses require multimodal nanoparticles. In our study, the nanoparticles exhibited near-infrared fluorescence and magnetic properties associated with stem cell transfection with luciferase. The NIRF nanoparticle properties showed excitation/emission fluorescence intensity peaks of 757.9 and 779.4 nm, respectively, which correspond to the NIR wavelength range specified by the manufacturer. NIR molecular probes offer two major advantages over those that emit visible wavelengths for *in vivo* analyses: lower absorption of biological tissues compared to visible light, allowing photon penetration through tissue to assess deeper structures; and a high signal/noise ratio, which minimizes the effects of tissue autofluorescence[28].

The magnetic nanoparticle properties showed good contrast in T_2-weighted images due to r^2 relaxivity characteristics, which depend on temperature, magnetic field

intensity and the size, composition, concentration, magnetic moment, aggregation, and coating of nanoparticles[29]. The T_2-weighted MRI intensity signals of the samples showed dark images in the presence of MNP-IR750. Therefore, high nanoparticle concentrations lead to a high local inhomogeneity field, decreasing the intensity signal and resulting in short T_2 values[10]. The r^2 value of 115.1 ± 8.0 $mm^{-1}s^{-1}$ obtained for MNP-IR750 is in accord with that of other commercial nanoparticles, such as feridex (size = 62 nm) and Resovist (size between 80 and 180 nm), which present r^2 values of 93 and 143 Mm-1s-1, respectively, correlated with the hydrodynamic size of these nanoparticles[30]. Thus, MNP-IR750 internalized in hBM-MSC_{Luc} presents high potential as a contrast agent for T_2-weighted MRI.

Among the lines of stem cells used in therapeutic approaches, MSCs present remarkable characteristics as neuronal markers *in vivo* as well as trophic factors such as brain-derived neurotrophic factor (BDNF), glial-derived neurotrophic factor (GDNF), VEGF, neurotrophin-3 (NT3), and fibroblast growth factor (FGF), in addition to thrombospondins released by these cells in response to the local microenvironment. These factors, associated with neurogenesis stimulation and angiogenesis immunomodulation, promote functional recovery[31]. These stem cells also stimulate astrocytes, which were used as a therapeutic target in the past because of their roles in maintaining neuronal function and effective endogenous repair.

Other relevant aspects of hMSCs relevant to their application in cellular therapy are their multipotency, biological characteristics, repair capacity, immunosuppressiveness, ease of isolation and expansion, and safety, without any possibility of malignant transformation after the infusion of allogeneic cells[32]. Bone marrow has been the major source of these cells, which directed the choices we made in this study.

The collection, isolation and immunophenotypic profiling of hBM-MSCs showed adequate results, confirming high levels of MSC markers (above of 93%) and low levels or absence of hematopoietic markers (below 3%) and leukocyte antigens. Such results are compatible with other studies on the same topic[33,34].

The nanoparticles tested showed a polydispersed size distribution and an average hydrodynamic diameter of 38.2 ± 0.5 nm, compatible with the manufacturer's specifications. They also showed adequate stability in DMEM-LG culture supplemented with 10% PBS over 18 h (time of incubation with the cells), avoiding agglomeration of nanoparticles, which may occur due to their interaction with the protein-supplemented and electrolyte-rich cell culture medium[35]. Another observed advantage was maintenance of the equilibrium of existing forces involved in the interaction between nanoparticles, such as electrostatic forces, Van der Waals forces, steric forces, and magnetic forces modulated *via* the Brownian motion associated with nanoparticles[35,36].

Another important aspect of the physical-chemical properties of nanoparticles in the cellular internalization process during nanoparticle uptake by cells is the electrophoretic mobility capacity of nanoparticles (zeta potential)[37]. Cells exhibit greater uptake of nanoparticles with a positive charge compared to those with a negative charge, which might be attributed to the attractive interaction between the negatively charged cell membrane and positively charged nanoparticles[38]. This phenomenon was a relevant factor in our study, due to the use of nanoparticles with a positive zeta potential of ξ = +29.2 ± 1.9 mV.

However, studies have demonstrated that shape, size and surface charge substantially influence nanoparticle internalization by cells[38,39]. Studies that have used nanoparticles with a negative zeta potential or a low positive zeta potential have included strategies for facilitating the internalization process, such as the use of transfection agents (poly(L-lysine) - PLL, protamine sulfate lipofectamine, among others)[40,41] or physical strategies (static or dynamic magnetic field) [42,43].

After labeling the cells with nanoparticles without any strategy for facilitating the internalization process, it was possible to verify that the use of nanoparticles with a positive zeta potential provided efficient labeling from the lowest nanoparticle concentrations to the highest concentration, based on Prussian blue staining. It was also possible to maintain the cellular morphological characteristics shown in optical microscopy images. Cellular viability assessed *via* MTT and BLI analyses was above 90% in all tested concentrations of nanoparticles, which varied from 0 to 50 μg Fe/mL. The same nanoparticle composition, with the exception of the type of fluorophore (rhodamine), resulted in little difference in cellular viability when assessed in the same range of nanoparticle concentrations (100% to 95%) using the MTT assay. However, a significantly high apoptosis rate was found in 100 μg Fe/mL (78% viability) in comparison to unlabeled cells, due to the toxic effect of a high concentration on stem cell viability[26,27,44]. A study by Addicott (2010) also showed that these nanoparticles maintained the immunophenotypic profile, even after labeling of hBM-MSCs[44].

Quantification of the nanoparticle load in cells *via* different imaging modalities (BLI, MRI and NIRF) provides indirect measurements of the load. Complementary analysis with ICP-MS has been performed in parallel in correlation analyses between indirect and direct measurements of nanoparticle load[10].

By analyzing the quantification results of the iron load/cell in different nanoparticle concentrations using MRI, ICP-MS and NIRF (Table 1), we could verify that the quantification of the iron load/cell *via* NIRF was over-estimated in relation to the ICP-MS values, mainly in the lowest concentrations (61% and 11% higher for 5 and 10 μg Fe/mL, respectively, *vs* 7, 3, 4 and 9% higher for 20, 30, 40, and 50 μg Fe/mL concentrations, respectively). The MRI quantification values also varied in relation to the ICP-MS values, but were underestimated at 29, 7, 2, 16, 9 and 6% for 5, 10, 20, 30, 40 and 50 μg Fe/mL, respectively, and the largest difference occurred in the lowest concentrations of nanoparticle tested (29% lower for 5 μg Fe/mL). This variability of results can be explained by a difference in sensitivity under each imaging modality, as MRI shows low sensitivity for small concentrations above 10^{-3} moles, whereas NIRF presents good sensitivity for ranges between 10^{-9} and 10^{-12} moles[45]. However, whether MRI and NIRF tracking of stem cells can reliably evaluate long-term cell engraftment and cell survival remains a controversial issue[46].

In this study, the maximum number of MNP-IR750 values adjusted based on an exponential curve showed values that were approximately 5% lower for MRI and NIRF in relation to ICP-MS. Under a constant value to achieve 63% of the maximum number of nanoparticles internalized, variations that were approximately 12% greater for NIRF and lower for MRI were detected in relation to ICP-MS values.

The correlation of the load quantification results based on images and spectrum techniques applied in our study *in vitro* (MRI, NIRF and ICP-MS) helped to improve the precision of these data and to understand the variation between the measurements according to the tested nanoparticle concentrations. Studies on multifunctional nanoparticles involving evaluations *via* multimodal images often show image analyses in a qualitative manner[26,27]. However, other studies either complement qualitative image analyses with techniques that permit nanoparticle quantification with more precision, such as inductively coupled plasma spectrometry[47,48], or use different approaches to quantify the nanoparticle load in cells by using image analysis[10,14,16]. However, none of these reported studies have included correlation analysis of the results obtained under each technique when applied in a quantitative way. This correlation could increase the accuracy of the obtained information, improving the interpretation of the analysis between the techniques as well as comparison with other studies. Therefore, the multimodal imaging analysis described above showed that MRI and NIRF presented a high correlation with ICP-MS, which is the *in vitro* gold standard for iron analysis[49]; the MRI results were lower than, while those of NIRF were greater than the ICP-MS results.

The sensitivity of triple-modal imaging was also analyzed *in vivo*. Experiment 1 showed that the NIRF and MRI signal intensity in the sham groups after 4 h of cell implantation was proportional to the tested nanoparticle concentrations (low, intermediate and high concentrations) and was constant in BLI images for all conditions analyzed. Experiment 2 also showed a difference in the triple-modal images between sham group and the stroke group after 6 d of cells implantation, using the same concentration of nanoparticles (50 μg Fe/mL of MNP-IR750), but in a different physiopathological process.

The BLI intensity results for experiment 1 showed little variability between the sham groups with labeled cells (S5, S20 and S50) and the sham group with unlabeled cells (S_control). This result was compatible with the decreased viability found in the *in vitro* study and corroborates other studies that have analyzed cell viability in the presence of similar nanoparticles at the same range of concentrations[26,27,44]. Considering cell viability under a high concentration of nanoparticles, experiment 2 showed maintenance of the BLI signal in both groups, even after 6 d of surgery procedures (craniectomy and stroke induction). The BLI intensity was high in the stroke_50 group, mainly near the stroke area, due to ischemic status, challenging the metabolic source for initiating the bioluminescence process[50]. The reduction of the BLI sign in the sham_50 group most likely resulted from the progressive biodistribution of grafted cells in the body[51].

Karp and Leng Teo[52] described MSC homing as "the arrest of MSCs within the vasculature of the respective tissue," followed by transmigration across the endothelium. These authors suggest that chemokines, cytokines, and growth factors released upon tissue injury provide migratory cues for stem cells implanted in a systemic or localized way. Concerning the homing capability of MSCs, many studies have indicated that systemically infused MSCs can migrate to injured, inflamed tissues and exert therapeutic effects[53]. Therefore, inflammation promotes chemotaxis of stem cells to the region of ischemia; this potential is initiated 24 h after injury and

stabilizes 5 to 7 d after ischemia, then decreases after 14 d[53]. Our results verified this reported kinetic observation, with *in vivo* bioluminescence images being found to be more intense after 6 d of lesion induction. Duan *et al*[46] verified the finding of significant chemotaxis of viable hBM-MSCs in ischemic areas.

Another optical image modality provided complementary information on both living and dead cells. NIRF intensity signal analysis *in vivo* showed high sensitivity in the detection of differences in nanoparticle concentrations, with an even greater difference being observed in *ex vivo* analysis (Experiment 1). These findings corroborate other studies that have indicated a strong linear relationship of signals with corresponding nanoparticle concentrations[14]. However, the signal was below the intensity detected in the *in vitro* study, due to the decreased attenuation caused by the presence of tissue[28]. Experiment 2 showed that the NIRF signal presented a good spatial resolution because MSCs were mainly concentrated at the injury site, with a small number of cells migrating to the periphery of the injury area; however, the NIRF signal decreased over time, due to exocytosis and cell division, thus diluting the signal in the target area[54].

The intensity of the MRI signal showed a remarkable region of hypointensity under the highest nanoparticle concentration, while similar results were found between the other lower concentrations, allowing good localization of cells labeled with SPIONs, due to the high structural resolution[27]. However, SPION-based MRI cannot provide reliable information on longitudinal viability and might overestimate the survival of SPION-labeled stem cells in other ischemic models. Duan *et al*[46] showed the dynamic changes in a low signal volume in MRI in a preclinical stroke model, due to a consistent pattern of change in the number of viable cells. Thus, MRI and NIRF present some challenges in the longitudinal monitoring of stem cells. Zhang *et al*[55] showed that cell grafts with SPION can be detected as a hypointense signal in T2 and T2* MRI imaging up to 6 wk after implantation; a few viable stem cells and many grafted cells that differentiate into astrocytes at 6 wk are observed. These results suggest that the iron-dependent signal in T2*-weighted imaging can lead to overestimation of the real number of viable cell grafts. Considering that the number of transplanted stem cells that home and survive in host organs in the first several h is generally very low[56], the gradual reduction in graft size most likely results from the progressively decreased survival of grafted cells. The histological data showed many extracellular iron particles and microglia/macrophages present at the implantation site at 6 wk. Therefore, the longitudinal cell viability observed *via* NIRF might represent overestimated data. The accuracy of such data can be affected by many factors, especially by cell death and concomitant microglia/macrophage accumulation potentially activated by immunoreaction. Thus, the biodistribution, proliferation and differentiation of transplanted cells decreases the NIRF signal over time and might result in overestimation, as observed for the MRI signal.

The BLI signal analyzed in the stroke model after cell therapy remained constant until 28 d after stroke induction, but disappeared after 6 d in the sham group. It has also been reported that 28 d after induction, the intensity of the BLI signal is significantly higher than following other implantations performed earlier (after 2 h or 1 wk of stroke induction)[51]. The reduction of the BLI sign observed in the sham group most likely resulted from the progressive biodistribution of grafted cells in the body. Our results showed that the stem cells were viable, even in a challenging microenvironment, due to a lack of O_2 and adenosine triphosphate (ATP), 6 d after ischemia induction. In conclusion, cell implantation is advised soon after stroke induction to increase the efficiency of cellular therapy monitored *via* the BLI signal.

Finally, we demonstrated that MNP-IR750 could be used to monitor cell grafts noninvasively, longitudinally, and repetitively, enabling the assessment of cell graft conditions *in vivo* after stroke for multimodal imaging assessment. The BLI signal of hBM-MSC_{Luc} showed the best imaging technique for functional and longitudinal assessment. The applicability of multimodal imaging should always be analyzed in accordance with the limitations and advantages of each technique involved.

ARTICLE HIGHLIGHTS

Research background

Mesenchymal stem cells (MSCs) have been widely tested for therapeutic efficacy in the ischemic brain, providing several benefits. A major obstacle for the clinical translation of these therapies has been the inability to noninvasively monitor the best route, cell doses, and collateral effects, while ensuring survival and effective biological functioning of the transplanted stem cells. Combined image modalities have improved the accuracy of cellular therapy, allowed the *in vivo* monitoring of the biodistribution and viability of transplanted stem cells due to associated new tracers such as multimodal nanoparticles with new labels and covers, resulting in low toxicity

and longtime residence in cells.

Research motivation

Although meta-analyses have examined the benefits of cell transplantation in experimental stroke, low viable cell retention after transplantation in ischemic brain areas still represents the major obstacle to the successful clinical translation of cell-based stroke repair approaches. The multimodal imaging techniques provide morpho-functional information for studying pathological events following ischemia, associated with new tracers. These innovations will contribute to further our comprehension of stem cell transplantation, allowing the assessment of therapeutic effects on a molecular scale.

Research objectives

In this study, we aim to evaluate the sensitivity of triple-modal imaging of stem cells labeled with multimodal nanoparticles with different iron concentrations and their cellular viability *in vitro* as well as the correlation of the quantification of the iron load between different techniques (ICP-MS, MRI and NIRF. In addition, we seek to verify whether these images of stem cells labeled with multimodal nanoparticles maintain the same properties after application in a stroke model. The results will help us to better understand the biodistribution, sensitivity and viability of stem cells labeled with nanoparticles in sham and stroke models.

Research methods

Isolated and immunophenotypically characterized hBM-MSCs were transduced with a lentivirus for BLI evaluation *in vitro* and *in vivo*. In addition, MNP-IR750 that had previously been characterized (hydrodynamic size, zeta potential, and optical properties) were used for labeling these cells and analyzing cell viability *via* MTT and BLI assays. The internalization process and quantification of the iron load in different concentrations of MNP-IR750 were analyzed *via* MRI, NIRF, and ICP-MS. In the *in vivo* study, the same labeled cells were implanted in the sham group and stroke group at different times and MNP-IR750 concentrations (after 4 h and after 6 d of cell implantation) to evaluate the sensitivity of triple-modal images.

Research results

The collection and isolation of hBM-MSCs after immunophenotypic characterization was demonstrated to be adequate for human bone marrow samples. After the transduction of these cells with luciferase, we detected a maximum BLI intensity of 2.0×10^8 photons/s in 10^6 hBM-MSC samples. Evaluation of the physicochemical characteristics of MNP-IR750 showed an average hydrodynamic diameter of 38.2 ± 0.5 nm, a zeta potential of +29.2 ± 1.9 mV and adequate colloidal stability, without agglomeration over 18 h. The iron load internalization process in hBM-MSCs showed a strong relationship of the signal with the corresponding MNP labeling concentration based on MRI, ICP-MS and NIRF. Cellular viability in the highest MNP-IR750 concentration showed a reduction of less than 10% compared to the control. The correlation analysis of the MNP-IR750 load internalized by hBM-MSCs between the MRI, ICP-MS and NIRF techniques showed the same correlation coefficient of 0.99. The evaluation of BLI, NIRF, and MRI signals *in vivo* and *ex vivo* after labeled hBM-MSCs were implanted in the animals showed sensitivity in the detection of MNP-IR750 concentrations of 5, 20 and 50 μg Fe/mL at 4 h and 6 d in the sham groups, with significant results regarding the time and image effect as well as the group effect when the sham and stroke groups were compared at 6 d.

Research conclusions

Our study demonstrates that MNP-IR750 can be used to monitor cell grafts noninvasively, longitudinally, and repetitively, enabling the assessment of cell graft conditions *in vivo* after stroke for multimodal imaging assessment. The BLI signal of hBM-MSC_{Luc} showed the best imaging technique for functional and longitudinal assessment.

Research perspectives

In summary, we highlight the importance of quantification of multimodal nanoparticles internalized by cells and the efficacy of signal detection under the triple-image modality in a stroke model. However, the applicability of multimodal imaging should always be analyzed in accordance with the limitations and advantages of each technique involved.

REFERENCES

1 **Phinney DG**, Prockop DJ. Concise review: mesenchymal stem/multipotent stromal cells: the state of transdifferentiation and modes of tissue repair--current views. *Stem Cells* 2007; **25**: 2896-2902 [PMID: 17901396 DOI: 10.1634/stemcells.2007-0637]

2 **Alvarim LT**, Nucci LP, Mamani JB, Marti LC, Aguiar MF, Silva HR, Silva GS, Nucci-da-Silva MP, DelBel EA, Gamarra LF. Therapeutics with SPION-labeled stem cells for the main diseases related to brain aging: a systematic review. *Int J Nanomedicine* 2014; **9**: 3749-3770 [PMID: 25143726 DOI: 10.2147/IJN.S65616]

3 **Wu Y**, Zhao RC. The role of chemokines in mesenchymal stem cell homing to myocardium. *Stem Cell Rev* 2012; **8**: 243-250 [PMID: 21706142 DOI: 10.1007/s12015-011-9293-z]

4 **Eggenhofer E**, Luk F, Dahlke MH, Hoogduijn MJ. The life and fate of mesenchymal stem cells. *Front Immunol* 2014; **5**: 148 [PMID: 24904568 DOI: 10.3389/fimmu.2014.00148]

5 **Fischer UM**, Harting MT, Jimenez F, Monzon-Posadas WO, Xue H, Savitz SI, Laine GA, Cox CS.

Pulmonary passage is a major obstacle for intravenous stem cell delivery: the pulmonary first-pass effect. *Stem Cells Dev* 2009; **18**: 683-692 [PMID: 19099374 DOI: 10.1089/scd.2008.0253]
6 **Au P**, Hursh DA, Lim A, Moos MC, Oh SS, Schneider BS, Witten CM. FDA oversight of cell therapy clinical trials. *Sci Transl Med* 2012; **4**: 149fs31 [PMID: 22932219 DOI: 10.1126/scitranslmed.3004131]
7 **Kircher MF**, Gambhir SS, Grimm J. Noninvasive cell-tracking methods. *Nat Rev Clin Oncol* 2011; **8**: 677-688 [PMID: 21946842 DOI: 10.1038/nrclinonc.2011.141]
8 **Li X**, Zhang XN, Li XD, Chang J. Multimodality imaging in nanomedicine and nanotheranostics. *Cancer Biol Med* 2016; **13**: 339-348 [PMID: 27807501 DOI: 10.20892/j.issn.2095-3941.2016.0055]
9 **Lee DE**, Koo H, Sun IC, Ryu JH, Kim K, Kwon IC. Multifunctional nanoparticles for multimodal imaging and theragnosis. *Chem Soc Rev* 2012; **41**: 2656-2672 [PMID: 22189429 DOI: 10.1039/c2cs15261d]
10 **Yang HM**, Park CW, Park S, Kim JD. Cross-linked magnetic nanoparticles with a biocompatible amide bond for cancer-targeted dual optical/magnetic resonance imaging. *Colloids Surf B Biointerfaces* 2018; **161**: 183-191 [PMID: 29080502 DOI: 10.1016/j.colsurfb.2017.10.049]
11 **Gupta AK**, Gupta M. Synthesis and surface engineering of iron oxide nanoparticles for biomedical applications. *Biomaterials* 2005; **26**: 3995-4021 [PMID: 15626447 DOI: 10.1016/j.biomaterials.2004.10.012]
12 **Li J**, Lee WY, Wu T, Xu J, Zhang K, Hong Wong DS, Li R, Li G, Bian L. Near-infrared light-triggered release of small molecules for controlled differentiation and long-term tracking of stem cells in vivo using upconversion nanoparticles. *Biomaterials* 2016; **110**: 1-10 [PMID: 27693946 DOI: 10.1016/j.biomaterials.2016.09.011]
13 **Zhang W**, Wang W, Yu DX, Xiao Z, He Z. Application of nanodiagnostics and nanotherapy to CNS diseases. *Nanomedicine (Lond)* 2018; **13**: 2341-2371 [PMID: 30088440 DOI: 10.2217/nnm-2018-0163]
14 **Chen G**, Lin S, Huang D, Zhang Y, Li C, Wang M, Wang Q. Revealing the Fate of Transplanted Stem Cells In Vivo with a Novel Optical Imaging Strategy. *Small* 2018; **14** [PMID: 29171718 DOI: 10.1002/smll.201702679]
15 **Sarkar D**, Spencer JA, Phillips JA, Zhao W, Schafer S, Spelke DP, Mortensen LJ, Ruiz JP, Vemula PK, Sridharan R, Kumar S, Karnik R, Lin CP, Karp JM. Engineered cell homing. *Blood* 2011; **118**: e184-e191 [PMID: 22034631 DOI: 10.1182/blood-2010-10-311464]
16 **Sibov TT**, Pavon LF, Miyaki LA, Mamani JB, Nucci LP, Alvarim LT, Silveira PH, Marti LC, Gamarra L. Umbilical cord mesenchymal stem cells labeled with multimodal iron oxide nanoparticles with fluorescent and magnetic properties: application for in vivo cell tracking. *Int J Nanomedicine* 2014; **9**: 337-350 [PMID: 24531365 DOI: 10.2147/IJN.S53299]
17 **Souza TKF**, Nucci MP, Mamani JB, da Silva HR, Fantacini DMC, de Souza LEB, Picanço-Castro V, Covas DT, Vidoto EL, Tannús A, Gamarra LF. Image and motor behavior for monitoring tumor growth in C6 glioma model. *PLoS One* 2018; **13**: e0201453 [PMID: 30048545 DOI: 10.1371/journal.pone.0201453]
18 **Mamani JB**, Pavon LF, Miyaki LA, Sibov TT, Rossan F, Silveira PH, Cárdenas WH, Amaro Junior E, Gamarra LF. Intracellular labeling and quantification process by magnetic resonance imaging using iron oxide magnetic nanoparticles in rat C6 glioma cell line. *Einstein (Sao Paulo)* 2012; **10**: 216-221 [PMID: 23052458 DOI: 10.1590/S1679-45082012000200016]
19 **Gamarra LF**, Amaro E, Alves S, Soga D, Pontuschka WM, Mamani JB, Carneiro SM, Brito GE, Figueiredo Neto AM. Characterization of the biocompatible magnetic colloid on the basis of Fe3O4 nanoparticles coated with dextran, used as contrast agent in magnetic resonance imaging. *J Nanosci Nanotechnol* 2010; **10**: 4145-4153 [PMID: 21128393 DOI: 10.1166/jnn.2010.2200]
20 **Paxinos G**, Watson Ch. The Rat Brain in Stereotaxic Coordinates. London: Academic Press 1998;
21 **da Silva H**, Nucci MP, Mamani JB, Mendez-Otero R, Nucci LP, Tannus A, Gamarra LF. Evaluation of temperature induction in focal ischemic thermocoagulation model. *PLoS One* 2018; **13**: e0200135 [PMID: 29975761 DOI: 10.1371/journal.pone.0200135]
22 **Giraldi-Guimardes A**, Rezende-Lima M, Bruno FP, Mendez-Otero R. Treatment with bone marrow mononuclear cells induces functional recovery and decreases neurodegeneration after sensorimotor cortical ischemia in rats. *Brain Res* 2009; **1266**: 108-120 [PMID: 19368806 DOI: 10.1016/j.brainres.2009.01.062]
23 **Nucci LP**, Silva HR, Giampaoli V, Mamani JB, Nucci MP, Gamarra LF. Stem cells labeled with superparamagnetic iron oxide nanoparticles in a preclinical model of cerebral ischemia: a systematic review with meta-analysis. *Stem Cell Res Ther* 2015; **6**: 27 [PMID: 25889904 DOI: 10.1186/s13287-015-0015-3]
24 **Saadatpour Z**, Rezaei A, Ebrahimnejad H, Baghaei B, Bjorklund G, Chartrand M, Sahebkar A, Morovati H, Mirzaei HR, Mirzaei H. Imaging techniques: new avenues in cancer gene and cell therapy. *Cancer Gene Ther* 2017; **24**: 1-5 [PMID: 27834357 DOI: 10.1038/cgt.2016.61]
25 **Key J**, Leary JF. Nanoparticles for multimodal in vivo imaging in nanomedicine. *Int J Nanomedicine* 2014; **9**: 711-726 [PMID: 24511229 DOI: 10.2147/IJN.S53717]
26 **Dabrowska S**, Del Fattore A, Karnas E, Frontczak-Baniewicz M, Kozlowska H, Muraca M, Janowski M, Lukomska B. Imaging of extracellular vesicles derived from human bone marrow mesenchymal stem cells using fluorescent and magnetic labels. *Int J Nanomedicine* 2018; **13**: 1653-1664 [PMID: 29593411 DOI: 10.2147/IJN.S159404]
27 **Ma L**, Li MW, Bai Y, Guo HH, Wang SC, Yu Q. Biological Characteristics of Fluorescent Superparamagnetic Iron Oxide Labeled Human Dental Pulp Stem Cells. *Stem Cells Int* 2017; **2017**: 4837503 [PMID: 28298928 DOI: 10.1155/2017/4837503]
28 **Zhang X**, Bloch S, Akers W, Achilefu S. Near-infrared molecular probes for in vivo imaging. *Curr Protoc Cytom* 2012; **Chapter** 12: Unit12.27 [PMID: 22470154 DOI: 10.1002/0471142956.cy1227s60]
29 **Lee N**, Choi Y, Lee Y, Park M, Moon WK, Choi SH, Hyeon T. Water-dispersible ferrimagnetic iron oxide nanocubes with extremely high r relaxivity for highly sensitive in vivo MRI of tumors. *Nano Lett* 2012; **12**: 3127-3131 [PMID: 22575047 DOI: 10.1021/nl3010308]
30 **Korchinski DJ**, Taha M, Yang R, Nathoo N, Dunn JF. Iron Oxide as an MRI Contrast Agent for Cell Tracking. *Magn Reson Insights* 2015; **8**: 15-29 [PMID: 26483609 DOI: 10.4137/MRI.S23557]
31 **Chopp M**, Li Y. Treatment of neural injury with marrow stromal cells. *Lancet Neurol* 2002; **1**: 92-100 [PMID: 12849513 DOI: 10.1016/S1474-4422(02)00040-6]
32 **Kim HJ**, Park JS. Usage of Human Mesenchymal Stem Cells in Cell-based Therapy: Advantages and Disadvantages. *Dev Reprod* 2017; **21**: 1-10 [PMID: 28484739 DOI: 10.12717/DR.2017.21.1.001]
33 **Yousefifard M**, Nasirinezhad F, Shardi Manaheji H, Janzadeh A, Hosseini M, Keshavarz M. Human bone marrow-derived and umbilical cord-derived mesenchymal stem cells for alleviating neuropathic pain in a spinal cord injury model. *Stem Cell Res Ther* 2016; **7**: 36 [PMID: 26957122 DOI: 10.1186/s13287-016-0295-2]

34 **Li XY**, Ding J, Zheng ZH, Li XY, Wu ZB, Zhu P. Long-term culture in vitro impairs the immunosuppressive activity of mesenchymal stem cells on T cells. *Mol Med Rep* 2012; **6**: 1183-1189 [PMID: 22923041 DOI: 10.3892/mmr.2012.1039]

35 **Moore TL**, Rodriguez-Lorenzo L, Hirsch V, Balog S, Urban D, Jud C, Rothen-Rutishauser B, Lattuada M, Petri-Fink A. Nanoparticle colloidal stability in cell culture media and impact on cellular interactions. *Chem Soc Rev* 2015; **44**: 6287-6305 [PMID: 26056687 DOI: 10.1039/c4cs00487f]

36 **Myers D**. Surfaces, interfaces, and colloids: principles and applications. New York: Wiley-VCH Publishers 1999; 40-78

37 **Zhang Y**, Yang M, Portney NG, Cui D, Budak G, Ozbay E, Ozkan M, Ozkan CS. Zeta potential: a surface electrical characteristic to probe the interaction of nanoparticles with normal and cancer human breast epithelial cells. *Biomed Microdevices* 2008; **10**: 321-328 [PMID: 18165903 DOI: 10.1007/s10544-007-9139-2]

38 **Hu L**, Mao Z, Gao Ch. Colloidal particles for cellular uptake and delivery. *J Mater Chem* 2009; **19**: 3108-3115 [DOI: 10.1039/B815958K]

39 **Cai YR**, Liu YK, Yan WQ, Hu QH, Tao JH, Zhang M, Shi ZL, Tang RK. Role of hydroxyapatite nanoparticle size in bone cell proliferation. *J Mater Chem* 2007; **17**: 3780-3787 [DOI: 10.1039/B705129H]

40 **Montet-Abou K**, Montet X, Weissleder R, Josephson L. Cell internalization of magnetic nanoparticles using transfection agents. *Mol Imaging* 2007; **6**: 1-9 [PMID: 17311760 DOI: 10.2310/7290.2006.00028]

41 **Lee JH**, Jung MJ, Hwang YH, Lee YJ, Lee S, Lee DY, Shin H. Heparin-coated superparamagnetic iron oxide for in vivo MR imaging of human MSCs. *Biomaterials* 2012; **33**: 4861-4871 [PMID: 22475532 DOI: 10.1016/j.biomaterials.2012.03.035]

42 **Vaněček V**, Zablotskii V, Forostyak S, Růžička J, Herynek V, Babič M, Jendelová P, Kubinová S, Dejneka A, Syková E. Highly efficient magnetic targeting of mesenchymal stem cells in spinal cord injury. *Int J Nanomedicine* 2012; **7**: 3719-3730 [PMID: 22888231 DOI: 10.2147/IJN.S32824]

43 **Adams CF**, Pickard MR, Chari DM. Magnetic nanoparticle mediated transfection of neural stem cell suspension cultures is enhanced by applied oscillating magnetic fields. *Nanomedicine* 2013; **9**: 737-741 [PMID: 23751375 DOI: 10.1016/j.nano.2013.05.014]

44 **Addicott B**, Willman M, Rodriguez J, Padgett K, Han D, Berman D, Hare JM, Kenyon NS. Mesenchymal stem cell labeling and in vitro MR characterization at 1.5 T of new SPIO contrast agent: Molday ION Rhodamine-B™. *Contrast Media Mol Imaging* 2011; **6**: 7-18 [PMID: 20690161 DOI: 10.1002/cmmi.396]

45 **Townsend D**, Cheng Zh, Georg D, Drexler W, Moser E; Townsend D, Cheng Zh, Georg D, Drexler W, Moser E. Grand challenges in biomedical physics. *Front Phys* 2013; **1**: 1-6 [DOI: 10.3389/fphy.2013.00001]

46 **Duan X**, Lu L, Wang Y, Zhang F, Mao J, Cao M, Lin B, Zhang X, Shuai X, Shen J. The long-term fate of mesenchymal stem cells labeled with magnetic resonance imaging-visible polymersomes in cerebral ischemia. *Int J Nanomedicine* 2017; **12**: 6705-6719 [PMID: 28932115 DOI: 10.2147/IJN.S146742]

47 **Schweiger C**, Hartmann R, Zhang F, Parak WJ, Kissel TH, Rivera Gil P. Quantification of the internalization patterns of superparamagnetic iron oxide nanoparticles with opposite charge. *J Nanobiotechnology* 2012; **10**: 28 [PMID: 22781560 DOI: 10.1186/1477-3155-10-28]

48 **Vandeputte C**, Thomas D, Dresselaers T, Crabbe A, Verfaillie C, Baekelandt V, Van Laere K, Himmelreich U. Characterization of the inflammatory response in a photothrombotic stroke model by MRI: implications for stem cell transplantation. *Mol Imaging Biol* 2011; **13**: 663-671 [PMID: 20700767 DOI: 10.1007/s11307-010-0395-9]

49 **Dadashzadeh ER**, Hobson M, Henry Bryant L, Dean DD, Frank JA. Rapid spectrophotometric technique for quantifying iron in cells labeled with superparamagnetic iron oxide nanoparticles: potential translation to the clinic. *Contrast Media Mol Imaging* 2013; **8**: 50-56 [PMID: 23109392 DOI: 10.1002/cmmi.1493]

50 **Aswendt M**, Adamczak J, Tennstaedt A. A review of novel optical imaging strategies of the stroke pathology and stem cell therapy in stroke. *Front Cell Neurosci* 2014; **8**: 226 [PMID: 25177269 DOI: 10.3389/fncel.2014.00226]

51 **Jang KS**, Lee KS, Yang SH, Jeun SS. In vivo Tracking of Transplanted Bone Marrow-Derived Mesenchymal Stem Cells in a Murine Model of Stroke by Bioluminescence Imaging. *J Korean Neurosurg Soc* 2010; **48**: 391-398 [PMID: 21286474 DOI: 10.3340/jkns.2010.48.5.391]

52 **Karp JM**, Leng Teo GS. Mesenchymal stem cell homing: the devil is in the details. *Cell Stem Cell* 2009; **4**: 206-216 [PMID: 19265660 DOI: 10.1016/j.stem.2009.02.001]

53 **Gurtner GC**, Werner S, Barrandon Y, Longaker MT. Wound repair and regeneration. *Nature* 2008; **453**: 314-321 [PMID: 18480812 DOI: 10.1038/nature07039]

54 **Santoso MR**, Yang PC. Magnetic Nanoparticles for Targeting and Imaging of Stem Cells in Myocardial Infarction. *Stem Cells Int* 2016; **2016**: 4198790 [PMID: 27127519 DOI: 10.1155/2016/4198790]

55 **Zhang F**, Duan X, Lu L, Zhang X, Chen M, Mao J, Cao M, Shen J. In Vivo Long-Term Tracking of Neural Stem Cells Transplanted into an Acute Ischemic Stroke model with Reporter Gene-Based Bimodal MR and Optical Imaging. *Cell Transplant* 2017; **26**: 1648-1662 [PMID: 29251112 DOI: 10.1177/0963689717722560]

56 **Dimmeler S**, Ding S, Rando TA, Trounson A. Translational strategies and challenges in regenerative medicine. *Nat Med* 2014; **20**: 814-821 [PMID: 25100527 DOI: 10.1038/nm.3627]

P- Reviewer: Grawish ME, Hassan AI, Haider KH

S- Editor: Ma YJ **L- Editor:** A **E- Editor:** Bian YN

World Journal of Stem Cells

Submit a Manuscript: https://www.f6publishing.com

World J Stem Cells 2019 February 26; 11(2): 124-146

DOI: 10.4252/wjsc.v11.i2.124

ISSN 1948-0210 (online)

CASE REPORT

Improved guided bone regeneration by combined application of unmodified, fresh autologous adipose derived regenerative cells and plasma rich in growth factors: A first-in-human case report and literature review

Önder Solakoglu, Werner Götz, Maren C Kiessling, Christopher Alt, Christoph Schmitz, Eckhard U Alt

ORCID number: Önder Solakoglu (0000-0002-0046-3457); Werner Götz (0000-0001-9975-5793); Maren C Kiessling (0000-0001-9261-6993); Christopher Alt (0000-0003-1487-4502); Christoph Schmitz (0000-0002-4065-1241); Eckhard U Alt (0000-0002-6687-139X).

Author contributions: Solakoglu Ö, Götz W, Alt C, and Alt EU designed the report; Solakoglu Ö and Götz W collected the patient's clinical data; Solakoglu Ö, Götz W, Kiessling MC, Alt C, Schmitz C, and Alt EU analyzed the data and wrote the paper.

Informed consent statement: Consent was obtained from the patient for publication of this report and any accompanying images.

Conflict-of-interest statement: All authors have no conflicts of interest to report.

Önder Solakoglu, External Visiting Lecturer, Dental Department of the University Medical Center Hamburg-Eppendorf, Hamburg 20246, Germany

Önder Solakoglu, Clinic for Periodontology and Implantology, Hamburg 22453, Germany

Werner Götz, Department of Orthodontics, Center of Dento-Maxillo-Facial Medicine, University of Bonn, Bonn 53111, Germany

Maren C Kiessling, Christoph Schmitz, Institute of Anatomy, Faculty of Medicine, LMU Munich, Munich 80336, Germany

Christopher Alt, Eckhard U Alt, InGeneron GmbH, Munich 80331, Germany

Eckhard U Alt, InGeneron, Inc., Houston, TX 77054, United States

Eckhard U Alt, Isar Klinikum Munich, 80331 Munich, Germany

Corresponding author: Önder Solakoglu, DDS, MSc, PhD, Adjunct Professor, Clinic for Periodontology and Implantology, Groß Borsteler Str. 9, Hamburg 22453, Germany. solakoglu@fpi-hamburg.de
Telephone: +49-40-515050
Fax: +49-40-53997289

Abstract

BACKGROUND

Novel strategies are needed for improving guided bone regeneration (GBR) in oral surgery prior to implant placement, particularly in maxillary sinus augmentation (GBR-MSA) and in lateral alveolar ridge augmentation (LRA). This study tested the hypothesis that the combination of freshly isolated, unmodified autologous adipose-derived regenerative cells (UA-ADRCs), fraction 2 of plasma rich in growth factors (PRGF-2) and an osteoinductive scaffold (OIS) (UA-ADRC/PRGF-2/OIS) is superior to the combination of PRGF-2 and the same OIS alone (PRGF-2/OIS) in GBR-MSA/LRA.

CASE SUMMARY

A 79-year-old patient was treated with a bilateral external sinus lift procedure as well as a bilateral lateral alveolar ridge augmentation. GBR-MSA/LRA was performed with UA-ADRC/PRGF-2/OIS on the right side, and with PRGF-

Manuscript source: Unsolicited manuscript

Received: October 9, 2018
Peer-review started: October 9, 2018
First decision: November 14, 2018
Revised: December 7, 2018
Accepted: January 10, 2019
Article in press: January 11, 2019
Published online: February 26, 2019

2/OIS on the left side. Biopsies were collected at 6 wk and 34 wk after GBR-MSA/LRA. At the latter time point implants were placed. Radiographs (32 mo follow-up time) demonstrated excellent bone healing. No radiological or histological signs of inflammation were observed. Detailed histologic, histomorphometric, and immunohistochemical analysis of the biopsies evidenced that UA-ADRC/PRGF-2/OIS resulted in better and faster bone regeneration than PRGF-2/OIS.

CONCLUSION
GBR-MSA with UA-ADRCs, PRGF-2, and an OIS shows effectiveness without adverse effects.

Key words: Case report; Cell-based therapy; Guided bone regeneration; Maxillary sinus augmentation; Lateral alveolar ridge augmentation; Unmodified autologous adipose-derived regenerative cells; Stem cells

Core tip: Novel strategies are needed in oral surgery for improving guided bone regeneration in maxillary sinus augmentation prior to implant placement. We demonstrate that the combination of freshly isolated, unmodified autologous adipose-derived regenerative cells, fraction 2 of plasma rich in growth factors and an osteoinductive scaffold is superior to the combination of fraction 2 of plasma rich in growth factors and the same osteoinductive scaffold alone. This novel procedure may contribute to a decreased healing period and increased bone quality in rehabilitation of the edentulous posterior maxilla as well as in other regenerative techniques in pre-implant bone augmentation procedures.

Citation: Solakoglu Ö, Götz W, Kiessling MC, Alt C, Schmitz C, Alt EU. Improved guided bone regeneration by combined application of unmodified, fresh autologous adipose derived regenerative cells and plasma rich in growth factors: A first-in-human case report and literature review. *World J Stem Cells* 2019; 11(2): 124-146
URL: https://www.wjgnet.com/1948-0210/full/v11/i2/124.htm
DOI: https://dx.doi.org/10.4252/wjsc.v11.i2.124

INTRODUCTION

The main causes of tooth loss are periodontal disease and dental caries[1]. Replacing missing or lost teeth with osseointegrated dental implants has been highly successful in the treatment of single, partial, or complete edentulism[2]. However, insufficient bone volume is a common problem occurring in the rehabilitation of the edentulous posterior maxilla with implant-supported prostheses[3-5]. Both the presence of the maxillary sinus and atrophy of the alveolar process after tooth extraction or loss contribute to this problem. Therefore, it is often necessary to perform vertical alveolar ridge augmentation to enable implant placement and integration. A well-studied technique in this context is maxillary sinus membrane elevation with autologous bone or a variety of biomaterials (*i.e.*, a form of guided bone regeneration in maxillary sinus augmentation; thereafter, "GBR-MSA")[3-6]. However, for the following reasons there is a need for developing novel strategies for improving GBR-MSA.

First, autologous bone is considered to be the gold standard in GBR-MSA due to its osteogenic, osteoinductive, and osteoconductive properties including lack of immunogenicity[7,8]. However, autologous bone grafts may show a number of disadvantages, such as increased operation time, donor site morbidity, post-operative discomfort, limitations in bone quantity and volume, unpredictable bone quality, reduced volume stability, and fast resorption rate[9-13]. It may also be only effective under good recipient conditions. Furthermore, the intraoral amount of autologous bone is limited, and therefore extraoral donor sites are needed for larger defects. Extraoral donor sites like the iliac crest may lead to further discomfort for the patient and an even higher morbidity rate compared to intraoral donor sites.

Second, while allografts have osteogenic properties, their probable osteoinductive and osteoconductive functions are still discussed contradictorily[7,11,14-16]. Especially the

osteoconductive property of bone allografts leads to a significant higher volume stability compared to autologous bone, although it is still resorbable and will be degraded into autologous bone. Demineralized freeze-dried bone allografts were shown to be osteoinductive and osteoconductive due to the release of bone morphogenetic proteins[17], although clinical outcomes comparing mineralized and demineralized freeze-dried bone allografts were reported to be similar[18]. Studies *in vitro* and animal investigations revealed osteoinductive functions of demineralized freeze-dried bone allografts by recruiting cells and ectopic bone formation[19]. Disadvantages of allogeneic materials may be a protracted vascularization, slow remodeling and resorption or longer time for osseointegration, and the risk of immunogenic reactions[15-18].

Third, several experimental studies on animal models[20,21], clinical studies[22-24], and an earlier meta-analysis[25] indicated that platelet-rich plasma (PRP) can increase new bone formation in maxillary sinus augmentation when used in combination with autologous or allogeneic graft material. The use of PRP is based on the premise that it contains large quantities of growth factors, including platelet derived growth factor, insulin-like growth factor-1, and transforming growth factor-β that may enhance osteogenesis[26-28]. However, a number of recent systematic reviews and meta-analyses came to the conclusion that PRP has no significant impact on bone formation as well as on implant survival in maxillary sinus augmentation[29-31].

Based on multidisciplinary expert consultation the aim of the present study was to test (using a first-in-human, split-mouth single case study design) the hypothesis that in GBR-MSA the combination of freshly isolated, unmodified autologous adipose derived regenerative cells (UA-ADRCs), fraction 2 of plasma rich in growth factors (PRGF-2), and an osteoinductive scaffold (OIS) is superior to the combination of PRGF-2 and the same OIS alone. Due to the fact that preliminary data were not available, the present study tested the null hypothesis that the combination of UA-ADRCs, PRGF-2, and an OIS in GBR-MSA is not more effective than the combination of PRGF-2 and the same OIS alone.

CASE PRESENTATION

Chief complaints

A 79-year-old male patient presented with a partly failing maxillary dentition to the clinic of the principal investigator who specialized in periodontology and implant dentistry. The patient reported that his major concern was a functional occlusion resulting in restoration of an aesthetic smile.

History of present illness

The patient reported extensive restorative treatment in the past as well as the loss of several premolar and molar teeth.

History of past illness

No specific past illness was reported that was directly related to the present illness. However, the patient reported reduced oral hygiene in the past, including lack of supragingival plaque control and limited motivation for oral hygiene.

Personal and family history

No specific personal and family history was reported that was directly related to the present illness.

Physical examination upon admission

The clinical examination upon admission revealed a reduced vertical dimension of occlusion and loss of several premolar and molar teeth. Furthermore, advanced periodontal defects were present around several teeth in the anterior maxilla as well as around maxillary and mandibular molar teeth. Most of the remaining maxillary teeth had a guarded to hopeless prognosis.

Laboratory examinations

No laboratory examinations were performed upon admission.

Imaging examinations

A panoramic radiograph was performed upon admission (*i.e.*, at time point T0; the time course of the present study is summarized in Table 1) showed the loss of several premolar and molar teeth and revealed that the residual bone height of the edentulous posterior maxilla below the antrum and the ridge crest was less than 3 mm on both sides (Class D according to[32]) (Figure 1).

Table 1 Overview on the treatments performed in the present study.

Treatments	Time point	Procedures
Pre-phase	T0	Evaluation of the patient
Preparatory steps	T1 (4 mo after T0)	Preparation of plasma rich in growth factors (PRGF-2); isolation of unmodified, autologous adipose derived regenerative cells (UA-ADRCs)
1	T1 (GBR-MSA)	Extraction of tooth # 14; ridge preservation and external sinus lift procedures
2	T2 (6 wk after T1)	Extraction of teeth # 11, #12 and #22; collection of the first biopsies
3	T3 (34 wk after T1)	Placement of implants; collection of the second biopsies
4	T4 (1 yr after T3)	Extraction of tooth #18; placement of healing abutments
5	T5 (6 wk after T4)	Placement of the definitive prosthetic telescopic bridge
	T6 (32 mo after T1)	Last radiologic follow-up

In order to prevent potential identification of the patient the timeline was coded.

MULTIDISCIPLINARY EXPERT CONSULTATION

Önder Solakoglu, DDS, Head of the Clinic for Periodontology and Implantology (Hamburg, Germany)

The residual bone height of the edentulous posterior maxilla as well as of the alveolar bone crest height around the remaining maxillary teeth did not justify immediate implant placement. Therefore, extensive bone augmentation procedures (GBR-MSA) were necessary prior to implant placement. According to the literature, residual bone height of the edentulous posterior maxilla below the antrum and the ridge crest of less than 3 mm shall be treated with a lateral approach involving a bone grafting material and delayed implant placement[33].

To date, the combination of PRGF-2 instead of PRP and an OIS appears to be the most advanced procedure for GBR-MSA. This is due to the fact that a recent experimental study on rats showed that PRGF-2 has more availability for bone regeneration than PRP[34]. The use of a combination of PRGF-2 (prepared using the PRGF-Endoret technology; BTI, Miñano, Spain) and a mineralized cancellous bone particulate allograft (MCBPA) (Puros Cancellous Particulate Allograft; Zimmer Biomet Dental, Palm Beach Gardens, FL, United States) is the current standard procedure for GBR-MSA at the Clinic for Periodontology and Implantology (Hamburg, Germany).

Eckhard U. Alt, MD, PhD, Professor, Chairman of the Board of InGeneron (Houston, TX, United States) and of Isar Klinikum (Munich, Germany)

It appears feasible to further improve GBR-MSA by the application of stem cells (for recent reviews on the use of stem cells in regenerative dentistry[35-37]). Among the different types of mesenchymal stem cells, cells derived from adipose tissue (either freshly isolated or culture-expanded) have emerged as a promising tool for GBR[4,38,39]. The freshly isolated cells are named stromal vascular fraction or ADRCs, and the cultured cells are named adipose-derived stem cells (ASCs). It should be mentioned that some studies on animal models suggested that bone marrow stem cells (BMSCs) may demonstrate greater differentiation into osteoblasts than ADRCs and ASCs[40,41] and might be more useful than ADRCs or ASCs in GBR-MSA[42]. However, bone marrow has a significantly lower stem cell density than adipose tissue (0.01% *vs* 5%), and harvesting adipose tissue is much less painful than harvesting bone marrow because the former is less invasive than the latter[43-45]. Furthermore, focusing exclusively on the potential to differentiate into osteoblasts would fail to take into account the known effect of indirect stimulation of bone regeneration by ADRCs and ASCs, which led to the same amount of measured regenerated bone volume after 6 wk in a study that compared the bone regeneration effect of BMSCs and ASCs in a rabbit craniectomy model[40].

Furthermore, several studies demonstrated that the combination of ADRCs or ASCs with an OIS is a more effective strategy for GBR than the use of an OIS alone (reviewed in[46-48]). Moreover, it was hypothesized that the application of ADRCs or ASCs in combination with an OIS and osteogenic/angiogenic growth factors may

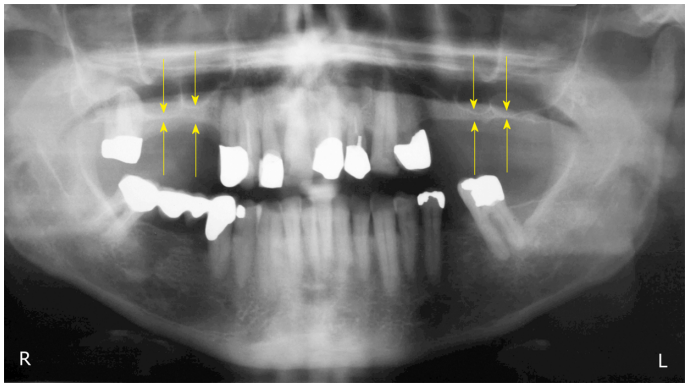

Figure 1 Panoramic radiograph at T0. The yellow arrows indicate the reduced bone height of the edentulous posterior maxilla below the antrum and the ridge crest of less than 3 mm on both sides. R: Right; L: Left.

help to optimize clinical procedures[46]. In this regard the following must be kept in mind: (1) Compared to cultured and potentially modified ASCs, freshly isolated, unmodified ADRCs have the advantage of lower safety requirements because it is not necessary to culture and/or modify the cells; (2) Several non-enzymatic and enzymatic systems for isolating ADRCs were developed (reviewed in[49]). It was reported that cell yield may vary considerably[50]. Moreover, it was shown that in general, non-enzymatic isolation of ADRCs yielded fewer cells than enzymatic (mechanical) isolation[51,52]. To our knowledge, the greatest difference in cell yield between enzymatic and non-enzymatic isolation of ADRCs was reported for the Transpose RT system and the proprietary Matrase Reagent (both from InGeneron, Inc., Houston, TX, United States)[53] (this study is discussed in detail below); and (3) Some clinical studies on cell-based therapies reported the production of donor-specific antibodies after application of allogeneic cells[54,55]. This is not the case when using autologous cells.

In summary, the combination of enzymatically isolated, UA-ADRCs with PRGF-2 and an OIS may be optimal for GBR-MSA.

Werner Götz, MD, PhD, Director of the Laboratory for Orthodontic Basic Research, University of Bonn (Bonn, Germany)

The use of a combination of UA-ADRCs, PRGF-2, and an OIS appears promising but has not yet been reported in GBR-MSA or in guided bone regeneration in general. Thus, it is justified to test this combination in a first-in-human, split-mouth single case study. Furthermore, it is recommended to perform comprehensive histologic, histomorphometric, and immunohistochemical analysis of biopsies of the newly formed bone collected at different time points after GBR-MSA.

Christoph Schmitz, MD, PhD, Head of the Department of Neuroanatomy at LMU Munich (Munich, Germany)

Contemporary histomorphometric analysis of bone biopsies may be insufficient to assess the significance of a combination of UA-ADRCs, PRGF-2, and an OIS in GBR-MSA because it does not provide a detailed analysis of the relative amount (area/area) of bone, allograft, fibrin and connective tissue, adipocytes, arteries, and veins in biopsies of the newly formed bone. However, the latter can be achieved with design-based stereology[56].

FINAL DIAGNOSIS

Loss of several premolar and molar teeth, with residual bone height of the edentulous posterior maxilla as well as of the alveolar bone crest height around the remaining maxillary teeth considered insufficient for implant placement. Justification for treatment with a novel combination of UA-ADRCs, PRGF-2, and an OIS in a first-in-human, split-mouth single case study, carefully controlled by comprehensive histologic, design-based stereologic, and immunohistochemical analysis of biopsies of the newly formed bone collected at different time points after GBR-MSA.

TREATMENT

The present single-case study was approved by the ethics committee of the Federal Dental Association Hamburg (Hamburg, Germany) (no. PV5211). Written informed consent was obtained from the patient to participate in this study after verbal and written information provided by the principal investigator.

During a 4 mo pre-phase the patient's reduced oral hygiene was significantly improved by oral hygiene advice and supragingival plaque control.

During the first treatment, venous blood (8 × 9 mL = 72 mL) was withdrawn from the patient's arm and was processed into PRGF using the PRGF-Endoret technology (BTI, Miñano, Spain) according to the manufacturer's instructions for use. After centrifugation, PRGF-2 was collected and activated with PRGF Activator (BTI).

Furthermore, human subcutaneous adipose tissue was obtained using liposuction. To this end, the periumbilical abdominal area was surgically disinfected. Then, local anesthesia was achieved by infiltrating the periumbilical subcutaneous adipose tissue with 150 mL of modified Klein tumescent solution[57], comprising lactated Ringer solution, adrenaline (1:1000; 1 mg/mL) and 2% lidocaine (20 mg/mL). Fifteen minutes later a stab incision was made 15 cm lateral of the umbilicus, bilaterally. Lipoaspiration was performed using the Coleman method[58] using a 4-hole blunt tipped cannula (3 mm × 150 mm) (part of the LCK-15 Lipoaspiration Collection Kit; InGeneron) and a 60 cm^3 Luer-Lock Toomey-Syringe (also part of the LCK-15 Kit; InGeneron). After liposuction, pressure was applied to the wounds. Then the wounds were closed using adhesive bandage strips (Leukosilk; BSN Medical GmbH, Hamburg, Germany). The lipoaspirate (100 mL) was divided into four aliquots of 25 mL each. Then, all aliquots were processed using the Transpose RT system (InGeneron) for isolating UA-ADRCs from the adipose tissue. Specifically, each aliquot was incubated together with Matrase Reagent (InGeneron) for 1 h. The latter was performed in the processing unit under agitation at 39 °C according to the manufacturer's instructions for use. The total procedure time was 70 min.

Approximately 7 g (2 × 2 cubic centimeters of 0.25-1.0 mm particle size and 1 x 3 cubic centimeters of 1-2 mm particle size) of Puros Cancellous Particulate Allograft (Zimmer Biomet Dental, Palm Beach Gardens, FL, United States) were rehydrated with 1.5 mL of PRGF-2 and a suspension of UA-ADRCs (approximately 50 × 10^6 cells in 3 mL saline) (hereafter referred to as MCBPA/PRGF-2/UA-ADRCs). This was done within 30 min after completion of the PRGF processing and immediately after completion of isolating the UA-ADRCs (Figure 2A). Another 7 g of the same MCBPA were rehydrated with 1.5 ml of PRGF-2 and 3 mL of saline (hereafter referred to as MCBPA/PRGF-2/saline).

After the patient was prepared for surgery and anesthetized *via* local infiltration with Ultracain-DS Forte (Sanofi-Aventis, Frankfurt/Main, Germany), the maxillary tooth 14 was extracted using a minimal traumatic approach with periotomes. Following careful extraction with special emphasis on preservation of the buccal plate of bone, the extraction sockets were examined for potential perforation and fenestration. Curettage of the extraction site was performed to remove all soft tissue debris as well as granulation tissue and to promote healing by stimulating bleeding from the osseous base. Additionally, a bilateral external sinus lift procedure using the Tatum technique[59] was performed. The lateral window access was prepared in the areas of the first molars on both sides using a very atraumatic piezosurgery approach (Mectron, Cologne, Germany) to a size of approximately 10 mm × 7 mm (length × height) in order to allow for sufficient overview into the sinus cavity and to minimize the reduction of cortical bone for overall stability (Figure 2B). Then, the MCBPA/PRGF-2/UA-ADRCs was loosely packed into the prepared right maxillary sinus (Figure 2C), and the MCBPA/PRGF-2/saline into the prepared left maxillary sinus. Afterwards, all sites were covered with a resorbable native pericardium membrane (CopiOs Extend Membrane; Zimmer Biomet Dental) in order to promote the ingrowth of new bone by excluding epithelial migration into the grafted sites. Finally, a soft tissue flap extension[60,61] was surgically performed and primary closure without tension was achieved using vertical and horizontal cross mattress sutures using Gore-Tex Suture (W.L. Gore and Associates, Inc., Flagstaff, AZ, United States) (Figure 2D). The anterior maxillary teeth 11, 12 and 22 were initially preserved for aesthetic reasons and scheduled for extraction 6.5 wk later (Figure 3A).

Analgesics (Paracetamol 500 mg, t.i.d.) and prophylactic antibiotics (Amoxicillin 500 mg, t.i.d.) were prescribed for 7 d postoperatively. Tooth brushing in the surgical area was restricted for the first 2 wk. In addition, chlorhexidine mouthwash was prescribed to maintain the oral flora and prevent infection. Sutures were removed on the 10th postoperative day, and routine monitoring appointments were held at monthly intervals to evaluate healing.

Six weeks after the first treatment, the patient was reappointed and the maxillary anterior teeth # 11, 12, and 22 were extracted (second treatment) using the same approach as applied to the maxillary posterior tooth # 14 during the first treatment.

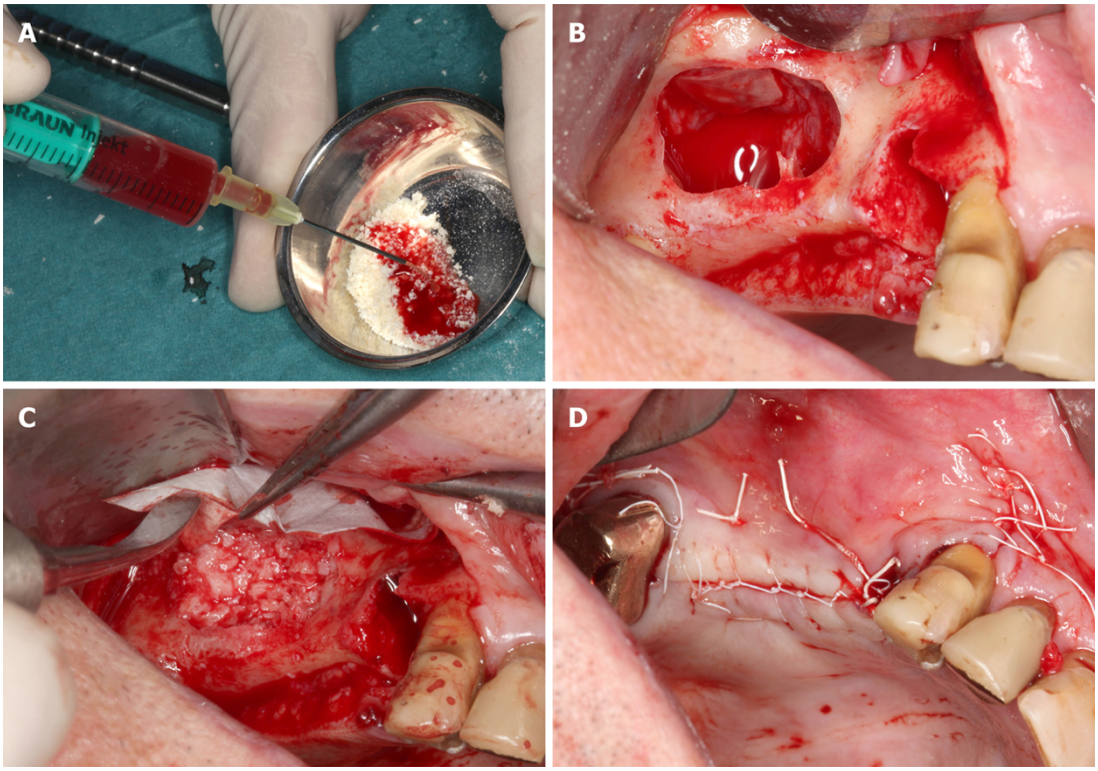

Figure 2 Details of the procedures performed immediately before and during the first surgery (guided bone regeneration-maxillary sinus augmentation). A: Rehydration of the MCBPA with PRGF-2 and UA-ADRCs; B: Preparation of the right maxillary sinus with a lateral external window after atraumatic extraction of tooth # 14 (the Schneiderian membrane was elevated); C: Filling of the right sinus cavity with loosely packed MCBPA/PRGF-2/UA-ADRCs; D: Achievement of primary closure without tension on the right side using horizontal mattress as well as a continuous half-hitch sutures. MCBPA: Mineralized cancellous bone particulate allograft; PRGF-2: Fraction 2 of plasma rich in growth factors; UA-ADRCs: Unmodified autologous adipose-derived regenerative cells.

During this procedure, biopsies of the areas grafted during the first treatment with the MCBPA/PRGF-2/UA-ADRCs (right) and the MCBPA/PRGF-2/saline (left) were collected using a trephine bur (length: 18 mm; inner diameter: 2.6 mm; outer diameter: 3.2 mm; Trepan Bur 227A.204.032; Komet Dental, Lemgo, Germany). Biopsies were fixed by immersion in 4% buffered formaldehyde at room temperature. After at least 1 d of fixation they were prepared for histologic and immunohistological analysis (described in detail below).

The postoperative management (prescription of analgesics, antibiotics, and chlorhexidine mouthwash, restriction of tooth brushing in the surgical area, removal of sutures, and routine monitoring) was the same as performed after the first treatment.

The patient was reappointed again at 34 wk after the second treatment and prepared for dental implant placement surgery (third treatment). Anesthesia was induced *via* local infiltration of Ultracain-DS Forte (Sanofi-Aventis). Then, an osteotomy for implant placement was initially prepared in the alveolar bone using a trephine bur that was identical to the one used during the second treatment (Trepan Bur 227A.204.032; Komet Dental), and biopsies of the areas grafted during the first treatment with the MCBPA/PRGF-2/UA-ADRCs (right side) and the MCBPA/PRGF-2/saline (left side) were collected (these biopsies were handled and processed in the same way as the biopsies that were collected during the second treatment). The osteotomies for implant placement were prepared by sequential cutting to the radiographically determined length with surgical drills in graduated diameters according to the dental implant manufacturer's instructions of use. Implants were then placed according to the manufacturer's recommendations (ASTRA TECH implants with cover screw, Dentsply, Mannheim, Germany). Implants of the following dimensions were inserted into the finally prepared osteotomies: regions 16 and 26: 5.0 S × 11 mm; region 14: 4.0 S × 13 mm; regions 12, 15, and 25: 4.0 S × 11 mm; and region 22: 3.5 S × 11 mm. All implants achieved a high primary stability of 25-30 Ncm insertion torque. The implant access holes were closed with cover screws prior to primary soft tissue closure as performed during the first treatment (Figure 3B). The postoperative management was the same as performed after the first and second treatments.

Twelve months after the third treatment, radiographs were taken and

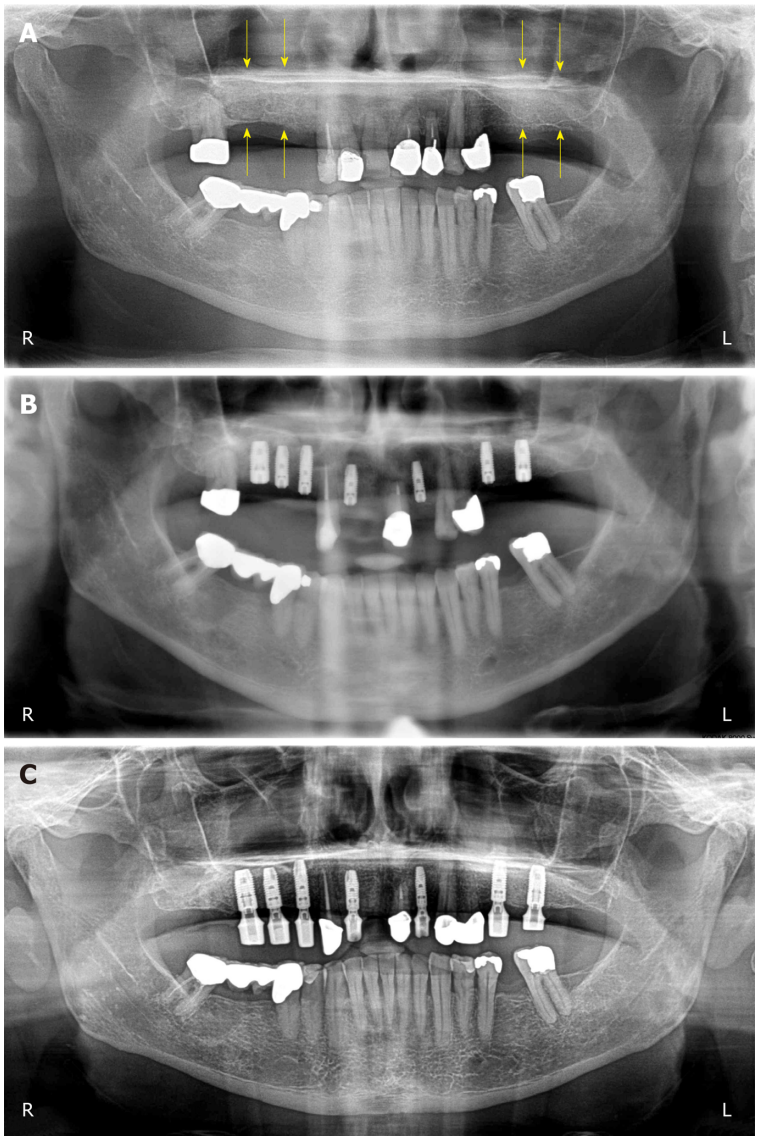

Figure 3 Clinical findings. A: Panoramic radiograph taken immediately after the first surgery (GBR-MSA). The yellow arrows indicate the restored bone height of the edentulous posterior maxilla on both sides; B: Panoramic radiograph taken after the third surgery (placement of implants at 34 wk after GBR-MSA); C: Panoramic radiograph taken at 32 mo after the first treatment. R: Right; L: Left.

demonstrated excellent bone healing around the dental implants, within the augmented sinus, and the extraction sockets (Figure 4) (fourth treatment) (note that the long time between the third and the fourth treatment was due to constraints of time on the side of the patient; from a medical point of view the fourth treatment could have been performed already at 4 mo after the third treatment). No radiological signs of inflammation were observed. The patient was reappointed again and prepared for uncovering of the implants and implant abutment placement surgery as well as extraction of tooth #18. Anesthesia was induced *via* local infiltration of Ultracain-DS Forte (Sanofi-Aventis). Localized mucoperiosteal flaps were raised and the cover screws were removed from the implant access holes. The implant access holes were rinsed using 2% chlorhexidine solution and were then covered with ASTRA Tech Implant healing abutments ('Gingivaformer') of the following dimensions: regions 16 and 26: 5.5 mm × 4.0 mm; regions 12, 14, 15, and 25: 4.5 mm × 4.0 mm; and region 22: 3.5 mm × 4.0 mm.

Prior to closure of the implant access hole, the healing abutment screws were covered with 2% chlorhexidine gel in order to minimize bacterial contamination. The healing abutments were placed using a torque of 20 Ncm according to the manufacturer's recommendations. All implants were surrounded with very sufficient three-dimensional bone volume and demonstrated excellent stability (Figure 4). No clinical signs of inflammation were observed. Tooth # 18 was carefully extracted using a piezosurgery device as described above. Following achievement of primary closure

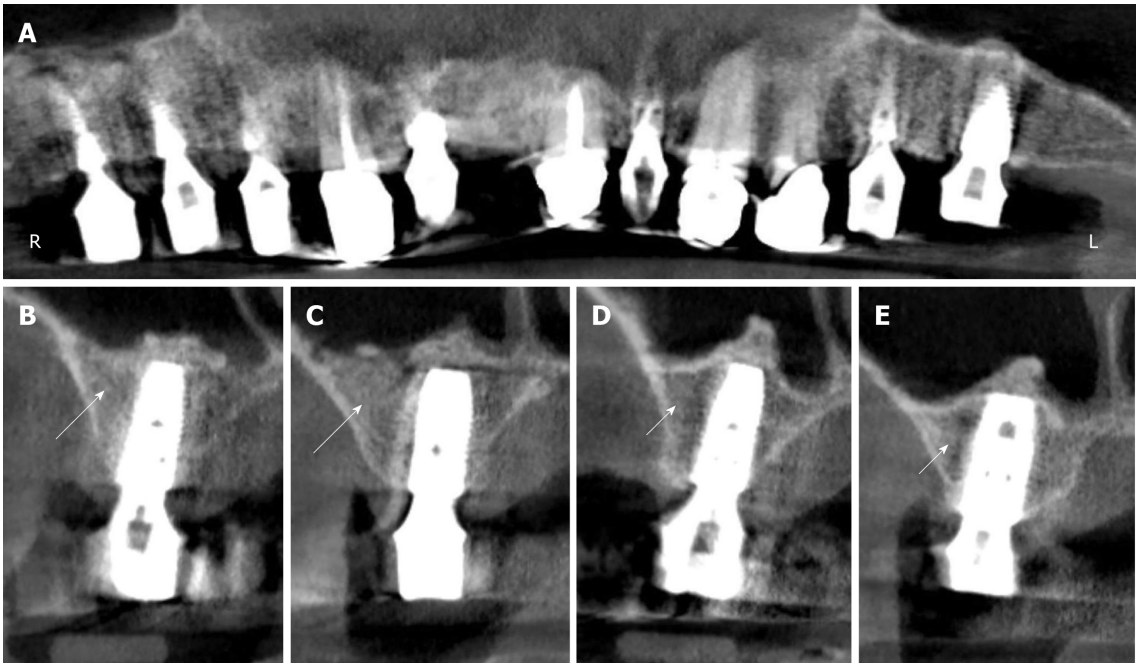

Figure 4 Digital volume tomography radiographs taken after the fourth surgery (1 year after the placement of implants and 20 mo after guided bone regeneration-maxillary sinus augmentation). A: Panoramic view; B-E: Detailed view on selected regions 15 (B), 16 (C), 25 (D), and 26 (E). With the application of unmodified autologous adipose-derived regenerative cells (UA-ADRCs) the bone around the implants in regions 15 and 16 appeared larger in area and denser (arrows in B, C) than without the application of UA-ADRCs in regions 25 and 26 (arrowheads in D, E).

around the healing abutments as described for the other treatments, the same postoperative care regimen was administered as described above and the sutures were removed approximately 10 d postoperatively.

Six weeks after placement of the healing abutments, the definitive prosthetic telescopic bridge (prepared by Dr. Johanna Hevelke, Winsen/Luhe, Germany) was placed.

Histologic processing of the biopsies was performed at the Department of Orthodontics, Center of Dento-Maxillo-Facial Medicine, University of Bonn, Bonn, Germany. To this end, the fixed biopsies were decalcified in 4.1% EDTA solution at room temperature for about 7 d, changing the EDTA solution every 24 h. Then, the biopsies were hydrated, followed by rehydration in an ascending series of ethanol. Afterwards they were embedded in paraffin and cut into 3 μm thick serial longitudinal sections. The sections were mounted on Superfrost Plus slides (Gerhard Menzel, Braunschweig, Germany). Sections representing positions within the biopsies near the longitudinal axis were stained with hematoxylin and eosin stain, or were processed by immunohistochemistry. Finally, all sections were coverslipped with DePeX (Serva, Heidelberg, Germany).

Relative amounts (area/area) of bone, allograft, connective tissue and fibrin, adipocytes, arteries, and veins were determined on the sections that were stained with hematoxylin and eosin stain using point counting as described in detail in[56] (Figure 1B). The distance between the points was 110 μm in XY directions, resulting in a mean total number of 943 (range, 662-1172) points per section. Analyses were performed with a computerized stereology workstation consisting of a modified light microscope (Axioskop; Carl Zeiss Microscopy, Jena, Germany) with Plan-Neofluar objectives 2.5 × (numerical aperture [NA] = 0.075) and 10 × (NA = 0.3) (Carl Zeiss Microscopy), motorized specimen stage (BioPrecision2; Ludl Electronics, Hawthorne, NY, United States), stage controller (MAC 6000 XY; Ludl Electronics), focus encoder (MT 1271; Heidenhain, Traunreut, Germany), CCD color video camera (1,600 x 1,200 pixels; MBF Bioscience, Williston, VT, United States), and stereology software (Stereo Investigator version 10; MBF Bioscience).

After deparaffinizing and rehydrating, sections were rinsed for 10 min in TBS. Histochemical detection of tartrate-resistant acid phosphatase was performed with a specific Acid Phosphatase staining kit (Sigma-Aldrich, Steinheim, Germany) according to the staining protocol of the manufacturer. For immunohistochemistry, endogenous peroxidase was blocked in a methanol/H_2O_2 (Merck, Darmstadt, Germany) solution for 45 min in the dark. Then, sections were pretreated with TBS containing 1% bovine serum albumin at room temperature for 20 min. Afterwards,

sections were digested with 0.4% pepsin at 37 °C for 10 min, followed by incubation with the primary antibodies in a humid chamber. Table 2 summarizes details of the antibodies and the incubation protocols.

Antibody binding was detected with the peroxidase-conjugated EnVision anti-mouse system (Dako, Glostrup, Denmark) or the horseradish peroxidase-conjugated EnVision anti-rabbit/anti-goat secondary antibodies (Dako) that were diluted 1:50 and incubated at room temperature for 30 min. Visualization of peroxidase activity was performed using diaminobenzidine resulting in a brown staining product. Mayer's hematoxylin was used for counterstaining the sections. In order to perform specificity controls, primary antibodies were omitted and TBS or normal horse serum was applied. In other control experiments, both primary and secondary antibodies were omitted. Fetal human bone or mandibular bone (*i.e.*, tissues carrying known antigens) were used as positive controls. Qualitative histological evaluations were performed blinded by one of the authors.

Digital photography was used to produce the photomicrographs shown in Figure 5A and 5B. To this end, on average 41 (range, 30-45) images were captured for each composite using a computerized stereology workstation. The latter consisted of a modified light microscope (Axio Imager 2; Carl Zeiss Microscopy) with an EC Plan Neofluar 10 × objective (NA = 0.3) (Carl Zeiss Microscopy), motorized specimen stage for automatic sampling (H101A; Prior Scientific Instruments, Cambridge, United Kingdom), focus encoder (MT 1271; Heidenhain), CCD color video camera (1388 x 1040 pixels; AxioCam MRc; Carl Zeiss Microscopy), and stereology software (Stereo Investigator version 10; MBF Bioscience). The Virtual Slice module of the Stereo Investigator software (MBF Bioscience) was used to create the montages. The photomicrographs shown in Figure 5C and 5D, Figure 6 and Figure 7 were produced by digital photography (all components from Carl Zeiss Microscopy) using an AxioCam MRc camera attached to an AxioScope 2 microscope and AxioVision 4.7 software using the following objectives: Epiplan 20 × (NA = 0.40) and Plan-Neofluar 40 × (NA = 0.75). Corel Photo-Paint X7 and Corel Draw X7 (both versions 17.5.0.907; Corel, Ottawa, Canada) were used to construct the final figures. Contrast and brightness were only marginally adjusted, which did not alter the appearance of the original materials.

OUTCOME AND FOLLOW-UP

The patient was very satisfied with the maxillary restoration regarding aesthetics, function, phonetics, and cleansibility (Figure 8). The last radiologic follow-up examination took place at 32 mo after the GBR-MSA surgery (Figure 3C).

The biopsies that were collected at 6 wk after GBR-MSA showed the formation of a network of cancellous bony trabeculae by appositional membranaceous osteogenesis in different developmental stages around allogeneic fragments. The newly formed bone (asterisks in Figure 5A and 5B) consisted of fibrous bone. Typically, newly formed bone spicules contained nuclei of allogeneic remnants that showed basophilic staining and contained empty osteocyte lacunae (arrows in Figure 5A and 5B). Most surfaces of the newly formed trabeculae were covered by osteoblasts with underlying osteoid (arrowheads in Figure 5A and 5B). With the application of UA-ADRCs a higher bone lining cell density was achieved than without UA-ADRCs. No signs of active inflammation or necrosis could be recognized in either biopsy.

The biopsies that were collected at 34 wk after GBR-MSA showed a similar morphology as the biopsies that were collected at 6 wk after GBR-MSA. However, bone formation seemed to be increased with a decreased percentage of allogeneic remnants (arrows in Figure 5C and 5D) and fibrous bone. Newly formed cancellous bone was in an advanced stage of remodeling, appearing as lamellar bone (asterisks in Figure 5C and 5D) with fibrous bone remnants incorporated. Fewer adipocytes developed after the application of UA-ADRCs than without UA-ADRCs (arrowheads in Figure 5C and 5D).

At higher magnification, the biopsy that was collected at 6 wk after GBR-MSA with the application of UA-ADRCs showed regions with early osteogenic condensations within a highly cellular surrounding. Specifically, osteoclasts appeared on the surface of natural and allogeneic bone (arrowheads in Figure 5E). Such regions with early osteogenic condensations were not observed at 6 wk after GBR-MSA without application of UA-ADRCs. Rather, osteogenesis appeared more discrete in this case (Figure 5F). Likewise, at 34 wk after GBR-MSA a higher cell density around newly formed cancellous bone was found after the application of UA-ADRCs (arrowheads in Figure 5G) than without UA-ADRCs (arrowheads in Figure 5H).

The results of the histomorphometric analysis are summarized in Figure 9. The

Table 2 Details of antibodies and incubation protocols used in the present study

Antibody	Isotype	Manufacturer	Dilution/incubation
runX2	Goat polyclonal	Santa Cruz Biotechnology (Dallas, TX, United States)	1:30, 4 °C, ON
Collagen type I	Rabbit monoclonal	Abcam (Cambridge, United Kingdom)	1:400, RT, 1 h
Alkaline phosphatase	Rabbit polyclonal	Quartett (Berlin, Germany)	Ready to use, 4 °C, ON
Von Willebrand factor	Rabbit polyclonal	Linaris (Dossenheim, Germany)	1:200, RT, 1h
CD146	Rabbit monoclonal	Abcam	1:50, RT, 1h
CD73	Mouse monoclonal	Antibodies-online (Atlanta, GA, United States)	1:100, 4 °C, ON
PPARγ	Mouse monoclonal	Santa Cruz Biotechnology	1:25, 4 °C, ON

ON: Overnight; RT: Room temperature.

application of UA-ADRCs resulted in a higher relative amount (area/area) of newly formed bone (+ 63% at 6 wk; + 44% at 34 wk), a higher relative amount of fibrin and collagen (+ 144% at 6 wk; + 78% at 34 wk) and a lower relative amount of adipocytes (- 83% at 34 wk) compared to the situation without application of UA-ADRCs. Besides this, the ratio of the relative amounts (area/area) of veins to arteries was 3.5 after the application of ADRCs and 4.7 without ADRCs at 34 wk after GBR-MSA.

Tartrate-resistant acid phosphatase immunostaining revealed middle-sized osteoclasts on the surface of newly formed and allogeneic bone and on debris accumulations at 6 wk after GBR-MSA, with a higher osteoclast density after the application of UA-ADRCs than without UA-ADRCs (arrows in Figure 6A and 6B). Only a few osteoclasts were found at 34 wk after GBR-MSA (arrows in Figure 6C and 6D).

Anti-runt-related transcription factor 2 immunoreactivity was found at 6 wk after GBR-MSA with the application of UA-ADRCs, but not in GBR-MSA without UA-ADRCs, in most osteoblasts and osteoblast-like cells (arrows in Figure 6E). Only very weak anti-runt-related transcription factor 2 immunoreactivity was found at 34 wk after GBR-MSA (Figure 6G and 6H).

Type I collagen appeared in osteoid seams (arrows in Figure 6I and 6J) and in a weak manner in the matrix of newly formed bone trabeculae (asterisks in Figure 6I and 6J) at 6 wk after GBR-MSA. At 34 wk after GBR-MSA the pattern of immunoreactivity for type I collagen was similar to the pattern observed at 6 wk after GBR-MSA but weaker (arrows and asterisks in Figure 6K and 6L).

The application of UA-ADRCs resulted in strong alkaline phosphatase (AP) immunoreactivity in osteoblasts, osteoblast-like cells, and fibroblasts in the intertrabecular connective tissue at 6 wk after GBR-MSA, while in GBR-MSA without UA-ADRCs only a few osteoblasts were immunoreactive for AP (arrows in Figure 6M and 6N). At 34 wk after GBR-MSA AP immunoreactivity appeared in some osteoblasts and osteoblast-like cells in a weak to moderate manner (arrows in Figure 6O and 6P).

Immunohistochemical detection of factor VIII/von Willebrand factor showed dense vascularization in all biopsies (arrows in Figure 7A-D), with the highest density at 6 wk after GBR-MSA with the application of UA-ADRCs. In GBR-MSA without UA-ADRCs, larger sinusoidal vessels were found at 34 wk after GBR-MSA and were located within the intertrabecular connective tissue (arrowheads in Figure 7D).

Vessel walls were strongly immunoreactive for CD146 in all biopsies (arrows in Figure 7E-H).

A strong intracellular, granular anti-CD 73 immunoreactivity was seen in all biopsies in subsets of fibroblasts and osteoblasts (arrows in Figure 7I-L), as well as in vessel walls (arrowheads in Figure 7I-L).

Nearly all osteoblasts and fibroblasts as well as a subset of osteocytes showed immunoreactivity for PPARγ at 6 wk after GBR-MSA (arrows in Figure 7M and 7N). Furthermore, PPARγ immunoreactivity was also found in vessel walls in areas with osteogenesis (arrowheads in Figure 7M and 7N). In general, a very similar pattern was found at 34 wk after the application of UA-ADRCs, whereas without UA-ADRCs immunoreactivity for PPARγ was restricted to vessel walls (arrows and arrowheads in Figure 7O and 7P).

The immunohistochemically negative control specimens displayed no immunoreactivity.

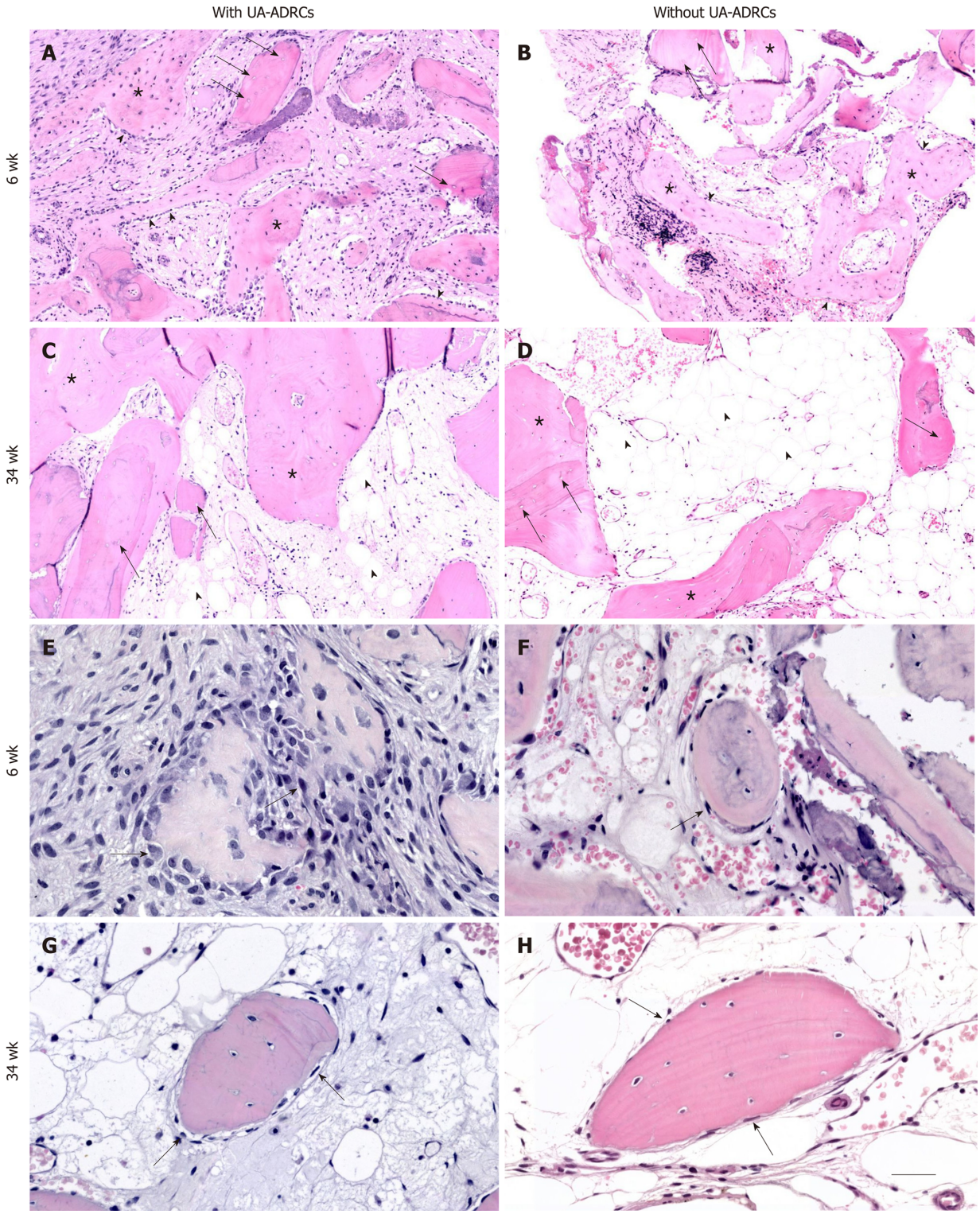

Figure 5 Histological findings. Representative photomicrographs of 3 μm thick paraffin sections stained with hematoxylin and eosin of biopsies that were collected at 6 wk (A, B, E, F) or 34 wk (C, D, G, H) after guided bone regeneration maxillary sinus augmentation with the application of UA-ADRCs (A, C, E, G) or without UA-ADRCs (B, D, F, H). In A-D the asterisks indicate newly formed bone and the arrows indicate empty osteocyte lacunae in allogeneic fragments. Furthermore, in A and B the arrowheads point to osteoblasts with underlying osteoid, while in C and D the arrowheads indicate adipocytes. In E-H the arrows indicate cells on the surface of newly formed bone. The scale bar in H represents 150 μm in A-D and 75 μm in E-H. UA-ADRCs: Unmodified autologous adipose-derived regenerative cells.

DISCUSSION

The present study is the first one in which a combination of freshly isolated UA-ADRCs, PRGF-2, and an OIS was used for GBR-MSA. Furthermore, our study is the first one in which cellular and histological effects of mesenchymal stem cells in human GBR-MSA were investigated with design-based stereology, histochemistry, and immunohistochemistry. The analysis of the biopsies that were collected at 6 wk and

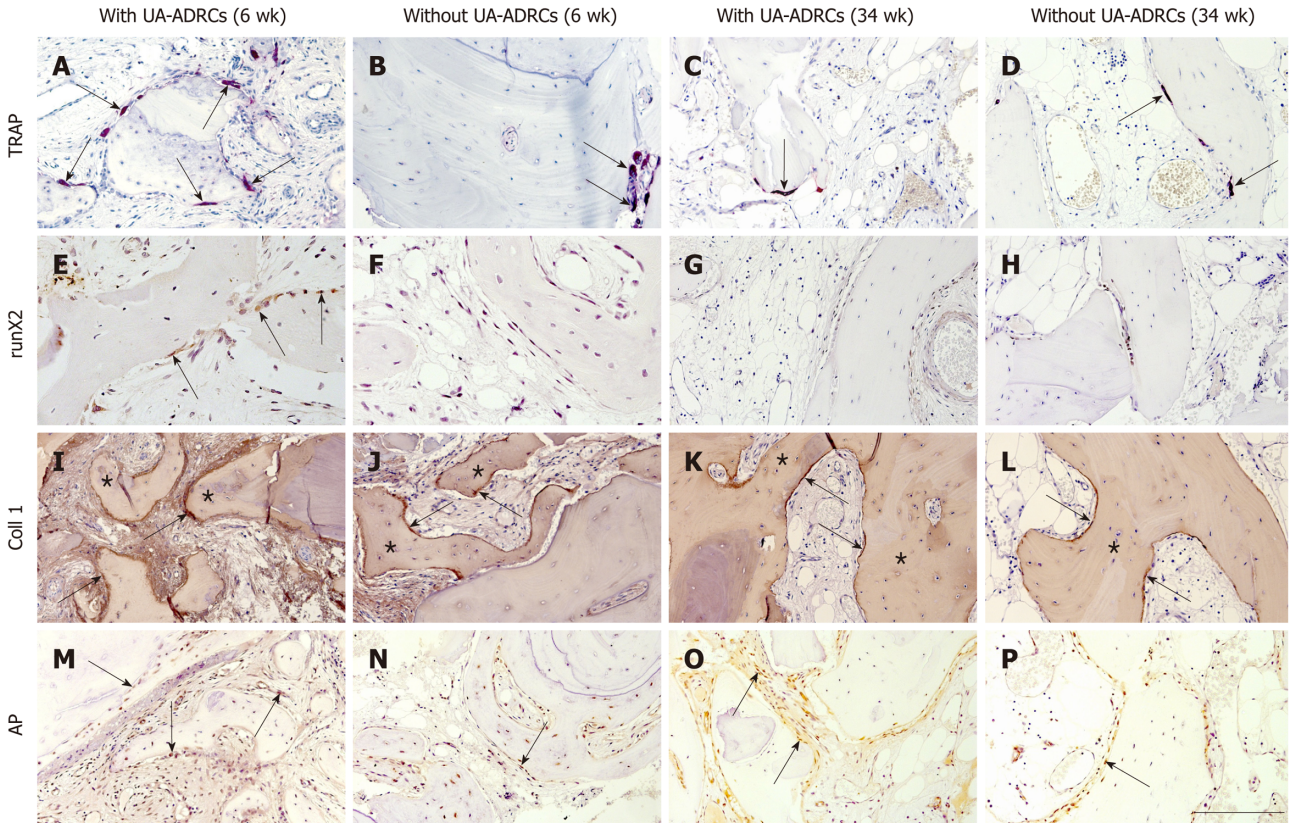

Figure 6 Histological findings. Representative photomicrographs of histochemical detection of tartrate-resistant acid phosphatase (TRAP) (A-D) as well as of immunohistochemical detection of Runt-related transcription factor 2 (runX2) (E-H), collagen 1 (Coll 1) (I-L), and alkaline phosphatase (AP) (M-P) in 3 μm thick paraffin sections of biopsies that were collected at 6 wk (A, B, E, F, I, J, M, N) or 34 wk (C, D, G, H, K, L, O, P) after GBR-MSA with the application of UA-ADRCs (A, C, E, G, I, K, M, O) or without UA-ADRCs (B, D, F, H, J, L, N, P). In A-D the arrows point to osteoclasts, in E to osteoblasts, in I-L to type I collagen in osteoid seams, and in M-P to AP immunostaining found in osteoblasts, osteoblast-like cells, and fibroblasts in the intertrabecular connective tissue. Furthermore, in I-L the asterisks indicate type I collagen in the matrix of newly formed bone trabeculae. The scale bar in P represents 200 μm in A-D and I-P, and 100 μm in E-H. UA-ADRCs: Unmodified autologous adipose-derived regenerative cells.

again at 34 wk after GBR-MSA showed that the combination of UA-ADRCs, PRGF-2, and the OIS resulted in better and faster bone regeneration than the combination of PRGF-2 and the same OIS alone. It is of note that our design-based stereologic finding of a higher relative amount of newly formed bone after GBR-MSA with the application of UA-ADRCs than without UA-ADRCs (+ 63% at 6 wk; + 44% at 34 wk) (Figure 9) was in line with our radiologic finding of more dense bone after the application of UA-ADRCs in regions 15 and 16 than without UA-ADRCs in regions 25 and 26 at 20 mo after GBR-MSA (Figure 4).

The results of the present study may open new horizons for the rehabilitation of the edentulous posterior maxilla and potentially for other regenerative techniques in pre-implant bone augmentation procedures like lateral and horizontal alveolar ridge augmentation, socket preservation, and bone grafting following large cystectomies. Specifically, the novel GBR-MSA approach presented here could result in a superior bone-implant-contact due to advanced new bone formation (Figure 9) and could also serve as the basis for reducing the time between GBR-MSA and the placement of implants in patients with residual bone height below the antrum and the ridge crest of less than 3 mm (Class D[32]). Besides this, our novel approach may allow for immediate implant placement in combination with bone augmentation procedures when the primary stability of the implant is provided. Moreover, the harvesting of ADRCs may result in less morbidity of the patient compared to bone marrow aspiration from the iliac crest area (addressed in the next paragraph). However, it will be the task of future studies to test these hypotheses.

GBR-MSA using mesenchymal stem cells (except of the use of UA-ADRCs) has been investigated in many preclinical and clinical studies, with and without OIS, and with and without use of PRP (reviewed in[62-64]). In most of these studies BMSCs, autologous bone marrow aspirate concentrate (BMAC), or periosteal derived stem cells were used. Histomorphometric analysis showed considerable differences in the relative amount (area/area) of newly formed bone at 24 wk after surgery, ranging between 13.5% using BMSCs and bovine bone material (BBM)[65] and 55.2% using

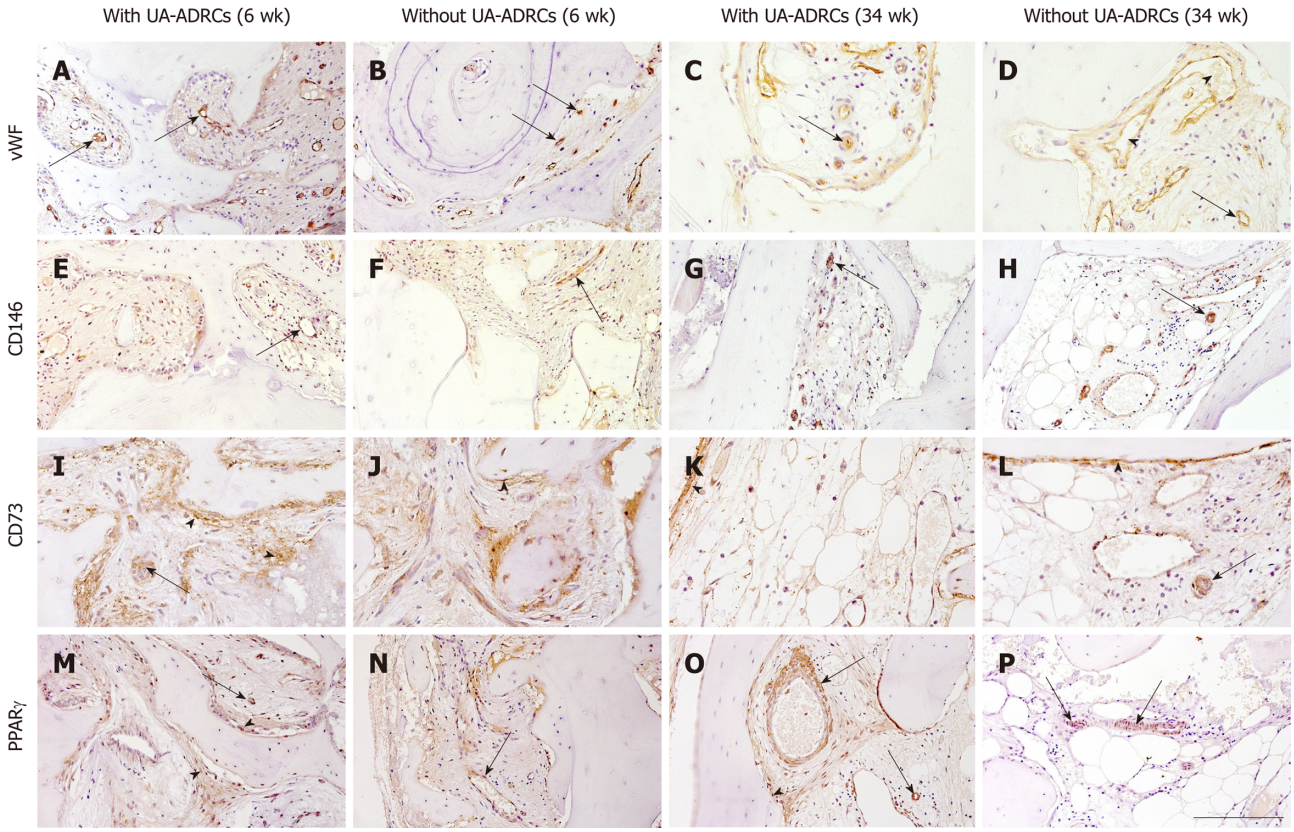

Figure 7 Histological findings. Representative photomicrographs of immunohistochemical detection of factor VIII/von Willebrand factor (vWF) (A-D), CD146 (E-H), CD73 (I-L), and peroxisome proliferator-activated receptor gamma (PPARγ) (M-P) in 3 μm thick paraffin sections of biopsies that were collected at 6 wk (A, B, E, F, I, J, M, N) or 34 wk (C, D, G, H, K, L, O, P) after GBR-MSA with the application of UA-ADRCs (A, C, E, G, I, K, M, O) or without UA-ADRCs (B, D, F, H, J, L, N, P). In all panels the arrows point to vessels. Furthermore, the arrowheads indicate sinusoidal vessels in D, and fibroblasts and osteoblasts in I-L, M, and O. The scale bar in P represents 200 μm in A-D and I-P, and 100 μm in E-H. GBR-MSA: Guided bone regeneration maxillary sinus augmentation; UA-ADRCs: Unmodified autologous adipose-derived regenerative cells.

BMAC and BBM[66]. This considerable difference and the fact that the relative amount (area/area) of cancellous bone in normal human bone is only approximately 25%[67] should give reason to accept the results of related studies only after having critically scrutinized the corresponding methodological details. For example, in a study that reported a relative amount of newly bone of 55.2% using BMAC and BBM[67] only small portions of the investigated specimens were shown, and histomorphometry was performed by inspecting the specimens with a 1.25× objective, which precludes to distinguish between empty osteocyte lacunae (representing scaffold) and cell bodies within osteocyte lacunae (representing newly formed bone). In any case, a meta-analysis of nine studies (seven animal and two human studies) in which the combination of mesenchymal stem cells and OIS *versus* OIS alone were compared, found a statistically significant positive effect of stem cells on the bone re-growth in GBR-MSA[63].

At first glance our design-based results (relative amount of newly formed bone of 24.2% at 34 wk after GBR-MSA) do not speak in favor of our approach compared to the use of BMSCs (among the six studies reviewed in[63] in which BMSCs were applied and histomorphometric analysis was performed at 24 wk after surgery, three studies reported a relative amount of newly formed bone of more than 24%). However, our decision to use UA-ADRCs rather than other types of cells (including ASCs, BMSCs, periosteal derived stem cells, allogeneic and/or modified ASCs/BMSCs, dental-derived mesenchymal stem cell-like cells (reviewed in[68]) or induced pluripotent stem cells) was based on the fact that UA-ADRCs are the only type of cell that allows immediate usage at point of care, with the lowest safety concerns in cell-based therapy as no culturing or modification is required. This is fundamentally different from all other types of cells that have been considered for cell-based therapies in dentistry (reviewed in[69]). Regarding safety concerns one must keep in mind that, *e.g.*, potential oncogenesis currently limits the clinical translation of induced pluripotent stem cells[70,71], and applying allogeneic cells may cause the production of donor-specific antibodies and cell induced immune response[54,55]. The only other cell-based therapy that allows immediate usage at point of care is autologous BMAC, which was

Figure 8 Documentation of clinical outcome. A, B: Intraoral ventral (A) and occlusal (B) views on the healing abutments in regions 12, 14, 15, 16, 22, 25, and 26 after the fourth treatment (1 year after the placement of implants and 20 mo after guided bone regeneration maxillary sinus augmentation). Note that the teeth # 13, 21, 23, and 24 are crowned; C, D: External (C) and internal (D) view of the prosthetic telescopic bridge; E: Intraoral view of the final prosthetic reconstruction.

investigated in two studies on GBR-MSA (BBM as OIS). One of these studies was a case report on a 46-year-old partially edentulous man, showing a relative amount of newly formed bone of 27% at 12 wk after surgery without control treatment[72]. The other study[73] was a randomized controlled trial (from the same lab as[72], published in the same year, and using exactly the same procedure for harvesting bone marrow aspirate as used in[72]), reporting a mean relative amount of newly formed bone of only 12.6% at 12 wk after surgery (n = 34 patients), with a mean relative amount of newly formed bone of only 14.3% at 12 wk after grafting BBM and autologous bone (n = 11 patients)[73]. It is of note that only in the latter study[73] whole specimens were shown and methodological details of the histomorphometric analysis were provided. The data of the latter study[73] are in line with the data obtained with our control treatment (Figure 7) and indicates that the use of UA-ADRCs may be more effective than the use of BMAC in GBR-MSA.

Detection of factors involved in osteogenesis and bone remodeling using histochemistry and immunohistochemistry is not frequently applied in studies on GBR-MSA in dentistry. Mostly, only selected factors were investigated. In line with former studies[74,75] we applied a broader panel of antibodies including vessel markers like factor VIII/von Willebrand factor. The immunostaining pattern obtained revealed similar findings as for remodeling of allografts[76]. However, the direct comparison of the immunolabeling of osteogenic factors like runt-related transcription factor 2 and AP between both sides showed stronger immunopositivity after the application of

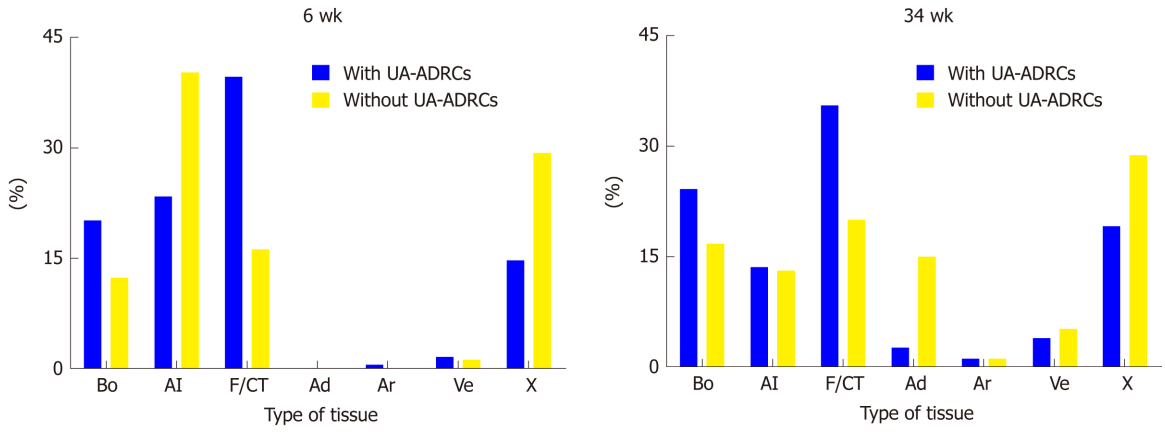

Figure 9 Results of histomorphometric analyses. Relative amounts (area/area) of bone (Bo), allograft (Al), fibrin and connective tissue (F/CT), adipocytes (Ad), arteries (Ar), veins (Ve) and artifacts (X) in 3 μm thick paraffin sections stained with hematoxylin and eosin stain of biopsies that were collected at 6 wk (on the left) or 34 wk (on the right) after guided bone regeneration maxillary sinus augmentation with the application of unmodified autologous adipose-derived regenerative cells (UA-ADRCs) or without UA-ADRCs. UA-ADRCs: Unmodified autologous adipose-derived regenerative cells.

UA-ADRCs, which underlines better and faster bone regeneration. The finding of middle-sized osteoclasts on the surface of newly formed and allogeneic bone and on debris accumulations at 6 wk after GBR-MSA, with a higher osteoclast density after the application of UA-ADRCs than without UA-ADRCs (Figure 5E, 5F, and Figure 6A-D), was in line with earlier reports in the literature[77,78] about osteoclasts involved in bone remodeling (which was increased after application of UA-ADRCs compared to the situation without UA-ADRCs). This phenomenon must not be confused with foreign material resorption by multinucleated giant cells[77]. That was not observed in the present study. The denser vascularization on the cell treated side (detected with both histomorphometry and anti-factor VIII/von Willebrand factor immunohistochemistry) that was treated with UA-ARDCs underlines the importance of the coupling of angiogenesis and osteogenesis in bone regeneration[79].

We did not characterize the UA-ADRCs isolated from lipoaspirate with the Transpose RT system and Matrase Reagent (both from InGeneron) in the present study. However, a very recent study compared cell suspensions that were obtained by isolating cells from lipoaspirate from 12 healthy donors using the Transpose RT system and Matrase Reagent (thereafter: "TRT-MR cell suspensions") with cell suspensions that were obtained by isolating cells from lipoaspirate from the same donors just mechanically (*i.e.*, using the Transpose RT system but without Matrase Reagent) (thereafter: "TRT cell suspensions")[53]. It was found that the mean cell yield (numbers of cells/g of processed lipoaspirate) was approximately twelve times higher in TRT-MR cell suspensions than in TRT cell suspensions ($P < 0.001$), and cells in TRT-MR cell suspensions formed on average 16 times more colony forming units (considered to be an indicator of stemness) per g lipoaspirate than cells in TRT cell suspensions ($P < 0.001$)[53]. Of note, the mean relative number of viable cells in TRT-MR cell suspensions (85.9% ± 1.1%; mean ± SE) exceeded the proposed minimum threshold for the viability of cells in the stromal vascular fraction of 70% established by the International Federation for Adipose Therapeutics and Science[80], whereas the mean relative number of viable cells in TRT suspensions (61.7% ± 2.6%) did not ($P < 0.001$)[53]. On the other hand, cells in TRT-MR cell suspensions exhibited no statistically significant differences in the expression of regenerative cell-associated genes such as Oct4, Hes1, and Klf4 compared to cells in TRT cell suspensions[53].

The same study demonstrated that upon stimulation with specific differentiation media cells in TRT-MR and TRT cell suspensions were independently able to differentiate into cells from all three germ layers (*i.e.*, into the adipogenic, osteogenic, hepatogenic, and neurogenic lineages)[53]. The latter is in line with earlier findings that adult stem cells may obtain any of the lineages but depend on constant induction of differentiation and re-confirmation by signals released and communicated from the local microenvironment[81-83]. If this information and confirmation is missing or ceases, adult stem cells stop differentiating[84,85]. In fact, only true stem cells are able to continue their expected differentiation pathway as supported by the local microenvironment[86-88]. This is one of several reasons why adult stem cell therapy with UA-ARDCs is very safe[89-91]. In contrast, safety concerns have been raised regarding stem cell therapy with cultured adult stem cells because with higher passages an increased rate of potential malignant transformation may occur[92-94].

A study on fresh, uncultured cells that were isolated from adipose tissue of pigs

using the Transpose RT system and Matrase Reagent showed that approximately 40% of cells in the stromal vascular fraction were immunopositive for CD29 (thereafter: $CD29^+$) and $CD44^+$[95], which are markers of adipose tissue-derived stem cells[50,96]. Furthermore, on average only 9% of the cells were $CD45^+$ (a marker of blood derived cells[50]), and on average only 11% of the cells were $CD31^+$ (a marker of endothelial cells[50]). Another study on fresh, uncultured cells that were isolated from adipose tissue of horses using a predecessor of the Transpose RT system (ARC system; InGeneron) and Matrase Reagent found the highest relative gene expression of osteocalcin (a gene associated with the osteogenic lineage[97]) when investigating these cells for the relative gene expression of CD44, CD73, CD90, CD105, CD146, and CD166 (mesenchymal stem cell surface markers), CD34 and CD45 (hematopoietic markers), CD31 (endothelial cell marker), type-1 collagen, PPARγ2 (a gene associated with the adipogenic lineage), and osteocalcin[98]. Collectively, these data underline the osteogenic potential of the UA-ADRCs used in the present study.

We used PRGF-2 rather than PRP because our clinical experience is in line with data from a recent experimental study on rats that showed that PRGF-2 has more availability for bone regeneration than PRP[34]. The content of PRGF-2 prepared using the PRGF-Endoret technology (BTI) was investigated in several studies in the literature. Most relevant to the results of the present study was the demonstration of high amounts of growth factors in PRGF-2[98], *i.e*. on average approximately 14000 pg/mL of platelet derived growth factor-AB, 46000 pg/mL of transforming growth factor-β 1, 220 pg/mL of vascular endothelial growth factor, 400 pg/mL hepatocyte growth factor, 83000 pg/mL insulin-like growth factor-1, and 600 pg/mL endothelial growth factor (note that what was named "PRGF F3" in[98] is now named "Fraction 2 of PRGF" according to BTI, and the latter terminology was used in the present study). Several pilot studies described the use of PRGF in GBR-MSA[99-101]. Furthermore, it was shown that PRGF can stimulate the proliferation, migration, and chemotaxis of osteoblasts *in vitro* and enhance the osteblasts' autocrine expression of vascular endothelial growth factor and hepatocyte growth factor that are proangiogenic factors[98]. Both vascular endothelial growth factor and hepatocyte growth factor are contained in PRGF-2[98] and were also identified within the ASCs' secretome (reviewed in[102]). A recent study showed that PRGF can induce proliferation and migration of human-derived ASCs and reduce senescence and autophagocytosis of these cells *in vitro*[103]. The same study[103] confirmed our own finding that human-derived ASCs can efficiently differentiate into osteocytes or adipocytes when cultured in osteogenic or adipogenic induction medium, respectively[53,104], but also demonstrated that this process is enhanced in the presence of PRGF[103]. Accordingly, our finding that the treatment with MCBPA/PRGF-2/UA-ADRCs resulted in the formation of 44% more bone and 83% fewer adipocytes in the biopsies collected at 34 wk after GBR-MSA (Figure 9) cannot be directly attributed to the action of PRGF-2 on UA-ADRCs. Rather, it is reasonable to hypothesize that cues from the local extracellular environment affected the properties of the UA-ADRCs in terms of proliferation and specific osteogenic differentiation (c.f.[105]), and this process was enhanced by PRGF-2.

GBR-MSA has been performed using a number of grafting materials, including autologous bone grafts, allografts, and xenografts[106]. An earlier meta-analysis published in 1998 found that the survival rates of implants placed in grafted maxillary sinuses did not depend on whether autologous, allogeneic, or alloplastic grafts were used[107]. However, when focusing on the total bone volume, another meta-analysis published in 2010 concluded that autologous bone should still be considered the gold standard in MSA surgery[108]. On the other hand, the latter study stated that the consequence of the total bone volume for implant survival is still unknown[108]. A recent meta-analysis based on 16 original studies found that the implant survival rate was 99.6% when a biomaterial was used during surgery compared to 96.0% when no graft material was used (the follow-up period was 48 to 60 mo in this study)[109]. However, these data should be handled cautiously because only two studies in this meta-analysis were performed with autologous bone grafts, and in 10 out of the 16 included studies (six out of seven studies without interpositional graft material) the average preoperative bone height was more than 5 mm, which represents Class C according to[32] and does not resemble the situation addressed in the present study. We used the Puros Cancellous Particulate Allograft (Zimmer Biomet Dental) because it fulfills all of the following criteria that are considered essential for an OIS in the literature (reviewed in[110]: volume stability of at least 4 mo after implantation, full biocompatibility and resorbability, and possibility for loading with stem cells and growth factors.

The patient who was investigated in our study was 79-years-old. The statistical life expectancy of 80-year-old men and women has increased 7.7 years and 9.2 years, respectively in Germany[111]. Thus, one can expect an increasing demand for the

restoration of an aesthetic smile and a functional occlusion by patients aged 79 and older (and of course by younger patients) in the future. On the other hand, some authors have argued that age-related progressive decline in mechanical strength of tissue could be due to loss of resident stem cell number and function and have raised concerns regarding the use of autologous adult stem cell therapy in older patients[112]. Indeed, an earlier study[113] found that the number and multilineage differentiation potential of ASCs declined with the age of healthy volunteers, combined with increased expression of cyclin-dependent kinase inhibitor p16ink4a and CHEK1 (*i.e.*, genes associated with senescence)[112]. These and other data reported in the literature have motivated patients to start cryopreserving ADRCs from lipoaspirate[112]. However, a recent pilot study showed that two samples of ADRCs collected from a healthy person at age 72 years and again at age 84 years showed the same cell yield and ADRC subpopulation composition without change in the proliferation rates of ASCs (obtained by culturing the ADRCs), as well as the capability of tri-lineage differentiation of both cell cultures[112]. Another recent pilot study showed that protein expression profiles of human umbilical vein endothelial cells that were co-cultured under oxidative stress conditions with ADRCs from three healthy persons aged 42, 45, and 47 years did not differ from protein expression profiles of human umbilical vein endothelial cells that were co-cultured under identical conditions with ADRCs from three healthy persons aged 61 and 62 (two persons) years[114]. Collectively, these data with the results of the present study, indicate (albeit preliminary) that using freshly isolated UA-ADRCs from patients aged 79 years and older is a valid approach for GBR-MSA. Effects of aging on PRGF-2 have, to our knowledge, not been reported.

There are limitations to the present study. First, only a single patient was investigated. However, from an ethical point of view, this appears justified in a first-in-human pilot study. It goes without saying that the efficacy and safety of our novel approach must be confirmed in future studies (including well-designed randomized controlled trials) on a larger number of patients. Second, only a single combination of a certain dose of UA-ADRCs, PRGF-2, and a certain OIS was tested. However, the same was done in most other feasibility studies on cell-based therapies for GBR-MSA. Third, we did not investigate the combination of UA-ADRCs and MCBPA. Rather, we used MCBPA/PRGF-2/saline as a control treatment because we wanted to compare the effects of UA-ADRCs in GBR-MSA with an established procedure (a similar decision was taken in an earlier study[79] that compared a combination of BMAC and BBM with a combination of autologous bone and BBM in GBR-MSA rather than BBM alone). Fourth, we were unable to determine whether (and, if so, how many) UA-ADRCs differentiated into osteoblasts. This is due to the fact that UA-ADRCs can in principle not be labeled and, thus not be quantified.

CONCLUSION

The present study suggests that GBR-MSA with a combination of UA-ADRCs, PRGF-2, and an OIS is effective, leading to a significant increase in the relative amount of newly formed bone and of dense fibrous tissue as well as less unwanted new adipose tissue formation without adverse effects. The results of our study support further evaluation of UA-ADRCs (including the isolation procedure used), dose, and combination with PRFG-2 and an OIS in future clinical trials under strict criteria. Besides this, the results presented here may also be of relevance to other fields of regenerative dentistry using stem cells (reviewed in[115-117]), as well as for GBR in general. The results depicted in Figure 9 indicate that the addition of stem cells induces more bone formation already after 6 wk than achieved without stem cells after 6 mo. This clinically relevant shortening of time to implant should be evaluated by future studies.

ACKNOWLEDGEMENTS

We thank Aschauer B, Müller-Bay I, and van Dyck S for technical support.

REFERENCES

1 **Laudenbach JM**, Simon Z. Common dental and periodontal diseases: evaluation and management. *Med Clin North Am* 2014; **98**: 1239-1260 [PMID: 25443675 DOI: 10.1016/j.mcna.2014.08.002]

2 **Moraschini V**, Poubel LA, Ferreira VF, Barboza Edos S. Evaluation of survival and success rates of dental implants reported in longitudinal studies with a follow-up period of at least 10 years: a systematic

review. *Int J Oral Maxillofac Surg* 2015; **44**: 377-388 [PMID: 25467739 DOI: 10.1016/j.ijom.2014.10.023]
3 **Lundgren S**, Cricchio G, Hallman M, Jungner M, Rasmusson L, Sennerby L. Sinus floor elevation procedures to enable implant placement and integration: techniques, biological aspects and clinical outcomes. *Periodontol 2000* 2017; **73**: 103-120 [PMID: 28000271 DOI: 10.1111/prd.12165]
4 **Esposito M**, Felice P, Worthington HV. Interventions for replacing missing teeth: augmentation procedures of the maxillary sinus. *Cochrane Database Syst Rev* 2014; CD008397 [PMID: 24825543 DOI: 10.1002/14651858.CD008397.pub2]
5 **Starch-Jensen T**, Jensen JD. Maxillary Sinus Floor Augmentation: a Review of Selected Treatment Modalities. *J Oral Maxillofac Res* 2017; **8**: e3 [PMID: 29142655 DOI: 10.5037/jomr.2017.8303]
6 **Al-Dajani M**. Recent Trends in Sinus Lift Surgery and Their Clinical Implications. *Clin Implant Dent Relat Res* 2016; **18**: 204-212 [PMID: 25274014 DOI: 10.1111/cid.12275]
7 **Jamjoom A**, Cohen RE. Grafts for Ridge Preservation. *J Funct Biomater* 2015; **6**: 833-848 [PMID: 26262646 DOI: 10.3390/jfb6030833]
8 **Rogers GF**, Greene AK. Autogenous bone graft: basic science and clinical implications. *J Craniofac Surg* 2012; **23**: 323-327 [PMID: 22337435 DOI: 10.1097/SCS.0b013e318241dcba]
9 **Sakkas A**, Wilde F, Heufelder M, Winter K, Schramm A. Autogenous bone grafts in oral implantology-is it still a "gold standard"? A consecutive review of 279 patients with 456 clinical procedures. *Int J Implant Dent* 2017; **3**: 23 [PMID: 28573552 DOI: 10.1186/s40729-017-0084-4]
10 **Sanz M**, Vignoletti F. Key aspects on the use of bone substitutes for bone regeneration of edentulous ridges. *Dent Mater* 2015; **31**: 640-647 [PMID: 25882277 DOI: 10.1016/j.dental.2015.03.005]
11 **Wang W**, Yeung KWK. Bone grafts and biomaterials substitutes for bone defect repair: A review. *Bioact Mater* 2017; **2**: 224-247 [PMID: 29744432 DOI: 10.1016/j.bioactmat.2017.05.007]
12 **Yamada M**, Egusa H. Current bone substitutes for implant dentistry. *J Prosthodont Res* 2018; **62**: 152-161 [PMID: 28927994 DOI: 10.1016/j.jpor.2017.08.010]
13 **Nkenke E**, Neukam FW. Autogenous bone harvesting and grafting in advanced jaw resorption: morbidity, resorption and implant survival. *Eur J Oral Implantol* 2014; **7** Suppl 2: S203-S217 [PMID: 24977256]
14 **García-Gareta E**, Coathup MJ, Blunn GW. Osteoinduction of bone grafting materials for bone repair and regeneration. *Bone* 2015; **81**: 112-121 [PMID: 26163110 DOI: 10.1016/j.bone.2015.07.007]
15 **Troeltzsch M**, Troeltzsch M, Kauffmann P, Gruber R, Brockmeyer P, Moser N, Rau A, Schliephake H. Clinical efficacy of grafting materials in alveolar ridge augmentation: A systematic review. *J Craniomaxillofac Surg* 2016; **44**: 1618-1629 [PMID: 27622971 DOI: 10.1016/j.jcms.2016.07.028]
16 **Danesh-Sani SA**, Engebretson SP, Janal MN. Histomorphometric results of different grafting materials and effect of healing time on bone maturation after sinus floor augmentation: a systematic review and meta-analysis. *J Periodontal Res* 2017; **52**: 301-312 [PMID: 27534916 DOI: 10.1111/jre.12402]
17 **Monje A**, O'Valle F, Monje-Gil F, Ortega-Oller I, Mesa F, Wang HL, Galindo-Moreno P. Cellular, Vascular, and Histomorphometric Outcomes of Solvent-Dehydrated vs Freeze-Dried Allogeneic Graft for Maxillary Sinus Augmentation: A Randomized Case Series. *Int J Oral Maxillofac Implants* 2017; **32**: 121-127 [PMID: 27529782 DOI: 10.11607/jomi.4801]
18 **Wood RA**, Mealey BL. Histologic comparison of healing after tooth extraction with ridge preservation using mineralized versus demineralized freeze-dried bone allograft. *J Periodontol* 2012; **83**: 329-336 [PMID: 21749166 DOI: 10.1902/jop.2011.110270]
19 **Miron RJ**, Sculean A, Shuang Y, Bosshardt DD, Gruber R, Buser D, Chandad F, Zhang Y. Osteoinductive potential of a novel biphasic calcium phosphate bone graft in comparison with autographs, xenografts, and DFDBA. *Clin Oral Implants Res* 2016; **27**: 668-675 [PMID: 26227281 DOI: 10.1111/clr.12647]
20 **Roldán JC**, Knueppel H, Schmidt C, Jepsen S, Zimmermann C, Terheyden H. Single-stage sinus augmentation with cancellous iliac bone and anorganic bovine bone in the presence of platelet-rich plasma in the miniature pig. *Clin Oral Implants Res* 2008; **19**: 373-378 [PMID: 18261122 DOI: 10.1111/j.1600-0501.2007.01465.x]
21 **Lee HJ**, Choi BH, Jung JH, Zhu SJ, Lee SH, Huh JY, You TM, Li J. Maxillary sinus floor augmentation using autogenous bone grafts and platelet-enriched fibrin glue with simultaneous implant placement. *Oral Surg Oral Med Oral Pathol Oral Radiol Endod* 2007; **103**: 329-333 [PMID: 17321442 DOI: 10.1016/j.tripleo.2006.03.010]
22 **Kassolis JD**, Rosen PS, Reynolds MA. Alveolar ridge and sinus augmentation utilizing platelet-rich plasma in combination with freeze-dried bone allograft: case series. *J Periodontol* 2000; **71**: 1654-1661 [PMID: 11063400 DOI: 10.1902/jop.2000.71.10.1654]
23 **Rodriguez A**, Anastassov GE, Lee H, Buchbinder D, Wettan H. Maxillary sinus augmentation with deproteinated bovine bone and platelet rich plasma with simultaneous insertion of endosseous implants. *J Oral Maxillofac Surg* 2003; **61**: 157-163 [PMID: 12618990 DOI: 10.1053/joms.2003.50041]
24 **Wiltfang J**, Schlegel KA, Schultze-Mosgau S, Nkenke E, Zimmermann R, Kessler P. Sinus floor augmentation with beta-tricalciumphosphate (beta-TCP): does platelet-rich plasma promote its osseous integration and degradation? *Clin Oral Implants Res* 2003; **14**: 213-218 [PMID: 12656882 DOI: 10.1034/j.1600-0501.2003.140212.x]
25 **Bae JH**, Kim YK, Myung SK. Effects of platelet-rich plasma on sinus bone graft: meta-analysis. *J Periodontol* 2011; **82**: 660-667 [PMID: 21091351 DOI: 10.1902/jop.2010.100529]
26 **Nikolidakis D**, Jansen JA. The biology of platelet-rich plasma and its application in oral surgery: literature review. *Tissue Eng Part B Rev* 2008; **14**: 249-258 [PMID: 18601587 DOI: 10.1089/ten.teb.2008.0062]
27 **Intini G**. The use of platelet-rich plasma in bone reconstruction therapy. *Biomaterials* 2009; **30**: 4956-4966 [PMID: 19573909 DOI: 10.1016/j.biomaterials.2009.05.055]
28 **Roffi A**, Di Matteo B, Krishnakumar GS, Kon E, Filardo G. Platelet-rich plasma for the treatment of bone defects: from pre-clinical rational to evidence in the clinical practice. A systematic review. *Int Orthop* 2017; **41**: 221-237 [PMID: 27888295 DOI: 10.1007/s00264-016-3342-9]
29 **Lemos CA**, Mello CC, dos Santos DM, Verri FR, Goiato MC, Pellizzer EP. Effects of platelet-rich plasma in association with bone grafts in maxillary sinus augmentation: a systematic review and meta-analysis. *Int J Oral Maxillofac Surg* 2016; **45**: 517-525 [PMID: 26775635 DOI: 10.1016/j.ijom.2015.07.012]
30 **Pocaterra A**, Caruso S, Bernardi S, Scagnoli L, Continenza MA, Gatto R. Effectiveness of platelet-rich plasma as an adjunctive material to bone graft: a systematic review and meta-analysis of randomized controlled clinical trials. *Int J Oral Maxillofac Surg* 2016; **45**: 1027-1034 [PMID: 26987695 DOI: 10.1016/j.ijom.2016.02.012]
31 **Abdalla RIB**, Alqutaibi AY, Kaddah A. Does the adjunctive use of platelet-rich plasma to bone graft

during sinus augmentation reduce implant failure and complication? Systematic review and meta-analysis. *Quintessence Int* 2018; **49**: 139-146 [PMID: 29292406 DOI: 10.3290/j.qi.a39616]
32 **Misch CE**. Available bone and dental implant treatment plans. In: Misch CE, editor. Contemporary Implant Dentistry. 3rd ed. St. Louis: Mosby 2008; 178-199
33 **Jensen OT**, Shulman LB, Block MS, Iacono VJ. Report of the Sinus Consensus Conference of 1996. *Int J Oral Maxillofac Implants* 1998; **13** Suppl: 11-45 [PMID: 9715571]
34 **Eda T**, Takahashi K, Kanao S, Aoki A, Ogura N, Ito K, Tsukahara H, Suemitsu M, Kuyama K, Kondoh T. Comparison study between plasma rich in growth factors and platelet-rich plasma for osteoconduction in rat calvaria. *J Oral Maxillofac Surg Med Pathol* 2017; **29**: 563-569 [DOI: 10.1016/j.ajoms.2017.06.011]
35 **Parnia F**, Yazdani J, Maleki Dizaj S. Applications of Mesenchymal Stem Cells in Sinus Lift Augmentation as a Dental Implant Technology. *Stem Cells Int* 2018; **2018**: 3080139 [PMID: 29760723 DOI: 10.1155/2018/3080139]
36 **Niño-Sandoval TC**, Vasconcelos BC, D Moraes SL, A Lemos CA, Pellizzer EP. Efficacy of stem cells in maxillary sinus floor augmentation: systematic review and meta-analysis. *Int J Oral Maxillofac Surg* 2018 [PMID: 29759309]
37 **Miguita L**, Mantesso A, Pannuti CM, Deboni MCZ. Can stem cells enhance bone formation in the human edentulous alveolar ridge? A systematic review and meta-analysis. *Cell Tissue Bank* 2017; **18**: 217-228 [PMID: 28233169 DOI: 10.1007/s10561-017-9612-y]
38 **Barba M**, Di Taranto G, Lattanzi W. Adipose-derived stem cell therapies for bone regeneration. *Expert Opin Biol Ther* 2017; **17**: 677-689 [PMID: 28374644 DOI: 10.1080/14712598.2017.1315403]
39 **Bhattacharya I**, Ghayor C, Weber FE. The Use of Adipose Tissue-Derived Progenitors in Bone Tissue Engineering - a Review. *Transfus Med Hemother* 2016; **43**: 336-343 [PMID: 27781021 DOI: 10.1159/000447494]
40 **Han DS**, Chang HK, Kim KR, Woo SM. Consideration of bone regeneration effect of stem cells: comparison of bone regeneration between bone marrow stem cells and adipose-derived stem cells. *J Craniofac Surg* 2014; **25**: 196-201 [PMID: 24406577 DOI: 10.1097/SCS.0000000000000378]
41 **Hayashi O**, Katsube Y, Hirose M, Ohgushi H, Ito H. Comparison of osteogenic ability of rat mesenchymal stem cells from bone marrow, periosteum, and adipose tissue. *Calcif Tissue Int* 2008; **82**: 238-247 [PMID: 18305886 DOI: 10.1007/s00223-008-9112-y]
42 **Zhang W**, Zhang X, Wang S, Xu L, Zhang M, Wang G, Jin Y, Zhang X, Jiang X. Comparison of the use of adipose tissue-derived and bone marrow-derived stem cells for rapid bone regeneration. *J Dent Res* 2013; **92**: 1136-1141 [PMID: 24097853 DOI: 10.1177/0022034513507581]
43 **Yu H**, Lu K, Zhu J, Wang J. Stem cell therapy for ischemic heart diseases. *Br Med Bull* 2017; **121**: 135-154 [PMID: 28164211 DOI: 10.1093/bmb/ldw059]
44 **Fraser JK**, Wulur I, Alfonso Z, Hedrick MH. Fat tissue: an underappreciated source of stem cells for biotechnology. *Trends Biotechnol* 2006; **24**: 150-154 [PMID: 16488036 DOI: 10.1016/j.tibtech.2006.01.010]
45 **Aust L**, Devlin B, Foster SJ, Halvorsen YD, Hicok K, du Laney T, Sen A, Willingmyre GD, Gimble JM. Yield of human adipose-derived adult stem cells from liposuction aspirates. *Cytotherapy* 2004; **6**: 7-14 [PMID: 14985162 DOI: 10.1080/14653240310004539]
46 **Tajima S**, Tobita M, Mizuno H. Current status of bone regeneration using adipose-derived stem cells. *Histol Histopathol* 2018; **33**: 619-627 [PMID: 29094748 DOI: 10.14670/HH-11-942]
47 **Romagnoli C**, Brandi ML. Adipose mesenchymal stem cells in the field of bone tissue engineering. *World J Stem Cells* 2014; **6**: 144-152 [PMID: 24772241 DOI: 10.4252/wjsc.v6.i2.144]
48 **Zanetti AS**, Sabliov C, Gimble JM, Hayes DJ. Human adipose-derived stem cells and three-dimensional scaffold constructs: a review of the biomaterials and models currently used for bone regeneration. *J Biomed Mater Res B Appl Biomater* 2013; **101**: 187-199 [PMID: 22997152 DOI: 10.1002/jbm.b.32817]
49 **Oberbauer E**, Steffenhagen C, Wurzer C, Gabriel C, Redl H, Wolbank S. Enzymatic and non-enzymatic isolation systems for adipose tissue-derived cells: current state of the art. *Cell Regen (Lond)* 2015; **4**: 7 [PMID: 26435835 DOI: 10.1186/s13619-015-0020-0]
50 **van Dongen JA**, Tuin AJ, Spiekman M, Jansma J, van der Lei B, Harmsen MC. Comparison of intraoperative procedures for isolation of clinical grade stromal vascular fraction for regenerative purposes: a systematic review. *J Tissue Eng Regen Med* 2018; **12**: e261-e274 [PMID: 28084666 DOI: 10.1002/term.2407]
51 **Condé-Green A**, Kotamarti VS, Sherman LS, Keith JD, Lee ES, Granick MS, Rameshwar P. Shift toward Mechanical Isolation of Adipose-derived Stromal Vascular Fraction: Review of Upcoming Techniques. *Plast Reconstr Surg Glob Open* 2016; **4**: e1017 [PMID: 27757339 DOI: 10.1097/GOX.0000000000001017]
52 **Aronowitz JA**, Lockhart RA, Hakakian CS. Mechanical versus enzymatic isolation of stromal vascular fraction cells from adipose tissue. *Springerplus* 2015; **4**: 713 [PMID: 26636001 DOI: 10.1186/s40064-015-1509-2]
53 **Valenzuela N**, Alt C, Winnier GE, Alt EU. Isolation of adipose tissue derived regenerative cells from human subcutaneous tissue with or without the use of enzymatic reagent. 2018 Preprint. bioRxiv:485318. [DOI: 10.1101/485318]
54 **Panés J**, García-Olmo D, Van Assche G, Colombel JF, Reinisch W, Baumgart DC, Dignass A, Nachury M, Ferrante M, Kazemi-Shirazi L, Grimaud JC, de la Portilla F, Goldin E, Richard MP, Leselbaum A, Danese S; ADMIRE CD Study Group Collaborators. Expanded allogeneic adipose-derived mesenchymal stem cells (Cx601) for complex perianal fistulas in Crohn's disease: a phase 3 randomised, double-blind controlled trial. *Lancet* 2016; **388**: 1281-1290 [PMID: 27477896 DOI: 10.1016/S0140-6736(16)31203-X]
55 **Álvaro-Gracia JM**, Jover JA, García-Vicuña R, Carreño L, Alonso A, Marsal S, Blanco F, Martínez-Taboada VM, Taylor P, Martín-Martín C, DelaRosa O, Tagarro I, Díaz-González F. Intravenous administration of expanded allogeneic adipose-derived mesenchymal stem cells in refractory rheumatoid arthritis (Cx611): results of a multicentre, dose escalation, randomised, single-blind, placebo-controlled phase Ib/IIa clinical trial. *Ann Rheum Dis* 2017; **76**: 196-202 [PMID: 27269294 DOI: 10.1136/annrheum-dis-2015-208918]
56 **Schmitz C**, Hof PR. Design-based stereology in neuroscience. *Neuroscience* 2005; **130**: 813-831 [PMID: 15652981 DOI: 10.1016/j.neuroscience.2004.08.050]
57 **Klein JA**. Tumescent technique for local anesthesia improves safety in large-volume liposuction. *Plast Reconstr Surg* 1993; **92**: 1085-98; discussion 1099-100 [PMID: 8234507 DOI: 10.1097/00006534-199311000-00014]
58 **Coleman WP 4th, Hendry SL 2nd**. Principles of liposuction. *Semin Cutan Med Surg* 2006; **25**: 138-144

[PMID: 17055393 DOI: 10.1016/j.sder.2006.06.006]
59 **Tatum H**. Maxillary and sinus implant reconstructions. *Dent Clin North Am* 1986; **30**: 207-229 [PMID: 3516738 DOI: 10.1016/0011-3840(86)90013-4]
60 **El Chaar ES**. Soft tissue closure of grafted extraction sockets in the posterior maxilla: the rotated pedicle palatal connective tissue flap technique. *Implant Dent* 2010; **19**: 370-377 [PMID: 20881807 DOI: 10.1097/ID.0b013e3181ed06cd]
61 **Ronda M**, Stacchi C. A Novel Approach for the Coronal Advancement of the Buccal Flap. *Int J Periodontics Restorative Dent* 2015; **35**: 795-801 [PMID: 26509982 DOI: 10.11607/prd.2232]
62 **Mangano FG**, Tettamanti L, Sammons RL, Azzi L, Caprioglio A, Macchi A, Mangano C. Maxillary sinus augmentation with adult mesenchymal stem cells: a review of the current literature. *Oral Surg Oral Med Oral Pathol Oral Radiol* 2013; **115**: 717-723 [PMID: 23313230 DOI: 10.1016/j.oooo.2012.09.087]
63 **Mangano FG**, Colombo M, Veronesi G, Caprioglio A, Mangano C. Mesenchymal stem cells in maxillary sinus augmentation: A systematic review with meta-analysis. *World J Stem Cells* 2015; **7**: 976-991 [PMID: 26240683 DOI: 10.4252/wjsc.v7.i6.976]
64 **Correia F**, Pozza DH, Gouveia S, Felino A, Faria E Almeida R. The applications of regenerative medicine in sinus lift procedures: A systematic review. *Clin Implant Dent Relat Res* 2018; **20**: 229-242 [PMID: 29205768 DOI: 10.1111/cid.12561]
65 **Wildburger A**, Payer M, Jakse N, Strunk D, Etchard-Liechtenstein N, Sauerbier S. Impact of autogenous concentrated bone marrow aspirate on bone regeneration after sinus floor augmentation with a bovine bone substitute--a split-mouth pilot study. *Clin Oral Implants Res* 2014; **25**: 1175-1181 [PMID: 23875876 DOI: 10.1111/clr.12228]
66 **Pasquali PJ**, Teixeira ML, de Oliveira TA, de Macedo LG, Aloise AC, Pelegrine AA. Maxillary Sinus Augmentation Combining Bio-Oss with the Bone Marrow Aspirate Concentrate: A Histomorphometric Study in Humans. *Int J Biomater* 2015; **2015**: 121286 [PMID: 26543482 DOI: 10.1155/2015/121286]
67 **Parisien M**, Cosman F, Morgan D, Schnitzer M, Liang X, Nieves J, Forese L, Luckey M, Meier D, Shen V, Lindsay R, Dempster DW. Histomorphometric assessment of bone mass, structure, and remodeling: a comparison between healthy black and white premenopausal women. *J Bone Miner Res* 1997; **12**: 948-957 [PMID: 9169355 DOI: 10.1359/jbmr.1997.12.6.948]
68 **Hynes K**, Menicanin D, Gronthos S, Bartold PM. Clinical utility of stem cells for periodontal regeneration. *Periodontol 2000* 2012; **59**: 203-227 [PMID: 22507067 DOI: 10.1111/j.1600-0757.2012.00443.x]
69 **Egusa H**, Sonoyama W, Nishimura M, Atsuta I, Akiyama K. Stem cells in dentistry--part I: stem cell sources. *J Prosthodont Res* 2012; **56**: 151-165 [PMID: 22796367 DOI: 10.1016/j.jpor.2012.06.001]
70 **Ahmed RP**, Ashraf M, Buccini S, Shujia J, Haider HKh. Cardiac tumorigenic potential of induced pluripotent stem cells in an immunocompetent host with myocardial infarction. *Regen Med* 2011; **6**: 171-178 [PMID: 21391851 DOI: 10.2217/rme.10.103]
71 **Zhang Y**, Wang D, Chen M, Yang B, Zhang F, Cao K. Intramyocardial transplantation of undifferentiated rat induced pluripotent stem cells causes tumorigenesis in the heart. *PLoS One* 2011; **6**: e19012 [PMID: 21552563 DOI: 10.1371/journal.pone.0019012]
72 **Schmelzeisen R**, Gutwald R, Oshima T, Nagursky H, Vogeler M, Sauerbier S. Making bone II: maxillary sinus augmentation with mononuclear cells--case report with a new clinical method. *Br J Oral Maxillofac Surg* 2011; **49**: 480-482 [PMID: 20678831 DOI: 10.1016/j.bjoms.2010.06.020]
73 **Sauerbier S**, Rickert D, Gutwald R, Nagursky H, Oshima T, Xavier SP, Christmann J, Kurz P, Menne D, Vissink A, Raghoebar G, Schmelzeisen R, Wagner W, Koch FP. Bone marrow concentrate and bovine bone mineral for sinus floor augmentation: a controlled, randomized, single-blinded clinical and histological trial--per-protocol analysis. *Tissue Eng Part A* 2011; **17**: 2187-2197 [PMID: 21529247 DOI: 10.1089/ten.TEA.2010.0516]
74 **Götz W**, Gerber T, Michel B, Lossdörfer S, Henkel KO, Heinemann F. Immunohistochemical characterization of nanocrystalline hydroxyapatite silica gel (NanoBone(r)) osteogenesis: a study on biopsies from human jaws. *Clin Oral Implants Res* 2008; **19**: 1016-1026 [PMID: 18828818 DOI: 10.1111/j.1600-0501.2008.01569.x]
75 **Friedmann A**, Gissel K, Konermann A, Götz W. Tissue reactions after simultaneous alveolar ridge augmentation with biphasic calcium phosphate and implant insertion--histological and immunohistochemical evaluation in humans. *Clin Oral Investig* 2015; **19**: 1595-1603 [PMID: 25511386 DOI: 10.1007/s00784-014-1385-0]
76 **Hawthorne AC**, Xavier SP, Okamoto R, Salvador SL, Antunes AA, Salata LA. Immunohistochemical, tomographic, and histological study on onlay bone graft remodeling. Part III: allografts. *Clin Oral Implants Res* 2013; **24**: 1164-1172 [PMID: 22775764 DOI: 10.1111/j.1600-0501.2012.02528.x]
77 **Brunel G**, Brocard D, Duffort JF, Jacquet E, Justumus P, Simonet T, Benqué E. Bioabsorbable materials for guided bone regeneration prior to implant placement and 7-year follow-up: report of 14 cases. *J Periodontol* 2001; **72**: 257-264 [PMID: 11288801 DOI: 10.1902/jop.2001.72.2.257]
78 **Mordenfeld A**, Hallman M, Johansson CB, Albrektsson T. Histological and histomorphometrical analyses of biopsies harvested 11 years after maxillary sinus floor augmentation with deproteinized bovine and autogenous bone. *Clin Oral Implants Res* 2010; **21**: 961-970 [PMID: 20497443 DOI: 10.1111/j.1600-0501.2010.01939.x]
79 **Tian T**, Zhang T, Lin Y, Cai X. Vascularization in Craniofacial Bone Tissue Engineering. *J Dent Res* 2018; **97**: 969-976 [PMID: 29608865 DOI: 10.1177/0022034518767120]
80 **Bourin P**, Bunnell BA, Casteilla L, Dominici M, Katz AJ, March KL, Redl H, Rubin JP, Yoshimura K, Gimble JM. Stromal cells from the adipose tissue-derived stromal vascular fraction and culture expanded adipose tissue-derived stromal/stem cells: a joint statement of the International Federation for Adipose Therapeutics and Science (IFATS) and the International Society for Cellular Therapy (ISCT). *Cytotherapy* 2013; **15**: 641-648 [PMID: 23570660 DOI: 10.1016/j.jcyt.2013.02.006]
81 **Rezza A**, Sennett R, Rendl M. Adult stem cell niches: cellular and molecular components. *Curr Top Dev Biol* 2014; **107**: 333-372 [PMID: 24439812 DOI: 10.1016/B978-0-12-416022-4.00012-3]
82 **Dong L**, Hao H, Han W, Fu X. The role of the microenvironment on the fate of adult stem cells. *Sci China Life Sci* 2015; **58**: 639-648 [PMID: 25985755 DOI: 10.1007/s11427-015-4865-9]
83 **Wabik A**, Jones PH. Switching roles: the functional plasticity of adult tissue stem cells. *EMBO J* 2015; **34**: 1164-1179 [PMID: 25812989 DOI: 10.15252/embj.201490386]
84 **Trosko JE**. Induction of iPS cells and of cancer stem cells: the stem cell or reprogramming hypothesis of cancer? *Anat Rec (Hoboken)* 2014; **297**: 161-173 [PMID: 24293264 DOI: 10.1002/ar.22793]
85 **Zhang B**, Wang M, Gong A, Zhang X, Wu X, Zhu Y, Shi H, Wu L, Zhu W, Qian H, Xu W. HucMSC-

Exosome Mediated-Wnt4 Signaling Is Required for Cutaneous Wound Healing. *Stem Cells* 2015; **33**: 2158-2168 [PMID: 24964196 DOI: 10.1002/stem.1771]
86 **Phinney DG**, Prockop DJ. Concise review: mesenchymal stem/multipotent stromal cells: the state of transdifferentiation and modes of tissue repair--current views. *Stem Cells* 2007; **25**: 2896-2902 [PMID: 17901396 DOI: 10.1634/stemcells.2007-0637]
87 **Kara RJ**, Bolli P, Karakikes I, Matsunaga I, Tripodi J, Tanweer O, Altman P, Shachter NS, Nakano A, Najfeld V, Chaudhry HW. Fetal cells traffic to injured maternal myocardium and undergo cardiac differentiation. *Circ Res* 2012; **110**: 82-93 [PMID: 22082491 DOI: 10.1161/CIRCRESAHA.111.249037]
88 **Malliaras K**, Zhang Y, Seinfeld J, Galang G, Tseliou E, Cheng K, Sun B, Aminzadeh M, Marbán E. Cardiomyocyte proliferation and progenitor cell recruitment underlie therapeutic regeneration after myocardial infarction in the adult mouse heart. *EMBO Mol Med* 2013; **5**: 191-209 [PMID: 23255322 DOI: 10.1002/emmm.201201737]
89 **Ra JC**, Shin IS, Kim SH, Kang SK, Kang BC, Lee HY, Kim YJ, Jo JY, Yoon EJ, Choi HJ, Kwon E. Safety of intravenous infusion of human adipose tissue-derived mesenchymal stem cells in animals and humans. *Stem Cells Dev* 2011; **20**: 1297-1308 [PMID: 21303266 DOI: 10.1089/scd.2010.0466]
90 **Hoffman AM**, Dow SW. Concise Review: Stem Cell Trials Using Companion Animal Disease Models. *Stem Cells* 2016; **34**: 1709-1729 [PMID: 27066769 DOI: 10.1002/stem.2377]
91 **Toyserkani NM**, Jørgensen MG, Tabatabaeifar S, Jensen CH, Sheikh SP, Sørensen JA. Concise Review: A Safety Assessment of Adipose-Derived Cell Therapy in Clinical Trials: A Systematic Review of Reported Adverse Events. *Stem Cells Transl Med* 2017; **6**: 1786-1794 [PMID: 28722289 DOI: 10.1002/sctm.17-0031]
92 **Røsland GV**, Svendsen A, Torsvik A, Sobala E, McCormack E, Immervoll H, Mysliwietz J, Tonn JC, Goldbrunner R, Lønning PE, Bjerkvig R, Schichor C. Long-term cultures of bone marrow-derived human mesenchymal stem cells frequently undergo spontaneous malignant transformation. *Cancer Res* 2009; **69**: 5331-5339 [PMID: 19509230 DOI: 10.1158/0008-5472.CAN-08-4630]
93 **Xu S**, De Becker A, De Raeve H, Van Camp B, Vanderkerken K, Van Riet I. In vitro expanded bone marrow-derived murine (C57Bl/KaLwRij) mesenchymal stem cells can acquire CD34 expression and induce sarcoma formation in vivo. *Biochem Biophys Res Commun* 2012; **424**: 391-397 [PMID: 22771324 DOI: 10.1016/j.bbrc.2012.06.118]
94 **Pan Q**, Fouraschen SM, de Ruiter PE, Dinjens WN, Kwekkeboom J, Tilanus HW, van der Laan LJ. Detection of spontaneous tumorigenic transformation during culture expansion of human mesenchymal stromal cells. *Exp Biol Med (Maywood)* 2014; **239**: 105-115 [PMID: 24227633 DOI: 10.1177/1535370213506802]
95 **Haenel A**, Ghosn M, Karimi T, Vykoukal J, Kettlun C, Shah D, Dave A, Valderrrabano M, Schulz D, Azares A, Raizner A, Alt E. Unmodified, autologous adipose-derived regenerative cells improve cardiac function, structure and revascularization in a porcine model of chronic myocardial infarction. 2018 Preprint. BioRxiv:286468. [DOI: 10.1101/286468]
96 **Badimon L**, Oñate B, Vilahur G. Adipose-derived Mesenchymal Stem Cells and Their Reparative Potential in Ischemic Heart Disease. *Rev Esp Cardiol (Engl Ed)* 2015; **68**: 599-611 [PMID: 26028258 DOI: 10.1016/j.rec.2015.02.025]
97 **Lombardi G**, Perego S, Luzi L, Banfi G. A four-season molecule: osteocalcin. Updates in its physiological roles. *Endocrine* 2015; **48**: 394-404 [PMID: 25158976 DOI: 10.1007/s12020-014-0401-0]
98 **Anitua E**, Tejero R, Zalduendo MM, Orive G. Plasma rich in growth factors promotes bone tissue regeneration by stimulating proliferation, migration, and autocrine secretion in primary human osteoblasts. *J Periodontol* 2013; **84**: 1180-1190 [PMID: 23088531 DOI: 10.1902/jop.2012.120292]
99 **Anitua E**, Prado R, Orive G. A lateral approach for sinus elevation using PRGF technology. *Clin Implant Dent Relat Res* 2009; **11** Suppl 1: e23-e31 [PMID: 19438953 DOI: 10.1111/j.1708-8208.2009.00159.x]
100 **Taschieri S**, Corbella S, Del Fabbro M. Use of plasma rich in growth factor for schneiderian membrane management during maxillary sinus augmentation procedure. *J Oral Implantol* 2012; **38**: 621-627 [PMID: 23072223 DOI: 10.1563/AAID-JOI-D-12-00009]
101 **Khouly I**, Pardiñas López S, Aliaga I, Froum SJ. Long-Term Implant Survival After 100 Maxillary Sinus Augmentations Using Plasma Rich in Growth Factors. *Implant Dent* 2017; **26**: 199-208 [PMID: 28207599 DOI: 10.1097/ID.0000000000000561]
102 **Salgado AJ**, Reis RL, Sousa NJ, Gimble JM. Adipose tissue derived stem cells secretome: soluble factors and their roles in regenerative medicine. *Curr Stem Cell Res Ther* 2010; **5**: 103-110 [PMID: 19941460 DOI: 10.2174/157488810791268564]
103 **Mellado-López M**, Griffeth RJ, Meseguer-Ripolles J, Cugat R, García M, Moreno-Manzano V. Plasma Rich in Growth Factors Induces Cell Proliferation, Migration, Differentiation, and Cell Survival of Adipose-Derived Stem Cells. *Stem Cells Int* 2017; **2017**: 5946527 [PMID: 29270200 DOI: 10.1155/2017/5946527]
104 **Bai X**, Sadat S, Gehmert S, Alt E, Song YH. VEGF receptor Flk-1 plays an important role in c-kit expression in adipose tissue derived stem cells. *FEBS Lett* 2007; **581**: 4681-4684 [PMID: 17850794 DOI: 10.1016/j.febslet.2007.08.063]
105 **Kusuma GD**, Carthew J, Lim R, Frith JE. Effect of the Microenvironment on Mesenchymal Stem Cell Paracrine Signaling: Opportunities to Engineer the Therapeutic Effect. *Stem Cells Dev* 2017; **26**: 617-631 [PMID: 28186467 DOI: 10.1089/scd.2016.0349]
106 **Hegde R**, Prasad K, Shroff KK. Maxillary sinus augmentation using sinus membrane elevation without grafts - A Systematic Review. *J Indian Prosthodont Soc* 2016; **16**: 317-322 [PMID: 27746593 DOI: 10.4103/0972-4052.191289]
107 **Tong DC**, Rioux K, Drangsholt M, Beirne OR. A review of survival rates for implants placed in grafted maxillary sinuses using meta-analysis. *Int J Oral Maxillofac Implants* 1998; **13**: 175-182 [PMID: 9581402 DOI: 10.1016/S0020-1383(98)00055-2]
108 **Klijn RJ**, Meijer GJ, Bronkhorst EM, Jansen JA. A meta-analysis of histomorphometric results and graft healing time of various biomaterials compared to autologous bone used as sinus floor augmentation material in humans. *Tissue Eng Part B Rev* 2010; **16**: 493-507 [PMID: 20334505 DOI: 10.1089/ten.TEB.2010.0035]
109 **Silva LD**, de Lima VN, Faverani LP, de Mendonça MR, Okamoto R, Pellizzer EP. Maxillary sinus lift surgery-with or without graft material? A systematic review. *Int J Oral Maxillofac Surg* 2016; **45**: 1570-1576 [PMID: 27765427 DOI: 10.1016/j.ijom.2016.09.023]
110 **Hosseinpour S**, Ghazizadeh Ahsaie M, Rezai Rad M, Baghani MT, Motamedian SR, Khojasteh A. Application of selected scaffolds for bone tissue engineering: a systematic review. *Oral Maxillofac Surg*

2017; **21**: 109-129 [PMID: 28194530 DOI: 10.1007/s10006-017-0608-3]
111 **Destatis Statistisches Bundesamt**. Die Angeforderte Seite IST Nicht Verfügbar. 2018; Available from: URL: https://www.destatis.de/DE/ZahlenFakten/GesellschaftStaat/Bevoelkerung/Sterbefaelle/Tabellen/Lebenserwartung.pdf
112 **Kokai LE**, Traktuev DO, Zhang L, Merfeld-Clauss S, DiBernardo G, Lu H, Marra KG, Donnenberg A, Donnenberg V, Meyer EM, Fodor PB, March KL, Rubin JP. Adipose Stem Cell Function Maintained with Age: An Intra-Subject Study of Long-Term Cryopreserved Cells. *Aesthet Surg J* 2017; **37**: 454-463 [PMID: 28364523 DOI: 10.1093/asj/sjw197]
113 **Alt EU**, Senst C, Murthy SN, Slakey DP, Dupin CL, Chaffin AE, Kadowitz PJ, Izadpanah R. Aging alters tissue resident mesenchymal stem cell properties. *Stem Cell Res* 2012; **8**: 215-225 [PMID: 22265741 DOI: 10.1016/j.scr.2011.11.002]
114 **Kim SW**, Choi JW, Lee CY, Lee J, Shin S, Lim S, Lee S, Kim IK, Lee HB, Hwang KC. Effects of donor age on human adipose-derived adherent stromal cells under oxidative stress conditions. *J Int Med Res* 2018; **46**: 951-964 [PMID: 28984178 DOI: 10.1177/0300060517731684]
115 **Egusa H**, Sonoyama W, Nishimura M, Atsuta I, Akiyama K. Stem cells in dentistry--Part II: Clinical applications. *J Prosthodont Res* 2012; **56**: 229-248 [PMID: 23137671 DOI: 10.1016/j.jpor.2012.10.001]
116 **Miran S**, Mitsiadis TA, Pagella P. Innovative Dental Stem Cell-Based Research Approaches: The Future of Dentistry. *Stem Cells Int* 2016; **2016**: 7231038 [PMID: 27648076 DOI: 10.1155/2016/7231038]
117 **Amrollahi P**, Shah B, Seifi A, Tayebi L. Recent advancements in regenerative dentistry: A review. *Mater Sci Eng C Mater Biol Appl* 2016; **69**: 1383-1390 [PMID: 27612840 DOI: 10.1016/j.msec.2016.08.045]

P- Reviewer: Fatkhudinov T, He SQ, Zheng YW
S- Editor: Ma YJ **L- Editor:** Filipodia **E- Editor:** Bian YN

Baishideng®

Published By Baishideng Publishing Group Inc
7901 Stoneridge Drive, Suite 501, Pleasanton, CA 94588, USA
Telephone: +1-925-2238242
Fax: +1-925-2238243
E-mail: bpgoffice@wjgnet.com
Help Desk: https://www.f6publishing.com/helpdesk
https://www.wjgnet.com